UNIVERSITAT DE BARCELONA

Insights in the pathogenesis of the aortic aneurysm in Marfan syndrome and new therapeutic approaches

Isaac Rodriguez Rovira

UNIVERSITAT DE BARCELONA

Insights in the pathogenesis of the aortic aneurysm in Marfan syndrome and new therapeutic approaches

Ph.D. degree in Biomedicine by the
University of Barcelona

Submitted by:

Isaac Rodríguez Rovira

This work was performed at the Department of Biomedical Sciences of the Faculty of Medicine and Health Sciences of the University of Barcelona under the supervision of Dr. Gustavo Egea Guri.

Isaac Rodríguez Rovira
PhD Student

Dr. Gustavo Egea Guri
Director and tutor

Programa de Doctorat de Biomedicina

Table of contents

ABBREVIATIONS

ALO	Allopurinol
CVD	Cardiovascular disease
ECM	Extracellular matrix
ER	Endoplasmatic reticulum
Fbn1	Fibrillin-1
H_2O_2	Hydrogen peroxide
iNOS	Induced nitric oxide synthase
LAP	Latent associated peptide
LLC	Large latent complex
LOX	Lysyl Oxidases
LTBP	Latent binding protein
MFS	Marfan syndrome
MMP	Metaloproteinases
NO	Nitric oxide
NOX4	NADPH oxidases
O_2-	Radical superoxide
O_2	Oxygen
OH^-	Radical hydroxil
$ONOO^-$	Peroxinytrite
ROS	Reactive oxygen species
SOD	Superoxide dismutase
TAAD	Toracic aortic aneurysm and dissection
TGF-ß	Transforming growth factor beta
TGFRs	Transforming growth factor receptors
VSMC	Vascular smooth muscle cells
XDH	Xanthine deydrogenase
XO	Xanthine oxidase
XOR	Xanthine oxidoreductase

1. Introduction

1.1. The aorta: Anatomy and histology

The aorta is the primary and largest artery in the body (Koeppen et al. 2010). In a healthy adult human, the aorta measures approximately 1.2 m in length and has a diameter of around 26 mm, which is progressively reduced in diameter, and from which emerges many arteries. Eventually, these arteries lead to billions of capillaries, which then progressively converge to form a single vena cava back to the heart (Hutchinson et al. 2010; Back et al. 2013). The aorta serves as the direct collector of blood ejected by the heart standardizing the blood flow all over the circulatory system (Testut et al. 1983).

1.1.1. Anatomy of the aorta

The aorta presents one end emerging from the left ventricle of the heart and the other ending at a bifurcation at the lower back (Mann et al. 2015). The aorta is divided into ascending thoracic aorta, aortic arch, and descending thoracic and abdominal segments. The aorta descending portion feeds the thoracic organs as it descends along the spine, travels through the diaphragm, branches to feed the abdominal organs, and then divides into the two iliac arteries that serve the lower limbs. Furthermore, the aortic arch is the origin of the blood arteries that nourish the brain and upper limbs. (Figure 1) (Mann et al. 2015; Gartner et al 2008).

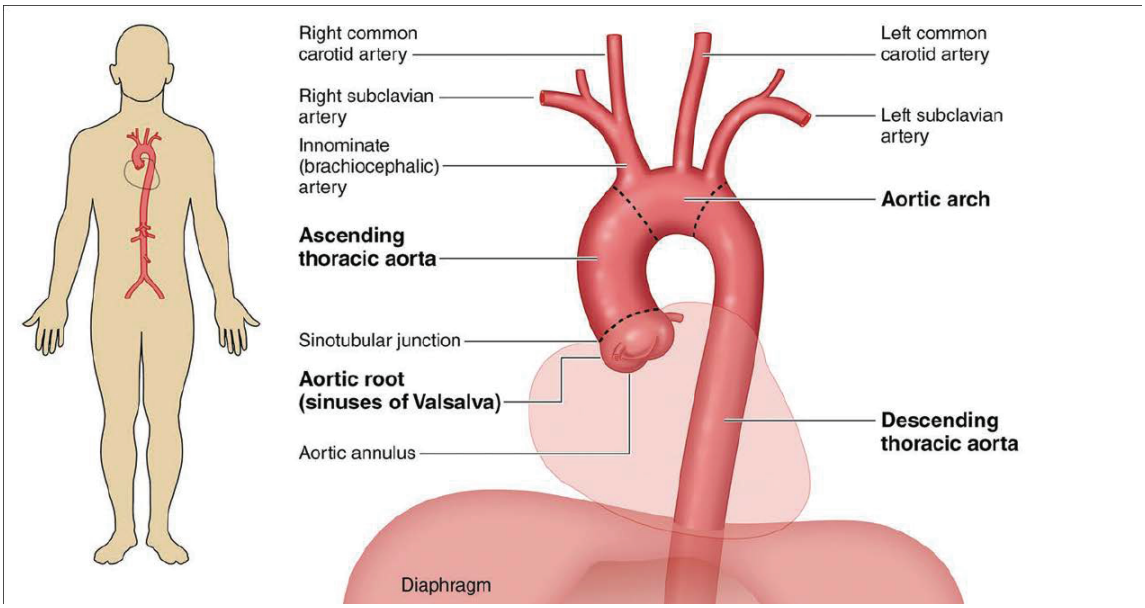

Figure 1. The anatomy of the aorta and its branches. Modified from Isselbacher EM et al 2022.

The ascending aorta consists of two main parts: the aortic root and the ascending tubular aorta, which is a vertical tube connecting to the aortic arch. The sinotubular junction marks the border between these two segments of the ascending aorta (Mann et al. 2015). Inside the heart, the aortic root is a naturally dilated space that houses the aortic semilunar valve. This valve controls the flow of blood into the aorta. It is a tricuspid valve composed of three cusps or leaflets that passively open during systole when blood is ejected, and passively close during diastole to prevent backward blood flow to the heart (Gartner et al. 2008). The tube-like structure of the aortic root comprises three rounded dilations called Valsalva sinuses. Furthermore, the origins of the coronary arteries, which supply blood to the cardiac tissue, arise from these sinuses.

1.1.2. Histology of the aorta

The aorta is categorized as an elastic artery due to its structural design, which facilitates the passive propulsion of blood forward. Its wall is divided into three layers known as tunicae intima, media, and adventitia (Figure 2) (Wagensein et al 2009). The innermost layer, called the tunica intima, consists of a continuous monolayer of endothelial cells and a thin layer of loose connective tissue beneath them (Kierszenbaum et al. 2016). Together, these components cover the inner surface of the vessel. The middle and thickest layer, known as the tunica media, is composed of elastic lamellae alternating with layers of vascular
smooth muscle cells (VSMCs) that are arranged circumferentially.

The outermost layer, referred to as the tunica adventitia, is composed of loose fibroelastic connective tissue enriched in longitudinally arranged collagen I fibers, containing fibroblasts, macrophages, small nerves, and small blood vessels. Oxygen and nutrients are supplied to the aortic wall through simple diffusion from the lumen on one side. In the case of thick aortic walls (found in humans but not in mice), oxygen and nutrients are also provided by the *vasa vasorum* capillary network, which extends from the adventitia to the outer layers of the tunica media. The internal elastic lamina separates the tunica intima from the media, while the external elastic one marks the boundary between the tunica media and the adventitia (Ross et al. 2004).

The tunica media, which constitutes a significant portion of the aortic wall's thickness, possesses a complex and interconnected matrix structure. It contains elastic lamellae, which are fenestrated sheets of elastic fibers organized into multiple concentric cylinders. The spaces between the lamellae, known as interlamellar spaces, are occupied by VSMCs. These cells are

surrounded by other components of the extracellular matrix (ECM) such as collagen I and III fibers, a variety of proteoglycans, signaling factors, and fibronectin (O'Connell et al. 2008; Dingemans et al. 2000)

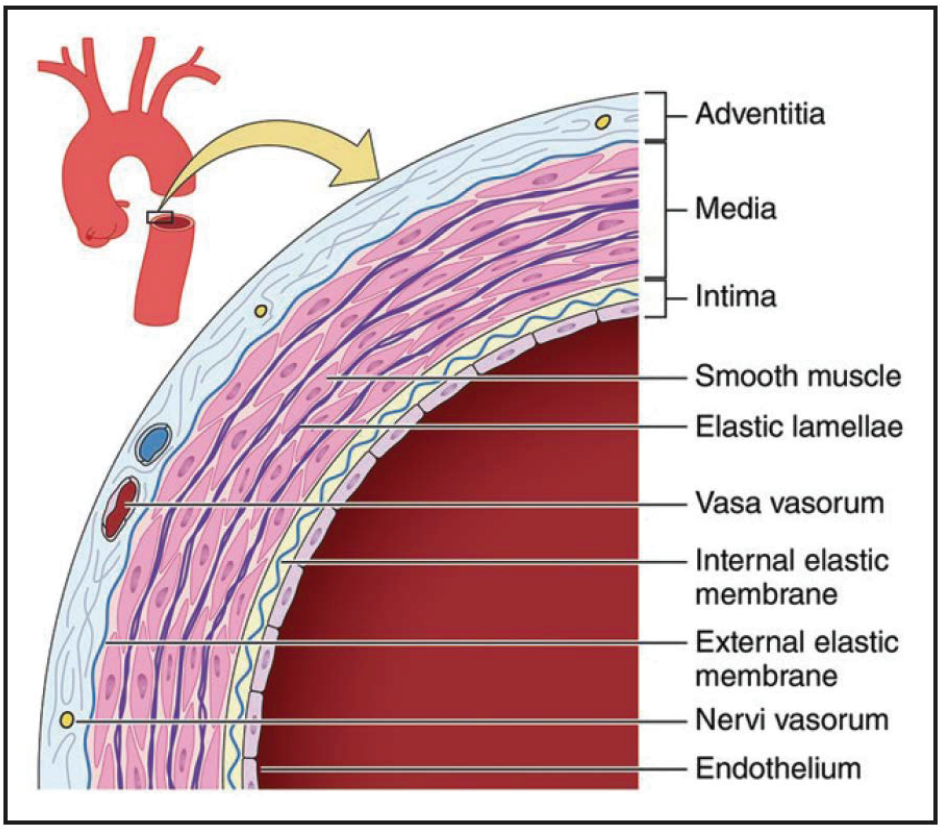

Figure 2. Diagram depicting the histological components of the aortic wall. Image from Isselbacher EM et al. 2022.

1.1.3. Aortic protein composition

1.1.3.1. Elastic lamellae

Elastic lamella is made of a rubber-like material and largely contribute to the expansion of the aortic wall during normal systolic pressure (Boron et al. 2005). When the aorta is in diastole pressure or not pressurized at all, the lamellae appear wavy (Wolinsky et al. 1964).

In cross-section, traditional histological preparations of the aortic wall reveal elastic lamellae arranged in almost evenly spaced parallel layers. The number of lamellae varies depending on the species and vessel size. For example, adult mice aortas have an average of 7 to 8 lamellae, while humans have 40 to 70 lamellae. Although the lamellae appear as parallel layers, they branch out regularly, resulting in varying numbers of lamellae in different anatomical positions within the same section of the aorta (Wolinsky et al. 1967).

Furthermore, the tunica media contains numerous direct connections between adjacent lamellae, creating a dense network of elastic fibers within the interlamellar spaces. This network forms cage-like structures that separate neighboring VSMCs and often establish connections with them (O'Connell et al. 2008).

1.1.3.2. Microfibrils

The microfibrils involved in the assembly of elastin consist of polymers of ensembled fibrilin-1 (Fbn1) moieties with an average diameter of approximately 10-15 nm (Karimi et al. 2016). These microfibrils are stabilized by crosslinks catalyzed by the protein-glutamine γ-glutamyltransferase 2 (formerly known as tissue transglutaminase) (Kielty et al. 2007). The formation of microfibrils serves as a scaffold or template for the subsequent deposition of tropoelastin monomers in a manner that allows for the crosslinking of lysine residues by lysyl oxidases (LOX) (Wagenseil et al. 2009).

In addition to their structural role, microfibrils also play a regulatory role in various morphogenetic and tissue homeostatic processes. They directly interact with cells through cell-matrix interactions and indirectly modulate the activity of growth factors such as the transforming growth factor beta (TGF-β) and the bone morphogenetic protein (BMP). Signaling pathways induced by these growth factors are crucial for cell survival, differentiation, tissue morphogenesis, homeostasis, and responses to injury. Therefore, the integrity of microfibrils is vital for the overall maintenance of tissues (Wagenseil et al. 2009; Kielty et al. 2007).

In the human genome, there are three types of fibrillins (fibillins 1, 2, and 3), with FBN1 being the most abundant in the mature aorta. Fibrillins interact with various molecules, including integrins, elastin, heparin sulfate, proteoglycans, TGF-β binding proteins, and some BMPs (Jondeau et al. 2011). Fibrillin-1 plays a crucial role in sequestering and regulating the activity of growth factors, particularly TGF-β, which is essential for tissue homeostasis. Disruption of these interactions and deregulation of TGF-β activity have been implicated in a variety of diseases (El-Hamamsy et al. 2009).

1.1.4. Aortopathies

The structural integrity of the aortic wall is crucial for its function in facilitating blood flow. Maintaining the proper structure is essential for effective vessel function (El-Hamamsy et al. 2009; Tsamis et al. 2013). However, in certain vascular diseases, the aortic structure undergoes significant alterations, compromising its vital role in blood circulation. Aortic diseases encompass a range of conditions, including atherosclerotic stenosis, ulcers, calcification, thromboembolic disease, aneurysms, pseudoaneurysms, intramural hematoma, aortic tumors, and dissections. Similar to other arterial diseases, the development of aortic diseases can be asymptomatic over an extended period or present acutely (Erbel et al. 2014).

An aneurysm is characterized as the abnormal enlargement of an artery, typically reaching a size that is at least 1.5 times larger than its normal dimensions. In the case of the abdominal aorta, a commonly accepted threshold for defining it as an aneurysm is a diameter of more than 3 cm (Calero et al. 2016).

1.1.4.1. Etiology of aortic aneurysms

The etiology of aortic aneurysms is primarily attributed to the degeneration of the aortic wall caused by atherosclerosis, particularly in the abdominal region (Lavall et al. 2012; Cozijnsen et al. 2011). Several risk factors, including age, male gender, cigarette smoking, atherosclerotic cardiovascular disease, and hypertension, are associated with the development of aneurysms. Genetic connective tissue disorders such as Marfan syndrome, Loeys-Dietz syndrome, and vascular Ehlers-Danlos syndrome, as well as congenital anomalies of the aortic valve (e.g., bicuspid aortic valve), familial genetic variants affecting proteins like aortic smooth muscle actin, myosin-11, Fibrillin-1, SMAD3, TGF-β and TGF-β receptor type-2, inflammatory diseases (syphilitic, Takayasu and giant cell aortitis), and trauma, are also recognized causes of aortic aneurysms (Lavall et al. 2012; Cozijnsen et al. 2011). It is important to note that genetically triggered aneurysms exhibit distinct characteristics compared to atherosclerotic aneurysms (Mann et al. 2015). Many individuals with connective tissue disorders also have a bicuspid aortic valve, which further increases the risk of aortic rupture and mortality. Additionally, patients with an aortic aneurysm face an elevated risk of cardiovascular events, often unrelated to the aneurysm itself, but likely influenced by factors such as inflammation, smoking, or hypertension (Erbel et al. 2015).

1.1.4.2. Prognosis of aortic aneurysms

Aneurysms are characterized by their silent nature, often presenting no symptoms until an acute event occurs, such as aortic wall dissection or rupture, which can have lethal consequences. Dissection refers to the separation of layers in the aortic wall due to bleeding within the wall, often resulting in the formation of a false lumen. On the other hand, aortic rupture involves the complete breach of the vessel wall, leading to bleeding into the surrounding tissues and potentially fatal exsanguination. Unfortunately, only a minority of patients, ranging from 30% to 59%, survive sudden aneurysm rupture and manage to reach the hospital in time for treatment. Moreover, an additional 27% to 40% of patients who do reach the hospital succumb to the condition. The likelihood of aortic dissection occurring is closely related to the size of the aneurysm, with a higher probability as the aneurysm expands. In the ascending aorta, once the diameter exceeds 60 mm, there is a significant increase in the risk of acute complications. Therefore, early clinical diagnosis, along with regular monitoring and appropriate treatment, is crucial to prevent premature death resulting from aneurysm rupture (Chau et al. 2013; Tellides et al. 2017; Tremblay et al. 2011).

1.1.4.3. Diagnosis of aortic aneurysms

The natural progression of aneurysms involves the gradual enlargement of the aorta over several years, eventually leading to rupture (Mann et al. 2015). During the initial stages of growth, the aneurysm remains asymptomatic, and its detection often occurs incidentally through abdominal, or chest radiography conducted for other medical purposes. Once identified, ultrasound echography, such as echocardiography, is the primary imaging technique used for monitoring aortic aneurysms in clinical practice (Lavall et al. 2012; Cozijnsen et al. 2011). This method is preferred due to its ability to measure the size of the aorta, detect wall abnormalities, widespread availability, non-invasiveness, absence of risks, and low cost. However, since ultrasound measurements of vessel diameter may not always be accurate, experts recommend the use of computed tomography (CT) or magnetic resonance imaging (MRI) for follow-up and surgical planning in larger aneurysms. These imaging modalities provide comprehensive 3D visualization of the entire aorta, allowing for proper identification of affected areas. CT is favored for its shorter image acquisition and processing time and wide availability. On the other hand, MRI, although contraindicated for patients with metal implants, does not involve harmful ionizing radiation like CT and is therefore highly suitable for serial follow-up

studies in individuals with known aortic conditions. Additionally, MRI enables visualization and measurement of blood flow, facilitating the assessment of pulse wave velocities and wall shear stress (Chau et al. 2013; Tremblay et al. 2011).

1.1.4.4. Aortic dissections

Aortic dissection is the prevailing form of acute aortic syndrome. It arises when there is a tear in the inner layer of the aorta, allowing blood to pass through the tear and enter the middle layer known as the aortic media. This tear causes a longitudinal splitting of the intima, forming a dissection flap that separates the true lumen from a newly formed false lumen (Figure 3). The dissection flap can progress either in an antegrade or retrograde direction, leading to a range of life-threatening complications, such as acute aortic regurgitation, myocardial ischemia, cardiac tamponade, acute stroke, or malperfusion syndromes (Isselbacher et al. 2022; Chau et al 2013).

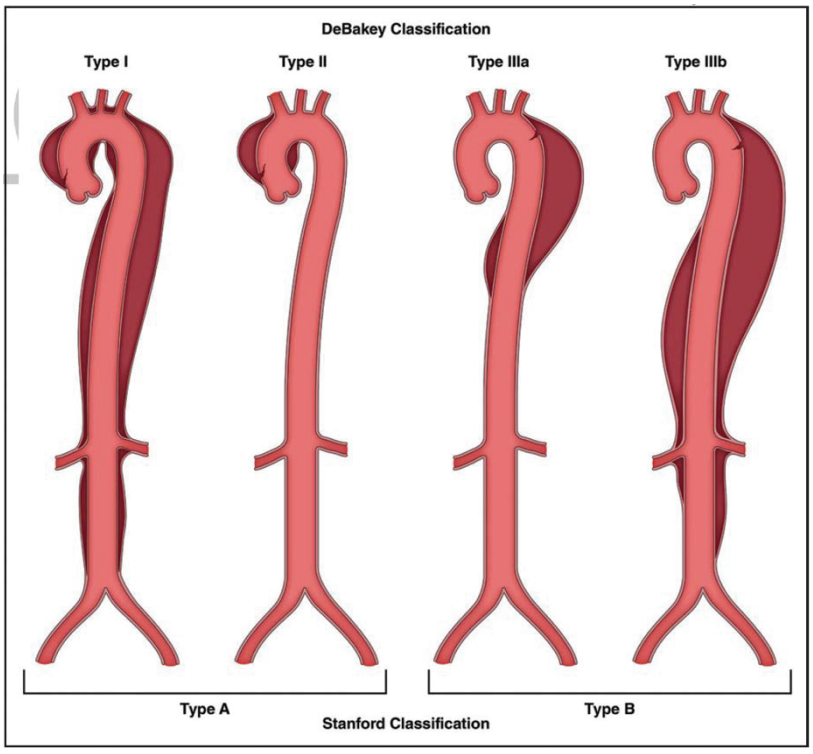

Figure 3. Classification of acute aortic dissection. The DeBakey and Stanford classification systems are widely used to classify aortic dissections. The DeBakey system provides more detailed anatomical information, while the Stanford system is simpler and primarily differentiates dissections involving the ascending thoracic aorta from those that do not. Image from Isselbacher EM et al. 2022.

The blood flowing within the false lumen has the potential to rupture back through the intima into the true lumen, creating a reentry tear. Alternatively, if the blood in the false lumen tears

through the outer media and adventitia, it results in aortic rupture. The incidence of aortic dissection is estimated to be between 5 and 30 cases per million people per year, with a higher prevalence in men. Most dissections occur in individuals aged 50 to 70 years, although patients with Marfan syndrome (MFS), bicuspid aortic valve, Loeys-Dietz syndrome, and vascular Ehlers-Danlos syndrome usually present at younger ages.

If left untreated, acute aortic dissection of the ascending aorta can be extremely fatal, especially in symptomatic patients. The mortality rate rises rapidly, reaching 1% to 2% per hour after the onset of symptoms. Patients who experience complications such as cardiac tamponade (with or without cardiogenic shock), acute myocardial ischemia or infarction, stroke, or organ malperfusion are at an even higher risk of mortality. Among patients with uncomplicated acute type B aortic dissection, the 30-day mortality rate is 10%. However, when complications such as malperfusion or rupture arise in patients with acute type B aortic dissection, the mortality rate increases to 20% by day 2 and further to 25% by day 30 (Isselbacher et al. 2022; Chau et al 2013).

1.2. Marfan syndrome

Marfan Syndrome is an autosomal dominant multisystemic connective tissue disorder, affecting approximately 1.5 to 17.2 individuals per 100,000 live births. The disease primarily manifests through skeletal, ocular, and cardiovascular symptoms. The underlying cause of MFS is a mutation in the gene responsible for encoding fibrillin 1, *FBN1* in humans and *Fbn1* in mouse.

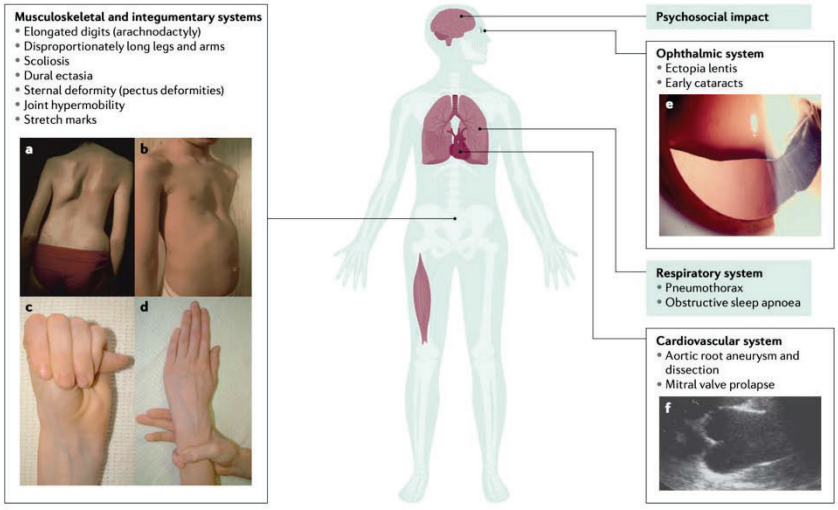

Figure 4. Clinical manifestations of Marfan syndrome. Image obtained from Milewicz et al. 2022

Fibrillin 1 is a structural glycoprotein forming the microfibrils, which along with elastin, constitute the elastic fibers of the connective tissues. To date, nearly 3.000 different *FBN1* mutations with varying and little-known functional effects have been identified (Dietz et al 1991, Sakai et al 2016, Milewicz et al. 2005; Milewicz et al. 2022)).

1.2.1. *FBN1*

MFS is the result of various mutations that can occur in the *FBN1* gene located to chromosome 15q21.1. This gene is quite large, consisting of 11,756 base pairs, and it encodes a 350 kDa heavy ECM glycoprotein called fibrillin 1 (Dietz et al. 1991). Fibrillin-1 is the basic component of microfibrils, which are structural elements measuring 10-20 nm and found throughout the body in both elastic and non-elastic connective tissues (Sakai et al 2016, Robinson et al 2002). These microfibrils interact with different ECM components such as elastin and collagen, thereby contributing to the formation of elastic fibers. The arrangement of elastic fibers varies depending on the tissue, ranging from parallel bundles as seen in the aorta to isolated fibers as occurring in the skin and the lung (Ramirez et al. 2007).

FBN1 consists primarily of 47 epidermal growth factor (EGF)-like domains, interspersed with seven characteristic domains of each eight cysteines (TB/8-Cys). The EGF-like domains contain six highly conserved cysteine residues that form intramodule disulphide bonds and induce β-sheet formation of the protein. In addition, 43 of the 47 EGF-like domains contain calcium binding consensus sequences (Ramirez et al. 2007; Reinhard et al. 1997).

1.2.2. Cardiovascular manifestations of Marfan syndrome and other systems manifestations

Cardiovascular problems are the most serious side effects of MFS. Around 77% of patients with MFS manifest progressive aortic root enlargement and ascending aortic aneurysms that often ends with the dissection and subsequent the fatal rupture of the aorta (Milewicz et al. 2005; Karnebeek et al. 2001). The only treatments for aortic problems are β-adrenergic receptor blockers, and preventive or emergency surgical repair. Even though aortic surgical repair has considerably extended the life expectancy of MFS patients, many still need additional procedures, frequently at locations other than the aorta's initial site of dilatation or rupture. Other cardiovascular issues include aortic insufficiency, mitral valve regurgitation, and the most

common valvular anomaly, mitral valve prolapse (Figure 4) (Karnebeek et al. 2001; Faivre et al. 2007).

The most apparent phenotype of MFS patients is at musculoskeletal level *Pectus excavatum* and *pectus carinatum* as well usually accompanied by abnormally high stature, dolichostenomelia (exceptionally long limbs), and arachnodactyly (abnormally long fingers and toes) are the characteristics that are most frequently associated with the condition (Scherer et al. 1988; Loeys et al. 2010). Spine abnormalities such scoliosis (an improper lateral curvature of the spine) and kyphosis (an unnatural curve of the upper back), whose growth is linked to increasing pain in the spine area (ref), are another characteristic of MFS (Sponseller et al. 1995). Additionally, Marfan individuals experience failure to rebuild skeletal muscle following damage or assault as well as muscular myopathies (Cohn et al. 2007).

About 50% of Marfan patients experience ectopia lentis, which is the dislocation of the eye lens and can affect one or both eyes simultaneously (ref). The stretching of the tunica scleralis, which results in zonular fiber rupture and lens displacement, is the cause of ocular diseases in MFS (Maumenee et al. 1981). Additionally, spontaneous pneumothorax—the uncoupling of the lung from the chest wall by the accumulation of air in the pleural space—has been documented in MFS patients (Karpman et al. 2011). Shortness of breath, chest pain, oxygen deprivation, and an accelerated heart rate can all be symptoms of spontaneous pneumothorax. Even while a modest spontaneous pneumothorax typically only has to be monitored, MFS patients have been known to have recurring and even contralateral pneumothorax that require surgery (Viveiro et al. 2013; Mo et al. 2014; Kohler et al. 2013). Another common symptom in MFS patients are obstructive and central sleep apneas (Rybczynski et al. 2010).

1.2.3. The aortic aneurysm in Marfan syndrome

Aside from their structural function in the ECM, microfibrils also serve as reservoirs for certain signaling molecules. Specifically, TGF-β is bound and rendered inactive by latent TGF-β binding proteins (LTBPs) attached to microfibrils. In the context of MFS, where there is insufficient or dysfunctional fibrillin 1, abnormal assembly of the lamellae occurs, leading to impaired mechano-transduction in VSMCs and an elevated level of bioactive TGF-β (Cañadas et al. 2010).

The presence of reduced or mutated fibrillin-1 results in the formation of weakened lamellae that prematurely deteriorate under the normal blood pressure forces, thereby providing inadequate mechanical cues to VSMCs. Furthermore, VSMCs in the MFS aorta experience heightened signaling due to the pathological overactivation of TGF-β, which triggers excessive phosphorylation of SMAD and MAPK (formerly ERK) proteins through TGF-β receptors (TGFRs). These signals prompt the excessive release of matrix metalloproteinases (MMPs), leading to inappropriate tissue remodeling and further weakening of the aortic wall and finally promoting the aortic aneurysm formation (Figure 5) (Wilson et al. 2016; De Backer et al. 2015).

This explanatory model of pathogenesis provides valuable insights into the progression of MFS-related aneurysms and serves as a prototype for understanding thoracic aortic aneurysms and dissections (TAAD) caused by other factors. However, there are still gaps in our understanding of this model that require further investigation. One notable aspect is the role of TGF-β in aneurysm progression. In MFS patients, elevated levels of circulating TGF-β have been found to correlate positively with the diameter of the aortic root, suggesting its potential as a biomarker for aortic risk (Jondeau et al. 2011; De Backer et al. 2015).

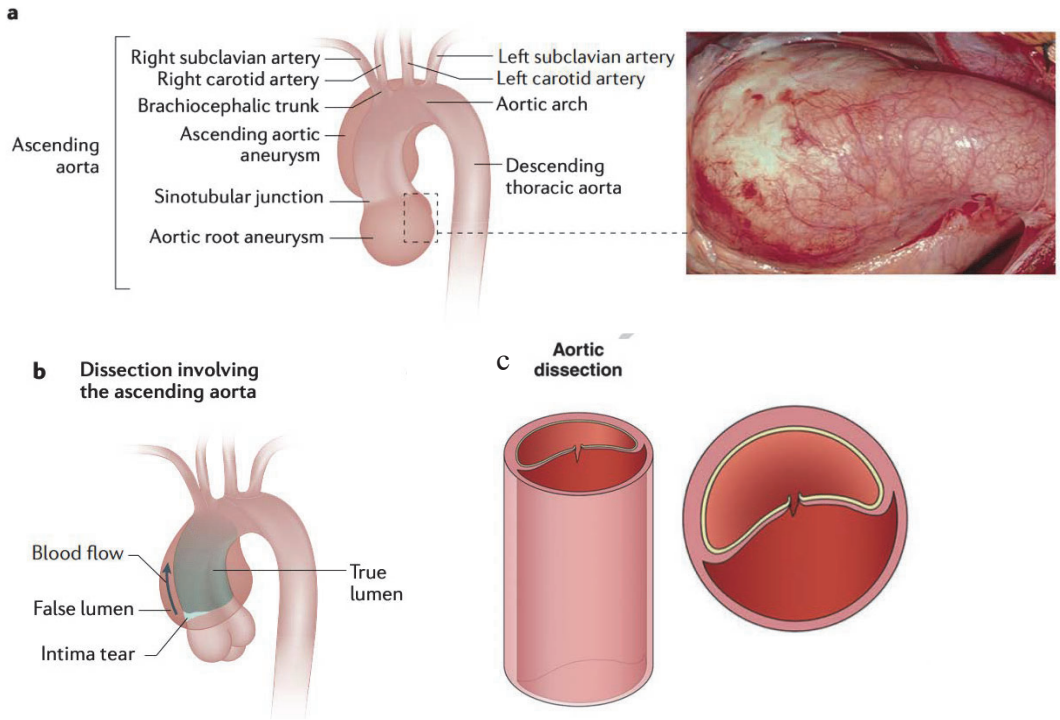

Figure 5. Aortic root aneurysm and ascending aortic dissection in MFS patient. (a) On the left, schematic aortic root aneurysm, on the right, photo of an aortic root aneurysm. (b) Schematic aortic root dissection. MFS patients present type A aortic dissections. (c) Schematic transversal aortic root dissection. Images taken and modified from Milewicz et al. 2021 and modified from Isselbacher; et al 2022, respectively)

1.3. TGF-ß signaling is regulated by fibrillin-1

TGF-β is essential for various developmental processes and maintaining a balanced relationship between cells and the ECM to ensure tissue homeostasis. Dysregulation of TGF-β has been implicated in a wide range of diseases, including fibrosis, cancer, autoimmune disorders, and vascular diseases. Fibrillin-1 is a vital component of the ECM contributing to the temporal and spatial regulation of the versatile TGF-ß (Neptune et al. 2003; Chaudhry et al. 2007).
Fibrillin-1, in addition to its structural role, also plays a significant physiological role in the regulation of TGF-β activation. TGF-β is initially secreted as a large latent complex (LLC), which is covalently attached to LTBP (Dijke et al. 2007; Isogai et al. 2003). The interaction between LTBP and Fibrillin-1 is facilitated by their shared 8-Cys module, which is a unique feature of both proteins (Gordon et al. 2008).

1.3.1. TGF-ß release in the ECM

To initiate signaling, TGF-β needs to bind to its receptor (see below). This requires the release of the LLC, which contains the mature form of TGF-β from both Fibrillin-1 microfibrils and the ECM. The displacement of LLC from Fibrillin-1 can be triggered by the displacement of LTBP. Elastase, a proteolytic enzyme, degrades the microfibrils, leading to the release of fragments of Fibrillin-1. These fragments compete with LTBP for binding at their own N-terminal, displacing LTBP in the process (Dijke et al. 2007; Chaudry et al. 2007;).

In addition, proteases such as plasmin and thrombin cleave the hinge region of LTBP, which allows for the release of LLC from the ECM. The LTBP N-terminal fragment remains bound to the ECM while the LLC is freed. Recent research has also highlighted the role of BMPs in LLC release. BMPs cleave the LTBP hinge region at specific sites, resulting in the release of a free LLC complex (Annes et al. 2003).

Overall, the release of LLC from microfibrils and the ECM involves a complex interplay of proteolytic enzymes, LTBP displacement, and cleavage events mediated by elastase, plasmin, thrombin, and BMPs. These processes are crucial for activating TGF-β signaling and facilitating its role in various physiological and pathological processes (Ge et al. 2006).

1.3.2. TGF-ß activation

To activate TGF-β, the mature active cytokine needs to be cleaved from the latency-associated peptide (LAP) complex, allowing for receptor binding and signaling. This activation process can occur through integrin-independent mechanisms after the release of the LLC from the ECM, or it can be integrin-associated at different stages of extracellular release. However, in all cases, the LAP complex is the direct target (Dijke et al. 2007; Annes et al. 2003).

One well-accepted integrin-independent mechanism involves the cleavage of LAP by matrix MMPs, which releases the active mature form of TGF-β. MMPs have diverse functions and are involved in wound healing responses, ECM degradation, and remodeling. ECM degradation may contribute to the lack of TGF-β targeting to the ECM and the increased activation of TGF-β. In turn, TGF-β has been shown to transcriptionally control the activation of MMPs, creating a positive feedback loop between TGF-β and MMPs (Yu et al. 2000; Lu et al. 2011; Krstic et al. 2014).

Changes in pH can also activate TGF-β independently of integrins. Acidic environments can lead to the disintegration of LAP, releasing active TGF-β. Reactive oxygen species (ROS) are another mechanism for TGF-β activation. ROS mostly produced by NADPH oxidases and mitochondria, can alter the conformation of LAP and expose active TGF-β. Conversely, TGF-β signaling promotes the production of ROS by activating NADPH oxidase, interfering with mitochondrial function, and suppressing antioxidant enzymes. This creates a vicious cycle of global redox imbalance that favors TGF-β-induced tissue fibrosis under non-homeostatic conditions. This ROS point will be explained in next points (Lyons et al. 1988; Liu et al. 2015; Barcellos-Hoff et al. 1996).

1.3.3. TGF-ß receptors

TGF-β mediates its signaling effects through a receptor complex composed of two types of receptors from the serine/threonine kinase family. This receptor complex family consists of 12 members, including 7 type I receptors and 5 type II receptors, all dedicated to signaling by the TGF-β superfamily. The transmembrane receptors of the TGF-β superfamily have a structural organization of approximately 500 amino acids, which includes a cysteine-rich extracellular

ligand binding domain at the N-terminal, a transmembrane domain, and a serine/threonine kinase domain at the C-terminal (Manning et al. 2002; Shi et al. 2003).

TGF-β, including its isoforms (TGF-β1, TGF-β2, and TGF-β3), signals through a heterocomplex formed by the TGF-β type II receptor (TBRII) and either of the TGF-β type I receptors (TBRI). The TBRI type can be ALK5, which induces the classical canonical SMAD2-dependent signaling, or ALK1, which induces SMAD1/5 phosphorylation. Other members of the TGF-β superfamily signal through different combinations of specialized type I and type II receptors. The TBRI has a distinctive sequence called the GS domain, which is located N-terminal to the intracellular kinase domain. Successful activation of TBRI involves transphosphorylation of its GS domain by TBRII upon ligand binding (Shi et al. 2003; Di Guglielmo et al. 2003).

An additional type of auxiliary TGF-β receptor, TBRIII (including endoglin and betaglycan), mainly assist the low-affinity TGF-β2 isoform in binding TBRII but also in a lesser extent to TGF-ß1.
TGF-β does not directly interact with TBRI alone but has a high affinity for TBRII and binds to its ectodomain. Recruitment of TBRI allows for the assembly of the receptor complex and subsequent phosphorylation. However, the heterocomplex formation involves not only one TGF-β ligand but a ligand dimer and four receptor molecules. Each receptor binds one ligand at a time, and TBRI and TBRII bind adjacent positions on the ligand surface. The reason for TGF-β changing its affinity for TBRI once it is bound to TBRII is not yet clear, but a hypothetical model suggests a conformational change in TGF-β that exposes a binding site for TBRI once it is bound to TBRII (Sankar et al. 1995).

Regardless of the specific mechanism, the binding of the ligand dimer to TBRII and the inclusion of TBRI in the complex bring the receptors close enough to enable transphosphorylation of TBRI by TBRII. While TBRI requires phosphorylation, TBRII kinase is thought to be constitutively active, although the regulatory process is not well understood. The GS region of TBRI not only serves as a critical phosphorylation site but also functions to prevent phosphorylation and activation of the receptor complex. Proteins such as 12 kDa FK506-Binding Protein (FKBP12) can bind to the unphosphorylated GS region and inhibit the phosphorylation of TBRI by TBRII, thereby regulating TGF-β signaling at the receptor level (Hart et al. 2002; Huse et al. 1999).

1.3.4. TGF-ß in Marfan syndrome

Under normal physiological conditions, TGF-β remains inactive due to controlled binding of LTBP to Fibrillin-1. However, in MFS, the fragmentation of microfibrils caused by insufficient or dysfunctional Fibrillin-1 disrupts the binding capacity of LTBP, resulting in increased levels of active TGF-β in the ECM (Figure 6). This dysregulation of TGF-β has emerged as a significant molecular factor in the progression of aneurysms, a common manifestation of MFS. Studies using animal models of MFS have demonstrated that inhibiting TGF-β activity using TGF-β neutralizing antibodies or inhibiting its expression via cross-activating pathways can reduce the formation of aneurysms. Additionally, in MFS patients, higher circulating levels of TGF-β have been found to positively correlate with the diameter of the aortic root, suggesting its potential as a biomarker for aortic risk assessment (Holm et al. 2011; Lavoie et al. 2005).

The increased presence of TGF-β in the environment surrounding VSMCs in the aorta has direct implications for cellular function, including impaired tissue repair, attenuated immune responses, and limited angiogenesis. This highlights that the dysregulation of TGF-β extends beyond structural deficiencies and contributes to various cellular changes associated with MFS-related complications. These insights into the dysregulation of TGF-β in MFS challenge the simple notion that structural abnormalities caused by Fibrillin-1 are the only ones responsible for aneurysm formation. Instead, they present an opportunity for targeted therapeutic approaches aimed at modulating TGF-β signaling to mitigate the progression of aneurysms in MFS patients (Habashi et al. 2011; Cook et al. 2015).

1.3.5. TGF-ß inhibitory peptides

In the last decade, several anti-TGF-ß peptides have been developed to avoid the excessive TGF-ß bioavailability (Llopiz et al. 2009). Among these peptides, P144 is a hydrophobic peptide derived from the membrane-proximal ligand-binding domain of β-glycan (Murillo et al. 2015). It is designed to hinder the interaction between TGF ligands and their receptors by blocking the extracellular domains of TGFRs III (Ezquerro et al. 2003). Another soluble peptide, P17 (KRIWFIPRSSWYERA), was generated from a phage library (Dotor et al. 2007) and exhibits relative affinity binding to TGF-β1, TGFβ2, and TGFβ3 of 100%, 80%, and 30%, respectively (Santiago et al. 2005). The inhibitory effects of both peptides have been demonstrated in in vivo

and in vitro models of fibrosis and scleroderma, showing their potential therapeutic value in blocking the TGFβ pathway and preventing collagen fiber accumulation (Llopiz et al. 2018).

P144 is a hydrophobic peptide derived from the extracellular region of the human TGFR type III . Studies have demonstrated that P144 can enhance the effectiveness of antitumor immunotherapy in thymoma and melanoma cell lines. Furthermore, P144 has been suggested to have immunomodulatory properties in the cellular response to tumors, stimulating the production of cytokines in melanoma that redirect the cellular response against tumors (Gallo-Oller et al. 2016) .

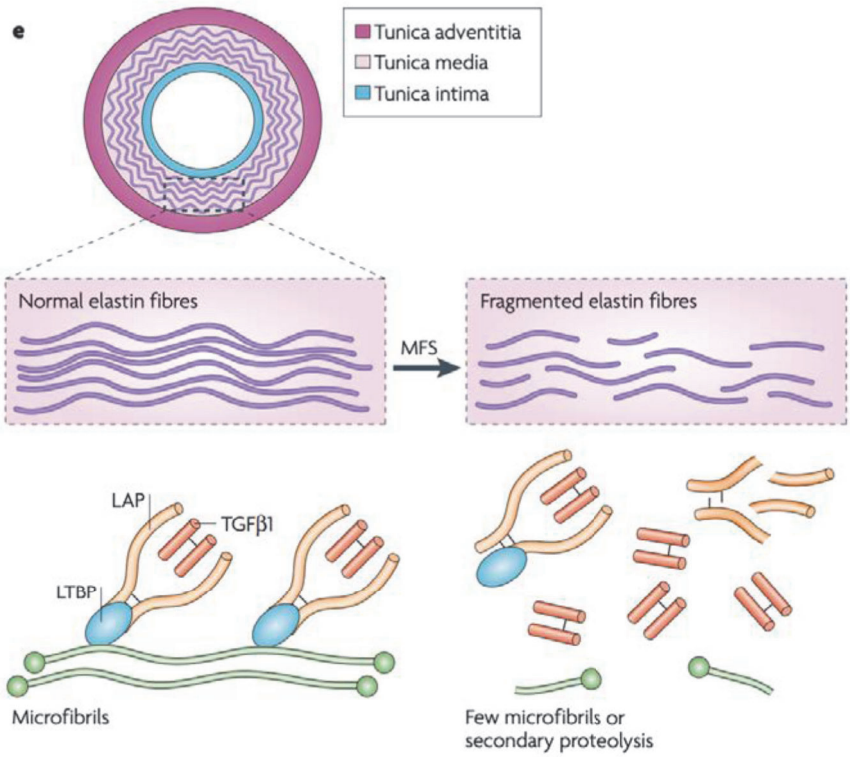

Figure 6. TGF-ß in MFS. In MFS, fragmented elastin fibers can be observed in the aorta, which are associated with the release of the large latent TGFβ complex and active TGFβ1. Modified from Dijke et al. 2007.

1.4. Oxidative eustress and distress

Oxidative (di)stress refers to an imbalance between the production of reactive oxygen species (ROS) and the body's antioxidant defenses, which can result in tissue damage. ROS are produced extensively as a natural byproduct of various biochemical processes and can also be intentionally generated, for example, by activated neutrophils (Sies et al. 2017).

When there is low exposure to oxidants, specific targets can be addressed for redox signaling, which is referred to as oxidative eustress. However, high exposure to oxidants can disrupt redox signaling and cause damage to biomolecules, leading to oxidative distress (Figure 7). Adaptive stress responses are activated to modulate and counteract these effects. The outcome of this interplay between oxidative stress and adaptive responses contributes to both health and disease processes (Sies et al. 2017; Sies et al 2020; Sies et al 2023).

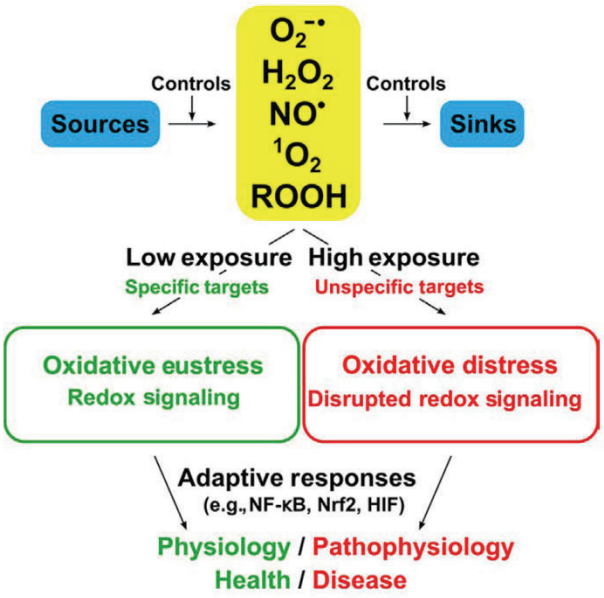

Figure 7. Schema representing the influence of low and high exposure to ROS generating oxidative eustress and oxidative distress. Image taken from: Sies et al. 2020.

1.4.1. Reactive oxygen species

ROS are small molecules formed by the partial reduction of molecular oxygen (O_2), and they play important roles in vital biological processes such as cellular respiration and aerobic metabolism. However, O_2 is a double-edged sword because reactive oxygen intermediates can easily convert into toxic compounds that cause cell damage by oxidizing proteins, lipids, carbohydrates, and nucleic acids. The primary ROS products formed during the partial reduction of O_2 include superoxide radical (O_2^-), and hydrogen peroxide (H_2O_2), which further react to produce hydroxyl radical (OH^-). O_2^- is a negatively charged species with an unpaired electron

and cannot diffuse across biological membranes. It can rapidly react with Fe-S clusters to generate H_2O_2, with Fe^{2+} to form OH• through the Fenton reaction, or with superoxide dismutase (SOD) to dismutate into H_2O_2 and O_2. O_2^- can be formed by the catalytic activity of peroxidases, such as myeloperoxidase. Importantly, the reaction between O_2^- and nitric oxide (NO) produces the highly reactive and harmful peroxynitrite ($ONOO^-$), which can be either a nitrogen- or oxygen-centered radical species. Unlike O_2^-, H_2O_2 is not a free radical and is much more stable. It can cross membranes through aquaporins and is produced constitutively in mitochondria, the ER membrane, and by NADPH oxidase NOX4. H_2O_2 can be formed through the spontaneous or enzymatic dismutation of O_2^- by SOD (Sies et al. 2020; Egea et al. 2020).

1.4.2. ROS sources

Endogenous ROS and free radicals are primarily produced in environments with high oxygen consumption, such as intracellular organelles like mitochondria, endoplasmic reticulum (ER), peroxisomes, and the plasma membrane (Egea et al 2020). In mammals, the main enzymatic sources of ROS are (Figure 8):

- Mitochondrial respiratory chain: During oxidative phosphorylation in mitochondria, O_2 is reduced to H_2O along the electron transport chain. This process generates O_2•−, with complexes I and III in the internal membrane of mitochondria being the major sites of O_2•− production (Brand et al. 2010)
- Cytochrome P450: The catalytic cycle of cytochrome P450, involved in metabolizing organic substrates, utilizes O_2 and produces O_2•− and H2O2 as by-products (Yasui et al. 2005).
- Flavoenzyme Ero1 and ER protein-folding processes: The ER, through protein-folding processes and the activity of flavoenzyme Ero1, generates ROS, particularly H_2O_2, as a by-product of disulfide bond formation for oxidative protein folding. Increased oxidative stress in the ER can stimulate mitochondrial ROS production through Ca^{2+} leakage (Araki et al. 2012).
- NADPH oxidases (NOX): NOX enzymes, mainly present in vascular tissue but also found in nonvascular tissues, catalyze the reduction of O2 in the presence of NADPH to generate O2•− and other ROS. Mammals have seven isoforms (NOX1–5, DUOX1, and DUOX2), with different levels of action and activation mechanisms (Lassègue et al. 2012).

- Xanthine oxidase (XO): XO is an enzyme involved in purine nucleotide catabolism. It generates O2•− and H2O2 as it oxidizes hypoxanthine to xanthine and further to uric acid (Lacy et al. 1998)
- Lipoxygenases: Lipoxygenases catalyze the conversion of polyunsaturated fatty acids into leukotrienes and lipoxins, which are involved in cellular signaling pathways. They generate O2•− in the presence of reducing co-substrates (Kukreja et al. 1986).
- Nitric oxide synthases (NOS): NOS enzymes are responsible for synthesizing nitric oxide (NO), an important signaling molecule. However, under certain conditions, NOS can become uncoupled and generate O2•− instead of NO, leading to impaired NO-dependent functions and the formation of toxic $ONOO^-$ (Förstermann et al. 2006).

These enzymatic machineries contribute to the endogenous production of ROS and free radicals within cells and organelles, playing a role in various physiological and pathological processes.

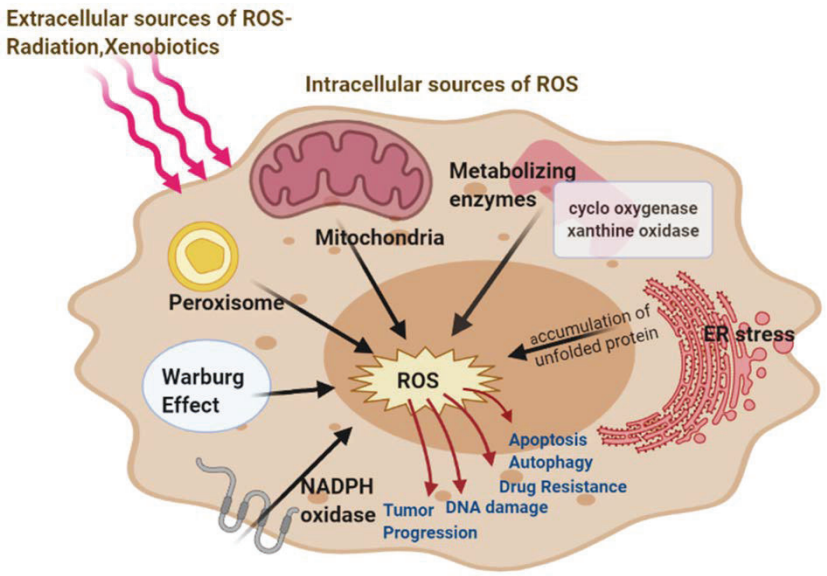

Figure 8. Sources of ROS in the cell. Image taken from Arfin, S.; Jha, N.K.; Jha, S.K.; Kesari, K.K.; Ruokolainen, J.; Roychoudhury, S.; Rathi, B.; Kumar, D. Oxidative Stress in Cancer Cell Metabolism. Antioxidants 2021, 10, 642. https://doi.org/10.3390/antiox10050642

1.4.3. Oxidative distress in cardiovascular diseases (CVD)

Oxidative stress primarily contributes to the initiation of atherosclerosis, a process characterized by early endothelial inflammation that triggers the generation of ROS by recruited macrophages. Subsequently, circulating LDL cholesterol undergoes oxidation by ROS, leading to

the formation of foam cells and the accumulation of lipids. These events ultimately result in the formation of an atherosclerotic plaque. Both in vivo and ex vivo studies have provided substantial evidence supporting the role of oxidative stress in the ischemia, hypertension, cardiomyopathy, cardiac hypertrophy, and congestive heart failure (Akhtar et al. 2010; Martinez-Revelles et al. 2017).

1.4.4. Oxidative distress in MFS

It is well-established that TGF-β signaling indirectly contributes to oxidative stress by promoting ROS production and/or inhibiting antioxidant systems, particularly in conditions such as fibrosis, tumorigenesis, and cerebral ischemia. The involvement of TGF-β-mediated oxidative stress has been demonstrated in MFS, where TGF-β signaling indirectly regulates the expression of NADPH oxidase NOX4 in both MFS patients and mouse models (Jimenez-Altayó et al. 2018; Gordon et al. 2008; Krstic et al. 2015; Lou et al. 2018).

The initial evidence supporting the involvement of oxidative stress in MFS was obtained from a study that investigated endothelial function in MFS mice. The study revealed that the relaxation ability of the aortic segments affected by TAAD in Fbn1C1041G/+ mice was significantly impaired due to the downregulation of endothelial nitric oxide synthase (eNOS)/AKT signaling, which leads to reduced NO production (Chung et al. 2007). However, when MFS aortic tissue was preincubated with various ROS inhibitors, the acetylcholine-induced aortic relaxation improved. Moreover, the expression levels of ROS-producing enzymes, such as XO, NOX, and inducible nitric oxide synthase (iNOS), were found to increase, while SOD levels decreased in MFS aortic tissue (Yang et al. 2010).

In another study, it was discovered that endothelial dysfunction could be prevented in MFS mice lacking the *Nox4* gene, providing the first evidence of the involvement of NADPH oxidases in the progression of MFS aortic aneurysm. Both MFS aortic tissue and SMC derived from MFS patients exhibited overexpression of NOX4. The MFS mouse model lacking Nox4 gene expression exhibited preserved elastic fiber integrity and a significant reduction in aortic aneurysm progression, particularly in 9-month-old mice. Interestingly, this protective effect was not observed in younger mice, suggesting that NOX4 plays a negative role in aneurysm progression during later stages of the disease. Similar protective effects of Nox4 have been

observed in cerebral arteries and the aorta of both MFS mice and patients (Jimenez-Altayó et al. 2019).

Another study in the mitochondria concluded that the extracellular matrix regulates the mitochondrial function of VSMCs and plays a crucial role in the development of aortic aneurysm in MFS (Oller et al. 2021).

Finally, they identified a mutation in the 3'UTR of the FBN1 gene in patients with MFS. This mutation suggests that the involvement of the ER stress response is a molecular mechanism in the formation of aortic aneurysm in these patients (Siegert et al. 2019).

Overall, the impaired vasomotor function in MFS is attributed to an imbalance between ROS-producing proteins, including NOX4, and ROS-scavenging proteins. Additionally, recent studies have implicated inducible iNOS in MFS aneurysm formation. Increased levels of iNOS have been observed in MFS mice and human aortic tissue, and the administration of an iNOS inhibitor quickly normalized aortic size, suggesting a role for iNOS in the pathogenesis of MFS. REFERENCIA?

1.5. Xanthine oxidase

Xanthine oxidoreductase (XOR), which was initially discovered in milk by Schardinger et al. 1902, belongs to the highly conserved molybdoenzyme family (Kisker et al. 1997). XOR exists in two interconvertible forms known as xanthine dehydrogenase (XDH) and xanthine oxidase (XO). XO exclusively reduces oxygen, while XDH can reduce either oxygen or NAD+ but has a higher affinity for the latter (Waud & Rajagopalan et al. 1976). Both forms catalyze the conversion of hypoxanthine to xanthine and xanthine to uric acid (UA), which are the final steps in the purine degradation pathway. XOR is composed of several cofactors, including molybdopterin (Mo-Co), two iron-sulfur centers (Fe2-S2), and flavin adenine dinucleotide (FAD) (Berry et al. 2003).

In cells and in biological fluids XOR exhibits the dehydrogenase and oxidase activity. However, there is an exception observed in activated leukocytes, where XOR demonstrates XO activity. In this case, through univalent and divalent electron transfers to O_2, XOR generates O_2^- and H_2O_2 respectively. These ROS play a functional role in activating endothelial cells and contribute to the cytocidal phase of phagocytosis (Battelli et al. 2014; Polito et al. 2021).

The reversible or irreversible transition from XDH to XO also occurs in various pathological conditions, including hypoxia and reoxygenation, ischemia and reperfusion, viral infections, toxic tissue injury, radiation damage, and organ preservation and transplantation. In such circumstances, XOR-derived ROS can trigger an inflammatory response and exacerbate tissue damage through their cytotoxic effects (Battelli et al. 2014; Battelli et al. 2016).

Furthermore, once XOR is released from hepatocytes and enters the bloodstream and undergoes its conversion from its dehydrogenase form to the oxidase form, the oxidase form of XOR has a strong affinity for the glycosaminoglycans present on the surface of endothelial cells. This bound XOR plays a crucial role as a systemic regulator of redox balance and influences various important functions of endothelial cells (Figure 9) (Fernandez et al. 2018; Bortolotti et al. 2021).

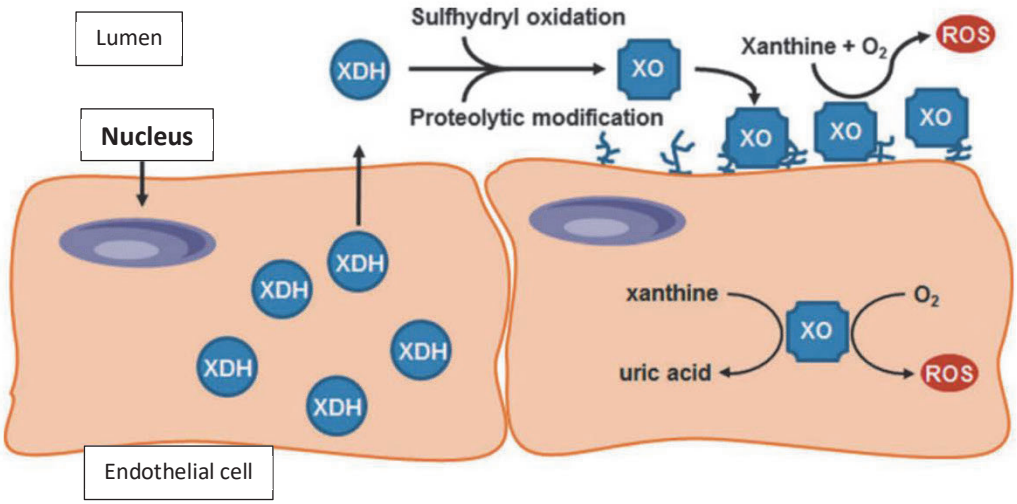

Figure 9. XOR mechanism of action in the endothelial cells in vasculature. Modified from Fernandez et al. 2018.

In terms of its roles in the inflammatory reaction, XOR associated with the endothelium generates ROS and nitrogen species (RNS). These oxidants activate endothelial cells, leading to increased permeability and the formation of inflammatory exudate. Additionally, XOR-derived oxidants induce the expression of adhesion molecules on the inner surface of the microcirculation, promoting the activation of leukocytes, their migration across the endothelium, and their movement towards the inflammatory stimulus. Furthermore, activated phagocytes release cytokines, which further enhance XOR expression and contribute to the

production of oxidant products that can be destructive to cells (Battelli et al. 2018; Bortolotti et al. 2021).

1.5.1. Xanthine oxidase and CVD

The activity of XOR and its products has a significant impact on the redox balance and is associated with various effects on the vascular endothelium and vessel walls, which hold great relevance for the cardiovascular system. XOR-derived ROS and oxidative stress can lead to endothelial dysfunction, contributing to the development and progression of atherosclerosis (Figure 10). Furthermore, the postulated intracellular pro-oxidant effect of uric acid in the vascular system can stimulate the proliferation of smooth muscle cells, activate the renin-angiotensin system, and inhibit the synthesis of nitric oxide. These effects can promote hypertension and CVD (Kotozaki et al 2023) .

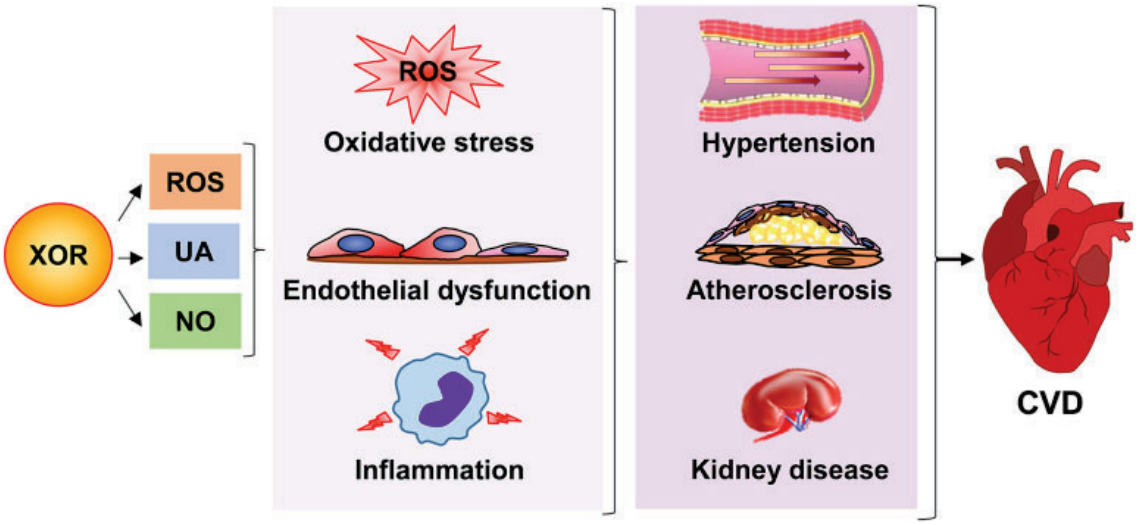

Figure 10. XOR contribution in CVD. XOR is involved in the generation of ROS, UA and NO, all together can contribute in generating CVD. Image taken from Polito et al. 2021.

Other studies have shown that the serum levels of XOR activity is significantly higher in patients with hypertension compared to dialyzed patients with chronic renal disease or control subjects. In heart failure, XOR activity is upregulated due to increased expression induced by inflammatory cytokines, as well as augmented substrate supply resulting from hypoxia, catabolic dominance, insulin resistance, cell death, and cachexia. This leads to increased production of both uric acid and ROS. Although uric acid is an established marker of several pathological heart conditions, therapies targeting urate-lowering other than XOR inhibition fail

to produce the expected beneficial effects if hyperuricemia played a primary pathogenic role in heart failure (Neogi et al. 2012; Miah et al. 2022)

1.5.2. Dual role of uric acid: antioxidant or prooxidant

Uric acid is the final product of the XOR catabolism. In humans and great apes, there can be abnormal accumulation of UA in plasma and certain tissues (Maiuolo et al. 2016). However, in rodents, UA is rapidly catabolized by uricase into allantoin, which is much more soluble in water than UA. In humans, allantoin has been proposed as a biomarker for oxidative stress since it is not produced metabolically. Several epidemiological studies suggest a potential association between elevated serum UA levels and cardiovascular risk factors, although this relationship remains controversial. Thus, UA plays a dual role in redox biopathology (Seet et al. 2010; Kanbay et al. 2013). On one hand, it contributes up to 50% of the total antioxidant capacity in human biological fluids, and higher UA levels have been hypothesized to provide protection against certain CNS diseases induced by peroxynitrite and inflammation. On the other hand, when UA accumulates in the cytoplasm or in an acidic/hydrophobic environment, it can act as a pro-oxidant(Kanbay et al. 2013; Vasalle et al. 2016; Kang et al. 2014).

UA has been detected in the walls of aortic aneurysms and arteries with atherosclerotic plaque in humans, and there is evidence of a positive association between serum UA levels and aortic dilatation and dissection. However, it is important to note that studies on UA formation have revealed that its impact on prognosis and cardiovascular events could not solely be attributed to UA itself, but also to the formation of ROS during XOR activity. The combined effect of elevated UA levels, ROS formation, and increased XOR activity could significantly contribute to endothelial dysfunction and heart failure associated with oxidative stress, potentially including aortopathies (Masi et al. 2019; Cortese et al. 2019; Yu et al. 2020; Lee et al. 2020).

2. RATIONALE AND OBJECTIVES

The main objective of this thesis is to contribute to new knowledge in the cardiovascular pathomechanisms occurring in the Marfan syndrome and based on them to test when possible new treatments that interfere in the formation and/or progression of the aortopathy. To this aim, we use the following experimental working models:

1. Aortic samples from patients with Marfan syndrome that were subjected to reparatory surgery.
2. A MFS mouse model (*Fbn1*$^{C1041G/+}$) which is representative of the type of mutation most frequently occurred in patients. This mouse model recapitulates rather well most of the clinical signs observed in patients obviously including the aortic aneurysm but only occasionally ends in dissection and rupture.

Therefore, to achieve the main aim of this Thesis, we address the following specific objectives:

1. Objective 1: Evaluate the effect of an anti-TGF-ß peptide (P144) in the formation and progression of the aortic aneurysm in Marfan syndrome. Rationale: Since there is a TGF-β hypersignaling associated to the MFS aortopathy, the use of the anti-TGF-β peptide P144, which has been demonstrated to be greatly effective against liver cancer, could also block or mitigate the aortopathy in MFS.

2. Objective 2: Study the contribution of XOR in the progression of aortic aneurysm in Marfan syndrome. Rationale: we previously shown redox stress in aortic samples from MFS patients and mice where a significant part of it was generated by NADPH oxidase NOX4. Nonetheless, we realized that other redox sources should also participate in the process. Together NOXes, XOR is other important source of redox stress in CVD but its contribution to the Marfan aortopathy is almost unknown.

3. Objective 3: Determine the impact of uric acid in the progression of aortic aneurysm in Marfan syndrome. Rationale: The activity of XOR produces ROS (anion superoxide and hydrogen peroxide) whereas the catabolite produced is uric acid. Uric acid is the main physiological antioxidant present in blood plasma. Therefore, with this on mind, we

wanted to know whether uric acid has some impact for itself in the aortopathy in MFS. We hypothesized that it could limit in some extent the progression of the aortopathy.

3. SCIENTIFIC PUBLICATIONS

OBJECTIVE 1: Evaluate the effect of an anti-TGF-ß peptide (P144) on the formation and progression of aortic aneurysm in Marfan syndrome.

Arce C, Rodríguez-Rovira I, De Rycke K, Durán K, Campuzano V, Fabregat I, Jiménez-Altayó F, Berraondo P, Egea G.

Anti-TGFβ (Transforming Growth Factor β) Therapy With Betaglycan-Derived P144 Peptide Gene Delivery Prevents the Formation of Aortic Aneurysm in a Mouse Model of Marfan Syndrome.

Arterioscler Thromb Vasc Biol. 2021 doi: 10.1161/ATVBAHA.121.316496)

Arteriosclerosis, Thrombosis, and Vascular Biology

BASIC SCIENCES

Anti-TGFβ (Transforming Growth Factor β) Therapy With Betaglycan-Derived P144 Peptide Gene Delivery Prevents the Formation of Aortic Aneurysm in a Mouse Model of Marfan Syndrome

Cristina Arce, Isaac Rodríguez-Rovira, Karo De Rycke, Karina Durán, Victoria Campuzano, Isabel Fabregat, Francesc Jiménez-Altayó, Pedro Berraondo, Gustavo Egea

OBJECTIVE: We investigated the effect of a potent TGFβ (transforming growth factor β) inhibitor peptide (P144) from the betaglycan/TGFβ receptor III on aortic aneurysm development in a Marfan syndrome mouse model.

APPROACH AND RESULTS: We used a chimeric gene encoding the P144 peptide linked to apolipoprotein A-I via a flexible linker expressed by a hepatotropic adeno-associated vector. Two experimental approaches were performed: (1) a preventive treatment where the vector was injected before the onset of the aortic aneurysm (aged 4 weeks) and followed-up for 4 and 20 weeks and (2) a palliative treatment where the vector was injected once the aneurysm was formed (8 weeks old) and followed-up for 16 weeks. We evaluated the aortic root diameter by echocardiography, the aortic wall architecture and TGFβ signaling downstream effector expression of pSMAD2 and pERK1/2 by immunohistomorphometry, and *Tgfβ1* and *Tgfβ2* mRNA expression levels by real-time polymerase chain reaction. Marfan syndrome mice subjected to the preventive approach showed no aortic dilation in contrast to untreated Marfan syndrome mice, which at the same end point age already presented the aneurysm. In contrast, the palliative treatment with P144 did not halt aneurysm progression. In all cases, P144 improved elastic fiber morphology and normalized pERK1/2-mediated TGFβ signaling. Unlike the palliative treatment, the preventive treatment reduced *Tgfβ1* and *Tgfβ2* mRNA levels.

CONCLUSIONS: P144 prevents the onset of aortic aneurysm but not its progression. Results indicate the importance of reducing the excess of active TGFβ signaling during the early stages of aortic disease progression.

GRAPHIC ABSTRACT: A graphic abstract is available for this article.

Key Words: AAV expression vector ■ aortic aneurysm ■ apolipoproteins ■ betaglycan ■ echocardiography ■ genetic therapy ■ Marfan syndrome ■ TGF-beta

Marfan syndrome (MFS) is a severe, systemic genetic disorder of the connective tissue that causes aortic aneurysm, ocular lens dislocation, emphysema, and bone overgrowth.[1–7] MFS is caused by heterozygous mutations in the fibrillin-1 gene (*FBN1*).[8,9] The most characteristic cardiovascular structural manifestation of MFS is found in the aortic root and the ascending aorta, where the aortic wall is dilated, and the tunica media shows fragmentation, disorganization, and loss of elastic fibers.[10–12] *FBN1* mutations lead to progressive weakening and dilation of the aortic root and its subsequent rupture and dissection. However, it is accepted that clinical manifestations of MFS arise not only due to the abnormal structural properties of fibrillin-1 microfibrils but also to dysregulation of TGFβ signaling, which is primarily caused by the loss of microfibrils as a reservoir for latent TGFβ.[13–16] This view was formed thanks to the availability of mouse models with

Correspondence to: Professor Gustavo Egea, Departamento de Biomedicina, Facultad de Medicina y Ciencias de la Salud, Universidad de Barcelona, c/ Casanova 143, 08036 Barcelona, Catalunya, Spain. Email gegea@ub.edu

The Data Supplement is available with this article at https://www.ahajournals.org/doi/suppl/10.1161/ATVBAHA.121.316496.

For Sources of Funding and Disclosures, see page e450.

Arterioscler Thromb Vasc Biol is available at www.ahajournals.org/journal/atvb

Nonstandard Abbreviations and Acronyms

AAV	adeno-associated virus/vector
Ang II	angiotensin II
ECM	extracellular matrix
HDLs	high-density lipoproteins
MFS	Marfan syndrome
P144	AAVApolinkerP144
PA	palliative treatment
PE	preventive treatment
PS	physiological serum
RT-PCR	real-time polymerase chain reaction
TGFβ	transforming growth factor β
VSMC	vascular smooth muscle cell
WT	wild type

Highlights

- P144, a peptide derived from the extracellular domain of betaglycan/TGFβ (transforming growth factor β) receptor III, is constitutively expressed in a murine model of Marfan syndrome (*Fbn1*$^{C1041G/+}$) by adeno-associated vector-mediated gene therapy.
- P144 blocks the formation of the ascending aortic aneurysm but not its progression once already formed.
- P144 also prevents aortic wall disarray and ERK1/2-mediated TGFβ hypersignaling occurring in Marfan syndrome.
- P144 reduces the Marfan syndrome-associated mRNA overexpression of TGFβs1 and 2 in the aortic wall.

reduced *Fbn1* expression. In MFS patients and mice, an increase was seen in the active form of TGFβ.[17–20] Furthermore, neutralizing anti-TGFβ antibodies prevented aortic aneurysm growth in a mouse model of MFS.[21,22] In MFS, excessive TGFβ signaling enhances proteolysis of the extracellular matrix (ECM), apoptosis, and phenotypic differentiation of vascular smooth muscle cells (VSMC), as well as (trans)differentiation of VSMC and fibroblasts to myofibroblasts.[14,20,23]

TGFβ mediates its effects through ligand binding to a receptor that initiates signaling via phosphorylation of SMADs or ERK1/2 proteins (among others).[24,25] However, the hyperactivation of TGFβ signaling as a determinant trigger factor of aneurysm formation has been experimentally questioned[26] based on the following observations: (1) the treatment of Marfan mice (*Fbn1*$^{mgR/mgR}$) with an anti-TGFβ antibody (1D11) was associated with a trend to disrupt, rather than prevent, aortic wall structure and aneurysm in early stages[22]; (2) no differences were detected in active TGFβ or pSMAD levels in latent TGFβ binding protein 3 in the observed reduced aortopathy in Marfan mice in an LTBP3 (latent transforming growth factor beta-binding protein 3) knockout background[27]; (3) TGFβ receptor II disruption in postnatal VSMC accelerated aneurysm growth and impaired aortic wall homeostasis[28]; and (4) young MFS mice showed aortic dilation without altered TGFβ signaling in aortic VSMC. Moreover, aortic dilation and tunica media structural disruption were exacerbated by superimposed deletion of TGFβRII with the concomitant decreased activation of VSMC TGFβ signaling.[29] Besides disputed dysregulation of TGFβ signaling, other molecular mechanisms suggested as determinants in aortic pathogenesis include abnormal mechanosensing of aortic wall stress mediated by increased Ang II (angiotensin II) signaling and VSMC phenotypic switching.[20,30–34] Free active and latent ECM-linked TGFβ superfamily ligands interact with a variety of plasma membrane receptors of the aortic mural cells (mainly VSMC). Receptors are type I (TβRI/ALKs), type II (TβRII), and type III (TβRIII/betaglycan).[35] Betaglycan is a proteoglycan that contains a large extracellular domain, a single-pass transmembrane region and a short cytoplasmic domain, and is the most abundant TGFβ receptor in many cell types.[36,37] Betaglycan was shown to bind all 3 TGFβ isoforms (TGFβ1, β2, and β3) with near nanomolar affinity, but with a slight preference for TGFβ2,[38] which binds TβRII with an affinity 200- to 500-fold weaker than TGFβ1.[38–40] The betaglycan ectodomain undergoes shedding, which renders both membrane-bound and soluble forms. The membrane-bound form serves as a TGFβ signaling agonist, acting as a local reservoir for TGFβ ligands, as well as presenting them to other TGFβ superfamily receptors (types I and II), which modulate the resulting signaling output. In contrast, the soluble form of betaglycan binds ligands in the extracellular space and effectively reduces this ligand's availability to cell surface signaling receptors, thus inhibiting downstream signaling.[41] For this reason, soluble betaglycan was postulated as a potential therapeutic target to control TGFβ superfamily signaling responses.

Many therapeutic strategies have been developed to interfere with TGFβ signaling and almost every component of the TGFβ pathway has been targeted for drug development.[42,43] Among others, ligand-competitive peptides have progressed to clinical development. This is the case of the P144 peptide, which encompasses amino acids 730 to 743 from the TGFβ domain of the membrane and soluble forms of betaglycan.[44] The rationale for its use as a potential therapeutic drug is based on the peptide imitating soluble betaglycan, sequestering TGFβ from transmembrane signaling receptors and consequently antagonizing TGFβ stimulatory signaling.[44] Importantly, in the presence of P144, the TGFβ signaling response is not fully abolished but simply reduced. This

avoids potential undesirable secondary effects associated with the absence of TGFβ, such as the mid- to long-term risk of tumor promotion after using neutralizing anti-TGFβ antibodies or anti-TGFβ receptors I/II drugs.[45] P144 has been successfully used to block TGFβ-induced damage in murine models of scleroderma,[46] periprosthetic capsular, cardiac, liver, pulmonary and epidural fibrosis,[47–51] glioblastoma,[52] hypertension,[53,54] liver metastasis,[55] and colon cancer.[56]

Here, we evaluate P144 as a therapeutic tool to abrogate the pathogenesis of aortic aneurysm in a nonlethal mouse model of MFS (*Fbn1*$^{C1041G/+}$). However, P144 has a poor pharmacokinetic profile due to its short half-life in blood circulation.[44] To solve this problem, the peptide was fused with apolipoprotein A-I, and the resulting fusion protein expressed via an adeno-associated viral vector (AAV). A single administration of this vector therapy induced sustained expression of the transgene in the liver during the entire life of the mice.[55] The fusion protein circulates in plasma incorporated into HDLs (high-density lipoproteins), preventing the apolipoprotein A-I the intrinsic hydrophobicity of P144, stabilizing the peptide. This viral vector enables sustained in vivo transgene expression of the P144 peptide. Our work has additional interest because a recent study reported a significant increase in TβRIII/betaglycan protein levels in cultured fibroblasts from MFS patients with dominant-negative *FBN1* mutations, which in turn correlated with *Tgfβ1* mRNA expression.[57]

MATERIALS AND METHODS

The data that support the findings of this study are available from the corresponding author upon reasonable request.

Please see the Major Resources Table in the Data Supplement.

Murine Model

Fbn1$^{C1041G/+}$ mice (hereafter, MFS mice) were obtained from The Jackson Laboratory (Bar Harbor, ME 04609, United States) and used as a validated MFS animal model. MFS and sex- and age-matched wild-type (WT) littermates were maintained on a C57BL/6J genetic background. All mice were housed in a controlled environment (12/12-hour light/dark cycle) and provided with ad libitum access to food and water. Animal care and colony maintenance conformed to the European Union (Directive 2010/63/EU) and Spanish guidelines (RD 53/2013) for the use of experimental animals. Ethical approval was obtained from the local animal ethics committee (CEEA and the Government of Catalonia, protocol approval number 9517-118/7).

AAV Production

AAV production was performed as previously indicated.[55] Cotransfection of 293T cells was performed with a transfer plasmid carrying the transgene of interest (ApolinkerP144) and the pDP8.ape packaging plasmid (PlasmidFactory, Bielefeld, Germany) to generate AAV particles of serotype 8. The transfection was performed using polyethylenimine MAXMW 25 000; Polyscience, Warrington, PA) for 48 hours. Then, the virus was purified from cell lysates using an iodixanol gradient and buffer exchange with 50 mL centrifugal filters (Amicon Ultra-15 Centrifugal Filter Concentrator, Merck, Ireland). Viral titers in terms of viral copies per milliliter (vg/mL) were determined by quantitative real-time polymerase chain reaction (RT-PCR).

Quantitative RT-PCR

Total liver and ascending aorta mRNA from WT and MFS mice were isolated using TRI reagent (Sigma, Dorset, United Kingdom). Sample concentration and purity were determined in a Nanodrop 1000 spectrophotometer (ThermoScientific). RNA was treated with DNase I and reverse-transcribed to cDNA with MMLV RT in the presence of RNase OUT (all reagents from Invitrogen) according to the manufacturer's instructions.

Expression of the AAVApolinkerP144 (P144) and *Tgfβ1* and *Tgfβ2* transcripts was determined by quantitative RT-PCR using SYBR Green Supermix (Bio-Rad Laboratories, Hercules, CA) and specific primers for each gene (Table I in the Data Supplement). As *Gapdh* or *H3f3a* transcript levels remain unchanged across experimental conditions, the expression of these housekeeping genes was used to standardize gene expression. The amount of each transcript was expressed by the formula $2^{\Delta\Delta Ct(H3f3)-Ct(gene)}$ where Ct is the point at which gene fluorescence rises significantly above background fluorescence. RT-PCR reactions were performed using Bio-Rad reagents in accordance with the manufacturer's recommended protocol.

Study Design and Animal Handling

To evaluate the therapeutic effect of the P144 peptide by gene transfer for the treatment of MFS-associated aortic aneurysm, 4- or 8-week-old male and female WT and MFS mice were infraorbitally injected with physiological serum (PS), AAV encoding luciferase, or AAVApolinkerP144 (P144) expression vectors.[28] Preventive (PE) and palliative (PA) experimental treatments were performed. A representative scheme of both experimental protocols is shown in Figure I in the Data Supplement. In PE treatment, PS and P144 expression vector were single injected into 4-week-old WT and MFS mice until 8 weeks old (4 weeks of treatment; PE1) and 24 weeks old (20 weeks of treatment; PE2). For the PA treatment, PS, luciferase, or P144 expression vectors were single injected into 8-week-old mice until 24 weeks old (16 weeks of treatment; PA). At the respective outcome time points, mice were subjected to echocardiographic analysis, liver and aorta were isolated, fixed for paraffin embedding or immersed in RNA Later (R-0901, Sigma Aldrich), frozen and stored at −80 °C. WT and MFS mice received a single injection of PS or the respective luciferase or P144 expression vectors (4×10^{12} vg/mice in PS). In the PA approach, a group of WT and MFS mice, injected or not with luciferase and P144 vectors, also received losartan and the combination of both P144 and losartan (P144+losartan). Losartan was dissolved in drinking water (bottles kept away from the light) to a final concentration of 0.6 g/L, giving an estimated daily dose of 40 to 60 mg/kg per day.

Echocardiography

Two-dimensional transthoracic echocardiography was performed in all animals under 1.5% inhaled isoflurane. Each animal was scanned 12 to 24 hours before euthanize. Images were obtained with a 10 to 13 MHz phased array linear transducer (IL12i GE Healthcare, Madrid, Spain) in a Vivid Q system (GE Healthcare, Madrid, Spain). Images were recorded and later analyzed offline using commercially available software (EchoPac v.08.1.6, GE Healthcare, Madrid, Spain). Proximal aortic segments were assessed in a parasternal long-axis view. The aortic root aorta diameter was measured from inner edge to inner edge in end diastole at the level of the sinus of Valsalva. All echocardiographic measurements were performed in a blinded manner by 3 independent investigators, at 2 different periods, and with no knowledge of genotype and treatment.

Histomorphometry

Ascending aorta segments were fixed in 10% formaldehyde and embedded in paraffin. Paraffin blocks were sectioned into 5 μm slices. The tunica media was delimited using bright field images corresponding to polarized light. Aortic elastic fiber ruptures were quantified by counting the number of big fiber breaks in tissue sections stained with Verhoeff-Van Gieson. Breaks larger than 20 μm were defined as evident large discontinuities in the normal circumferential continuity of each elastic lamina in the aortic media (see Figure 2C for a representative example). They were counted along the length of each elastic lamina for 4 different, representative images of 2 nonconsecutive sections of the same aorta. The mean was calculated for each sample and then for each animal. Images were captured using a Leica Leitz DMRB microscope (40× oil immersion objective) equipped with a Leica DC500 camera and were analyzed with Fiji Image J Analysis software. In addition, tunica media thickness was measured in the same paraffin sections. All measurements were performed in a blinded manner by 3 observers with no knowledge of genotype and treatment.

Immunolocalization

Consecutive 5 μm paraffin sections were stained with anti-apolipoprotein A-I (1:50; Santa-Cruz; sc-30089), anti-pSMAD2 (1:100; 3108S, Cell Signaling), and anti-pERK1/2 (1:50; 9101S, Cell Signaling) antibodies. For unmasking epitopes, sections were treated with 1 mol/L Tris-EDTA, 0.05% Tween, pH 9 for pSMAD2, and anti-apolipoprotein A-I or with 10 mmol/L sodium citrate, 0.05% tween, pH 6 for pERK1/2. Thereafter, sections were rinsed in PBS and incubated for 20 minutes with ammonium chloride (50 mmol/L, pH 7.4) to block free aldehyde groups. Sections were permeabilized using 0.3% triton X-100 for 10 minutes and treated with BSA blocking buffer (1%) for 2 hours before overnight incubation with the primary antibody in a humidified chamber at 4 °C. Subsequently, sections were rinsed with PBS, followed by 1 hour incubation at room temperature with the secondary antibody goat anti-rabbit Alexa 647 (1:1000; Invitrogen, A-21246). Finally, sections were rinsed with PBS and counterstained with DAPI (1:10 000). Negative controls were processed in the same manner in the absence of the primary antibody. For quantitative analysis, 4 areas of each immunostained paraffin section were quantified. The mean was first calculated for each sample and then for each animal. For apolipoprotein A-I immunostaining, the fluorescence results were expressed as the integrated density per unit area of the whole aortic wall. All analyses were performed using Image J software and an in-house developed macro for automated image analysis from pictures taken with ×40 objective magnification.

Statistical Analysis

All data shown in the present study are reported as means±SEM. n refers to the number of mice used for the in vivo experiments. GraphPad Prism 9 software was used for the statistical analysis, where $P \leq 0.05$ was already considered significant. Normal distribution and equal variance data were verified with the IBM SPSS Statistics Base 22.0 before parametric tests were used. Then, data were analyzed using 2-way ANOVA with Tukey post-test for multiple comparisons or the Student *t* test was used when only 2 groups were compared. For nonparametric test data, the Kruskal-Wallis test with Dunn posttest for multiple comparisons was applied. The statistical test applied in each case is indicated in each figure legend.

RESULTS

AAVApolinkerP144 Expression Levels in MFS Mouse Tissues

ApolinkerP144 is a fusion protein that contains the anti-TGFβ peptide P144 fused via a flexible linker to the apolipoprotein A-I, the main component of HDLs. This fusion protein is stably produced by AAV particles of serotype 8. This serotype has the highest liver transduction efficiency in mice with a reduced immunogenicity profile.[58] To check the production of the fusion protein in MFS mice, we evaluated its expression by quantitative RT-PCR in liver and ascending aorta. As an internal control, we used the same vector containing luciferase instead of P144. As expected, liver cells highly expressed the P144 fusion protein transcript. Moreover, the ascending aorta also significantly expressed the P144 transcript, although to a lesser extent than liver (Figure IIA in the Data Supplement). Therefore, the liver and the aorta ensure the constitutive expression and bloodstream presence of the P144 fusion protein throughout the entire treatment period. To corroborate the presence of apolipoprotein A-I-P144 in the aortic wall, we performed immunofluorescence staining for apolipoprotein A-I as anti-P144 antibodies are not available. P144 injected WT and MFS mice showed significantly more immunofluorescent signal in the aortic wall (media and adventitia layers together) than noninjected animals (Figure IIB in the Data Supplement).

Aortic Aneurysm Evolution in MFS Mice

Before the injection of AAV, we evaluated by echocardiography the aortic root dilation in MFS mice of different ages to obtain a reference pattern of the temporal evolution of aortic aneurysm in our murine MFS model under our animal

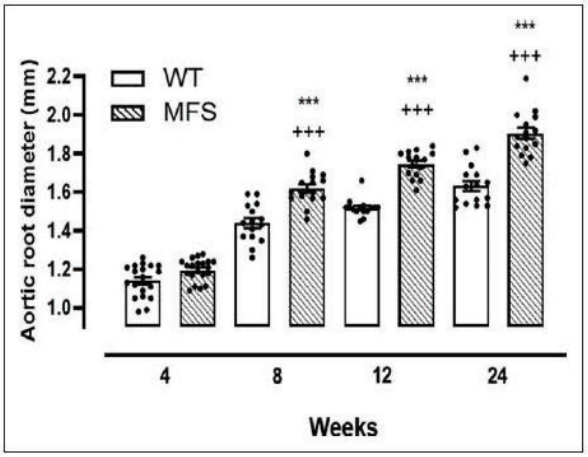

Figure 1. Aortic root dilation progression in Marfan syndrome (MFS) mice.
Comparative analysis of the aortic root diameter (mm) of wild-type (WT) and MFS (*Fbn1*$^{C1041G/+}$) mice of different age groups subjected to transthoracic echocardiography. See Table II in the Data Supplement for specific values. Statistical analysis: 2-way ANOVA and Tukey posttest ***$P \leq 0.001$ between WT and MFS, and $^{+++}P \leq 0.001$ between experimental MFS groups.

room conditions. MFS mice showed clear aortic root dilation at 8 weeks old, which progressively increased in 12- and 24-week-old mice. However, no significant changes were detected in the aortic root diameter in 4-week-old MFS mice compared with WT animals (Figure 1 and Table II in the Data Supplement). The aortic root growth diameter (indicated by the aortic root growth rate) between 4- and 8-week-old mice was twice that of MFS compared with WT mice (0.11±0.02 versus 0.07±0.02 mm/wk, respectively). For older mice, the growth was almost the same between WT and MFS mice and their respective age groups (8 versus 12 and 12 versus 24 weeks; Table III in the Data Supplement). The analysis of the results taking sex into consideration showed no significant changes (Tables II and III in the Data Supplement).

Aortic Root Growth, Aortic Wall Histopathology, and TGFβ Signaling Analysis When P144 Is Administered Before the Onset of Aortic Aneurysm: PE

Using echocardiography, we first analyzed whether P144 affected aneurysm formation. It was reported that P144 significantly reduces TGFβ signaling both in vitro and in vivo.[44,55] The P144 expression vector was injected into young WT and MFS mice just after weaning (4 weeks old). At this age, the aortic root diameter in MFS mice was almost indistinguishable from that of WT mice (Figure 1). Four weeks after the P144 injection (8 weeks old; PE1), aortic root dilation in MFS mice did not occur, in contrast to PS-treated MFS animals (Figure 2A and Table IV in the Data Supplement). Next, we evaluated whether the absence of aortic dilation in 8-week-old P144-injected MFS mice was indeed a halt or simply a delay in aneurysm onset. To this end, 4-week-old MFS mice were injected with the P144 expression vector and the aortic root diameter examined at 24 weeks old (20 weeks of PE; PE2). Results clearly showed that the aortic aneurysm did not form in the long-term (Figure 2B and Table V in the Data Supplement). No significant differences were observed between males and females (Tables IV and V in the Data Supplement for PE1 and PE2, respectively). Not only was aortic aneurysm formation prevented by P144 but also the characteristic tunica media structural disarray that usually accompany it, such as elastic lamina breaks (Figure 2C) and the augmentation of aortic wall thickness (Figure 2D and Table VI in the Data Supplement).

In parallel to the histomorphometry analysis of the aortic wall, we examined the tunica media protein expression levels of TGFβ signaling downstream effectors pSMAD2 and pERK1/2 as representatives of the canonical and noncanonical TGFβ signaling pathways, respectively. To this end, using immunofluorescence, we evaluated the nuclear localization of both phosphorylated forms as indicative of TGFβ signaling activation. In contrast to pSMAD2, P144 treatment significantly reduced the characteristic nuclear translocation of pERK1/2 that occurs in nontreated MFS mice (Figure 3A and 3B, respectively).

Aortic Root Growth, Aortic Wall Histopathology, and TGFβ Signaling Analysis When P144 Is Administered Once the Aortic Aneurysm Is Already Formed: PA

Next, we evaluated the potential therapeutic effect of expressing P144 once the aneurysm is present. Initially, we performed a pilot experiment with P144 and luciferase-expressing AAV vectors (Figure III in the Data Supplement). WT and MFS mice of 8 weeks of age were injected with PS, luciferase, or P144. We measured the aortic root diameter after 16 weeks of treatment in 24-week-old mice, when the aortic aneurysm is consolidated (Figure 1). Aortic root dilation occurred in PS- and luciferase-injected MFS mice and was indistinguishable from untreated animals. Note that P144-expressing MFS mice tended to show a reduction in aortic diameter, although statistical significance was not reached. Considering these preliminary echocardiographic results and knowing the intrinsic variability of aortic root diameter observed in adult mice, we increased the mouse sample size. In addition, we included losartan and the combination of P144 and losartan (P144+losartan; Figure 4). The aim of including losartan in parallel with P144 treatment was, on one hand, to have a comparative framework, as losartan is a well-established effective anti-aortic aneurysm treatment,[21] and on the other hand, to investigate the

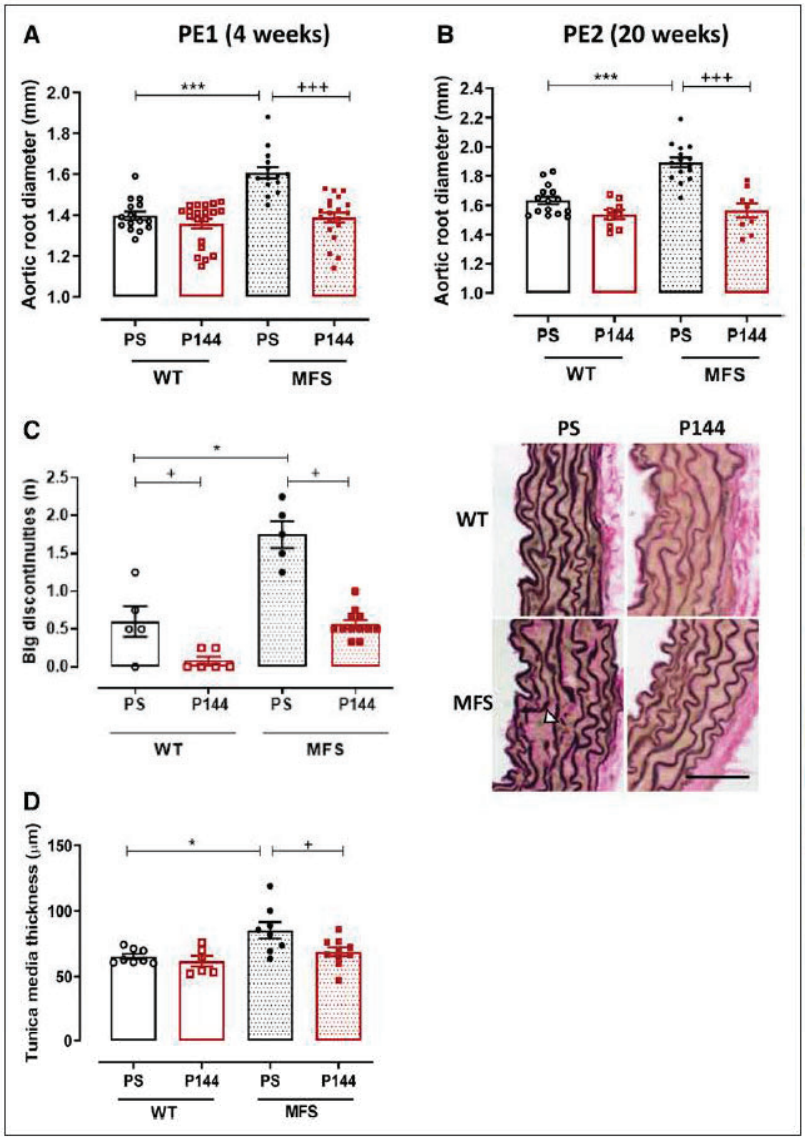

Figure 2. Aortic root dilation and aortic wall histomorphometry analysis in preventive P144 treatments. Aortic root diameter measured by echocardiography in wild-type (WT) and Marfan syndrome (MFS) mice of 4 wk of age treated with physiological serum (PS) or AAVApolinkerP144 (P144) for a period of 4 wk (PE1; **A**) or 20 wk (PE2; **B**); see respective Tables IV and V in the Data Supplement for specific values. **C**, Number of large discontinuities in the elastic lamina of the tunica of the ascending aorta (360°) from WT and MFS mice preventively treated (PE1) with PS or P144 expression vector. On the right, representative elastin histological staining (Elastin Verhoeff-Van Gieson) of the ascending aorta. White arrowhead indicates a representative large elastic discontinuity counted in the elastic lamina of MFS mouse aortic tissue. Bar 50 µm. **D**, Tunica media thickness (in µm) of the ascending aorta (360°) from WT and MFS mice preventively treated (PE1) with PS or P144 expression vector. See Table VI in the Data Supplement for specific values. All results are the mean±SEM. Two-way ANOVA and Tukey posttest (**A**, **B**, and **D**) and Kruskal-Wallis and Dunn posttest (**C**); $^{*,+}P \leq 0.05$, $^{***,+++}P \leq 0.001$; *significance between WT and MFS (genotype); +significance between experimental groups.

potential effectiveness of a combined therapy. Unlike losartan, P114 treatment definitively did not reduce the aortic root diameter (Figure 4A and Table VII in the Data Supplement). Note that P144 and losartan cotreatment produced the same reduction in aortic root diameter as losartan alone. As in PE, no differences were observed between males and females following the PA (Table VII in the Data Supplement).

When analyzing the aortic wall architecture, MFS mice showed a thicker aortic wall than WT mice, and losartan fully normalized the size (Figure 4B and Table VIII in the Data Supplement). This was also the case for P144 and its combined treatment with losartan. As expected, MFS mice showed large elastic lamina breaks, but P144, losartan, and P144+losartan treatments significantly reduced their number (Figure 4C).

The MFS-PS mice group showed a TGFβ-associated hypersignaling visualized by the increased presence of pSMAD2 and pERK1/2 in VSMC nuclei in the tunica media (Figure 5A and 5B, respectively, and Figure IV in the Data Supplement). This was not observed in MFS mice treated with P144, losartan, or their combined treatment, whose results were highly like those obtained in treated WT animals (Figure 5A and 5B; see Figure IV in the Data Supplement for representative images). Note that P144 protein expression in WT mice was innocuous.

Aortic TGFβ1 and TGFβ2 mRNA Expression Levels in P144-Treated MFS Mice

Since it was reported that betaglycan has a higher affinity for TGFβ2 than for TGFβ1 in vitro,[40] we next evaluated

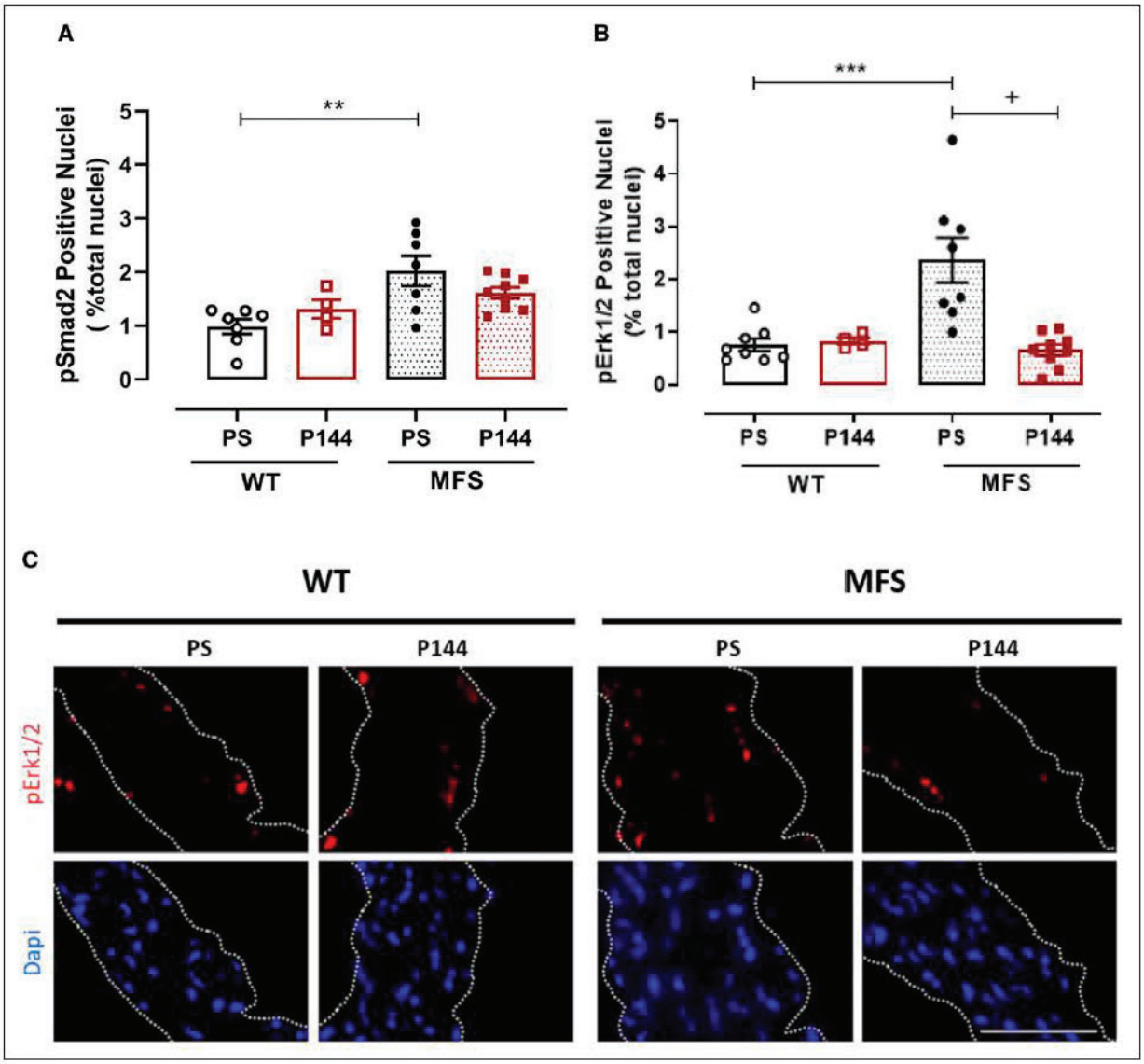

Figure 3. TGFβ (transforming growth factor β) signaling in the tunica media after preventive P144 treatment.
TGFβ signaling response evaluated by visualization of the nuclear localization of the phosphorylated forms of SMAD2 (pSmad2; **A**) and ERK1/2 (pErk1/2; **B** and **C**) in the tunica media of ascending aorta. **C**, Representative immunofluorescence staining for pERK1/2 performed in paraffin-embedded aortae from 4-wk-old wild-type (WT) and MFS (Marfan syndrome) mice treated with PS or P144 expression vector for 4 wk (PE1). Results are the mean±SEM. Kruskal-Wallis and Dunn posttest; *$P \leq 0.05$ and ***$P \leq 0.001$ between WT and MFS mice; $^{+}P \leq 0.05$ between experimental MFS groups.

whether the inhibition of aortic aneurysm formation following PE and PA treatments may have an impact on the bioavailability of TGFβ ligands due to changes in their gene expression. To this end, we evaluated *Tgfβ1* and *Tgfβ2* mRNA expression levels by RT-PCR in the aortic wall of treated and untreated WT and MFS mice. MFS animals showed significantly higher mRNA expression levels for both transcripts than WT mice regardless of the outcome age (8 and 24 weeks old). PE1 and PE2 treatments caused a significant reduction in the gene expression of both TGFβ ligands in MFS mice but not affecting WT ones (Figure 6A and 6B). Unlike the PE, the transcriptional levels of both TGFβ ligands following PA treatment were almost unaltered in MFS mice (Figure V in the Data Supplement). Therefore, P144 inhibits the overexpression of *Tgfβ1* and *Tgfβ2* in the aortic wall of MFS mice only when administered early in the aortic aneurysm but not later.

DISCUSSION

We here have examined the use of betaglycan/TGFβ receptor III-derived peptide P144 as a potential new therapeutic tool to interfere in the characteristic aortic aneurysm development in MFS. To this end, we have administered P144 via an AAV-based expression vector in MFS mice (C1041G/+) following a PE or PA

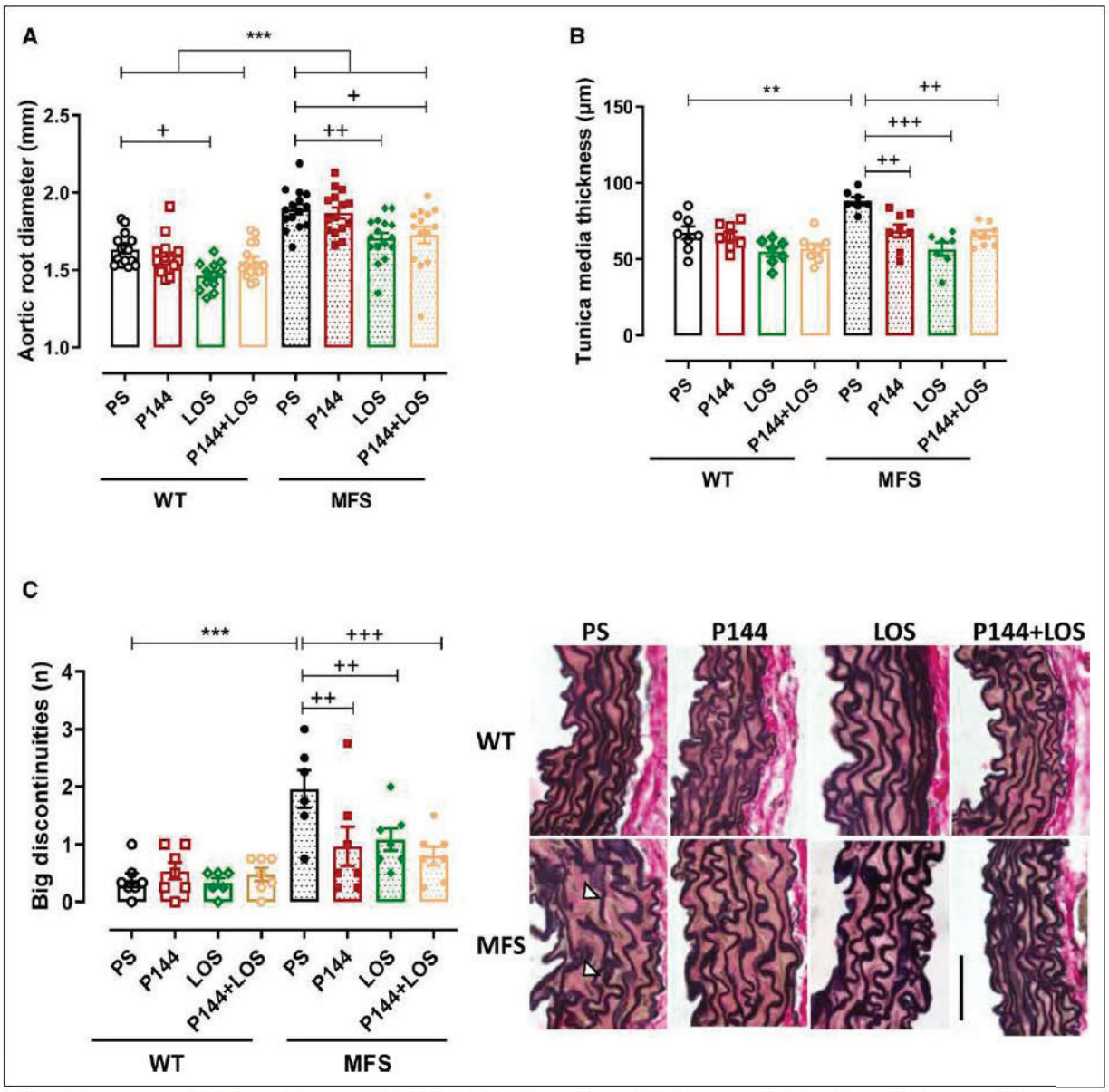

Figure 4. Aortic root dilation and aortic wall histomorphometric analysis of palliative P144 treatment (PA) and comparative study with losartan.

A, Aortic root diameter measured by echocardiography in 8-wk-old wild-type (WT) and Marfan syndrome (MFS) mice treated with PS, P144, losartan (LOS), or LOS+P144 for 16 wk. See Table VII in the Data Supplement for the specific values of each treatment. **B**, Tunica media thickness of the ascending aorta (360°) from WT and MFS mice. See Table VIII in the Data Supplement for specific values. **C**, Number of large discontinuities in the elastic lamina of the tunica of the ascending aorta (360°) from WT and MFS mice. Representative elastin histological staining (Verhoeff-Van Gieson) of the aortic wall of WT and MFS mice subjected to the treatments indicated are shown on the right. White arrow indicates an example of a large elastic lamina discontinuity seen in the MFS mouse aortic media. Bar, 50 µm. Results are the mean±SEM. P144 indicates AAVApolinkerP144 expression vector; P144+LOS, mice expressing P144 and treated with losartan; and PS, physiological serum/vehicle. Two-way ANOVA followed by Tukey posttest. $^{**}P\leq0.01$, $^{***}P\leq0.001$ between WT and MFS mice groups (genotype); $^{+}P\leq0.05$, $^{++}P\leq0.01$, and $^{+++}P\leq0.001$ between the indicated experimental MFS groups.

approach, expressing P144 before or after the aneurysm was generated. The main results of our study are as follows: (1) P144 is constitutively expressed both in liver (as expected) and to a lesser but significant manner in aorta as well; (2) P144 fully blocks the formation of the aneurysm but not its progression once formed; (3) neither aortic wall disarray nor noncanonical TGFβ hypersignaling (ERK1/2 mediated) occurred when the aneurysm was prevented by P144; and (4) P144 injected early can normalize the intrinsic abnormally high *Tgfβ1* and *Tgfβ2* mRNA expression levels in MFS mice.

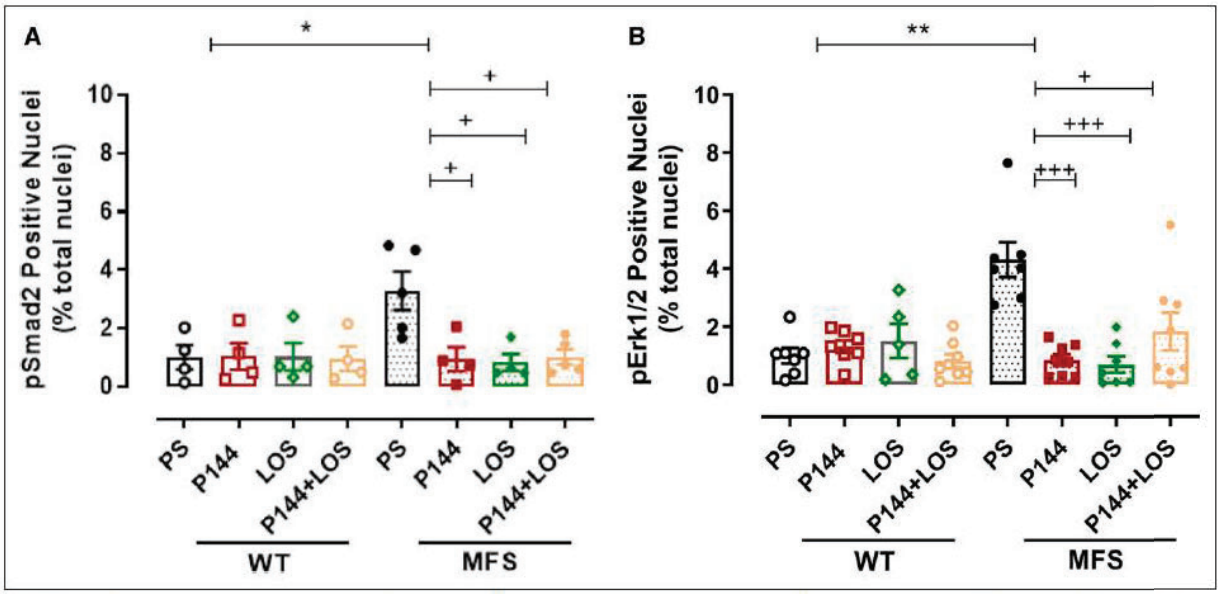

Figure 5. TGFβ (transforming growth factor β) signaling in the tunica media after palliative treatment with the P144 expression vector.

Analysis of activated phosphorylated forms of SMAD2 (**A**) and ERK1/2 (**B**) localized to nuclei of vascular smooth muscle cell (VSMC) of the tunica media of paraffin-embedded aortae from wild-type (WT) and Marfan syndrome (MFS) mice subjected to the experimental treatments indicated. Representative immunofluorescence images of each immunostaining and experimental group are shown in Figure IV in the Data Supplement. LOS indicates losartan; P144, constitutive expression of AAVApolinkerP144 expression vector; P144+LOS, constitutively expressing P144 cotreated with losartan; and PS, physiological serum/vehicle. Results expressed as the mean±SEM. Kruskal-Wallis and Dunn posttest; **P*≤0.05 and ****P*≤0.001 between WT and MFS (genotype); ^{+}P≤0.05, ^{++}P≤0.01, and ^{+++}P≤0.001 between the indicated experimental MFS groups.

Almost 2 decades ago, it was reported that TGFβ signaling was dysregulated in the aortic pathogenesis of MFS. This was based on the full normalization of the aortic wall in MFS mice, evaluated by echocardiography and histology using neutralizing anti-TGFβ antibodies and losartan (as AT1R activates TGFβ downstream effectors), and on the high structural similarity of fibrilin1 with LTBPs.[21,59] These observations immediately led to several clinical trials with losartan where the results were rather frustrating, as no clear improvement in aortic root progression was observed.[60,61] A short time later, new studies questioned TGFβ as a determinant primary trigger factor.[62] When our study was initiated, the TGFβ-based hypothesis was prevalent, and we postulated that the betaglycan-derived peptide P144 might be a promising therapeutic tool to regulate the abnormally increased bioavailability of active TGFβ in aortic mural cells. The use of the P144 peptide as an anti-TGFβ tool a priori afforded the advantage that it only causes partial inhibition of TGFβ signaling, and therefore a better safety profile than tools that completely abolish the signaling, thus in turn avoiding, to some extent, the risk of tumor formation.[62] In this respect, we observed that P144, preventively added, indeed abolished the overexpression of *Tgfβ1* and *Tgfβ2* transcripts in MFS mice without significantly affecting their normal levels in WT animals. These results indicate that only in MFS, where TGFβ ligands are overexpressed, P144 treatment not only seems to act as a sponge for their excess but also alters the transcription of both ligands, suggesting a feedback or direct regulatory effect within the wall itself. Nevertheless, this transcriptional effect is not surprising because, when using TGFβ inhibitors like galunisertib in liver cancer patients, it is observed that the inhibition of the TGFβ pathway by the drug is invariably accompanied by a significant reduction of TGFβ expression. Importantly, this behavior is used as a clinical diagnostic biomarker indicating that the treatment is working in the patients.[63] Moreover, changes in mRNA expression levels are not necessarily indicative of a reduced capability of P144 to sequester excess soluble TGFβ ligands with the subsequent reduction of circulating and local aortic levels of TGFβ, as would be the case at protein level.

The observation that the P144 peptide prevents aneurysm formation both in the short- and long-term, but not its progression once formed, confirms a divergent role for TGFβ in aortic aneurysm development and growth in MFS, as previously reported,[22,59] but with apparent disputed effects. Ramirez's laboratory showed that the impact of TGFβ on the formation and progression of aortic aneurysm varied (protective or detrimental) depending on when cytokine activity was intercepted and on the therapeutic agent used (neutralizing anti-TGFβ antibodies or losartan). They

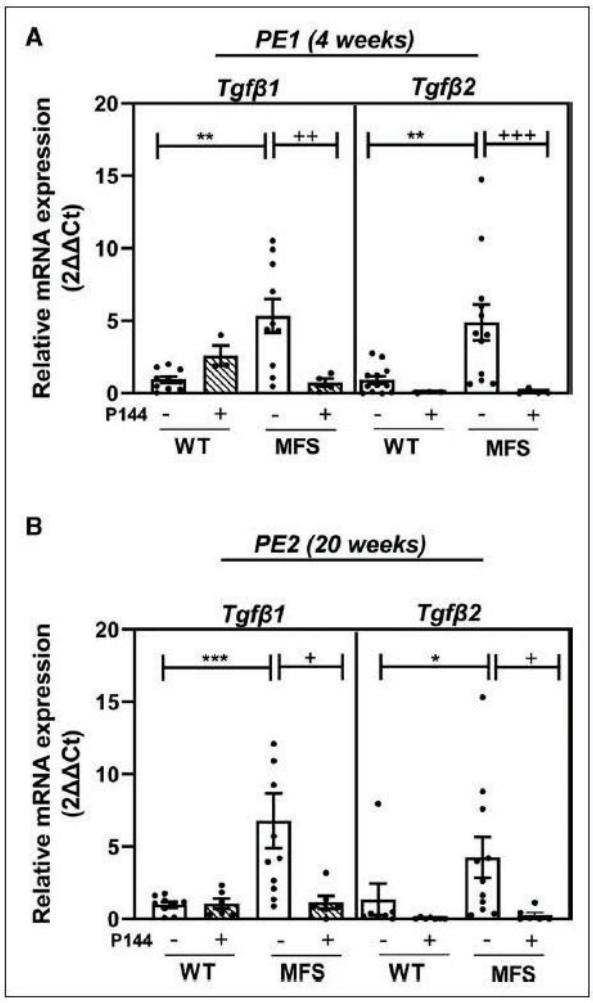

Figure 6. *Tgfβ1* and *Tgfβ2* mRNA expression levels in preventive P144 treatments.
Real-time polymerase chain reaction (RT-PCR) for *Tgfβ1* and *Tgfβ2* in wild-type (WT) and Marfan syndrome (MFS) mice (4 wk old) treated with P144 expression vector for 4 wk (PE1; **A**) or 20 wk (PE2; **B**). Results are the mean±SEM. mRNA expression values were normalized to *Gapdh* expression as a housekeeping control gene and reported as relative expression compared with WT using the $2^{-\Delta\Delta Ct}$ method. Kruskal-Wallis and Dunn posttest (**A**; PE1); and 2-way ANOVA followed by Tukey posttest (**B**; PE2). P144 indicates constitutive expression of AAVApolinkerP144 expression vector; and PS, physiological serum/vehicle. *$P\leq0.05$, **$P\leq0.01$, and ***$P\leq0.001$ between WT and MFS mice groups (genotype); $^{+}P\leq0.05$, $^{++}P\leq0.01$, and $^{+++}P\leq0.001$ between the indicated experimental MFS groups.

concluded that TGFβ hypersignaling is a secondary driver of aneurysm progression in MFS since blocking TGFβ in young MFS animals (mgR/mgR) at an early stage of the disease (2 weeks old/P16) exacerbated the aneurysm, whereas treatment at later stages was beneficial.[22] Along the same line of evidence, but using another MFS mouse model (C1041G/+), it was reported that the loss of physiological SMC-associated TGFβ signaling enhanced aortopathy after postnatal SMC-specific deletion of TβRII.[64] Strikingly, the aortopathy developed in the absence of detectable alterations in TGFβ signaling in young MFS mice. Moreover, thoracic and abdominal aortic disease, induced after Ang II infusion, were also both exacerbated when a pan-TGFβ neutralizing antibody was given to 8- to 12-week-old mice.[65] These results suggest that it is critical to maintain a physiological basal TGFβ signaling level for early normal aortic development and that its pathological imbalance will probably lead to the appearance of aortopathy. Our results are in accordance with this postulate, as P144 expression maintains TGFβ ligands and canonical (SMAD2) and noncanonical (ERK1/2) downstream signaling pathways at normal levels in MFS mice (C1041G/+). However, this was not the case when P144 was administered once aortic aneurysm progression had already started. It is possible, that at this stage, aortic P144 expression levels are not sufficient to reduce the overexpression and availability of bioactive soluble TGFβ ligand levels, therefore, becoming detrimental. Alternatively, but not mutually exclusive, it could be that other mechanisms are involved, mainly acting at advanced stages of aneurysm progression, and which also interfere in the expression and function of TGFβ, compensating, to some extent, the local inhibitory effect of P144. This would be case of Ang II-AT1R, whose TGFβ-independent dysregulated mechanisms, which participate in vascular mechanical stress, hemodynamic force, and kinetic energy, also primarily contribute to aortic aneurysm progression.[66–69] At the same time, they could also indirectly interfere in TGFβ-associated signaling, for example, in the SMAD pathway and in the own TGFβ ligands or their receptors expression levels,[60,70–72] being altogether determinant in aneurysm growth and rupture. In any case, it is clear from this and previous studies that TGFβ seems to be necessary but not sufficient in aortic formation and growth, and its signaling levels are also contextually critical in the time window in which its potential therapeutic effect finally becomes detrimental or beneficial.

Our results with betaglycan-derived P144 peptide highlight recent studies in which cultured fibroblasts from MFS patients with dominant-negative *FBN1* mutations showed increased betaglycan/TβRIII protein levels, which in turn correlated with increased *Tgfβ1* mRNA expression.[57] Membrane-bound betaglycan serves as a TGFβ signaling agonist acting as a local reservoir for TGFβ ligands and promoting their subsequent high-affinity interaction with other TGFβ receptors (TβRI and TβRII), also regulating their expression and membrane internalization.[73] In contrast, soluble betaglycan predominantly acts as a ligand-binding decoy, preventing the interaction of TGFβ ligands with cell surface receptors.[46] Therefore, presence in the bloodstream and local aorta expression of P144 acts as an antagonist to the intrinsic MFS-associated TGFβ hyperactivity, normalizing bioactive TGFβ ligands to physiological levels.

We are aware that our study has some limitations: (1) unlike preventive P144 treatment, the palliative approach did not reduce the aortic root diameter, conversely to aortic

wall organization and TGFβ signaling, which showed an almost total normalization. A possible explanation for this disparity is that the histological improvement might not be sufficient to have a functional (eg, mechanical) impact that can be resolved by echocardiography. However, this would not be the case for the PE in which the P144-treated mice were younger (4 week old), where the aorta is not yet fully structurally and functionally developed as in 8-week-old mice, age at which the PA was started. This functional and structural disparity of results has been previously observed in MFS experimental and clinical practice[74,75] although other studies showed a good correlation between both parameters[76,77]; (2) we cannot discard that P144 might affect blood pressure, but it is highly unlikely because previous studies in rodents clearly stated that blood pressure was unaffected by P144 treatments[48]; (3) most preclinical studies use the C1041G/+ mouse model, which slowly develops aortic aneurysm but rarely ends with aortic dissection. The mgR mouse model, which is a more severe model developing the disease and suitable to monitor the survival rate, would have been more appropriate for evaluating the natural progression of aneurysm to dissection that occurs in many MFS patients; (4) a priori, the PE with P144 in human patients does not seem as feasible as any other potential PA, but it cannot be discarded since it might be of help to those patients who suffer the disease but have not as yet developed the aneurysm; and (5) AAV particles of serotype 8 is not the most suitable AAV serotype to use for vasculature, although other serotypes do not largely transduce smooth muscle cells either.[78,79] However, an AAV-based expression strategy guarantees the continuous presence of P144 in the bloodstream (mostly coming from liver cells, but also locally from aortic cells), whose stability is facilitated by its linking to apolipoprotein A-I. The AAV-mediated expression approach has been very recently reported for oligonucleotide to AP-1 transcription factor in MFS.[80] This work shows a significant reduction of elastolysis in MFS mice (mgR/mgR),[80] which not only highlights the relevance of AP-1 in aortic wall organization but also reinforces the potential therapeutic use of AAV-based therapy for aortic diseases. AAV vector expression technology for treating some monogenetic diseases has been applied successfully and 2 AAV-based drugs have received Food and Drug Administration approval,[28] whose potential translational application is closer in time to that based on highly potential patient-derived induced pluripotent stem cells-based technology.[81–84] P144 administration via an AAV-based expression vector makes it especially attractive as AAVs are considered one of the most effective delivery tools for gene therapy due to their low toxicity and mild stimulation of immune responses, and they also facilitate a safe, long-term expression of the peptide.[85]

In conclusion, the P144 peptide, mimicking the role of the endogenous soluble domain of betaglycan, triggers a local compensatory negative signaling response in the aorta of MFS mice and blocks the onset of aortic aneurysm, but not progression once it is already formed. This preventive effect is associated with the inhibition of TGFβs1 and 2 overexpression and subsequent hyper-signaling (mainly ERK1/2 mediated) occurring in MFS aorta, bringing their expression levels to physiological levels. This observation is demonstrative of the importance of reducing the excess of TGFβ during the early stages of aortic disease progression in MFS.

ARTICLE INFORMATION

Received May 12, 2020; accepted June 9, 2021.

Affiliations

Department of Biomedical Sciences, School of Medicine and Health Sciences, University of Barcelona, Spain (C.A., I.R.-R., K.D.R., V.C., G.E.). Department of Cardiology, Hospital Clínic y Provincial de Barcelona, Spain (K.D.). Centro de Investigación Biomédica en Red de Enfermedades Raras (CIBERER), ISCIII, Spain (V.C.). Bellvitge Biomedical Research Institute (IDIBELL) and Centro de Investigación Biomédica en Red de Enfermedades Hepático-Digestivas (CIBEREHD), ISCIII, Spain (I.F.). Department of Therapeutic Pharmacology and Toxicology, School of Medicine, Neuroscience Institute, Autonomous University of Barcelona, Bellaterra, Spain (F.J.-A.). Program of Immunology and Immunotherapy, CIMA University of Navarra, Pamplona, Spain (P.B.). Navarra Institute for Health Research (IDISNA), Pamplona, Spain (P.B.). Institut d'Investigacions Biomèdiques August Pi i Sunyer (IDIBAPS), Barcelona, Spain (G.E.).

Acknowledgments

We thank Helena Kruyer for language editing and Dr Ana Paula Dantas for statistical advice.

Sources of Funding

This work was supported by grants from the National Marfan Association of the United States (NMF2015), MINECO from the Spanish Government (SAF2017-83039-R), and Fondo de Investigación Sanitaria-Fondo Europeo de Desarrollo Regional (FEDER) under Grant PI19/01128. G. Egea greatly acknowledges the invaluable support of Damelys Fumero and the Asociación Eutsi Gogor Danok Batera from the Basque Country for the research carried out in his lab I. Rodríguez-Rovira is a Spanish predoctoral fellow (FPI program).

Disclosures

None.

Supplemental Materials

Online Figures I–V
Online Tables I–VIII

REFERENCES

1. Pyeritz RE. The Marfan syndrome. *Annu Rev Med*. 2000;51:481–510. doi: 10.1146/annurev.med.51.1.481
2. De Paepe A, Devereux RB, Dietz HC, Hennekam RC, Pyeritz RE. Revised diagnostic criteria for the Marfan syndrome. *Am J Med Genet*. 1996;62:417–426. doi: 10.1002 /(SICI)1096-8628 (19960 424)62:4<417::A ID -AJMG15 >3.0.CO;2-R
3. Loeys BL, Dietz HC, Braverman AC, Callewaert BL, De Backer J, Devereux RB, Hilhorst-Hofstee Y, Jondeau G, Faivre L, Milewicz DM, et al. The revised Ghent nosology for the Marfan syndrome. *J Med Genet*. 2010;47:476–485. doi: 10.1136/jmg.2009.072785
4. Cañadas V, Vilacosta I, Bruna I, Fuster V. Marfan syndrome. Part 1: pathophysiology and diagnosis. *Nat Rev Cardiol*. 2010;7:256–265. doi: 10.1038/nrcardio.2010.30
5. Cañadas V, Vilacosta I, Bruna I, Fuster V. Marfan syndrome. Part 2: treatment and management of patients. *Nat Rev Cardiol*. 2010;7:266–276. doi: 10.1038/nrcardio.2010.31
6. De Backer J, Renard M, Campens L, Mosquera LM, De Paepe A, Coucke P, Callewaert B, Kodolitsch Yv. Marfan Syndrome and related heritable thoracic aortic aneurysms and dissections. *Curr Pharm Des*. 2015;21:4061–4075. doi: 10.2174/1381612821666150826093152
7. von Kodolitsch Y, De Backer J, Schüler H, Bannas P, Behzadi C, Bernhardt AM, Hillebrand M, Fuisting B, Sheikhzadeh S, Rybczynski

M, et al. Perspectives on the revised Ghent criteria for the diagnosis of Marfan syndrome. *Clin Genet*. 2015;8:137–155. doi: 10.2147/TACG.S60472
8. Dietz HC, Cutting GR, Pyeritz RE, Maslen CL, Sakai LY, Corson GM, Puffenberger EG, Hamosh A, Nanthakumar EJ, Curristin SM. Marfan syndrome caused by a recurrent de novo missense mutation in the fibrillin gene. *Nature*. 1991;352:337–339. doi: 10.1038/352337a0
9. Sakai LY, Keene DR, Renard M, De Backer J. FBN1: The disease-causing gene for Marfan syndrome and other genetic disorders. *Gene*. 2016;591:279–291. doi: 10.1016/j.gene.2016.07.033
10. Schlatmann TJ, Becker AE. Pathogenesis of dissecting aneurysm of aorta. Comparative histopathologic study of significance of medial changes. *Am J Cardiol*. 1977;39:21–26. doi: 10.1016/s0002-9149(77)80005-2
11. Hollister DW, Godfrey M, Sakai LY, Pyeritz RE. Immunohistologic abnormalities of the microfibrillar-fiber system in the Marfan syndrome. *N Engl J Med*. 1990;323:152–159. doi: 10.1056/NEJM199007193230303
12. Cook JR, Carta L, Galatioto J, Ramirez F. Cardiovascular manifestations in Marfan syndrome and related diseases; multiple genes causing similar phenotypes. *Clin Genet*. 2015;87:11–20. doi: 10.1111/cge.12436
13. Dietz HC. TGF-beta in the pathogenesis and prevention of disease: a matter of aneurysmic proportions. *J Clin Invest*. 2010;120:403–407. doi: 10.1172/JCI42014
14. Doyle JJ, Gerber EE, Dietz HC. Matrix-dependent perturbation of TGFβ signaling and disease. *FEBS Lett*. 2012;586:2003–2015. doi: 10.1016/j.febslet.2012.05.027
15. Gillis E, Van Laer L, Loeys BL. Genetics of thoracic aortic aneurysm: at the crossroad of transforming growth factor-β signaling and vascular smooth muscle cell contractility. *Circ Res*. 2013;113:327–340. doi: 10.1161/CIRCRESAHA.113.300675
16. Takeda N, Hara H, Fujiwara T, Kanaya T, Maemura S, Komuro I. TGF-β signaling-related genes and thoracic aortic aneurysms and dissections. *Int J Mol Sci*. 2018;19:2125. doi: 10.3390/ijms19072125
17. Neptune ER, Frischmeyer PA, Arking DE, Myers L, Bunton TE, Gayraud B, Ramirez F, Sakai LY, Dietz HC. Dysregulation of TGF-beta activation contributes to pathogenesis in Marfan syndrome. *Nat Genet*. 2003;33:407–411. doi: 10.1038/ng1116
18. Ng CM, Cheng A, Myers LA, Martinez-Murillo F, Jie C, Bedja D, Gabrielson KL, Hausladen JM, Mecham RP, Judge DP, et al. TGF-beta-dependent pathogenesis of mitral valve prolapse in a mouse model of Marfan syndrome. *J Clin Invest*. 2004;114:1586–1592. doi: 10.1172/JCI22715
19. Nataatmadja M, West J, West M. Overexpression of transforming growth factor-beta is associated with increased hyaluronan content and impairment of repair in Marfan syndrome aortic aneurysm. *Circulation*. 2006;114(1 Suppl):I371–I377. doi: 10.1161/CIRCULATIONAHA.105.000927
20. Crosas-Molist E, Meirelles T, López-Luque J, Serra-Peinado C, Selva J, Caja L, Gorbenko Del Blanco D, Uriarte JJ, Bertran E, Mendizábal Y, et al. Vascular smooth muscle cell phenotypic changes in patients with Marfan syndrome. *Arterioscler Thromb Vasc Biol*. 2015;35:960–972. doi: 10.1161/ATVBAHA.114.304412
21. Habashi JP, Judge DP, Holm TM, Cohn RD, Loeys BL, Cooper TK, Myers L, Klein EC, Liu G, Calvi C, et al. Losartan, an AT1 antagonist, prevents aortic aneurysm in a mouse model of Marfan syndrome. *Science*. 2006;312:117–121. doi: 10.1126/science.1124287
22. Cook JR, Clayton NP, Carta L, Galatioto J, Chiu E, Smaldone S, Nelson CA, Cheng SH, Wentworth BM, Ramirez F. Dimorphic effects of transforming growth factor-β signaling during aortic aneurysm progression in mice suggest a combinatorial therapy for Marfan syndrome. *Arterioscler Thromb Vasc Biol*. 2015;35:911–917. doi: 10.1161/ATVBAHA.114.305150
23. Jones JA, Spinale FG, Ikonomidis JS. Transforming growth factor-beta signaling in thoracic aortic aneurysm development: a paradox in pathogenesis. *J Vasc Res*. 2009;46:119–137. doi: 10.1159/000151766
24. Shi Y, Massagué J. Mechanisms of TGF-beta signaling from cell membrane to the nucleus. *Cell*. 2003;113:685–700. doi: 10.1016/s0092-8674(03)00432-x
25. Pardali E, Ten Dijke P. TGFβ signaling and cardiovascular diseases. *Int J Biol Sci*. 2012;8:195–213. doi: 10.7150/ijbs.3805
26. Mallat Z, Ait-Oufella H, Tedgui A. The pathogenic transforming growth factor-β overdrive hypothesis in aortic aneurysms and dissections: a mirage? *Circ Res*. 2017;120:1718–1720. doi: 10.1161/CIRCRESAHA.116.310371
27. Zilberberg L, Phoon CK, Robertson I, Dabovic B, Ramirez F, Rifkin DB. Genetic analysis of the contribution of LTBP-3 to thoracic aneurysm in Marfan syndrome. *Proc Natl Acad Sci U S A*. 2015;112:14012–14017. doi: 10.1073/pnas.1507652112
28. Li W, Li Q, Jiao Y, Qin L, Ali R, Zhou J, Ferruzzi J, Kim RW, Geirsson A, Dietz HC, et al. Tgfbr2 disruption in postnatal smooth muscle impairs aortic wall homeostasis. *J Clin Invest*. 2014;124:755–767. doi: 10.1172/JCI69942
29. Wei H, Hong-Hu J, Angelov S, Fox K, Yan J, Enstrom R, Smith A, Dichek D. Aortopathy in a mouse model of Marfan syndrome is not mediated by altered transforming growth factor ß signaling. *JAHA*. 2017;6:e004968. doi: 10.1161/JAHA.116.004968
30. Humphrey JD, Milewicz DM, Tellides G, Schwartz MA. Cell biology. Dysfunctional mechanosensing in aneurysms. *Science*. 2014;344:477–479. doi: 10.1126/science.1253026
31. Jeremy RW, Robertson E, Lu Y, Hambly BD. Perturbations of mechanotransduction and aneurysm formation in heritable aortopathies. *Int J Cardiol*. 2013;169:7–16. doi: 10.1016/j.ijcard.2013.08.056
32. Nolasco P, Fernandes CG, Ribeiro-Silva JC, Oliveira PVS, Sacrini M, de Brito IV, De Bessa TC, Pereira LV, Tanaka LY, Alencar A, et al. Impaired vascular smooth muscle cell force-generating capacity and phenotypic deregulation in Marfan Syndrome mice. *Biochim Biophys Acta Mol Basis Dis*. 2020;1866:165587. doi: 10.1016/j.bbadis.2019.165587
33. Dale M, Fitzgerald MP, Liu Z, Meisinger T, Karpisek A, Purcell LN, Carson JS, Harding P, Lang H, Koutakis P, et al. Premature aortic smooth muscle cell differentiation contributes to matrix dysregulation in Marfan Syndrome. *PLoS One*. 2017;12:e0186603. doi: 10.1371/journal.pone.0186603
34. Michel JB, Jondeau G, Milewicz DM. From genetics to response to injury: vascular smooth muscle cells in aneurysms and dissections of the ascending aorta. *Cardiovasc Res*. 2018;114:578–589. doi: 10.1093/cvr/cvy006
35. Nickel J, Ten Dijke P, Mueller TD. TGF-β family co-receptor function and signaling. *Acta Biochim Biophys Sin (Shanghai)*. 2018;50:12–36. doi: 10.1093/abbs/gmx126
36. López-Casillas F, Cheifetz S, Doody J, Andres JL, Lane WS, Massagué J. Structure and expression of the membrane proteoglycan betaglycan, a component of the TGF-beta receptor system. *Cell*. 1991;67:785–795. doi: 10.1016/0092-8674(91)90073-8
37. Wang XF, Lin HY, Ng-Eaton E, Downward J, Lodish HF, Weinberg RA. Expression cloning and characterization of the TGF-beta type III receptor. *Cell*. 1991;67:797–805. doi: 10.1016/0092-8674(91)90074-9
38. Kim SK, Henen MA, Hinck AP. Structural biology of betaglycan and endoglin, membrane-bound co-receptors of the TGF-beta family. *Exp Biol Med (Maywood)*. 2019;244:1547–1558. doi: 10.1177/1535370219881160
39. Bilandzic M, Stenvers KL. Betaglycan: a multifunctional accessory *Mol Cell Endocrinol*. 2011;339:180–189. doi: 10.1016/j.mce.2011.04.014
40. Mendoza V, Vilchis-Landeros MM, Mendoza-Hernández G, Huang T, Villarreal MM, Hinck AP, López-Casillas F, Montiel JL. Betaglycan has two independent domains required for high affinity TGF-beta binding: proteolytic cleavage separates the domains and inactivates the neutralizing activity of the soluble receptor. *Biochemistry*. 2009;48:11755–11765. doi: 10.1021/bi901528w
41. López-Casillas F, Payne HM, Andres JL, Massagué J. Betaglycan can act as a dual modulator of TGF-beta access to signaling receptors: mapping of ligand binding and GAG attachment sites. *J Cell Biol*. 1994;124:557–568. doi: 10.1083/jcb.124.4.557
42. Akhurst RJ, Hata A. Targeting the TGFβ signalling pathway in disease. *Nat Rev Drug Discov*. 2012;11:790–811. doi: 10.1038/nrd3810
43. Wagner AH, Zaradzki M, Arif R, Remes A, Müller OJ, Kallenbach K. Marfan syndrome: a therapeutic challenge for long-term care. *Biochem Pharmacol*. 2019;164:53–63. doi: 10.1016/j.bcp.2019.03.034
44. Dotor J, López-Vázquez AB, Lasarte JJ, Sarobe P, García-Granero M, Riezu-Boj JI, Martínez A, Feijoó E, López-Sagaseta J, Hermida J, et al. Identification of peptide inhibitors of transforming growth factor beta 1 using a phage-displayed peptide library. *Cytokine*. 2007;39:106–115. doi: 10.1016/j.cyto.2007.06.004
45. Llopiz D, Dotor J, Casares N, Bezunartea J, Díaz-Valdés N, Ruiz M, Aranda F, Berraondo P, Prieto J, Lasarte JJ, et al. Peptide inhibitors of transforming growth factor-beta enhance the efficacy of antitumor immunotherapy. *Int J Cancer*. 2009;125:2614–2623. doi: 10.1002/ijc.24656
46. Santiago B, Gutierrez-Cañas I, Dotor J, Palao G, Lasarte JJ, Ruiz J, Prieto J, Borrás-Cuesta F, Pablos JL. Topical application of a peptide inhibitor of transforming growth factor-beta1 ameliorates bleomycin-induced skin fibrosis. *J Invest Dermatol*. 2005;125:450–455. doi: 10.1111/j.0022-202X.2005.23859.x
47. Ruiz-De-Erenchun R, Dotor De Las Herrerías J, Hontanilla B. Use of the transforming growth factor-β1 inhibitor peptide in periprosthetic capsular fibrosis: experimental model with tetraglycerol dipalmitate. *Plast Reconstr Surg*. 2005;116:1370–1378. doi: 10.1097/01.prs.0000181694.07661.0d
48. Hermida N, López B, González A, Dotor J, Lasarte JJ, Sarobe P, Borrás-Cuesta F, Díez J. A synthetic peptide from transforming growth factor-beta1 type III receptor prevents myocardial fibrosis in spontaneously hypertensive rats. *Cardiovasc Res*. 2009;81:601–609. doi: 10.1093/cvr/cvn315
49. Ezquerro IJ, Lasarte JJ, Dotor J, Castilla-Cortázar I, Bustos M, Peñuelas I, Blanco G, Rodríguez C, Lechuga Mdel C, Greenwel P, et al. A synthetic peptide

from transforming growth factor beta type III receptor inhibits liver fibrogenesis in rats with carbon tetrachloride liver injury. *Cytokine*. 2003;22:12–20. doi: 10.1016/s1043-4666(03)00101-7
50. Arribillaga L, Dotor J, Basagoiti M, Riezu-Boj JI, Borrás-Cuesta F, Lasarte JJ, Sarobe P, Cornet ME, Feijoó E. Therapeutic effect of a peptide inhibitor of TGF-β on pulmonary fibrosis. *Cytokine*. 2011;53:327–333. doi: 10.1016/j.cyto.2010.11.019
51. Albiñana-Cunningham JN, Ripalda-Cemboráin P, Labiano T, Echeveste JI, Granero-Moltó F, Alfonso-Olmos M. Mechanical barriers and transforming growth factor beta inhibitor on epidural fibrosis in a rabbit laminectomy model. *J Orthop Surg Res*. 2018;13:72. doi: 10.1186/s13018-018-0781-6
52. Gallo-Oller G, Vollmann-Zwerenz A, Meléndez B, Rey JA, Hau P, Dotor J, Castresana JS. P144, a Transforming growth factor beta inhibitor peptide, generates antitumoral effects and modifies SMAD7 and SKI levels in human glioblastoma cell lines. *Cancer Lett*. 2016;381:67–75. doi: 10.1016/j.canlet.2016.07.029
53. Baltanás A, Miguel-Carrasco JL, San José G, Cebrián C, Moreno MU, Dotor J, Borrás-Cuesta F, López B, González A, Díez J, Fortuño A, et al. A synthetic peptide from transforming growth factor-β1 Type III receptor inhibits NADPH oxidase and prevents oxidative stress in the kidney of spontaneously hypertensive rats. *Antioxid Redox Sign*. 2013;19:1607–1618. doi: 10.1089/ars.2012.4653
54. Miguel-Carrasco JL, Baltanás A, Cebrián C, Moreno MU, López B, Hermida N, González A, Dotor J, Borrás-Cuesta F, Díez J, et al. Blockade of TGF-β 1 signalling inhibits cardiac NADPH oxidase overactivity in hypertensive rats. *Oxid Med Cell Longev*. 2012;2012:726940. doi: 10.1155/2012/726940
55. Medina-Echeverz J, Fioravanti J, Díaz-Valdés N, Frank K, Aranda F, Gomar C, Ardaiz N, Dotor J, Umansky V, Prieto J, et al. Harnessing high density lipoproteins to block transforming growth factor beta and to inhibit the growth of liver tumor metastases. *PLoS One*. 2014;9:e96799. doi: 10.1371/journal.pone.0096799
56. Medina-Echeverz J, Vasquez M, Gomar C, Ardaiz N, Berraondo P. Overexpression of apolipoprotein A-I fused to an anti-transforming growth factor beta peptide modulates the tumorigenicity and immunogenicity of mouse colon cancer cells. *Cancer Immunol Immunother*. 2015;64:717–725. doi: 10.1007/s00262-015-1681-9
57. Groeneveld ME, Bogunovic N, Musters RJP, Tangelder GJ, Pals G, Wisselink W, Micha D, Yeung KK. Betaglycan (TGFBR3) up-regulation correlates with increased TGF-β signaling in Marfan patient fibroblasts in vitro. *Cardiovasc Pathol*. 2018;32:44–49. doi: 10.1016/j.carpath.2017.10.003
58. Nakai H, Fuess S, Storm TA, Muramatsu S, Nara Y, Kay MA. Unrestricted hepatocyte transduction with adeno-associated virus serotype 8 vectors in mice. *J Virol*. 2005;79:214–224. doi: 10.1128/JVI.79.1.214-224.2005
59. Milewicz DM, Ramirez F. Therapies for thoracic aortic aneurysms and acute aortic dissections: old controversies and new opportunities. *Arterioscler Thromb Vas Biol*. 2019;39:126–136. doi: 10.1161/ATVBAHA.118.310956
60. Milewicz DM, Prakash SK, Ramirez F. Therapeutics targeting drivers of thoracic aortic aneurysms and acute aortic dissections: insights from predisposing genes and mouse models. *Annu Rev Med*. 2017;68:51–67. doi: 10.1146/annurev-med-100415-022956
61. Hoffman Bowman M, Eage KA, Milewicz DM. Update on clinical trials of Losartan with and without ß-blockers to block aneurysm growth in patients with Marfan syndrome: a review. *JAMA Cardiol*. 2019;4:702–707. doi: 10.1001/jamacardio.2019.1176
62. Tellides G. Further evidence supporting a protective role of transforming growth factor-β (TGFβ) in aortic aneurysm and dissection. *Arterioscler Thromb Vasc Biol*. 2017;37:1983–1986. doi: 10.1161/ATVBAHA.117.310031
63. Giannelli G, Santoro A, Kelley RK, Gane E, Paradis V, Cleverly A, Smith C, Estrem ST, Man M, Wang S, et al. Biomarkers and overall survival in patients with advanced hepatocellular carcinoma treated with TGF-βRI inhibitor galunisertib. *PLoS One*. 2020;15:e0222259. doi: 10.1371/journal.pone.0222259
64. Hu JH, Wei H, Jaffe M, Airhart N, Du L, Angelov SN, Yan J, Allen JK, Kang I, Wight TN, et al. Postnatal deletion of the type II transforming growth factor-β receptor in smooth muscle cells causes severe aortopathy in mice. *Arterioscler Thromb Vasc Biol*. 2015;35:2647–2656. doi: 10.1161/ATVBAHA.115.306573
65. Wang Y, Ait-Oufella H, Herbin O, Bonnin P, Ramkhelawon B, Taleb S, Huang J, Offenstadt G, Combadière C, Rénia L, et al. TGF-beta activity protects against inflammatory aortic aneurysm progression and complications in angiotensin II-infused mice. *J Clin Invest*. 2010;120:422–432. doi: 10.1172/JCI38136
66. Humphrey JD, Schwartz MA, Tellides G, Milewicz DM. Role of mechanotransduction in vascular biology: focus on thoracic aortic aneurysms and dissections. *Circ Res*. 2015;116:1448–1461. doi: 10.1161/CIRCRESAHA.114.304936
67. Milewicz DM, Trybus KM, Guo DC, Sweeney HL, Regalado E, Kamm K, Stull JT. Altered smooth muscle cell force generation as a driver of thoracic aortic aneurysms and dissections. *Arterioscler Thromb Vasc Biol*. 2017;37:26–34. doi: 10.1161/ATVBAHA.116.303229
68. Ramirez F, Caescu C, Wondimu E, Galatioto J. Marfan syndrome; a connective tissue disease at the crossroads of mechanotransduction, TGFβ signaling and cell stemness. *Matrix Biol*. 2018;71–72:82–89. doi: 10.1016/j.matbio.2017.07.004
69. Dorst DCH, Wagenaar NP, Pluijm I, Roos-Hesselink JW, Essers J, Danser AHJ. Transforming growth factor-β and the renin-angiotensin system in syndromic thoracic aortic aneurysms: implications for treatment [published online December 7, 2020]. *Cardiovasc Drugs Ther*. doi: 10.1007/s10557-020-07116-4
70. Touyz RM, Schiffrin EL. Signal transduction mechanisms mediating the physiological and pathophysiological actions of angiotensin II in vascular smooth muscle cells. *Pharmacol Rev*. 2000;52:639–672.
71. Rodríguez-Vita J, Sánchez-López E, Esteban V, Rupérez M, Egido J, Ruiz-Ortega M. Angiotensin II activates the Smad pathway in vascular smooth muscle cells by a transforming growth factor-beta-independent mechanism. *Circulation*. 2005;111:2509–2517. doi: 10.1161/01.CIR.0000165133.84978.E2
72. Shen YH, LeMaire SA, Webb NR, Cassis LA, Daugherty A, Lu HS. Aortic aneurysm and dissections series. *Arterioscler Thromb Vasc Biol*. 2020;40:e37–e46. doi: 10.1161/ATVBAHA.120.313991
73. Derynck R, Budi EH. Specificity, versatility, and control of TGF-ß family signaling. *Sci Signal*. 2019;12:eaav5183. doi: 10.1126/scisignal.aav5183
74. Mas-Stachurska A, Siegert AM, Batlle M, Gorbenko Del Blanco D, Meirelles T, Rubies C, Bonorino F, Serra-Peinado C, Bijnens B, Baudin J, et al. Cardiovascular benefits of moderate exercise training in Marfan syndrome: insights from an animal model. *J Am Heart Assoc*. 2017;6:e006438. doi: 10.1161/JAHA.117.006438
75. Gu X, He Y, Li Z, Han J, Chen J, Nixon JV. Echocardiographic versus histologic findings in Marfan syndrome. *Tex Heart Inst J*. 2015;42:30–34. doi: 10.14503/THIJ-13-3848
76. Gibson C, Nielsen C, Alex R, Cooper K, Farney M, Gaufin D, Cui JZ, van Breemen C, Broderick TL, Vallejo-Elias J, et al. Mild aerobic exercise blocks elastin fiber fragmentation and aortic dilatation in a mouse model of Marfan syndrome associated aortic aneurysm. *J Appl Physiol (1985)*. 2017;123:147–160. doi: 10.1152/japplphysiol.00132.2017
77. Chen JZ, Sawada H, Moorleghen JJ, Weiland M, Daugherty A, Sheppard MB. Aortic strain correlates with elastin fragmentation in fibrillin-1 hypomorphic mice. *Circ Rep*. 2019;1:199–205. doi: 10.1253/circrep.CR-18-0012
78. Denby L, Nicklin SA, Baker AH. Adeno-associated virus (AAV)-7 and -8 poorly transduce vascular endothelial cells and are sensitive to proteasomal degradation. *Gene Ther*. 2005;12:1534–1538. doi: 10.1038/sj.gt.3302564
79. Maeda Y, Ikeda U, Ogasawara Y, Urabe M, Takizawa T, Saito T, Colosi P, Kurtzman G, Shimada K, Ozawa K. Gene transfer into vascular cells using adeno-associated virus (AAV) vectors. *Cardiovasc Res*. 1997;35:514–521. doi: 10.1016/s0008-6363(97)00163-6
80. Remes A, Arif A, Franz M, Jungmann A, Zaradki M, Puehler T, Heckmann MMB, Frey N, Karck M, Kallenbach K, et al. AAV-mediated AP-1 decoy oligonucleotide expression inhibits aortic elastolysis in a mouse model of Marfan syndrome [published online January 20, 2021]. *Cardiovasc Res*. doi: 10.1093/cvr/cvab012
81. Davaapil H, Shetty DK, Sinha S. Aortic "disease-in-a-dish": mechanistic insights and drug development using iPSC-based disease modeling. *Front Cell Dev Biol*. 2020;8:550504. doi: 10.3389/fcell.2020.550504
82. Rurali E, Perrucci GL, Pilato CA, Pini A, Gaetano R, Nigro P, Pompilio G. Precise therapy for thoracic aortic aneurysm in marfan syndrome: a puzzle nearing its solution. *Prog Cardiovasc Dis*. 2018;61:328–335. doi: 10.1016/j.pcad.2018.07.020
83. Maguire EM, Xiao Q, Xu Q. Differentiation and application of induced pluripotent stem cell-derived vascular smooth muscle cells. *Arterioscler Thromb Vasc Biol*. 2017;37:2026–2037. doi: 10.1161/ATVBAHA.117.309196
84. Park JW, Yan L, Stoddard C, Wang X, Yue Z, Crandall L, Robinson T, Chang Y, Denton K, Li E, et al. Recapitulating and correcting marfan syndrome in a cellular model. *Int J Biol Sci*. 2017;13:588–603. doi: 10.7150/ijbs.19517
85. Samulski RJ, Muzyczka N. AAV-mediated gene therapy for research and therapeutic purposes. *Annu Rev Virol*. 2014;1:427–451. doi: 10.1146/annurev-virology-031413-085355

ONLINE SUPPLEMENTAL MATERIAL

ANTI-TGF-β THERAPY WITH P144 PEPTIDE GENE DELIVERY BLOCKS THE FORMATION BUT NOT THE PROGRESSION OF AORTIC ANEURYSM IN A MOUSE MODEL OF MARFAN SYNDROME

Cristina Arce[1], Isaac Rodríguez-Rovira[1], Karina Durán[2], Francesc Jiménez-Altayó[3], Isabel Fabregat[4], Pedro Berraondo[5,6], and Gustavo Egea[1,7,8]

[1]Department de Biomedicina, Facultat de Medicina i Ciències de la Salut, Universitat de Barcelona, Barcelona (Spain)
[2]Department of Cardiology, Hospital Clínic y Provincial de Barcelona, Barcelona (Spain)
[3]Departament de Farmacologia Terapèutica i Toxicologia, Facultat de Medicina, Institut de Neurociències, Universitat Autònoma de Barcelona, Bellaterra (Spain)
[4]Bellvitge Biomedical Research Institute (IDIBELL) and CIBEREHD, L'Hospitalet, Barcelona, Spain
[5]Program of Immunology and Immunotherapy, CIMA University of Navarra, Pamplona (Spain)
[6]Navarra Institute for Health Research (IDISNA), Pamplona (Spain)
[7]Institut d'Investigacions Biomèdiques August Pi i Sunyer (IDIBAPS), Barcelona (Spain)
[8]Institut de Nanociencies i Nanotecnologia (IN^{2}UB), Universitat de Barcelona, Barcelona (Spain)

SUPPLEMENTARY FIGURES

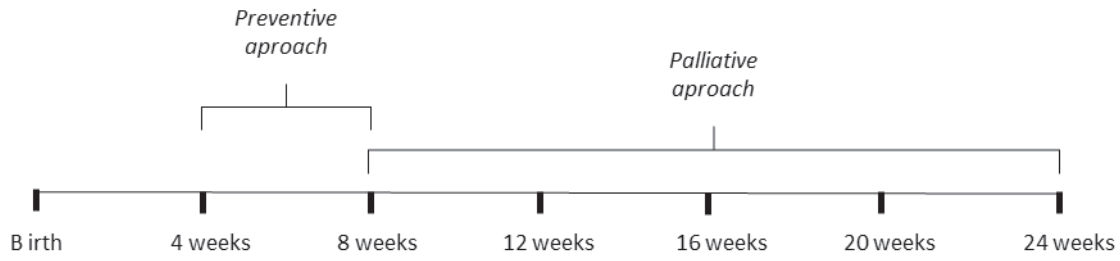

Supplementary Figure I. Representative scheme of the experimental protocols (preventive and palliative) performed in WT and MFS mice with AAV-P144 expression vector.

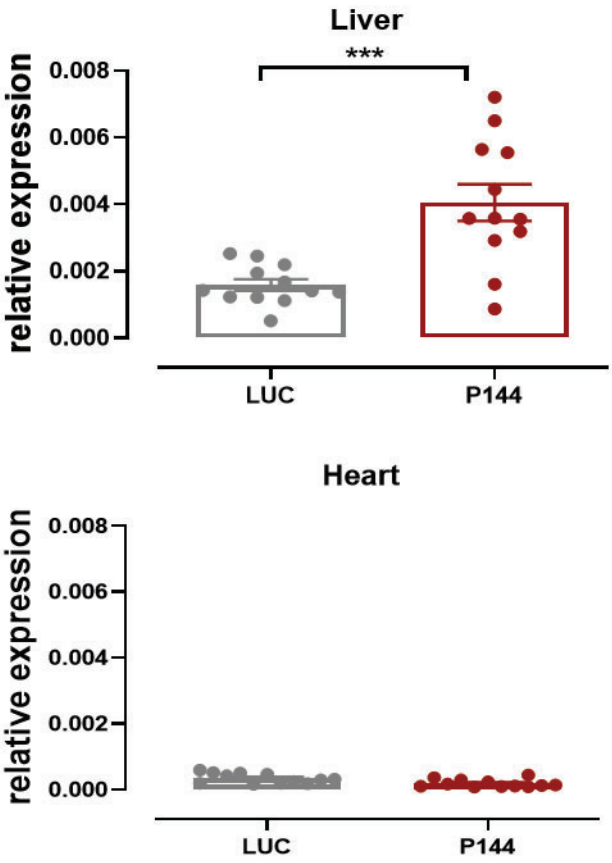

Supplementary Figure II. P144 expression in MFS mouse tissues. Quantitative RT-PCR analysis of P144 expression in liver and heart from MFS mice injected with PS or LUC or P144 expression vectors. Results expressed as mean±SEM. Statistical analysis: Student's *t* test. *P≤0.05, and ***P≤0.001.

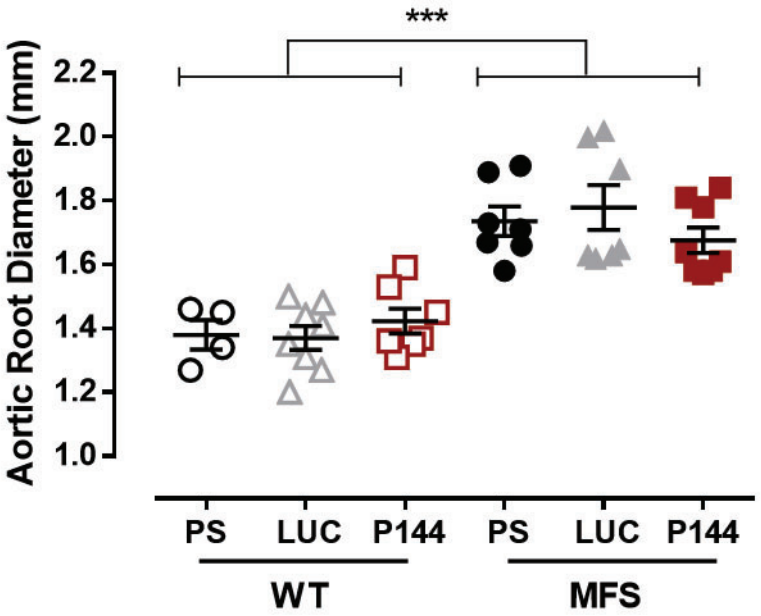

Supplementary Figure III. Pilot experiment to evaluate the aortic root diameter in the palliative P144 and LUC treatments in MFS mice. Aortic root diameter in WT and MFS mice (8 weeks-age) treated with physiological serum (PS), AAVLUC (LUC) or AAVApolinkerP144 (P144) for 16 weeks. Unlike LUC, P144 trend to reduced aortic root diameter but without reaching statistical significance. Results presented as mean ± SEM. ****P* ≤ 0,001 between WT and MFS mice groups (genotype). Two-way Anova followed by Tukey post-test.

SUPPLEMENTARY TABLES

Supplementary Table 1. Echocardiographic values of the aortic root diameter (in mm) of WT and MFS mice of different age groups.

Aortic root diameter				
Months	**WT**		**MFS**	
4	1.14±0.03	6	1.17±0.02	13
8	1.40±0.02	15	1.64±0.02^{*++++}	15
12	1.47±0.08^{++}	11	1.71±0.10^{*+++}	9
24	1.63±0.06^{+++}	15	1.89±0.03$^{******+++}$	15

*Indicates the statistical significance of WT vs. MFS mice of the same age; $^{+}$Indicates the statistical significance between WT or MFS mice of different ages. **,$^{++}$P≤ 0.01; ***,$^{+++}$P≤ 0.001

Supplementary Table 2. Echocardiographic values of aortic root diameter (in mm) of WT and MFS mice subjected to preventive treatment with the P144 expression vector for 4 weeks (from 4 to 8 weeks old).

Aortic root diameter at 8 weeks-age				
	WT		**MFS**	
PS	1.40±0.02	15	1.64±0.02***	15
P144	1.36±0.05	12	1.45±0.02^{+++}	15

*Indicates the statistical significance of WT vs. MFS mice of the same age; $^{+}$Indicates the statistical significance between WT or MFS mice of different ages. ***,$^{+++}$P≤0.001.

Supplementary Table 3. Aortic tunica media thickness (in μm) of WT and MFS mice subjected to preventive treatment with the P144 expression vector for 4 weeks (from 4 to 8 weeks old).

Tunica media thickness at 8 weeks-age				
	WT		**MFS**	
PS	64.80±3.50	8	85.25±6.33*	8
P144	61.80±4.10	6	68.80±3.33^{+}	10

*Indicates the statistical significance of WT vs. MFS mice of the same age; $^{+}$Indicates the statistical significance between WT or MFS mice of different ages. *,$^{+}$P≤0.05.

Supplementary Table 4. Echocardiographic values of the aortic root diameter (in mm) of WT and MFS mice subjected to palliative treatments with the P144

expression vector (P144) and losartan (LOS) for 16 weeks (from 8 to 24 weeks old).

Aortic Root at 24 weeks-age				
	WT		**MFS**	
PS	1.63±0.03	15	1.89±0.03***	15
P144	1.59±0.03	16	1.87±0.04	15
LOS	1.46±0.03^{+}	12	1.70±0.04^{++}	16
P144+LOS	1.56±0.03	15	1.73±0.05^{+}	14

*Indicates the statistical significance of WT vs. MFS mice of the same age; $^{+}$Indicates the statistical significance between WT or MFS mice of different ages. *,$^{+}$P≤ 0.05; **,$^{++}$P≤ 0.01; ***,$^{+++}$P≤ 0.001.

Supplementary Table 5. Aortic tunica media thickness (in μm) of WT and MFS mice subjected to palliative treatments with the P144 expression vector (P144) and losartan (LOS) for 16 weeks (from 8 to 24 weeks old)

Tunica media thickness at 24 weeks-age				
	WT		**MFS**	
PS	67.32±4.23	8	88.28±2.55**	7
P144	65.14±2.87	8	68.72±4.32^{++}	8
LOS	54.97±3.16	7	56.52±4.32^{+++}	7
P144+LOS	57.07±3.13	8	66.12±2.59^{++}	8

*Indicates the statistical significance of WT vs. MFS mice of the same age; $^{+}$Indicates the statistical significance between WT and MFS mice of different ages. **,$^{++}$P≤0.01; ***,$^{+++}$P≤0.001.

OBJECTIVE 2: Study the contribution of xanthine oxidoreductase (XOR) in the progression of aortic aneurysm in Marfan syndrome.

Rodríguez-Rovira I, Arce C, De Rycke K, Pérez B, Carretero A, Arbonés M, Teixidò-Turà G, Gómez-Cabrera MC, Campuzano V, Jiménez-Altayó F, Egea G.

Allopurinol blocks aortic aneurysm in a mouse model of Marfan syndrome via reducing aortic oxidative stress.

Free Radic Biol Med. 2022 20;193:538-550.
Doi:10.1016/j.freeradbiomed.2022.11.001.

Free Radical Biology and Medicine 193 (2022) 538–550

Contents lists available at ScienceDirect

Free Radical Biology and Medicine

journal homepage: www.elsevier.com/locate/freeradbiomed

Allopurinol blocks aortic aneurysm in a mouse model of Marfan syndrome via reducing aortic oxidative stress

Isaac Rodríguez-Rovira [a,1], Cristina Arce [a,1,3], Karo De Rycke [a,1,2], Belén Pérez [b], Aitor Carretero [c], Marc Arbonés [a], Gisela Teixidò-Turà [d,e], Mari Carmen Gómez-Cabrera [c], Victoria Campuzano [a,f], Francesc Jiménez-Altayó [b], Gustavo Egea [a,*]

[a] Department of Biomedical Sciences, University of Barcelona School of Medicine and Health Sciences, 08036, Barcelona, Spain
[b] Department of Pharmacology, Toxicology and Therapeutics, Neuroscience Institute, School of Medicine, Autonomous University of Barcelona, 08193, Cerdanyola del Vallès, Spain
[c] Department of Physiology, Faculty of Medicine, University of Valencia, CIBERFES, Fundación Investigación Hospital Clínico Universitario/INCLIVA, Valencia, Spain
[d] Department of Cardiology, Hospital Universitari Vall d'Hebron, Barcelona, Spain
[e] CIBER-CV, Vall d'Hebrón Institut de Recerca (VHIR), Barcelona, Spain
[f] Centro de Investigación Biomédica en Red de Enfermedades Raras (CIBERER), ISCIII, Spain

ARTICLE INFO

Keywords:
Aortic aneurysm
Allopurinol
Metalloproteinase
NOX4
NRF2
Oxidative stress
Uric acid
Xanthine oxidase

ABSTRACT

Background: Increasing evidence indicates that redox stress participates in MFS aortopathy, though its mechanistic contribution is little known. We reported elevated reactive oxygen species (ROS) formation and NADPH oxidase NOX4 upregulation in MFS patients and mouse aortae. Here we address the contribution of xanthine oxidoreductase (XOR), which catabolizes purines into uric acid and ROS in MFS aortopathy.

Methods and results: In aortic samples from MFS patients, XOR protein expression, revealed by immunohistochemistry, increased in both the tunicae intima and media of the dilated zone. In MFS mice (*Fbn1*$^{C1041G/+}$), aortic *XOR* mRNA transcripts and enzymatic activity of the oxidase form (XO) were augmented in the aorta of 3-month-old mice but not in older animals. The administration of the XOR inhibitor allopurinol (ALO) halted the progression of aortic root aneurysm in MFS mice. ALO administrated before the onset of the aneurysm prevented its subsequent development. ALO also inhibited MFS-associated endothelial dysfunction as well as elastic fiber fragmentation, nuclear translocation of pNRF2 and increased 3′-nitrotyrosine levels, and collagen maturation remodeling, all occurring in the tunica media. ALO reduced the MFS-associated large aortic production of H_2O_2, and NOX4 and MMP2 transcriptional overexpression.

Conclusions: Allopurinol interferes in aortic aneurysm progression acting as a potent antioxidant. This study strengthens the concept that redox stress is an important determinant of aortic aneurysm formation and progression in MFS and warrants the evaluation of ALO therapy in MFS patients.

1. Introduction

Marfan syndrome (MFS) is a relatively common inherited rare disease of the connective tissue caused by mutations in the gene encoding the extracellular matrix glycoprotein fibrillin-1 [1]. This multisystem disease mainly affects the skeleton (abnormally long bones and spine deformations), eyes (lens dislocation) and aorta (aortic root aneurysm). The latter commonly leads to aortic dissection and rupture, the main cause of reduced life expectancy in patients [2].

Reactive oxygen species (ROS) consist of radical (anion superoxide/ $O_2^{\cdot-}$ and hydroxyl radical/$HO^{\cdot}$) and non-radical (hydrogen peroxide/ H_2O_2) oxygen species, which are highly reactive chemicals formed by the partial reduction of oxygen. $O_2^{\cdot-}$ and H_2O_2 are the most frequently formed ROS and, under physiological concentrations, have important signaling functions (oxidative eustress) [3]. However, when ROS

* Corresponding author. Departament de Biomedicina, Facultat de Medicina i Ciències de la Salut, Universitat de Barcelona, c/ Casanova 143, 08036, Barcelona, Spain.
E-mail address: gegea@ub.edu (G. Egea).
[1] These three authors contributed equally to this work.
[2] Present address: Department of Biomolecular Medicine, Center for Medical Genetics, Ghent University, Ghent, Belgium.
[3] Present address: Department of Biology, University of Padova, Padova, Italy.

https://doi.org/10.1016/j.freeradbiomed.2022.11.001
Received 23 August 2022; Received in revised form 28 October 2022; Accepted 2 November 2022
Available online 5 November 2022

Nonstandard abbreviations

ALO	allopurinol
CRCs	cumulative concentration-response curves
3-NT	3′-nitrotyrosine
PA	palliative experimental treatment with allopurinol
PE	preventive experimental treatment with allopurinol
PE < ALO and PA < ALO	respective PE and PA treatments with subsequent allopurinol withdrawal

overwhelm the intrinsic cellular antioxidant system, either via an abnormal overproduction of ROS or reduction of their antioxidant capacity, they contribute to pathogenesis (oxidative stress), causing transient or permanent damage to nucleic acids, proteins, and lipids [4,5].

In the cardiovascular system, ROS are involved in, among other dysfunctions, the development of aortic abdominal aneurysms (AAA) through the regulation of inflammation induction, matrix metalloproteinases (MMPs) expression, vascular smooth muscle cell (VSMC) apoptosis and phenotypic changes and modifying extracellular matrix properties [6–10]. However, the impact of ROS on thoracic aortic aneurysm (TAA) of genetic origin, such as in MFS and Loeys-Dietz syndrome (LDS), is less known [11]. We and others have previously shown that ROS production is increased in MFS [12–18], although the specific generators of ROS and their respective impact on the formation and/or progression in either human or murine MFS aortic aneurysms is still poorly understood [19,20]. We reported the involvement of upregulated NADPH (nicotinamide adenine dinucleotide phosphate) oxidase 4 (NOX4) both in human and mouse MFS aortic samples and cultured VSMCs [17]. Nonetheless, besides NOX4, another important source of ROS in the cardiovascular system is xanthine oxidoreductase (XOR) [21].

XOR is involved in the final steps of nucleic acid-associated purine degradation and, particularly, in the conversion of hypoxanthine into xanthine and xanthine into urate. XOR exists in two forms that are derived from a single gene (*XDH*) [22]. The reduced form of XOR is referred to as xanthine dehydrogenase (XDH), and the oxidized form as xanthine oxidase (XO). XDH can be post-translationally modified to XO via proteolysis or oxidation of critical cysteines [23]. The XDH form has greater abundance and affinity for NAD^+ as the electron acceptor to generate NADH, which is a critical substrate for NADPH oxidases. Likewise, the XO form is mainly associated with the production of large amounts of O_2^- and H_2O_2 by preferentially using oxygen as the electron acceptor [24,25]. Under healthy conditions, XDH is constitutively expressed, and XO levels are low both in plasma and heart [26]. However, XDH conversion into XO is favored by hypoxia, low pH, ischemia, inflammation, and the presence of peroxynitrite and H_2O_2 itself [27–29]. XOR is widely distributed throughout the organism mainly in the liver and gut, but also present in intestine, lung, kidney, myocardium, brain and plasma [30]. In the vascular endothelium, XOR is bound to cell surface glycosaminoglycans [26]; the enhancement of endothelium attached XOR favors local ROS production with subsequent endothelial dysfunction [31]. XOR-derived anion superoxide (O_2^-) easily interacts with endothelial cell-generated nitric oxide (NO) forming peroxynitrite ($ONOO^-$), which in the endothelium of the tunica intima and VSMCs of the media irreversibly generates reactive nitrogen species (RNS) residues such as 3′-nitrotyrosine [32,33], which is usually used as a redox stress marker. Increased XOR levels have been reported in aortic samples from adult MFS mice [14] and LDS patients [34], even though the extent to which XOR contributes to TAA pathogenesis is unknown.

On the other hand, concomitantly to ROS production, XOR generates uric acid (UA), which in humans can pathologically accumulate in the plasma and some tissues. In rodents, UA is rapidly catabolized by uricase (absent in humans) to allantoin [35]. UA has a dual role in redox biology, acting as an antioxidant (both *in vitro* and *in vivo*) accounting for as much as 50% of the total antioxidant capacity of biological fluids in humans [36]. However, when UA accumulates in the cytoplasm or in acidic/hydrophobic milieu, it acts as a pro-oxidant promoting redox stress [36,37]. UA was found in the wall of human aortic aneurysms and atherosclerotic arteries [38] and there was a positive correlation between serum UA levels and aortic dilation and dissection [39,40]. Epidemiologic and biochemical studies on UA formation have demonstrated that it is not only UA itself that leads to a worse prognosis and increased cardiovascular events, but also ROS formed during XOR activity. Therefore, the resulting combined action of excessively formed UA and ROS surely contribute to oxidative stress-linked cardiovascular pathological events [41].

The aim of this study was to investigate the participation of XOR in MFS aortopathy in more detail and evaluate the effectiveness of the XOR inhibitor allopurinol (ALO) on the formation and/or progression of MFS-associated aortopathy. ALO is an analogue of hypoxanthine and, therefore, a competitive inhibitor of XOR [42]; it is a drug routinely prescribed to treat hypouricemic and hypertensive patients [43]. XOR also functions beyond its basic housekeeping role in purine catabolism, acting in oxidant signaling, which could contribute to exacerbating oxidative stress-associated MFS aortopathy. Therefore, since XOR is an important source of ROS in the cardiovascular system, we hypothesized that, together with upregulated NOX4 [17,44], the formation and/or progression of aortic aneurysm in MFS is favored by abnormal aortic XOR activity with the consequent dysfunctional increase in ROS levels (and likely UA and/or allantoin as well) exacerbating the oxidative stress-associated MFS aortopathy.

2. Material and methods

Please see Methods in Supplemental Materials [92–96].

3. Results

3.1. XOR is augmented in the dilated aorta of MFS patients

We evaluated protein levels by immunohistochemistry with specific anti-XOR antibodies in the aorta of MFS patients subjected to aortic reparatory surgery. Unlike the tunica adventitia, both the tunicae intima and media of the dilated aortic zone presented a significant increase in immunostaining compared with adjacent non-dilated and healthy aortae (Fig. 1), which is demonstrative of an increased protein expression of XOR associated with aortic aneurysm in MFS patients. No correlation between the intensity of the immunostaining and the age of the patients analyzed was observed.

3.2. XOR mRNA expression and enzymatic activity are only increased in the aorta of young MFS mice

We next evaluated whether XOR was also increased in the MFS mouse aorta. Firstly, we evaluated XOR transcriptional levels by RT-PCR in 3- and 6- and 9-month-old WT and MFS mice. Aortae from 3-month-old MFS mice showed significantly increased levels of *XOR* transcripts compared with age-matched WT animals. This increase was not observed in 6- or 9-month-old mice (Fig. 2A). Immunohistochemistry with anti-XOR antibodies confirmed the increased expression of XOR in the endothelial cell layer (intima) and in the media only in 3-month-old MFS aortic wall (Fig. 2B). The adventitia was also stained for XOR, but just like in the human aorta, nonsignificant changes were observed over the age.

To differentiate the functional contribution of the XDH and XO protein forms of XOR in the MFS aorta, we next measured their respective enzymatic activities in aortic lysates (see a representative assay in Fig. S2). The XO/XDH enzymatic activity ratio was significantly higher in 3-month-old but not in 6- or 9-month-old MFS mice (Fig. 2C),

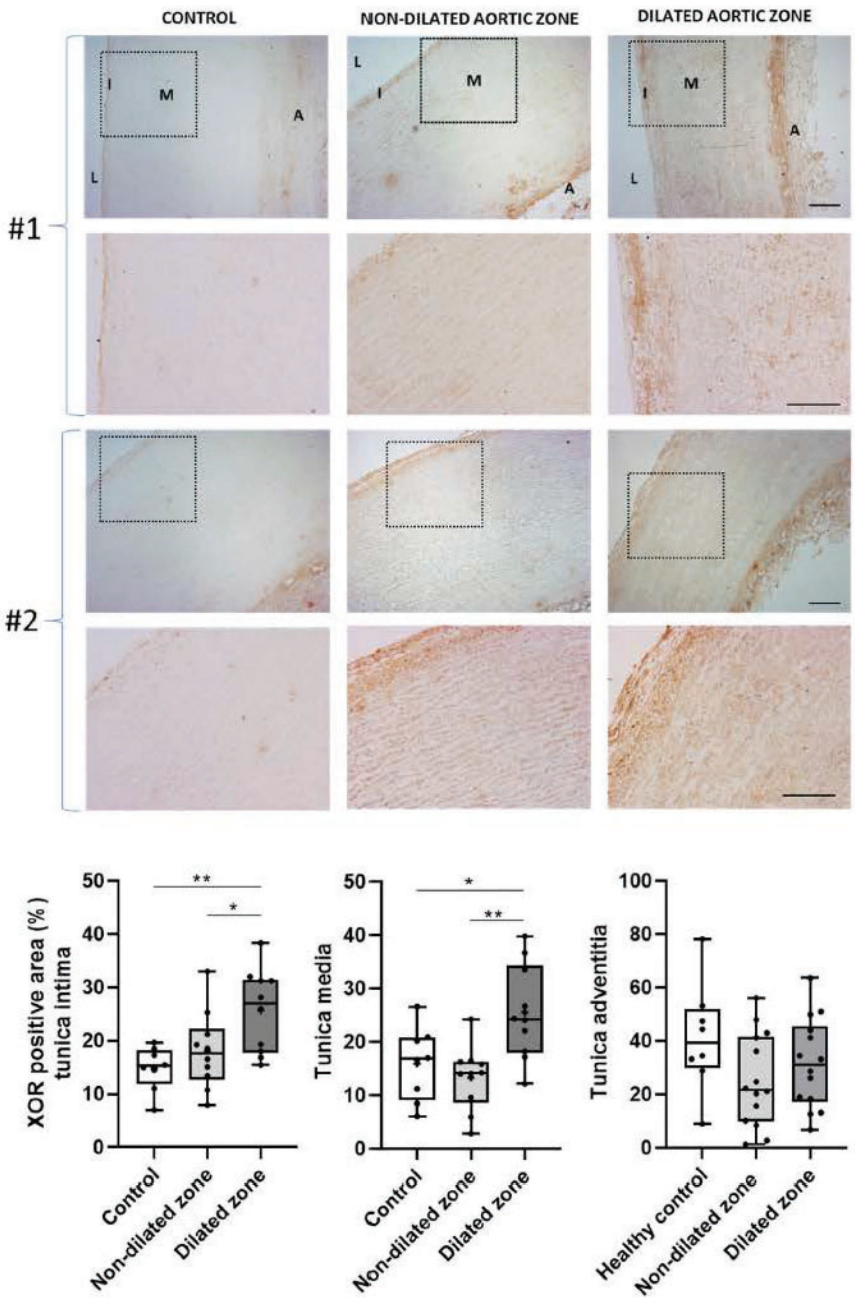

Fig. 1. Xanthine oxidoreductase is upregulated in the aorta of MFS patients. Representative images of XOR immunostaining in the ascending aorta from two healthy heart donors (control) and in the dilated and adjacent non-dilated aneurysmal zones of the aorta from two representative MFS patients (#1 and #2). The lower panels of each aortic sample are magnified images from the corresponding upper sample (black squares). L = lumen; I: tunica intima; M: tunica media; A: tunica adventitia. Below of images, quantitative analysis of immunolabeling results evaluated in tunicae intima, media, and adventitia. Bars, 100 μm. Statistical test analysis: One-way ANOVA; $*p \leq 0.05$ and $**p \leq 0.01$.

which is in accordance with transcriptional results (Fig. 2A). In this manner, results complement the previously reported upregulation of XOR in MFS mouse aortae [14].

3.3. Allopurinol inhibits the progression of aortic aneurysm and prevents its formation in MFS mice

The upregulation and activity of XOR in MFS aortae suggest its contribution to oxidative stress in MFS aortopathy. We hypothesized that the inhibition of its activity could ameliorate aortic aneurysm progression. To test this hypothesis, we treated WT and MFS mice with ALO. We first palliatively treated 2-month-old mice with ALO until 6 months of age (PA1; Fig. S1) and then evaluated aneurysm progression by ultrasonography. ALO significantly reduced the characteristic enlarged aortic root diameter occurring in MFS mice, the diameter obtained being highly similar to WT animals (Fig. 3A and Table S2). ALO did not cause any alteration in the aortic root diameter of WT mice. Moreover, no sex differences were observed regarding the effectiveness of ALO (Table S2).

We also evaluated aortic wall organization by histomorphology, quantifying the number of large elastic fiber ruptures as previously defined [45]. ALO treatment in MFS mice caused an apparent normalization of elastic fiber organization and integrity, their overall morphology being indistinguishable from non-treated WT animals (Fig. 3B).

ALO has also been safely administered during the late stages of

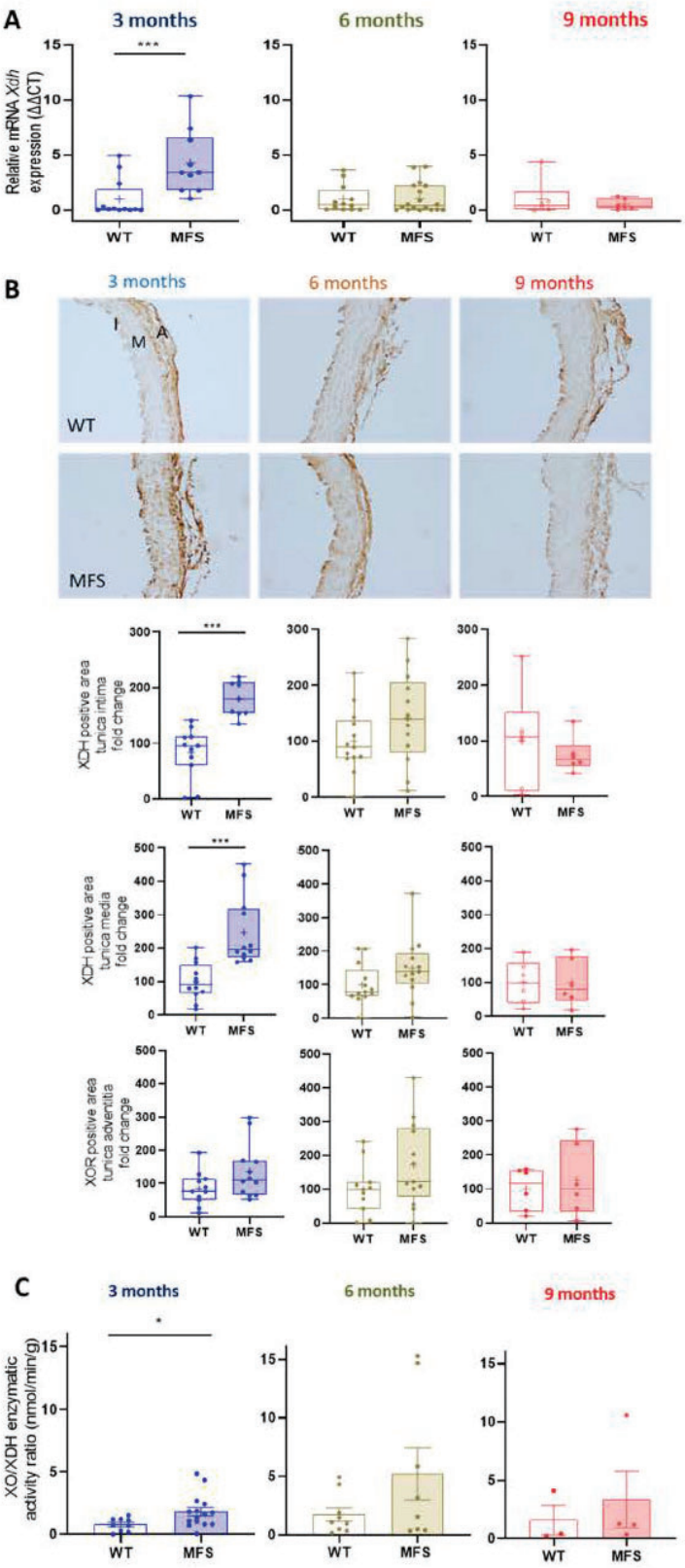

Fig. 2. XOR expression levels and enzymatic activity in the MFS mouse ascending aorta. (A) mRNA expression levels of XOR (*Xdh*) in WT and MFS mice of different ages (3-, 6- and 9-month-old). (B) XOR protein levels revealed by immunohistochemistry with anti-XOR antibodies in paraffin-embedded aortae from 3-, 6- and 9-month-old WT and MFS mice. Below of images, the quantitative analysis of the respective HRP immunostaining in tunicae intima (endothelial cell layer) (I), media (M) and adventitia (A). Bar, 100 μm. (C) XO/XDH enzymatic activity ratio in WT and 3-, 6-, and 9-month-old MFS mice. Data represented as boxplots. Statistical test analysis: Mann Whitney *U* test (A–C). ***$p \leq 0.001$ and *$p \leq 0.05$.

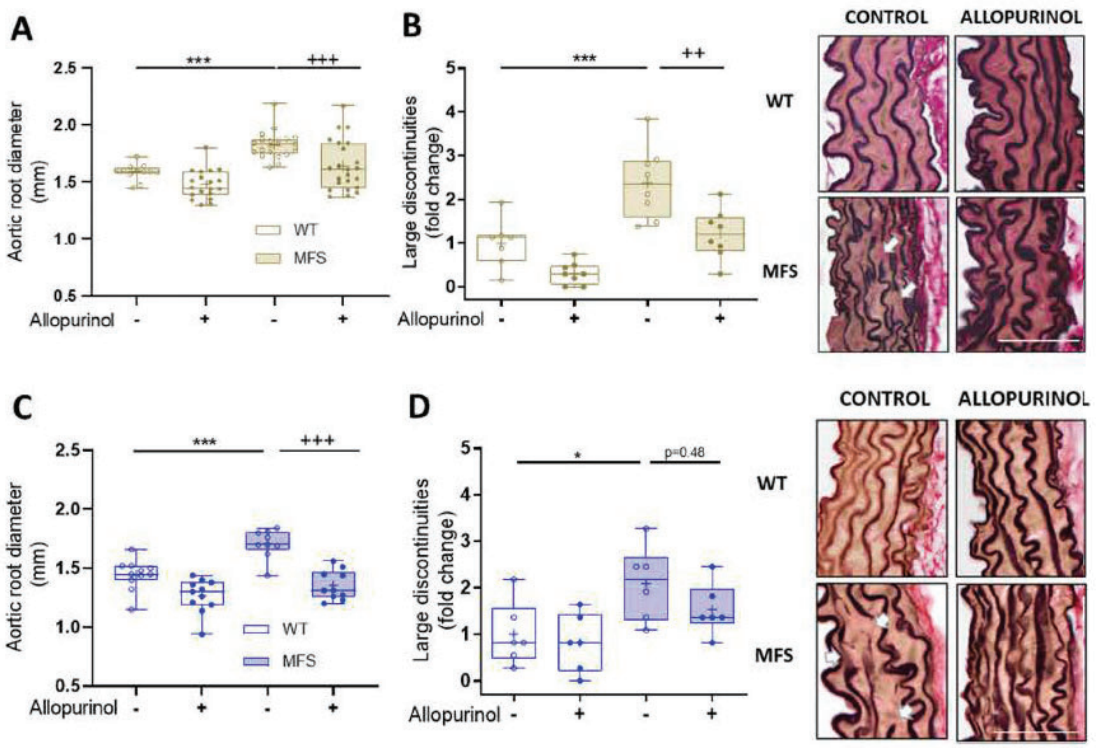

Fig. 3. Allopurinol prevents both the formation and progression of aortic root dilation in MFS mice. **(A)** Allopurinol halts the progression of aortic root dilatation in MFS mice measured by ultrasonography in WT and MFS mice of 6 months of age treated with allopurinol for 16 weeks (PA1). See also Table S2. **(B)** The number of large discontinuities in the elastic lamina of the aortic media from WT and MFS mice palliatively treated with allopurinol. **(C)** Allopurinol prevents the formation of aortic root dilatation in MFS mice measured by ultrasonography in 3-month-old WT and MFS mice preventively treated with allopurinol for 12 weeks (PE). See also Table S3. **(D)** Number of large discontinuities in the elastic lamina of the aortic media from WT and MFS mice preventively treated with allopurinol. On the right of panels B and D, representative Elastin Verhoeff-Van Gieson staining in paraffin sections of the ascending aorta. White arrows in B and D indicate examples of the large discontinuities analyzed. Bar, 100 μm. Data represented as boxplots. Statistical test analysis: Two-way ANOVA and Tukey post-test. $^{***/+++}p \leq 0.001$, $^{++}p \leq 0.01$ and $^{*}p \leq 0.05$; *effect of genotype; $^{+}$effect of treatment.

pregnancy, demonstrating efficiency in reducing uric acid, hypertension, and oxidative stress levels [46–49]. Therefore, we next evaluated whether ALO also prevented the formation of the aneurysm. ALO was administered to pregnant and lactating female mice and then to weaning offspring until the age of 3 months (PE; Fig. S1). ALO fully prevented aneurysm formation (Fig. 3C and Table S3), also showing a trend to reduce elastic fiber breaks (Fig. 3D).

We also analyzed the diameter of the tubular portion of the ascending aorta. In the PA1 treatment, ALO also normalized the diameter of MFS aortae (Fig. S3A; Table S4). However, this was not the case for the PE treatment (Fig. S3B; Table S5), likely because of the shorter ALO treatment and the younger age of the MFS mice treated, in which the ascending aorta was still not sufficiently affected as in the PA1 treatment.

3.4. The inhibition of aortopathy by allopurinol is reversible after drug withdrawal

We next examined whether the progression of the aortopathy inhibited by ALO was permanent or transient. To this end, we evaluated the aortic root diameter after the withdrawal of ALO following PA1 and PE treatments (PA1<ALO and PE < ALO, respectively; Fig. S1). When 6-month-old MFS animals were subjected to PA1 treatment with ALO and subsequently withdrawn from the drug for three months, until reaching 9 months of age, no statistical difference was obtained between their respective aortic root diameters (dashed red boxes of PA1<ALO 9-month-old MFS groups in Fig. S4A; Table S6). On the other hand, the 3-month-old animals subjected to PE treatment with ALO were withdrawn from the drug until reaching 6 months of age (WT and MFS groups labeled with red circles in Fig. S4B). There was no statistical difference between ALO-treated MFS groups regardless of whether ALO was subsequently withdrawn or not ($p = 0.08$) (dashed brown boxes of PE < ALO 6-month-old MFS groups in Fig. S4B; Table S7). Therefore, results show that the inhibitory effect of ALO on the aneurysm is only effective while the drug is administered.

3.5. Allopurinol prevents endothelial dysfunction in MFS ascending aorta

ROS generated by endothelial XOR could mediate alterations in the endothelial-associated vascular function by reducing NO bioavailability via direct interaction with O_2^- [32,33,50]. Previous evidence indicated that the MFS aorta shows endothelial dysfunction [14,51,52]. Thus, we analyzed the potential therapeutic effects of ALO treatment on endothelial function (Fig. 4). To this aim, we used wire-myography to measure the reactivity of endothelium-intact ascending aortas from 9-month-old MFS mice (PA2; Fig. S1), age at which, in our hands, endothelial dysfunctions were more clearly observed [52]. Firstly, we examined aortic root diameter in this mouse subset and the aneurysm was also inhibited after seven months of ALO treatment (PA2) (Fig. S5 and Table S8). Thereafter, ascending aortae were isolated, vessels were settled in the myograph and contracted with KCl to check their functionality (Fig. 4A). All aortae responded similarly to KCl (Fig. 4B and Table S10). The relaxant response to acetylcholine (ACh; Fig. 4A), mostly mediated by activation of endothelial NOS (NOS3), is an indicator of endothelial function. Untreated MFS mice showed a reduced sensitivity (pEC_{50}) to endothelium-dependent ACh-induced relaxation

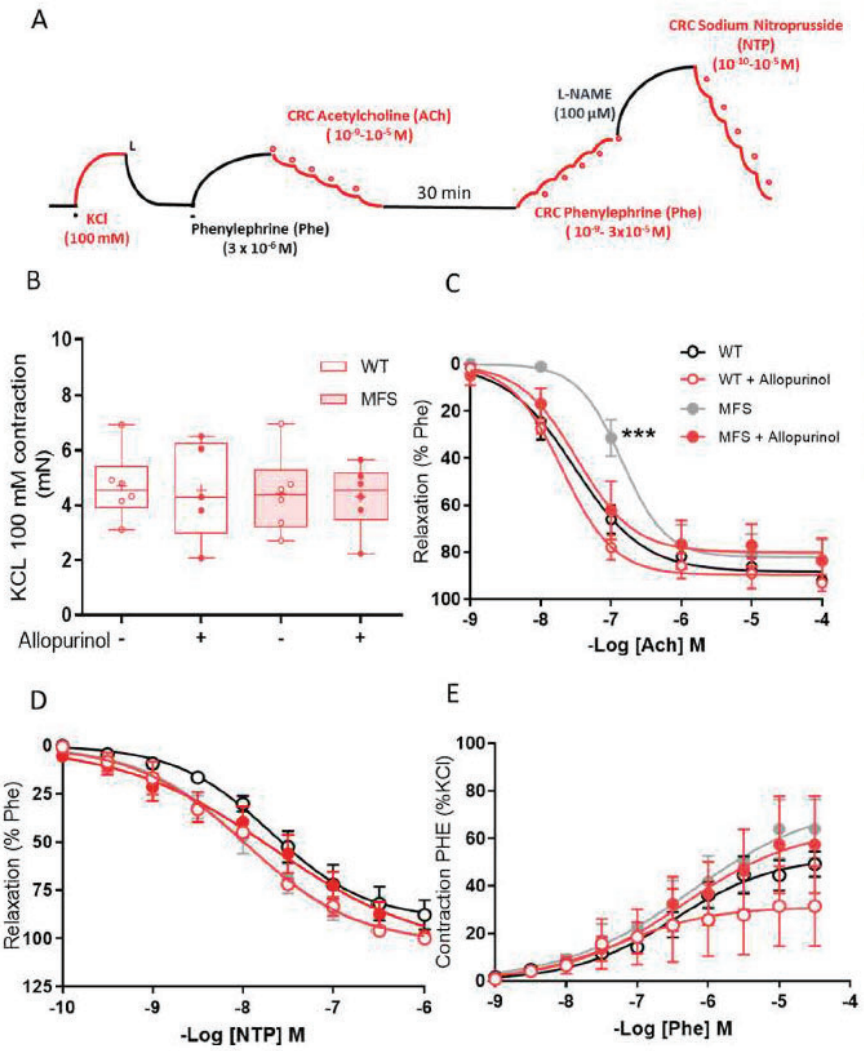

Fig. 4. Allopurinol prevents the endothelial vasodilation dysfunction of MFS aorta. (A) Experimental protocol for wire-myography experiments carried out in isolated 9-month-old ascending aorta from the diverse experimental groups indicated in the following panels. Red lines indicate where myographic measurements were obtained. (B) Physiological state test of aortic reactivity following the addition of KCl (100 mM). Data represented as boxplots. See also Table S10. (C) Relaxation of aortic reactivity following ACh addition. (D) Relaxation of reactivity after the addition of the NO donor sodium nitroprusside. (E) Contraction of aortic reactivity after the addition of phenylephrine. Data in C-E are mean ± SD. See also Tables S9 and S10. Statistical test tests: Two-way ANOVA and Tukey post-test (B); non-linear regression of data by fitting Phe/ACh/NTP concentration-response curves to a sigmoidal dose-response (C–E). ***$p \leq 0.001$. (For interpretation of the references to colour in this figure legend, the reader is referred to the Web version of this article.)

compared with WT (the curve shifted to the right in Fig. 4C/asterisks; Table S9), which indicated that ACh-mediated aortic relaxation was impaired in MFS mice and, therefore, demonstrative of dysfunctional endothelium. The treatment with ALO showed an ACh-induced relaxation in MFS aortae that was indistinguishable from WT animals (pEC_{50} 7.49 ± 0.19 and 7.52 ± 0.10, respectively) (Fig. 4C; Table S9), proving that ALO treatment normalizes endothelial function in MFS mice.

To check the participation of the NO/GC/cGMP pathway in the VSMCs of untreated MFS mice, we next added increased concentrations of the NO donor sodium nitroprusside (NTP) to aortae pre-contracted with phenylephrine (Phe) and the non-selective NOS inhibitor N (gamma)-nitro-L-arginine methyl ester (L-NAME; Fig. 4A), resulting in similar concentration-dependent aortic vasodilatations in untreated MFS and WT mice (Fig. 4D). No changes in the vasorelaxant response to NTP were observed following ALO administration either in WT or MFS mice (Fig. 4D; Table S9). We also evaluated the α_1-associated contractile response of ascending aortae when stimulated with different concentrations of Phe. Results were highly similar between non-treated MFS and WT ascending aortae or following ALO treatment (Fig. 4E; Table S10).

At this point of the study, there is an apparent inconsistency knowing that allopurinol is greatly inhibiting aortic aneurysm over the age in MFS mice (examined at 3-to-9 months old animals), but nevertheless XOR is only significantly increased in young animals (3 months-age). This means that other mechanisms directly or indirectly mediated by allopurinol must be affected. This conundrum is resolved below.

3.6. Allopurinol prevents increased levels of H_2O_2 in MFS aorta

Considering that ALO is clinically prescribed to treat hyperuricemia, we first measured UA and allantoin levels in blood plasma in WT and MFS mice to see potential changes associated with genotype or age or both. We noticed that neither UA nor allantoin, nor their ratio, showed any change between WT and MFS mice over age (Figs. S6A–C). Next, we analyzed whether ALO (PA1) reduced UA in blood plasma, but we observed that UA levels remained unaltered (Fig. S7). The possibility that the inhibition of aneurysm progression was mediated by reducing blood pressure as previously reported in other studies [53] was also discarded since systolic blood pressure values also remained unaltered (Fig. S8).

The aortopathy inhibition by ALO inhibiting XOR activity only happens in the early ages of MFS mice (3 months), but it cannot be explained in older animals. Therefore, other mechanism(s) must significantly participate in which redox stress should be directly or indirectly affected by ALO. In this regard, it was reported that ALO could directly scavenge ROS [54], thus, we measured ROS levels in blood

plasma and aorta from WT and MFS mice. We chose to measure H_2O_2 because it is the major ROS produced both by XOR under aerobic conditions [55], which occur in the heart and aorta, and by NOX4, which is upregulated in MFS aorta [17]. In blood plasma, we observed no differences with age between WT and MFS mice (Fig. S9). In contrast, ascending aorta rings from MFS mice showed significantly higher levels of H_2O_2 compared with WT mice of different ages (Fig. 5A). The *in vitro* administration of ALO to these aortic rings normalized H_2O_2 levels. This was also the case when ALO was administered *in vivo* in MFS mice (PE), whose aortic H_2O_2 levels were highly similar to those of untreated WT aortae (Fig. 5B). Therefore, ALO either prevented or inhibited the MFS-associated high levels of H_2O_2 in the ascending aorta irrespectively of *in vivo* or *in vitro* administration.

3.7. Allopurinol downregulates NOX4 and MMP2 expression in MFS aorta

Knowing that ALO blocks aortic aneurysm progression with age (3-, 6- and 9-month- old MFS mice), that aortic H_2O_2 levels also remain significantly elevated at these ages, and that XOR is only upregulated at early ages (3 months), we postulated that, regardless of its scavenging action, ALO could be directly or indirectly affecting other enzymatic H_2O_2 sources at the MFS aorta. In this regard, we next examined whether ALO treatments affected NOX4 expression, which greatly and directly produces H_2O_2 and whose expression and activity are abnormally increased in MFS aortae [17,18]. Thus, we evaluated NOX4 mRNA levels in the aorta of WT and MFS mice palliatively (PA1) and preventively (PE) treated with ALO. In both cases, ALO-treated MFS mice inhibited the characteristic upregulation of NOX4 in MFS aorta (Fig. 6A and B).

Another potential and complementary mechanism by which ALO, acting as an indirect antioxidant, could contribute to explaining the large reduction of MFS-associated aortic wall disarrays is by inhibiting the ROS-mediated activation of MPPs, as ROS are potent activators of MMPs [56]. MMP2 and MMP9, two well-known MMPs involved in MFS aortopathy [57] can be indirectly activated by ROS from their inactive-zymogen isoforms and via direct activation of their gene expression [58]. As expected, MFS aortae showed increased MMP2 protein levels in the tunica media compared with WT aorta. Both PE and PA1 ALO treatments inhibited the increased expression of MMP2 (Fig. 7).

3.8. Allopurinol prevents redox stress-associated injuries in the aortic tunica media of MFS mice

RNS can be produced due to the interaction of endothelial-generated NO and XDH-induced ROS [32,33]. Peroxynitrite and 3′-nitrotyrosine (3-NT) products are reliable redox stress biomarkers; immunohistochemical evaluation showed greater levels of 3-NT in the tunica media of MFS aortae. In both PA1 and PE approaches, ALO significantly prevented this increase (Figs. S10A and B).

The nuclear factor erythroid 2-related factor 2 (NRF2) is a key transcription factor that regulates the expression of several antioxidant defense mechanisms. Oxidative stress triggers its phosphorylation (pNRF2), being subsequently translocated to the nucleus to activate the expression response of physiological antioxidant enzymes [59]. Thus, we evaluated the nuclear presence of pNRF2 in aortic paraffin sections from WT and MFS mice treated with ALO after PA1 and PE treatments (Fig. 8A and B, respectively). Aortic media showed a higher presence of nuclear pNRF2 in MFS than WT VSMCs. This result demonstrated that

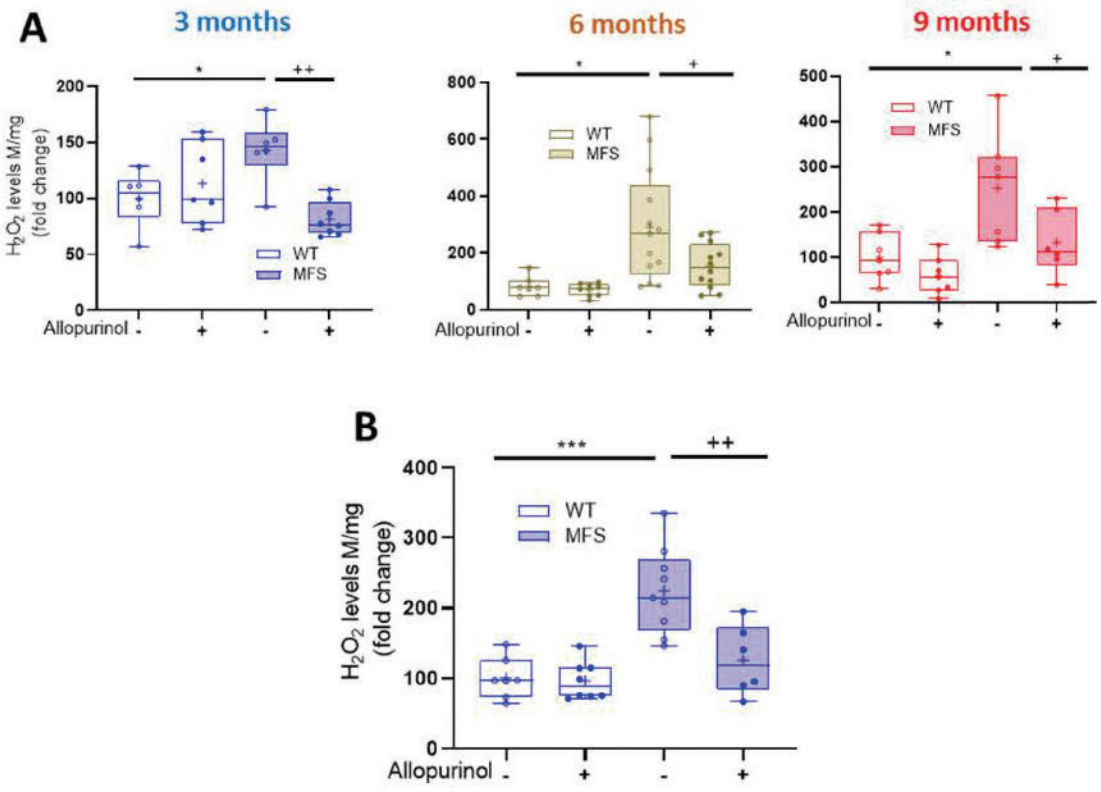

Fig. 5. High H_2O_2 levels generated in the ascending aorta of MFS mice are inhibited by allopurinol when administered both *in vitro* and *in vivo*. (A) H_2O_2 levels produced in ascending aortic rings over age in WT and MFS mice. Allopurinol was added *in vitro* to the assay containing aortic rings and the fluorescence signal measured after 2 h. (B) H_2O_2 levels measured in ascending aortic rings of WT and MFS mice preventively (PE) treated with allopurinol (*in vivo*). Data represented as boxplots. Statistical test analysis: Two-way ANOVA and Tukey's post-test $^{***}p \leq 0.001$, $^{++}p \leq 0.01$, $^{*/+}p \leq 0.05$; *effect of genotype; $^{+}$effect of treatment.

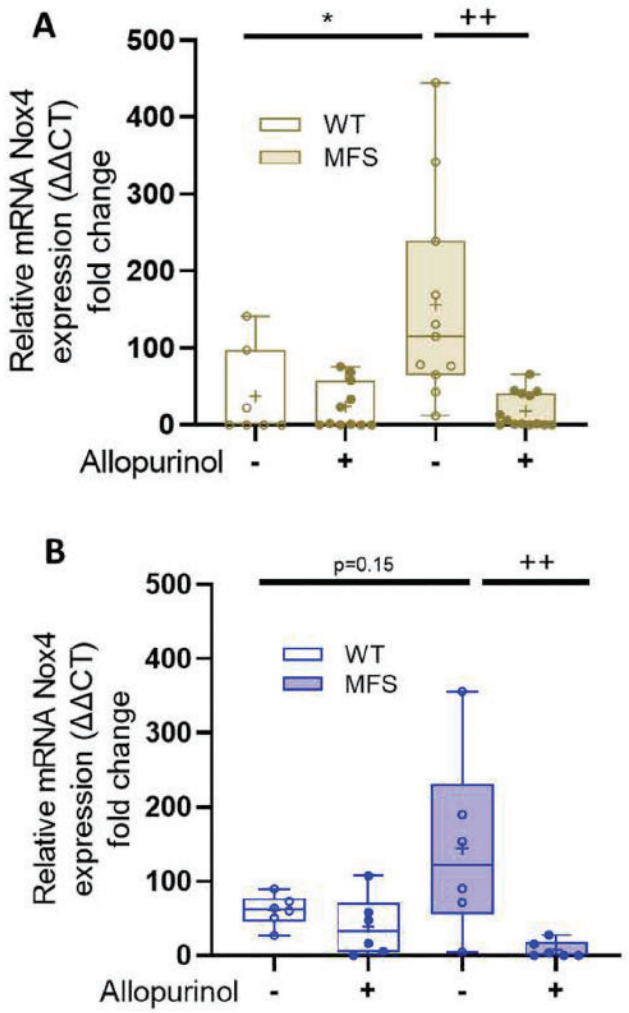

Fig. 6. Allopurinol prevents the upregulation of NADPH oxidase NOX4 in MFS aorta. mRNA expression levels of NOX4 in WT and MFS mice following the PA1 (A) or PE (B) allopurinol treatments. Statistical test analysis: Kruskal-Wallis and Dunn's multiple comparison test. $^{*/+}p \leq 0.05$ and $^{++}p \leq 0.01$; *effect of genotype; $^{+}$effect of treatment.

the MFS aorta suffered redox stress, which in turn triggered the endogenous antioxidant response. However, when ALO was administered to MFS mice, the number of pNRF2 stained nuclei was indistinguishable from WT aortae, regardless of the experimental treatment followed. This result is a logical consequence of the ALO-induced inhibition of the oxidative stress occurring in the MFS aorta.

Elastic fiber disruption in the MFS aorta is often accompanied by compensatory fibrotic-like remodeling supported by collagen overexpression and/or organization rearrangements occurring mainly in the tunica media [60]. This remodeling can be visualized under a polarized light microscope in paraffin-embedded aortae cross-sections stained with Picrosirius red [61]. We first evaluated total collagen content in the media quantifying Picrosirius staining and we did not observe any significant change (Fig. S11). We next analyzed green and red collagen fibers, which is illustrative of their different thickness and assembly compaction and, therefore, of their degree of maturity [62]. We observed an increase in immature (green) collagen fibers in the aortic tunica media of 6-month-old MFS mice (PA1 treatment). Notably, this collagen maturation remodeling was not produced after ALO treatment (PA1; Fig. 9). No differences were achieved in preventive ALO administration in MFS mice even though similar changes in green fibers tend to occur as well (Fig. S12). In PA1 and PE treatments, ALO did not reduce the increased trend of mature (red) collagen fiber formation (Fig. 9 and Fig. S12, respectively). Altogether, results indicated that ALO also reduced the collagen remodeling taking place in the aortic media of MFS mice.

4. Discussion

Over the last decade, significant progress has been made regarding the molecular mechanisms that participate in the formation and progression of aortic aneurysms in MFS but, until recently, current pharmacological approaches with angiotensin receptor blockers (ARBs; losartan), β blockers (atenolol) or both administered together have afforded uncertain results regarding halting or mitigating aortic aneurysm progression. Nonetheless, in a recent collaborative individual patient data meta-analysis of randomized trials for both treatments in MFS patients not submitted to aortic surgery, collected data showed that ARBs reduced the rate of increase of the aortic root Z score, even among those taking a β blocker [63]. Authors suggested that their additive combination would provide greater reductions in the rate of aortic enlargement than either treatment alone. Being undoubtedly good news, this does not rule out the possibility of using other new or repositioned complementary therapeutic options that specifically target other molecular processes having a relevant impact on aortopathy progression. With this idea in mind, the aim of our study was to obtain: (a) further insights into the contribution of redox stress to the molecular pathogenesis of aortic aneurysms. We have focused on XOR, which, jointly with NADPH oxidases, is a potent ROS-generating system in the cardiovascular system in health and disease; and (b) solid experimental evidence in a representative murine model of MFS to support a new pharmacological approach targeting redox stress (allopurinol), which could be easily translated to MFS patients.

This article produced several main findings: (i) XOR is upregulated in the aorta of both MFS patients and young mice; (ii) this upregulation is accompanied by increased enzymatic activity of the oxidase (XO) form in detriment of the dehydrogenase (XDH) from; (iii) the XOR inhibitor allopurinol (ALO) prevents both the formation and progression of aortic root dilation in MFS mice; (iv) this inhibitory effect is non-permanent since the withdrawal of ALO causes the reappearance of the aneurysm; (v) ALO prevents the characteristic MFS endothelial-dependent vasodilator dysfunction; (vi) ALO inhibits the MFS-associated increase of aortic H_2O_2 levels both *in vivo* and *in vitro* as well as the subsequent accompanying redox stress-associated reactions, such as accumulation of 3-NT, augmented nuclear translocation of pNRF2 and collagen remodeling of the aortic media; and (vii) ALO inhibits MFS-associated upregulation of NOX4 and reduces MMP2 expression in the aortic tunica media. Mechanistically, we postulated that ALO mitigates MFS aortopathy progression by acting as a potent antioxidant, both directly inhibiting XOR activity and scavenging ROS and indirectly downregulating NOX4 and MMP2 expression.

In aortic samples from MFS patients, XOR expression increased compared with healthy controls. This result was confirmed in MFS mice both at the protein and mRNA level. These changes were only observed in young (3-month-old) but not in older mice (6- and 9-month-old). It is possible that XOR upregulation only occurs while the aortic dilation undergoes rapid growth, which we found to occur until 3 months of age, becoming slower in older animals [45]. Nonetheless, no differences between WT and MFS aortae were observed regarding XOR activity in the study of the reactivity of MFS aorta [14], and after nitro-oleic acid treatment as a mediator in ERK1/2 and NOS2 expression in MFS aortopathy [64]. Explanations for this apparent discrepancy may be related to the different murine MFS models used (mgR/mgR and AngII infusion-induced acceleration of the aortopathy in MFS mouse, respectively) or the different XOR activity assays utilized, and/or even to local animal facility conditions.

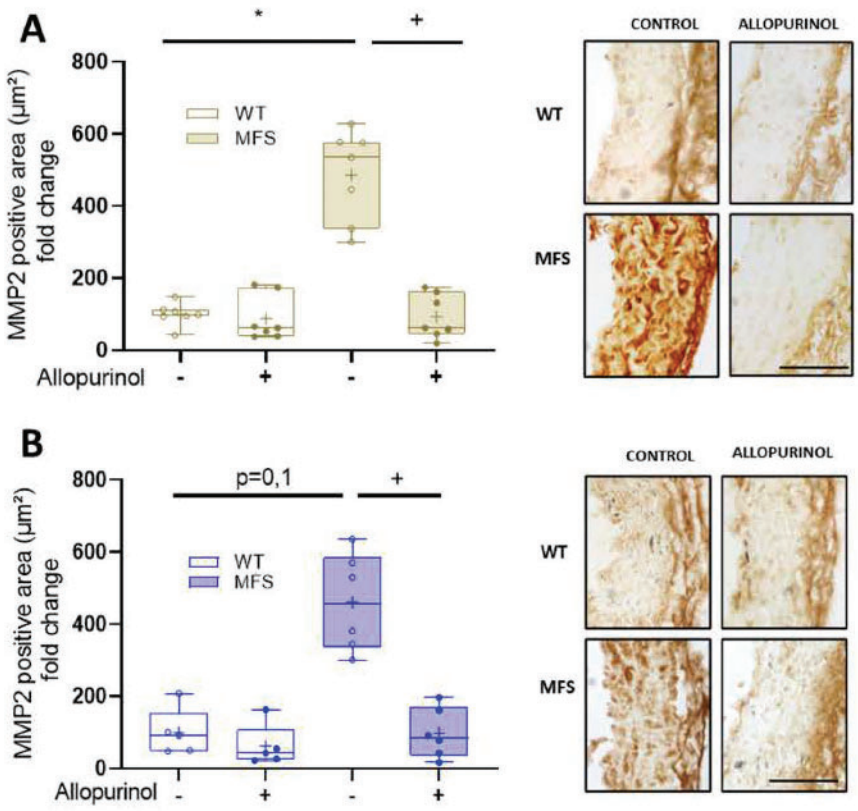

Fig. 7. Allopurinol reduces increased MMP2 levels in the tunica media of MFS aorta. MMP2 levels in the tunica media revealed by immunohistochemistry with anti-MMP2 antibodies in paraffin-embedded aortae from WT and MFS mice following palliative (PA1 (A) or preventive (PE) (B) administration of allopurinol. On the right, quantitative analysis of the respective HRP immunostaining. Bar, 100 µm. Statistical test analysis: Two-way ANOVA and Tukey's post-test $^{*/+}p \leq 0.05$. *Effect of genotype; $^{++}$effect of treatment.

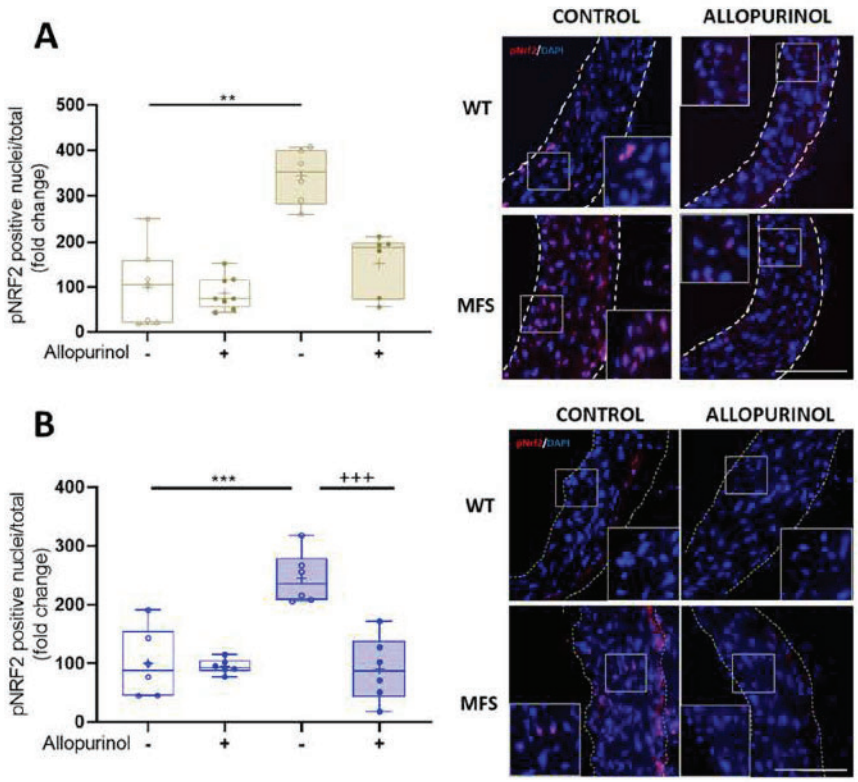

Fig. 8. Allopurinol inhibits the oxidative stress-associated increased nuclear translocation of pNRF2 in MFS aorta. Quantitative analysis and representative images of the nuclear translocation of the phosphorylated form of NRF2 in VSMCs of the tunica media of WT and MFS mice treated with allopurinol palliatively (PA1) (A) and preventively (PE) (B). Insets in the immunofluorescent images detail the nuclear localization of pNRF2. Bar, 100 µm. Statistical test: Kruskal-Wallis and Dunn's multiple comparison tests. $^{***/+++}p \leq 0.001$ $^{**}p \leq 0.01$; *effect of genotype; $^{+}$effect of treatment.

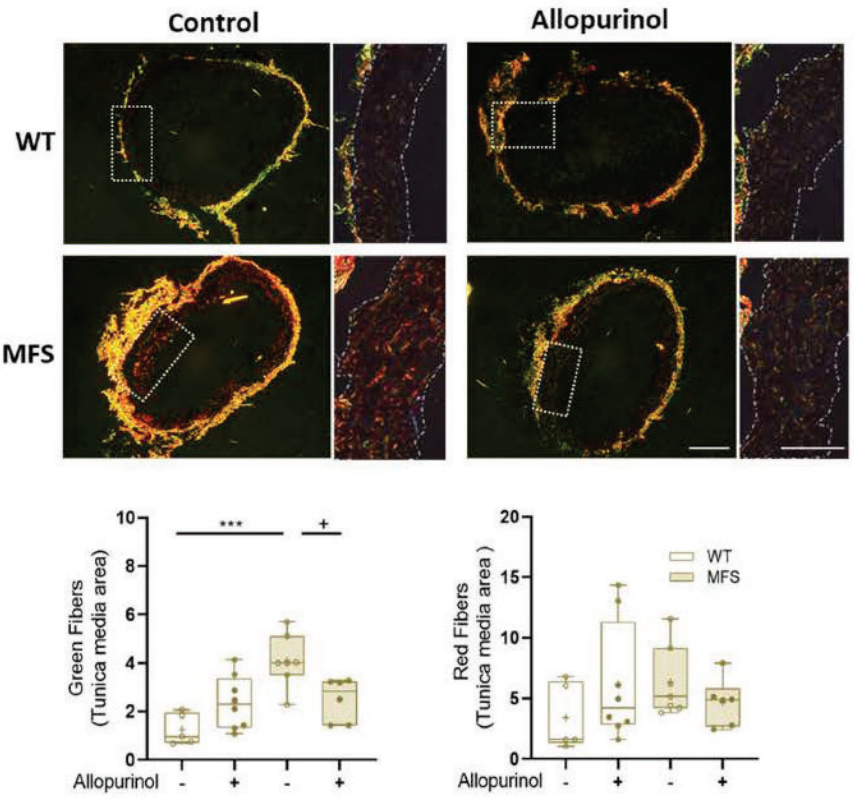

Fig. 9. Allopurinol reduces the MFS-associated collagen maturation remodeling of the tunica media. Immature (green) and mature (red) collagen fibers of the tunicae media and adventitia of WT and MFS aortae stained with Picrosirius red (see Fig. S11) visualized under the polarized microscope. WT and MFS mice were palliatively treated (PA1) or not with allopurinol. Representative fluorescent images of the whole aorta. On the right, images show the enhanced media outlined with white dots. Bar, 100 μm. The respective quantitative analysis of both types of collagen fibers is shown under the images. Statistical test: Kruskal-Wallis and Dunn's multiple comparison tests. ***$p \leq 0.001$ and $^{+}p \leq 0.05$; *effect of genotype; $^{+}$effect of treatment. (For interpretation of the references to colour in this figure legend, the reader is referred to the Web version of this article.)

ALO is a well-characterized specific inhibitor of XOR activity, mainly of the XO form [42], which was confirmed in the XOR enzymatic assay (Fig. S2). The main clinical actions of ALO are widely linked to UA-associated pathologies [65,66]. UA plasma levels were highly similar between MFS and WT animals, which at first glance discarded a UA-mediated effect in the aortopathy in MFS mice. Curiously, ALO did not cause the expected reduction of UA and/or allantoin plasma levels. However, it is important to highlight that the equivalent dose of ALO used here in mice (20 mg/kg/day) if administered to humans (~120 mg/day calculated for a weight of 70 Kg) [67] does not reduce normal plasma UA levels (≤6–7 mg/dL) [68]. Therefore, the blockade of MFS aortopathy by ALO is, in principle, not directly related to changes in UA, but to another accompanying mechanism(s).

Of note, ALO has a ROS lowering effect not necessarily related to its XOR inhibition activity, acting accordingly as a direct ROS scavenging moiety [68–71]. We demonstrated this possibility when ALO was added *in vitro* to MFS aortic rings, quickly attenuating their intrinsic increased H_2O_2 production levels, regardless of mouse age. Importantly, this reduction was also observed in aortic rings from MFS mice with the drug administered *in vivo*. In addition to the direct scavenging role of ALO, its effectiveness as a direct antioxidant can be reinforced, reducing the characteristic aortic upregulation of NOX4, knowing that NOX4 is the NADPH oxidase that directly generates H_2O_2 [72]. Pathological processes that usually accompany redox stress, such as the formation of 3-NT, pNRF2 nuclear translocation and fibrotic remodeling responses were all reduced or inhibited by ALO. The pathophysiological significance of these results in the MFS aortic media suggested several conclusions: (i) the accumulation of 3-NT is representative of abnormal RNS formation because of the pathological uncoupling of NO, which in turn leads to protein nitration via the formation of the highly reactive intermediate peroxynitrite and its subsequent product 3-NT [73]. This 3-NT upsurge in MFS aortic media is consistent with the recent demonstration of NO uncoupling in aneurysm formation in both MFS mice and patients [64,74,75]. Along this line of evidence, we identified actin as a nitrated protein target in MFS aorta from MFS patients [17], contributing, in this manner, to the reported damaged contractile properties of VSMCs in MFS [76]; (ii) redox stress is so elevated in MFS aorta that the intrinsic physiological antioxidant response mediated by the nuclear translocation of pNRF2 [60] is not high enough to compensate it. In contrast, ALO treatment allows this compensation, normalizing, to a large extent, the endogenous redox levels in MFS aorta and associated modifications; and (iii) ALO normalized the content of immature collagen (green) fibers, hence mitigating the collagen remodeling response that usually accompanies the aneurysm to compensate elastic fiber disarray. It would be interesting to know whether ALO is also able to prevent the characteristic phenotypic switch of VSMCs to a mixed contractile-secretory phenotype [77,78].

Of notice, ALO normalized ACh-stimulated vasodilator function, improving endothelial function. It is not a surprise given the reported effects of ALO on increasing NO bioavailability, totally or partially attributable to a reduction in ROS production [32]. Of notice, restoring the endothelial function is important since it has been reported in patients with MFS that flow-mediated dilatation (a noninvasive measurement of endothelial function) correlated with aortic dilatation [33].

In reference to the normalization by ALO treatments (PA1 and PE) of the structural aortic wall organization evidenced by the normalization of elastic laminae breaks, this effect could be explained by the inhibition of the ROS-mediated activation of MMP2 upregulation, which, together with MMP9, are two well-known MMPs upregulated and overactivated in MFS aorta [58]. Nonetheless, XOR itself can directly activate MMPs in a ROS-independent manner [79].

Finally, it cannot be discarded that ALO could also mediate its inhibitory action on aortopathy by acting as an anti-inflammatory agent [80] and/or also indirectly blocking the ROS-induced heat shock protein expression generating endoplasmic reticulum (ER) stress, which has an impact on abdominal and thoracic aortic aneurysms [81–84]. These two

possibilities deserve future attention.

We are aware that our study has some limitations: (i) ALO has a short half-life in plasma and is rapidly metabolized to oxypurinol, which has a longer lifespan [42]. It is possible that oxypurinol rather than allopurinol might be the primary metabolite that directly mediates the results we report herein. Nonetheless, in this respect, it is important to take into account that it is not recommended to administer higher doses of ALO in humans (>300 mg/day) because the high concentration of oxypurinol generated then acts as a pro-oxidant instead of antioxidant, favoring oxidative stress [68]; (ii) the MFS model used in our study (C1041G) is a very useful model to evaluate the temporal course of aortopathy (besides other clinical manifestations), but it is not the most suitable to evaluate the survival rate after ALO treatments. Other, more severe MFS murine models for aortic dissection and rupture, such as the *Fbn1* hypomorphic mouse (mgR/mgR) [85] or the AngiotensinII-induced accelerated model of MFS aortopathy [64], both leading to aortic dissection and rupture, would be more appropriate experimental murine models for this aim; and (iii) the aortic arch and descending thoracic aorta have not been studied; (iv) we have only studied ALO's effects on the cardiovascular system (TAA more specifically) because it is responsible for the life-threatening complication in MFS; and (v) even though ALO has been widely proven to be a safe and well-tolerated drug, it would also be of interest to evaluate if ALO has further beneficial or detrimental effects on other affected organ systems as MFS is a multisystemic disorder.

5. Conclusion

Our results definitively place redox stress among the molecular mechanisms that significantly participate in the pathogenesis of aortic aneurysm in MFS by the persistent high production levels of ROS mediated by upregulation of XOR (current study), the NADPH oxidase NOX4 [17], eNOS dysfunction [74] and mitochondrial electron transport-associated redox stress [86], all from studies performed both in MFS murine models and patients. How, and to what extent, do each of these interlinked mechanisms participate in aortic injury is currently unknown, but most likely they all act additively or synergistically to damage the aorta severely and permanently. We here demonstrated ALO's effectiveness, acting as a strong antioxidant drug in MFS aortae directly both as an inhibitor of XOR activity in early ages when XOR is overexpressed, and as ROS scavenger in the absence of XOR activity, and indirectly by downregulating NOX4 and MMP2 overexpression. ALO is an economic drug, which has been widely prescribed in clinical practice since the latter half of the last century and, most importantly, has been proven to be effective, safe, and usually well tolerated. ALO has been reported to present lower rates of cardiovascular events (related to hypertension) compared with non-treated patients [87]. Of note, a preprint study reported that febuxostat has similar effects to ALO, blocking MFS aortopathy [88]. Febuxostat is another specific XOR inhibitor not resembling purines or pyrimidines [89]. Some concerns regarding cardiovascular safety have been reported for febuxostat compared with ALO [90], but a recent study seems to refute this concern [91]. In sum, our results in MFS mice support the design of a clinical trial with ALO as having a potential beneficial effect in the pharmacological clinical practice of MFS patients. Last, but not least, such a potential benefit could only be obtained when the drug is administered chronically.

Sources of funding

This work has been funded by a poorly endowed grant from the Spanish Ministry of Science and Innovation PID2020-113634RB-C2 to GE and FJ-A, and PID2019-110906RB-I00 to MCG-C.

CRediT authorship contribution statement

Isaac Rodríguez-Rovira: Methodology, Investigation, Writing – review & editing. **Cristina Arce:** Methodology, Data curation, Formal analysis, Investigation, Writing – review & editing. **Karo De Rycke:** Methodology, Investigation, Writing – review & editing. **Belén Pérez:** Methodology, Investigation, Writing – review & editing. **Aitor Carretero:** Methodology, Writing – review & editing. **Marc Arbonés:** Methodology, Writing – review & editing. **Gisela Teixidò-Turà:** Supervision, Writing – review & editing. **Mari Carmen Gómez-Cabrera:** Funding acquisition, Supervision, Writing – review & editing. **Victoria Campuzano:** Investigation, Supervision, Writing – review & editing. **Francesc Jiménez-Altayó:** Methodology, Investigation, Funding acquisition, Supervision, Writing – review & editing. **Gustavo Egea:** Conceptualization, Funding acquisition, Supervision, Data curation, Investigation, Writing – original draft, Writing – review & editing.

Declaration of competing interest

None.

Acknowledgments

G.E. dedicates this article to the memory of Professor Mercedes Durfort i Coll (1943–2022). We deeply thank Isabel Fabregat and Hal Dietz for reviews and comments on previous versions of the manuscript, Ana Paula Dantas (IDIBAPS) and Coral Sanfeliu (CSIC) for helpful methodological advice with H_2O_2 fluorometric measurements, Helena Kruyer for patient editorial assistance, and Maria Encarnación Palomo and María Teresa Muñoz for excellent technical assistance and lab management, respectively.

Appendix A. Supplementary data

Supplementary data to this article can be found online at https://doi.org/10.1016/j.freeradbiomed.2022.11.001.

References

[1] H.C. Dietz, C.R. Cutting, R.E. Pyeritz, C.L. Maslen, L.Y. Sakai, G.M. Corson, E. G. Puffenberger, A. Hamosh, E.J. Nanthakumar, S. Curristin, et al., Marfan syndrome caused by a recurrent de novo missense mutation in the fibrillin gene, Nature 352 (1991) 337–339, https://doi.org/10.1038/352337a0.

[2] M.G. Keane, R.E. Pyeritz, Medical management of Marfan syndrome, Circulation 117 (2008) 2802–2813, https://doi.org/10.1161/CIRCULATIONAHA.107.693523.

[3] H. Sies, Oxidative eustress: on constant alert for redox homeostasis, Redox Biol. 41 (2021), 101867, https://doi.org/10.1016/j.redox.2021.101867.

[4] T.J. Costa, P.R. Barros, C. Arce, J.D. Santos, J. da Silva-Neto, G. Egea, A.P. Dantas, R.C. Tostes, F. Jiménez-Altayó, The homeostatic role of hydrogen peroxide, superoxide anion and nitric oxide in the vasculature, Free Radic. Biol. Med. 162 (2021) 615–635, https://doi.org/10.1016/j.freeradbiomed.2020.11.021.

[5] O. Chen, O. Wang, J. Zhu, O. Xiao, L. Zhang, Reactive oxygen species: key regulators in vascular health and diseases, Br. J. Pharmacol. 175 (2018) 1279–1292, https://doi.org/10.1111/bph.13828.

[6] F.J. Miller, W.J. Sharp, X. Fang, L.W. Oberley, T.D. Oberley, N.L. Weintraub, Oxidative stress in human abdominal aortic aneurysms, Arterioscler. Thromb. Vasc. Biol. 22 (2002) 560–565, https://doi.org/10.1161/01.ATV.0000013778.72404.30.

[7] M.L. McCormick, D. Gavrila, N.L. Weintraub, Role of oxidative stress in the pathogenesis of abdominal aortic aneurysms, Arterioscler. Thromb. Vasc. Biol. 27 (2007) 461–469, https://doi.org/10.1161/01.ATV.0000257552.94483.14.

[8] D. Sánchez-Infantes, M. Nus, M. Navas-Madroñal, J. Fité, B. Pérez, A.J. Barros-Membrilla, B. Soto, J. Martínez-González, M. Camacho, C. Rodriguez, et al., Oxidative stress and inflammatory markers in abdominal aortic aneurysm, Antioxidants 10 (2021) 602, https://doi.org/10.3390/antiox10040602.

[9] C. Aivatidi, G. Vourliotakis, S. Georgopoulos, F. Sigala, E. Bastounis, E. Papalambros, Oxidative stress during abdominal aortic aneurysm repair–biomarkers and antioxidant's protective effect: a review, Eur. Rev. Med. Pharmacol. Sci. 15 (2011) 245–252.

[10] J. Pincemail, J.O. Defraigne, J.P. Cheramy–Bien, N. Dardenne, A.F. Donneau, A. Albert, N. Labropoulos, N. Sakalihasan, On the potential increase of the oxidative stress status in patients with abdominal aortic aneurysm, Redox Rep. 17 (2012) 139–144, https://doi.org/10.1179/1351000212Y.0000000012.

[11] S.S. Portelli, B.D. Hambly, R.W. Jeremy, E.N. Robertson, Oxidative stress in genetically triggered thoracic aortic aneurysm: role in pathogenesis and therapeutic opportunities, Redox Rep. 26 (2021) 45–52, https://doi.org/10.1080/13510002.2021.1899473.

[12] J. Ejiri, N. Inoue, T. Tsukube, T. Munezane, Y. Hino, S. Kobayashi, K. Hirata, S. Kawashima, S. Imajoh-Ohmi, Y. Hayashi, et al., Oxidative stress in the

pathogenesis of thoracic aortic aneurysm Protective role of statin and angiotensin II type 1 receptor blocker, Cardiovasc. Res. 59 (2003) 988–996, https://doi.org/10.1016/s0008-6363(03)00523-6.
[13] C. Fiorillo, M. Becatti, M. Attanasio, L. Lucarini, N. Nassi, L. Evangelisti, M. C. Porciani, P. Nassi, G.F. Gensini, R. Abbate, et al., Evidence for oxidative stress in plasma of patients with Marfan syndrome, Int. J. Cardiol. 145 (2010) 544–546, https://doi.org/10.1016/j.ijcard.2010.04.077.
[14] H.H.C. Yang, C. van Breemen, A.W.Y. Chung, Vasomotor dysfunction in the thoracic aorta of Marfan syndrome is associated with accumulation of oxidative stress, Vasc. Pharmacol. 52 (2010) 37–45, https://doi.org/10.1016/j.vph.2009.10.005.
[15] E. Branchetti, P. Poggio, R. Sainger, E. Shang, J.B. Grau, B.M. Jackson, E.K. Lai, M. S. Parmacek, R.C. Gorman, J.H. Gorman, et al., Oxidative stress modulates vascular smooth muscle cell phenotype via CTGF in thoracic aortic aneurysm, Cardiovasc. Res. 100 (2013) 316–324, https://doi.org/10.1093/cvr/cvt205.
[16] A.M. Zúñiga-Muñoz, I. Pérez-Torres, V. Guarner-Lans, E. Núñez-Garrido, R. Velázquez Espejel, C. Huesca-Gómez, R. Gamboa-Ávila, M.E. Soto, Glutathione system participation in thoracic aneurysms from patients with Marfan syndrome, Vasa 46 (2017) 177–186, https://doi.org/10.1024/0301-1526/a000609.
[17] F. Jiménez-Altayó, T. Meirelles, E. Crosas-Molist, M.A. Sorolla, D.G. del Blanco, J. López-Luque, A. Mas-Stachurska, A.M. Siegert, F. Bonorino, L. Barberà, et al., Redox stress in Marfan syndrome: dissecting the role of the NADPH oxidase NOX4 in aortic aneurysm, Free Radic. Biol. Med. 118 (2018) 44–58, https://doi.org/10.1016/j.freeradbiomed.2018.02.023.
[18] F. Emrich, K. Penov, M. Arakawa, N. Dhablania, G. Burdon, A.J. Pedroza, T. K. Koyano, Y.M. Kim, U. Raaz, et al., Anatomically specific reactive oxygen species production participates in Marfan syndrome aneurysm formation, J. Cell Mol. Med. 23 (2019) 7000–7009, https://doi.org/10.1111/jcmm.14587.
[19] G. Egea, F. Jiménez-Altayó, V. Campuzano, Reactive oxygen species and oxidative stress in the pathogenesis and progression of genetic diseases of the connective tissue, Antioxidants 9 (2020) 2013, https://doi.org/10.3390/antiox9101013.
[20] J. Rysz, A. Gluba-Brzózka, R. Rokicki, B. Franczyk, Oxidative stress-related susceptibility to aneurysm in Marfan's syndrome, Biomedicines 9 (2021) 1171, https://doi.org/10.3390/biomedicines9091171.
[21] L. Polito, M. Bortolotti, M.G. Battelli, A. Bolognesi, Xanthine oxidoreductase: a leading actor in cardiovascular disease drama, Redox Biol. 24 (2021), 102195, https://doi.org/10.1016/j.redox.2021.102195.
[22] K. Ichida, Y. Amaya, K. Noda, S. Minoshima, T. Hosoya, O. Sakai, N. Shimizu, T. Nishino, Cloning of the cDNA encoding human xanthine dehydrogenase (oxidase): structural analysis of the protein and chromosomal location of the gene, Gene 133 (1993) 279–284, https://doi.org/10.1016/0378-1119(93)90652-j.
[23] C.M. Harris, S.A. Sanders, V. Massey, Role of the flavin midpoint potential and NAD binding in determining NAD versus oxygen reactivity of xanthine oxidoreductase, J. Biol. Chem. 274 (1999) 4561–4569, https://doi.org/10.1074/jbc.274.8.4561.
[24] F. Lacy, D.A. Gough, G.W. Schmid-Schönbein, Role of xanthine oxidase in hydrogen peroxide production, Free Radic. Biol. Med. 25 (1998) 720–727, https://doi.org/10.1016/s0891-5849(98)00154-3.
[25] M.G. Battelli, L. Polito, M. Bortolotti, A. Bolognesi, Xanthine oxidoreductase in drug metabolism: beyond a role as a detoxifying enzyme, Curr. Med. Chem. 23 (2016) 4027–4036, https://doi.org/10.2174/0929867323666160725091915.
[26] A. Sarnesto, N. Linder, K.O. Raivio, Organ distribution and molecular forms of human xanthine dehydrogenase/xanthine oxidase protein, Lab. Invest. 74 (1996) 48–56.
[27] H.P. Friedl, D.J. Smith, G.O. Till, P.D. Thomson, D.S. Louis, P.A. Ward, Ischemia-reperfusion in humans. Appearance of xanthine oxidase activity, Am. J. Pathol. 136 (1990) 491–495.
[28] S. Sakuma, Y. Fujimoto, Y. Sakamoto, T. Uchiyama, K. Yoshioka, H. Nishida, T. Fujita, Peroxynitrite induces the conversion of xanthine dehydrogenase to oxidase in rabbit liver, Biochem. Biophys. Res. Commun. 230 (1997) 476–479, https://doi.org/10.1006/bbrc.1996.5983.
[29] J.S. McNally, A. Saxena, H. Cai, S. Dikalov, D.G. Harrison, Regulation of xanthine oxidoreductase protein expression by hydrogen peroxide and calcium, Arterioscler. Thromb. Vasc. Biol. 25 (2005) 1623–1628, https://doi.org/10.1161/01.ATV.0000170827.16296.6e.
[30] D.A. Parks, D.N. Granger, Xanthine oxidase: biochemistry, distribution and physiology, Acta Physiol. Scand. Suppl. 548 (1986) 87–99.
[31] T. Maruhashi, I. Hisatome, Y. Kihara, Y. Higashi, Hyperuricemia and endothelial function: from molecular background to clinical perspectives, Atherosclerosis 278 (2018), 226231, https://doi.org/10.1016/j.atherosclerosis.2018.10.007.
[32] M. Houston, P. Chumley, R. Radi, H. Rubbo, B.A. Freeman, Xanthine oxidase reaction with nitric oxide and peroxynitrite, Arch. Biochem. Biophys. 355 (1998) 1–8, https://doi.org/10.1006/abbi.1998.0675.
[33] M. Takata, E. Amiya, M. Watanabe, K. Omori, Y. Imai, D. Fujita, H. Nishimura, M. Kato, T. Morota, K. Nawata, et al., Impairment of flow-mediated dilation correlates with aortic dilation in patients with Marfan syndrome, Heart Ves. 29 (2014) 478–485, https://doi.org/10.1007/s00380-013-0393-3.
[34] M.E. Soto, L.G. Manzano-Pech, V. Guarner-Lans, J.A. Díaz-Galindo, X. Vásquez, V. Castrejón-Tellez, R. Gamboa, C. Huesca, G. Fuentevilla-Alvárez, I. Pérez-Torres, Oxidant/antioxidant profile in the thoracic aneurysm of patients with the Loeys-Dietz syndrome, Oxid. Med. Cell. Longev. 2020 (2020), 5392454, https://doi.org/10.1155/2020/5392454.
[35] J. Maiuolo, F. Oppedisano, S. Gratteri, C. Muscoli, V. Mollace, Regulation of uric acid metabolism and excretion, Int. J. Cardiol. 213 (2016) 8–14, https://doi.org/10.1016/j.ijcard.2015.08.109.
[36] G. Glantzounis, E. Tsimoyiannis, A. Kappas, D. Galaris, Uric acid and oxidative stress, Curr. Pharmaceut. Des. 11 (2005) 4145–4151, https://doi.org/10.2174/138161205774913255.
[37] D.H. Kang, S.K. Ha, Uric Acid Puzzle: Dual Role as Anti-oxidant and Pro-oxidant, vol. 12, Electrolyte Blood Press, 2014, pp. 1–6, https://doi.org/10.5049/EBP.2014.12.1.
[38] P. Patetsios, W. Rodino, W. Wiisselink, D. Bryan, J.D. Kirwin, T.F. Panetta, Identification of uric acid in aortic aneurysms and atherosclerotic artery, Ann. N. Y. Acad. Sci. 800 (1996) 243–245, https://doi.org/10.1111/j.1749-6632.1996.tb33318.x.
[39] A.M. Esen, M. Akcakoyun, O. Esen, G. Acar, Y. Emiroglu, S. Pala, F. Kargin, H. Karapinar, O. Ozcan, I. Barutcu, Uric acid as a marker of oxidative stress in dilatation of the ascending aorta, Am. J. Hypertens. 24 (2011) 149–154, https://doi.org/10.1038/ajh.2010.219.
[40] W.L. Jiang, X. Qi, X. Li, Y.F. Zhang, Q.Q. Xia, J.C. Chen, Serum uric acid is associated with aortic dissection in Chinese men, Int. J. Cardiol. 202 (2016) 196–197, https://doi.org/10.1016/j.ijcard.2015.08.174.
[41] G. Ndrepepa, Uric acid and cardiovascular disease, Clin. Chim. Acta 484 (2018) 150–163, https://doi.org/10.1016/j.cca.2018.05.046.
[42] R.O. Day, G.G. Graham, M. Hicks, A.J. McLachlan, S.L. Stocker, K.M. Williams, Clinical pharmacokinetics and pharmacodynamics of allopurinol and oxypurinol, Clin. Pharmacokinet. 46 (2007) 623–644, https://doi.org/10.2165/00003088-200746080-00001.
[43] A. Kelkar, A. Kuo, W.H. Frishman, Allopurinol as a cardiovascular drug, Cardiol. Rev. 19 (2011) 265–271, https://doi.org/10.1097/CRD.0b013e318229a908.
[44] K. Huang, Y. Wang, K.L. Siu, Y. Zhang, H. Cai, Targeting feed-forward signaling of TGFβ/NOX4/DHFR/eNOS uncoupling/TGFβ axis with anti-TGFβ and folic acid attenuates formation of aortic aneurysms: novel mechanisms and therapeutics, Redox Biol. 38 (2021), 101757, https://doi.org/10.1016/j.redox.2020.101757.
[45] C. Arce, I. Rodríguez-Rovira, K. de Rycke, K. Durán, V. Campuzano, I. Fabregat, F. Jiménez-Altayó, P. Berraondo, G. Egea, Anti-TGFβ (Transforming Growth Factor β) therapy with betaglycan-derived P144 peptide gene delivery prevents the formation of aortic aneurysm in a mouse model of Marfan Syndrome, Arterioscler. Thromb. Vasc. Biol. 41 (2021) e440–e452, https://doi.org/10.1161/ATVBAHA.121.316496.
[46] N. Masaoka, Y. Nakajima, Y. Hayakawa, S. Ohgame, S. Hamano, M. Nagaishi, T. Yamamoto, Transplacental effects of allopurinol on suppression of oxygen free radical production in chronically instrumented fetal lamb brains during intermittent umbilical cord occlusion, J. Matern. Fetal Neonatal Med. 18 (2005) 1–7, https://doi.org/10.1080/14767050500127716.
[47] H.L. Torrance, M.J. Benders, J.B. Derks, C.M.A. Rademaker, A.F. Bos, P. van den Berg, M. Longini, G. Buonocore, M. Venegas, H. Baquero, G.H.A. Visser, F. van Bel, Maternal allopurinol during fetal hypoxia lowers cord blood levels of the brain injury marker S-100B, Pediatrics 124 (2009) 350–357, https://doi.org/10.1542/peds.2008-2228.
[48] J.B. Derks, M.A. Oudijk, H.L. Torrance, C. Rademaker, M.J. Benders, K.G. Rosen, T. Cindrova-Davies, A.S. Thakor, G.H.A. Visser, G.J. Burton, et al., Allopurinol reduces oxidative stress in the ovine fetal cardiovascular system following repeated episodes of ischemia-reperfusion, Pediatr. Res. 68 (2010) 374–380, https://doi.org/10.1203/PDR.0b013e3181ef7780.
[49] Y. Niu, A.D. Kane, C.M. Lusby, B.M. Allison, Y.Y. Chua, J.J. Kaandorp, R. Nevin-Dolan, T.J. Ashmore, H.L. Blackmore, J.B. Derks, et al., Maternal allopurinol prevents cardiac dysfunction in adult male offspring programmed by chronic hypoxia during pregnancy, Hypertension 72 (2018) 971–978, https://doi.org/10.1161/HYPERTENSIONAHA.118.11363.
[50] E.E. Kelley, A new paradigm for XOR-catalyzed reactive species generation in the endothelium, Pharmacol. Rep. 67 (2015) 669–674, https://doi.org/10.1016/j.pharep.2015.05.004.
[51] A.W.Y. Chung, K. Au Yeung, S.F. Cortes, G.G.S. Sandor, D.P. Judge, H.C. Dietz, C. van Breemen, Endothelial dysfunction and compromised eNOS/Akt signaling in the thoracic aorta during the progression of Marfan syndrome, Br. J. Pharmacol. 150 (2007) 1075–1083, https://doi.org/10.1038/sj.bjp.0707181.
[52] F. Jiménez-Altayó, A.M. Siegert, F. Bonorino, T. Meirelles, L. Barberà, A.P. Dantas, E. Vila, G. Egea, Differences in the thoracic aorta by region and sex in a murine model of Marfan syndrome, Front. Physiol. 8 (2017) 933, https://doi.org/10.3389/fphys.2017.00933.
[53] V. Agarwal, N. Hans, F.H. Messerli, Effect of allopurinol on blood pressure: a systematic review and meta-analysis, J. Clin. Hypertens. 15 (2013) 435–442, https://doi.org/10.1111/j.1751-7176.2012.00701.x.
[54] J. Robak, E. Marcinkiewicz, Scavenging of reactive oxygen species as the mechanism of drug action, Pol. J. Pharmacol. 47 (1995) 89–98.
[55] E.E. Kelley, N.K.H. Khoo, N.J. Hundley, U.Z. Malik, B.A. Freeman, M.M. Tarpey, Hydrogen peroxide is the major oxidant product of xanthine oxidase, Free Radic. Biol. Med. 48 (2010) 493–498, https://doi.org/10.1016/j.freeradbiomed.2009.11.012.
[56] M.G. Battelli, L. Polito, M. Bortolotti, A. Bolognesi, Xanthine oxidoreductase-derived reactive species: physiological and pathological effects, Oxid. Med. Cell. Longev. 2016 (2016), 3527579, https://doi.org/10.1155/2016/3527579.
[57] A.W. Chung, K. Au Yeung, G.G. Sandor, D.P. Judge, H.C. Dietz, C. van Breemen, Loss of elastic fiber integrity and reduction of vascular smooth muscle contraction resulting from the upregulated activities of matrix metalloproteinase-2 and -9 in the thoracic aortic aneurysm in Marfan syndrome, Circ. Res. 101 (2007) 512–522, https://doi.org/10.1161/CIRCRESAHA.107.157776.
[58] F. Valentin, J.L. Bueb, P. Kieffer, E. Tschirhart, J. Atkinson, Oxidative stress activates MMP-2 in cultured human coronary smooth muscle cells, Fundam. Clin.

Pharmacol. 19 (2005) 661–667, https://doi.org/10.1111/j.1472-8206.2005.00371.x.
[59] Q. Ma, Role of Nrf2 in oxidative stress and toxicity, Annu. Rev. Pharmacol. Toxicol. 53 (2013) 401–426, https://doi.org/10.1146/annurev-pharmtox-011112-140320.
[60] J.H.N. Lindeman, B.A. Ashcroft, J.W.M. Beenakker, M. van Es, N.B.R. Koekkoek, F. A. Prins, J.F. Tielemans, H. Abdul-Hussien, R.A. Bank, T.H. Oosterkamp, Distinct defects in collagen microarchitecture underlie vessel-wall failure in advanced abdominal aneurysms and aneurysms in Marfan syndrome, Proc. Natl. Acad. Sci. USA 107 (2010) 862–865, https://doi.org/10.1073/pnas.0910312107.
[61] L. Rittié, Method for Picrosirius red polarization detection of collagen fibers in tissue sections, Methods Mol. Biol. 1627 (2017) 395–407, https://doi.org/10.1007/978-1-4939-7113-8_26.
[62] J. López-Guimet, L. Peña-Pérez, R.S. Bradley, P. García-Canadilla, C. Disney, H. Geng, A.J. Bodey, P.J. Withers, B. Bijnens, M.J. Sherratt, et al., MicroCT imaging reveals differential 3D micro-scale remodelling of the murine aorta in ageing and Marfan syndrome, Theranostics 8 (2018) 6038–6052, https://doi.org/10.7150/thno.26598.
[63] A. Pitcher, E. Spata, J. Emberson, K. Davies, H. Halls, L. Holland, K. Wilson, C. Reith, A.H. Child, T. Clayton, et al., Marfan Treatment Trialists' Collaboration. Angiotensin receptor blockers and β blockers in Marfan syndrome: an individual patient data meta-analysis of randomised trials, Lancet 400 (2022) 822–831, https://doi.org/10.1016/S0140-6736(22)01534-3.
[64] F.S. Nettersheim, J. Lemties, S. Braumann, S. Geißen, S. Bokredenghel, R. Nies, A. Hof, H. Winkels, B.A. Freeman, A. Klinke, et al., Nitro-oleic acid (NO2-OA) reduces thoracic aortic aneurysm progression in a mouse model of Marfan syndrome, Cardiovasc. Res. (2021), https://doi.org/10.1093/cvr/cvab256 cvab256.
[65] C. Chen, J.M. Lü, Q. Yao, Hyperuricemia-related diseases and xanthine oxidoreductase (XOR) inhibitors: an overview, Med. Sci. Monit. 22 (2016) 2501–2512, https://doi.org/10.12659/msm.899852.
[66] M. Bove, A.F.G. Cicero, M. Veronesi, C. Borghi, An evidence-based review on urate-lowering treatments: implications for optimal treatment of chronic hyperuricemia, Vasc. Health Risk Manag. 13 (2017) 23–28, https://doi.org/10.2147/VHRM.S115080.
[67] S. Reagan-Shaw, M. Nihal, N. Ahmad, Dose translation from animal to human studies revisited, Faseb. J. 22 (2008) 659–661, https://doi.org/10.1096/fj.07-9574LSF.
[68] L.K. Stamp, T.R. Merriman, M.L. Barclay, J.A. Singh, R.L. Roberts, D.F. Wright, N. Dalbeth, Impaired response or insufficient dosage? Examining the potential causes of "inadequate response" to allopurinol in the treatment of gout, Semin. Arthritis Rheum. 44 (2014) 170–174, https://doi.org/10.1016/j.semarthrit.2014.05.007.
[69] D.K. Das, R.M. Engelman, R. Clement, H. Otani, M.R. Prasad, P.S. Rao, Role of xanthine oxidase inhibitor as free radical scavenger: a novel mechanism of action of allopurinol and oxypurinol in myocardial salvage, Biochem. Biophys. Res. Commun. 148 (1987) 314–319, https://doi.org/10.1016/0006-291x(87)91112-0.
[70] J. George, Role of urate, xanthine oxidase and the effects of allopurinol in vascular oxidative stress, Vasc. Health Risk Manag. 5 (2009) 265–272, https://doi.org/10.2147/vhrm.s4265.
[71] S.D. Ricardo, J.F. Bertram, G.B. Ryan, Podocyte architecture in puromycin aminonucleoside-treated rats administered tungsten or allopurinol, Exp. Nephrol. 3 (1995) 270–279.
[72] S.P. Gray, A.M. Shah, I. Smyrnias, NADPH oxidase 4 and its role in the cardiovascular system, Vasc. Biol. 1 (2019) H59–H66, https://doi.org/10.1530/VB-19-0014.
[73] R. Radi, Protein tyrosine nitration: biochemical mechanisms and structural basis of functional effects, Acc. Chem. Res. 46 (2013) 550–559, https://doi.org/10.1021/ar300234c.
[74] J. Oller, N. Méndez-Barbero, E.J. Ruiz, S. Villahoz, M. Renard, L.I. Canelas, A. M. Briones, R. Alberca, N. Lozano-Vidal, M.A. Hurlé, et al., Nitric oxide mediates aortic disease in mice deficient in the metalloprotease Adamts1 and in a mouse model of Marfan syndrome, Nat. Med. 23 (2017) 200–212, https://doi.org/10.1038/nm.4266.
[75] A. de la Fuente-Alonso, M. Toral, A. Alfayate, M.J. Ruiz-Rodríguez, E. Bonzón-Kulichenko, G. Teixido-Tura, S. Martínez-Martínez, M.J. Méndez-Olivares, D. López-Maderuelo, I. González-Valdés, et al., Aortic disease in Marfan syndrome is caused by overactivation of sGC-PRKG signaling by NO, Nat. Commun. 12 (2021) 2628, https://doi.org/10.1038/s41467-021-22933-3.
[76] D. Milewicz, D.C. Guo, V. Tran-Fadulu, A.L. Lafont, C.L. Papke, S. Inamoto, C. S. Kwartler, H. Pannu, Genetic basis of thoracic aortic aneurysms and dissections: focus on smooth muscle cell contractile dysfunction, Annu. Rev. Genom. Hum. Genet. 9 (2008) 283–302, https://doi.org/10.1146/annurev.genom.8.080706.092303.
[77] E. Crosas-Molist, T. Meirelles, J. López-Luque, C. Serra-Peinado, J. Selva, L. Caja, D. Gorbenko del Blanco, J.J. Uriarte, E. Bertran, Y. Mendizábal, et al., Vascular smooth muscle cell phenotypic changes in patients with Marfan syndrome, Arterioscler. Thromb. Vasc. Biol. 35 (2015) 960–972, https://doi.org/10.1161/ATVBAHA.114.304412.
[78] A.J. Pedroza, Y. Tashima, R. Shad, P. Cheng, R. Wirka, S. Churovich, K. Nakamura, N. Yokoyama, J.Z. Cui, C. Iosef, et al., Single-cell transcriptomic profiling of vascular smooth muscle cell phenotype Modulation in Marfan syndrome aortic aneurysm, Arterioscler. Thromb. Vasc. Biol. 40 (2020) 2195–2211, https://doi.org/10.1161/ATVBAHA.120.314670.
[79] W. Liu, G.A. Rosenberg, H. Shi, T. Furuichi, G.S. Timmins, L.A. Cunningham, K. J. Liu, Xanthine oxidase activates pro-matrix metalloproteinase-2 in cultured rat vascular smooth muscle cells through non-free radical mechanisms, Arch. Biochem. Biophys. 426 (2004) 11–17, https://doi.org/10.1016/j.abb.2004.03.029.
[80] N. Schlesinger, L. Brunetti, Beyond urate lowering: analgesic and anti-inflammatory properties of allopurinol, Semin. Arthritis Rheum. 50 (2019) 444–450, https://doi.org/10.1016/j.semarthrit.2019.11.009.
[81] J. Nishizawa, A. Nakai, K. Matsuda, M. Komeda, T. Ban, K. Nagata, Reactive oxygen species play an important role in the activation of heat shock factor 1 in Ischemic-reperfused heart, Circulation 99 (1999) 934–941, https://doi.org/10.1161/01.cir.99.7.934.
[82] A.M. Siegert, G. García Díaz-Barriga, A. Esteve-Codina, M. Navas-Madroñal, D. Gorbenko del Blanco, J. Alberch, S. Heath, M. Galán, G. Egea, A FBN1 3′UTR mutation variant is associated with endoplasmic reticulum stress in aortic aneurysm in Marfan syndrome, Biochim. Biophys. Acta, Mol. Basis Dis. 1865 (2019) 107–114, https://doi.org/10.1016/j.bbadis.2018.10.029.
[83] M. Navas-Madroñal, C. Rodriguez, M. Kassan, J. Fité, J.R. Escudero, L. Cañes, J. Martínez-González, M. Camacho, M. Galán, Enhanced endoplasmic reticulum and mitochondrial stress in abdominal aortic aneurysm, Clin. Sci. (Lond.) 133 (2019) 1421–1438, https://doi.org/10.1042/CS20190399.
[84] L. Pereira, S.Y. Lee, B. Gayraud, K. Andrikopoulos, S.D. Shapiro, T. Bunton, N. J. Biery, H.C. Dietz, L.Y. Sakai, F. Ramirez, Pathogenetic sequence for aneurysm revealed in mice underexpressing fibrillin-1, Proc. Natl. Acad. Sci. U.S.A. 96 (1999) 3819–3823, https://doi.org/10.1073/pnas.96.7.3819.
[85] J. Oller, E. Gabandé-Rodríguez, M.J. Ruiz-Rodríguez, G. Desdín-Micó, J.F. Aranda, R. Rodrigues-Diez, C. Ballesteros-Martínez, E.M. Blanco, R. Roldan-Montero, P. Acuña, et al., Extracellular tuning of mitochondrial respiration leads to aortic aneurysm, Circulation 143 (2021) 2091–2109, https://doi.org/10.1161/CIRCULATIONAHA.120.051171.
[86] R.L. MacIsaac, J. Salatzki, P. Higgins, M.R. Walters, S. Padmanabhan, A. F. Dominiczak, R.M. Touyz, J. Dawson, Allopurinol and cardiovascular outcomes in adults with hypertension, Hypertension 67 (2016) 535–540, https://doi.org/10.1161/HYPERTENSIONAHA.115.06344.
[88] H. Yagi, H. Akazawa, Q. Liu, K. Yamamoto, K. Nawata, A. Saga-Kamo, M. Umei, H. Kadowaki, R. Matsuoka, A. Shindo, et al., Aberrant mechanosensitive signaling underlies activation of vascular endothelial xanthine oxidoreductase that promotes aortic aneurysm formation in Marfan syndrome, bioRxiv (2022), https://doi.org/10.1101/2022.01.30.478356.
[87] M.E. Ernst, M.A. Fravel, Febuxostat: a selective xanthine-oxidase/xanthine-dehydrogenase inhibitor for the management of hyperuricemia in adults with gout, Clin. Therapeut. 31 (2009) 2503–2518, https://doi.org/10.1016/j.clinthera.2009.11.033.
[89] W.B. White, K.G. Saag, M.A. Becker, J.S. Borer, P.B. Gorelick, A. Whelton, B. Hunt, Gunawardhana L. Castillo, C Investigators. Cardiovascular safety of febuxostat or allopurinol in patients with gout, N. Engl. J. Med. 378 (2008) 1200–1210, https://doi.org/10.1056/NEJMoa1710895.
[90] I.S. Mackenzie, I. Ford, G. Nuki, J. Hallas, C.J. Hawkey, J. Webster, S.H. Ralston, M. Walters, M. Robertson, R.D. Caterina, et al., Long-term cardiovascular safety of febuxostat compared with allopurinol in patients with gout (FAST): a multicenter, prospective, randomized, open-label, non-inferiority trial, Lancet 396 (2020) 1745–1757, https://doi.org/10.1016/S0140-6736(20)32234-0.
[91] J. George, E. Carr, J. Davies, J.J. Belch, A. Struthers, High-dose allopurinol improves endothelial function by profoundly reducing vascular oxidative stress and not by lowering uric acid, Circulation 114 (2006) 2508–2516, https://doi.org/10.1161/CIRCULATIONAHA.106.651117.
[92] G. Lastra, C. Manrique, G. Jia, A.R. Aroor, M.R. Hayden, B.J. Barron, B. Niles, J. Padilla, J.R. Sowers, Xanthine oxidase inhibition protects against Western diet-induced aortic stiffness and impaired vasorelaxation in female mice, Am. J. Physiol. Regul. Integr. Comp. Physiol. 313 (2017) R67–R77, https://doi.org/10.1152/ajpregu.00483.2016.
[93] K.M. Kim, G.N. Henderson, X. Ouyang, R.F. Frye, Y.Y. Sautin, D.I. Feig, R. J. Johnson, A sensitive and specific liquid chromatography–tandem mass spectrometry method for the determination of intracellular and extracellular uric acid, J. Chromatogr. B Anal. Technol. Biomed. Life 877 (2009) 2032–2038, https://doi.org/10.1016/j.jchromb.2009.05.037.
[94] M.A.S. El Mubarak, Lamari, C. Kontoyannis, Simultaneous determination of allantoin and glycolic acid in snail mucus and cosmetic creams with high performance liquid chromatography and ultraviolet detection, J. Chromatogr. 1322 (2013) 49–53, https://doi.org/10.1016/j.chroma.2013.10.006.
[95] Y. Onetti, F. Jiménez-Altayó, M. Heras, E. Vila, A.P. Dantas, Western-type diet induces senescence, modifies vascular function in non-senescence mice and triggers adaptive mechanisms in senescent ones, Exp. Gerontol. 48 (2013) 1410–1419, https://doi.org/10.1016/j.exger.2013.09.004.
[96] J.S. Beckman, D.A. Parks, J.D. Pearson, P.A. Marshall, B.A. Freeman, A sensitive fluorometric assay for measuring xanthine dehydrogenase and oxidase in tissues, Free Radic. Biol. Med. 6 (1989) 607–615, https://doi.org/10.1016/0891-5849(89)90068-3.

SUPPLEMENTAL MATERIAL

ALLOPURINOL BLOCKS AORTIC ANEURYSM IN A MOUSE MODEL OF MARFAN SYNDROME BY REDUCING AORTIC OXIDATIVE STRESS

Short title: *Allopurinol inhibits Marfan syndrome aortopathy*

Isaac Rodríguez-Rovira[1,*], Cristina Arce[1,*,†], Karo De Rycke[1,*,¶], Belén Pérez[2], Aitor Carretero[3], Marc Arbonés[1], Gisela Teixidò-Turà[4], Mari Carmen Gómez-Cabrera[3], Victoria Campuzano[1,5], Francesc Jiménez-Altayó[2] and Gustavo Egea[1,#]

[1] Department of Biomedical Sciences, University of Barcelona School of Medicine and Health Sciences, 08036 Barcelona, Spain.

[2] Department of Pharmacology, Toxicology and Therapeutics, Neuroscience Institute, School of Medicine, Autonomous University of Barcelona, 08193 Cerdanyola del Vallès, Spain.

[3] Department of Physiology, Faculty of Medicine, University of Valencia, CIBERFES, Fundación Investigación Hospital Clínico Universitario/INCLIVA, Valencia, Spain.

[4] Department of Cardiology, Hospital Universitari Vall d'Hebron, Barcelona, Spain. CIBER-CV, Vall d'Hebrón Institut de Recerca (VHIR), Barcelona, Spain

[5] Centro de Investigación Biomédica en Red de Enfermedades Raras (CIBERER), ISCIII, Spain.

[#] Corresponding author: Gustavo Egea, Dept. Biomedicina, Facultat de Medicina i Ciències de la Salut, Universitat de Barcelona, c/ Casanova 143, 08036 Barcelona, Spain, +34648557759, gegea@ub.edu

* These authors contributed equally to this work.

¶ Present address: Department of Biomolecular Medicine, Center for Medical Genetics, Ghent University, Ghent, Belgium.

† Present address: Department of Biology, University of Padova, Padova, Italy.

CONTENT

1. MATERIAL AND METHODS

Human tissue collection, mice, and experimental designs

Healthy ascending aortic tissue was collected from heart donors via the organ donation organization at the Hospital Clínic i Provincial (Barcelona, Spain) and Hospital de Bellvitge (L'Hospitalet de Llobregat, Barcelona, Spain). The age and gender of heart donors were unknown because Spanish law protects personal information about organ donors. Ascending aortic aneurysm samples were collected from patients with Marfan syndrome (MFS) (with ages ranging from 17 to 60 years) undergoing aortic aneurysm repair surgery. All the patients in whom aortae were resected fulfilled MFS diagnostic criteria according to Ghent nosology, but no genetic information regarding putative *FBN1* mutations was available. For each patient, we obtained a 3 x 3 cm sample from two areas: the dilated zone, corresponding to the sinuses of Valsalva, and the adjacent virtually non-dilated aorta (according to the surgeon's opinion) corresponding to the distal ascending aorta. The aortae were maintained in cold saline solution or cardioprotective solution before delivery to the laboratory.

MFS mice with a fibrillin-1 mutation *(Fbn1*$^{C1041G/+}$*;* hereafter C1041G*)* (hereafter, MFS mice) were purchased from The Jackson Laboratory (B6.129-Fbn1tm1Hcd/J; Strain #012885/Common name: C1039G; Bar Harbor, ME

04609, USA). MFS and sex- and age-matched wild-type littermates (WT mice) were maintained in a C57BL/6J genetic background. All mice were housed according to the University of Barcelona institutional guidelines (constant room temperature at 22ºC, controlled environment 12/12-hour light/dark cycle, 60% humidity and *ad libitum* access to food and water).

WT and MFS mice were administered allopurinol (hereafter ALO) (A8003, Sigma-Aldrich) diluted in drinking water (20 mg/kg/day; 125 mg/mL) [92,93]. ALO was fully replaced each third day of treatment. We performed two experimental ALO treatment approaches: palliative (PA) and preventive (PE). For PA treatments, ALO was administered to mice of 2 months of age until 6-month-old (PA1) or 9-month-old (PA2) being a respective effective treatment of 4 and 7 months, respectively (Fig. S1). For PE treatment, ALO was administered to the pregnant WT mother, maintained after giving birth (lactation period of 25 days) and thereafter maintained in drinking water to weaned babies until three months of age. To evaluate whether ALO's effect on aortopathy was transient or permanent, the inhibitor was withdrawn from drinking water (<ALO) for a period of three months following the PE and PA1 experimental treatments with 6- and 9-month age endpoints (PE<ALO and (PA1<ALO, respectively; Fig. S1). At each outcome time points, mice were subjected to echocardiographic analysis. Both the ascending aorta and liver were dissected and fixed for paraffin embedding for (immuno)histological studies or immersed in RNA Later (R-0901, Sigma Aldrich), frozen in liquid nitrogen and stored at -80ºC for molecular tests.

Study approvals

Human tissues were collected with the required approval from the Institutional Clinical Review Board of Spanish clinical centers, and the patients' written consent conformed to the ethical guidelines of the 1975 Declaration of Helsinki. Patients were informed about the use for research studies of their extracted aortic samples. All aortic tissues described in the manuscript were those obtained from Spanish Marfan patients and heart donors. Due to the Spanish Data Protection Act, we do not have access to their clinical history or personal data.

Animal care and colony maintenance conformed to the European Union (Directive 2010/63/EU) and Spanish guidelines (RD 53/2013) for the use of experimental animals. Ethical approval was obtained from the local animal ethics committee (CEEA protocol approval number 10340).

Echocardiography

Two-dimensional transthoracic echocardiography was performed in all animals under 1.5% inhaled isoflurane. Each animal was scanned 12–24 hours before sacrifice. Images were obtained with a 10–13 MHz phased array linear transducer (IL12i GE Healthcare, Madrid, Spain) in a Vivid Q system (GE Healthcare, Madrid, Spain). Images were recorded and later analyzed offline using commercially available software (EchoPac v.08.1.6, GE Healthcare, Madrid, Spain). Proximal aortic segments were assessed in a parasternal long-axis view. The aortic root diameter was measured from inner edge to inner edge in end-diastole at the level of the sinus of Valsalva. All echocardiographic measurements were carried out in a blinded manner by two independent

investigators at two different periods, and with no knowledge of genotype or treatment.

Histology and histomorphometry

Paraffin-embedded tissue arrays of mice aortae from different experimental sets were cut into 5 μm sections. Elastic fiber ruptures were quantified by counting the number of large fiber breaks in tissue sections stained with Verhoeff-Van Gieson. Breaks larger than 20 μm were defined as evident large discontinuities in the normal circumferential continuity (360º) of each elastic lamina in the aortic media[45]. They were counted along the length of each elastic lamina in four different, representative images of three non-consecutive sections of the same ascending aorta. The number of sections studied for condition were usually of three, spacing 10 μm between them (2 sections). All measurements were carried out in a blinded manner by two different observers with no knowledge of genotype and treatment. Images were captured using a Leica Leitz DMRB microscope (40x oil immersion objective) equipped with a Leica DC500 camera and analyzed with Fiji Image J Analysis software.

Immunohistochemistry and immunofluorescence staining

For immunohistochemistry and/or immunofluorescence, paraffin-embedded aortic tissue sections (5 μm thick) were deparaffinized and rehydrated prior to unmasking the epitope. Horseradish peroxidase (HRP)-based immunohistochemistry was used to stain aortic tissue sections for XOR and 3'-nitrotyrosine (3-NT). To unmask XOR epitopes, aortic tissue sections were treated with a retrieval solution (10 mM sodium citrate, 0.05% Tween, pH 6) for

30 min in the steamer at 95ºC. No antigen retrieval was used for 3-NT. Next, sections were incubated for 10 min with peroxidase blocking solution (Dako Real Peroxidase-blocking solution), rinsed three times with PBS and then incubated with 1% BSA in PBS prior to overnight incubation at 4ºC with the respective primary polyclonal antibodies anti-XOR (1:50; Rockland 200-4183S) or anti-3-NT (1:200; Merck Millipore 06-284). On the next day, sections were incubated with the manufacturer's goat anti-rabbit secondary antibody solution (1:500; Abcam ab97051) for 1 h followed by the Liquid DAB+Substrate Chromogen System (Dako System HRP) for 1 min at room temperature. HRP-stained non-consecutive sections were visualized under a Leica Leitz DMRB microscope (40x immersion oil objective).

Immunofluorescence was used to stain pNRF2 in aortic sections. Sections were treated first with heat-mediated retrieval solution (1 M Tris-EDTA, 0.05% Tween, pH 9) for 30 min in the steamer at 95ºC. Next, sections were incubated for 20 minutes with ammonium chloride (NH_4Cl, 50 mM, pH 7.4) to block free aldehyde groups, followed by a permeabilization step using 0.3% Triton X-100 for 10 min and then treated with 1% BSA blocking buffer solution for 2 h prior to overnight incubation with monoclonal anti-pNRF2 (1:200; Abcam ab76026) in a humidified chamber at 4°C. On the next day, sections were rinsed with PBS, followed by 60 min incubation with the secondary antibody goat anti-rabbit Alexa 647 (1:1.000, A-21246, Invitrogen). Sections were counterstained with DAPI (1:10.000) and images were acquired using an AF6000 widefield fluorescent microscope.

For quantitative analysis of immunostainings, four areas of each ascending aorta section were quantified with Image J software. All measurements were carried out in a blinded manner by two independent investigators.

Uric acid, allantoin and hydrogen peroxide in blood plasma and in ascending aortic rings

Blood from mice was collected directly from the left ventricle just before the aortic tissue was dissected. Thereafter, the blood plasma was obtained by centrifugation of the blood at 3,000 rpm for 10 min at 4ºC and immediately stored frozen at -80 ºC.

Measurement of uric acid (UA) in blood plasma was evaluated by high-performance liquid chromatography (HPLC) with ultraviolet detection. The method used for UA extraction from biological samples was an adaptation of a method previously described[94]. The plasma (100 µl) was deproteinized with 10% trichloroacetic acid. Ten µl of supernatant was injected into the HPLC system consisting of a Perkin Elmer series 200 Pump, a 717 plus Autosampler, a 2487 Dual λ absorbance detector, and a reverse-phase ODS2 column (Waters, Barcelona, Spain; 4.6 mm·200 mm, 5 µm particle size). The mobile phase was methanol/ammonium acetate 5 mM/acetonitrile (1:96:3 v/v), which was run with an isocratic regular low flow rate of 1.2 mL/min and the wavelength UV detector was set at 292 nm. UA eluted at a retention time of 2.9 minutes. Quantification was performed by external calibration. The UA detection limit in plasma was 10 ng/mL

For the determination of allantoin in blood plasma, an adapted protocol was used as previously described [95]. Briefly, plasma (60 µl) was deproteinized

with acetonitrile (25 µl). Samples were centrifuged (5 min, 12,000 *g*). Ten µl of supernatant was injected into the HPLC system. Separation of allantoin was performed on a Synergy Hydro-RP C-18 reversed-phase column (250 × 4.6 mm I.D., 5 m particle size) from Phenomenex (Torrance, CA, USA). Allantoin elution (at 4 min) was performed with potassium dihydrogen phosphate (10 mM, pH 2.7): acetonitrile (85:15) and ultraviolet detection (at 235 nm).

Hydrogen peroxide (H_2O_2) was measured both in blood plasma and in freshly dissected aortic tissue (aortic rings) utilizing a commercial assay kit (ab102500 Abcam, Cambridge, UK). Non-deproteinized blood plasma from WT and MFS mice (50 µL) and standard dilutions were mixed with 50 µL of reaction Mix (composed of 48 µL of the assay buffer plus 1 µL OxiRed Probe + 1 µL HRP for fluorometric measures) and incubated (protected from daylight) for 10 min at room temperature. In the case of the aortic tissue, two types of measurements were carried out. On the one hand, H_2O_2 was measured in the aorta from mice that followed the preventive treatment with ALO (*in vivo* treatment); on the other hand, H_2O_2 was measured in the aorta in which ALO was directly added to the assay (*in vitro* treatment) Freshly dissected ascending aorta (the adventitia was quickly removed) were cut in two portions (3-4 mm thick each) corresponding to the proximal (the half close to the heart) and distal (the half close to the aortic arch) and maintained immersed in DMEM in the culture incubator at 37ºC and 5% CO_2 until time of the assay. Subsequently, each aortic portion was incubated with the reaction mix of the kit as indicated above for the blood plasma. For the *in vitro* approach, the dissected ascending aorta was treated as above with the difference that ALO (100 µM) was added to one of the two aortic portions while the other portion received the vehicle (physiological serum/PS).

Fluorometric readings were obtained at different times, reaching a plateau at 120 min. Results were normalized to the weight of the respective aortic portion. Fluorescence was measured with a Synergy fluorimeter (Ex/Em = 535/587 nm).

Myography tissue preparation and vascular reactivity

Segments of the ascending aorta from 9-month-old mice treated or not with ALO were dissected free of fat and placed in a cold physiological salt solution (PSS; composition in mM: NaCl 112; KCl 4.7; $CaCl_2$ 2.5; KH_2PO_4 1.1; $MgSO_4$ 1.2; $NaHCO_3$ 25 and glucose 11.1) gassed with 95% O_2 and 5% CO_2. Ascending aortic segments (2-3 mm) were set up on an isometric wire myograph (model 410A; Danish Myo Technology, Aarhus, Denmark) filled with PSS (37ºC; 95% O_2 and 5% CO_2) as previously described [96]. The vessels were stretched to 6 mN as reported [93], rinsed and allowed to equilibrate for 45 min. Tissues were then contracted twice with KCl (100 mM) every 5 min. After rinsing, vessels were left to equilibrate for an additional 30 min before starting the experiments. Vasodilatation caused by nitric oxide (NO) produced either by the endothelium itself (triggered by acetylcholine/ACh) or by the NO donor sodium nitroprusside (NTP) were determined by cumulative concentration-response curves (CRCs) of respective relaxation to ACh (10^{-9}-10^{-5} M) or NTP (10^{-10}-10^{-5} M) after phenylephrine (Phe; 3×10^{-6} M)-induced precontracted vessel. To study the impact of ALO on contractile responses triggered by α_1-adrenergic stimulation, the CRCs of Phe (10^{-9} to 3×10^{-5} M)-induced contraction were evaluated. Relaxations to ACh are expressed as a percentage of Phe-precontracted level. Contractions to Phe are expressed as a percentage of the tone generated by KCl. Data from CRCs were plotted using Graph Pad

Software version 8.0 (San Diego, CA, USA) with sigmoid curve fitting (variable slope) performed by non-linear regression. These curves were used to derive the values for E_{max} (the maximal relaxant response) and pEC_{50} (-log of the agonist concentration needed to produce 50% of E_{max}).

Quantitative Real-Time PCR

Total RNA from ascending aortae was extracted using Trizol© following manufacturer's recommendations (Invitrogen, USA). RNA concentration was quantified using Nanodrop (Agilent, USA). mRNA expression levels were determined by quantitative real-time PCR (qRT-PCR) using the SYBR green detection kit. mRNA levels encoding for XOR were expressed relative to *Gadph*, which was used as the housekeeping gene. qPCR reactions were performed following the protocol guidelines of the SYBR green master mix (ThermoFisher Scientific, Waltham, MA, USA). Briefly, reactions were performed in a total volume of 10 µL, including 5 µL of SYBR green PCR master mix, 2 µM of each primer, 2 µL of nuclease-free water, and 1 µL of the previously reverse-transcribed cDNA (25 ng) template on a 368-well iCycler iQ PCR plater (Bio-Rad). All reactions were carried out in duplicate for each sample. The thermocycling profile included 45 cycles of denaturation at 95 ºC for 15 seconds and annealing and elongation at 60ºC for 60 seconds. Cycle threshold (Ct) values for each gene were referenced to the internal control (comparative Ct (ΔΔCt)) and converted to the linear form relative to corresponding levels in WT aortae. The primer sequences for the murine genes used in this study are shown in Table S1.

Fluorometric assay for measuring the enzymatic activity of xanthine dehydrogenase (XDH) and xanthine oxidase (XO) forms

XO activity was determined in WT and MFS mice from liver and aorta (in which the adventitia was previously removed) lysates using a fluorimetry-based method [97]. Part of the liver and total aorta were homogenized with five volumes per gram of tissue of 0.25 M sucrose, 10 mM DTT, 0.2 mM PMSF, 0.1 mM EDTA and 50 mM K-phosphate, pH 7.4. Homogenates were centrifuged for 30 min at 15,000 *g* and the supernatants were obtained for XO activity. XO activity was measured by calculating the slope of the increase in fluorescence after adding pterin (0.010 mmol/L), which measures the conversion of pterin to isoxanthopterin. Total activity (XO+XDH) was likewise determined after adding methylene blue (0.010 mmol/L), which replaces NAD+ as an electron acceptor. The reaction was stopped by adding allopurinol (50 µmol/L). To calibrate the fluorescence signal, the activity of a standard concentration of isoxanthopterin was measured. The extent of dehydrogenase (XDH)-to-oxidase (XO) conversion was calculated from the proportion of XO activity divided by the total activities of XDH+XO. Values were expressed as nmol/min per g of protein. The protein concentration of homogenates was determined with the Bradford assay.

Blood pressure measurements

Systolic blood pressure measurements were acquired in 9-month-old animals by the tail-cuff method and using the Niprem 645 non-invasive blood pressure system (Cibertec, Madrid, Spain). Mice were positioned on a heating pad and all measurements were carried out in the dark to minimize stress. All animals were habituated to the tail-cuff by daily training one week prior to the final

measurements. Then, the systolic blood pressure was recorded over the course of three days. For quantitative analysis, the mean value of three measurements per day was used for each animal. All measurements were carried out in a blinded manner with no knowledge of genotype or experimental group.

Collagen content measurements

Collagen content was evaluated with the PicroSirius Red Staining method. Briefly, paraffin-embedded tissue arrays of mice aortae from different experimental sets were cut into 5 µm sections. Deparaffination was performed with xylene, and rehydration in 100% ethanol three times for 5 minutes, three times in 96% ethanol for 5 min and dH_2O for 5 min. After rehydration, samples were immersed in phophomolybdic acid 0,2% for 2 min and rinsed with distilled H_2O. Then, samples were immersed in picrosirius red (previously prepared with picric acid (Fluka 74069) and direct red 80 (Aldrich 365548) for 2 h. Afterward, samples were rinsed with distilled H_2O for 5 min and immersed in HCl 0,01 N for 2 min. To avoid background, unstaining was performed with ethanol 75º for 45 sec. Finally, slides were dehydrated with absolute ethanol for 5 min and fixated with xylene twice for 10 min each. Mount with DPX with coverslips. Images were captured using a Leica Leitz DMRB microscope (10x and 40x oil immersion objective) equipped with a Leica DC500 camera and analyzed with Fiji Image J Analysis software with a predesigned macro program.

Statistics

Data were presented either as bars showing mean ± standard error of the mean (SEM) or median±interquartile range (IQR) boxplots, in which the error bars

represent minimum and maximum values, the horizontal bars and the crosses indicate median and mean values, respectively, and the extremities of the boxes indicate interquartile ranges. Firstly, normal distribution and equality of error variance data were verified with Kolmogorov-Smirnov/Shapiro Wilk tests and Levene's test, respectively, using the IBM SPSS Statistics Base 22.0 before parametric tests were used. Differences between three or four groups were evaluated using one-way or two-way ANOVA with Tukey's *post-hoc* test if data were normally distributed, and variances were equal or Kruskal-Wallis test with Dunn's *post-hoc* test if data were not normally distributed. For comparison of two groups, the unpaired t-test was utilized when the data were normally distributed, and variances were equal or the Mann-Whitney U test if data did not follow a normal distribution. A value of $P \leq 0.05$ was considered statistically significant. Data analysis was carried out using GraphPad Prism software (version 9.1.2; GraphPad Software, La Jolla, CA). Outliers (ROUT 2%, GraphPad Prism software) were removed before analysis.

SUPPLEMENTAL FIGURES AND FIGURE LEGENDS

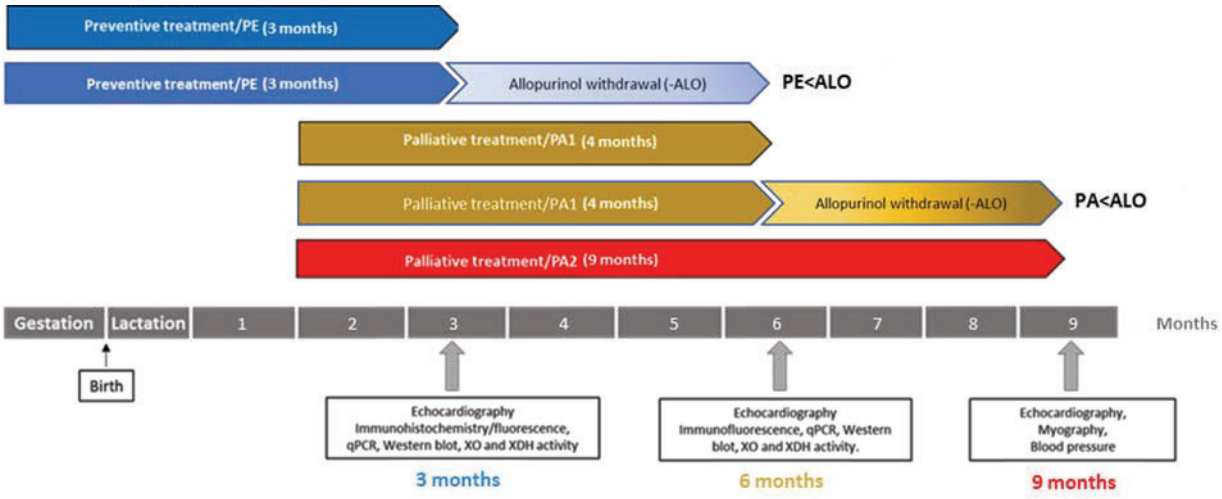

Figure S1. Representative scheme of the experimental protocols for allopurinol treatments. PE: preventive allopurinol (ALO) treatment (endpoint at 3-month-old); PA: palliative allopurinol treatments PA1 and PA2 whose difference between them being the duration of treatment, which was 4 months (endpoint at 6-month-old mice) and 7 months (endpoint at 9-month-old mice), respectively. PE<ALO: preventive allopurinol treatment followed by the subsequent drug withdrawal for 3 months (endpoint at 6-months-old); PA1<ALO: palliative allopurinol treatment followed by the subsequent drug withdrawal for 3 months (endpoint at 9-month-old). Note that each endpoint duration protocol has a different code color, which is maintained for the figures and supplemental figures shown throughout the manuscript: blue (PE), brown (PA1) and red (PA2).

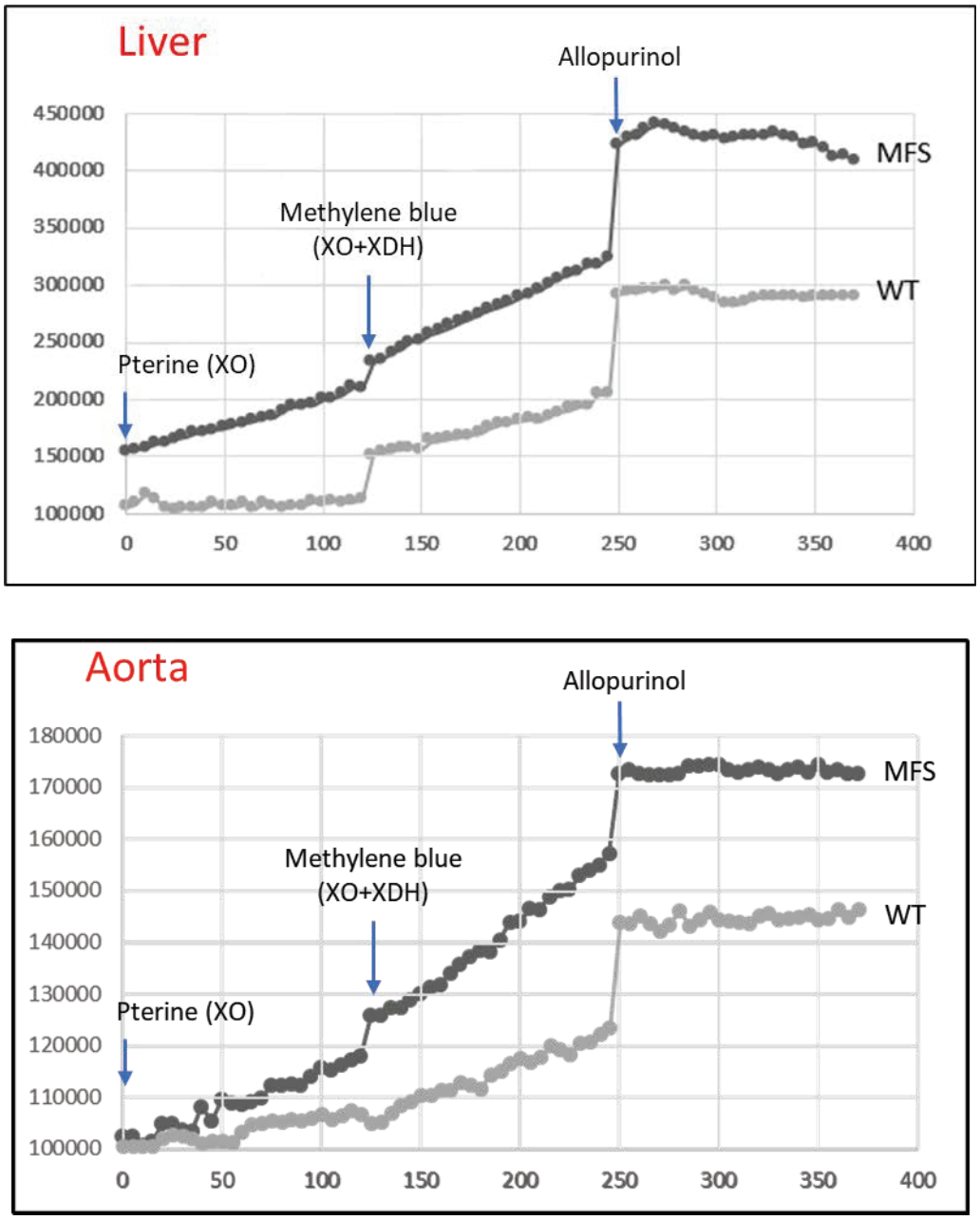

Figure S2. Fluorometric assay for measuring xanthine dehydrogenase (XDH) and oxidase (XO) enzymatic activity in liver and aortic tissues. Liver (as positive control of the assay) and aortic WT and MFS lysates had pterine added as a specific substrate for XO and methylene blue for total XOR (XO+XDH) activity. Allopurinol was added at the end of the assay to check its effectiveness in inhibiting total XDH activity. Units in the Y axis are fluorescence arbitrary units.

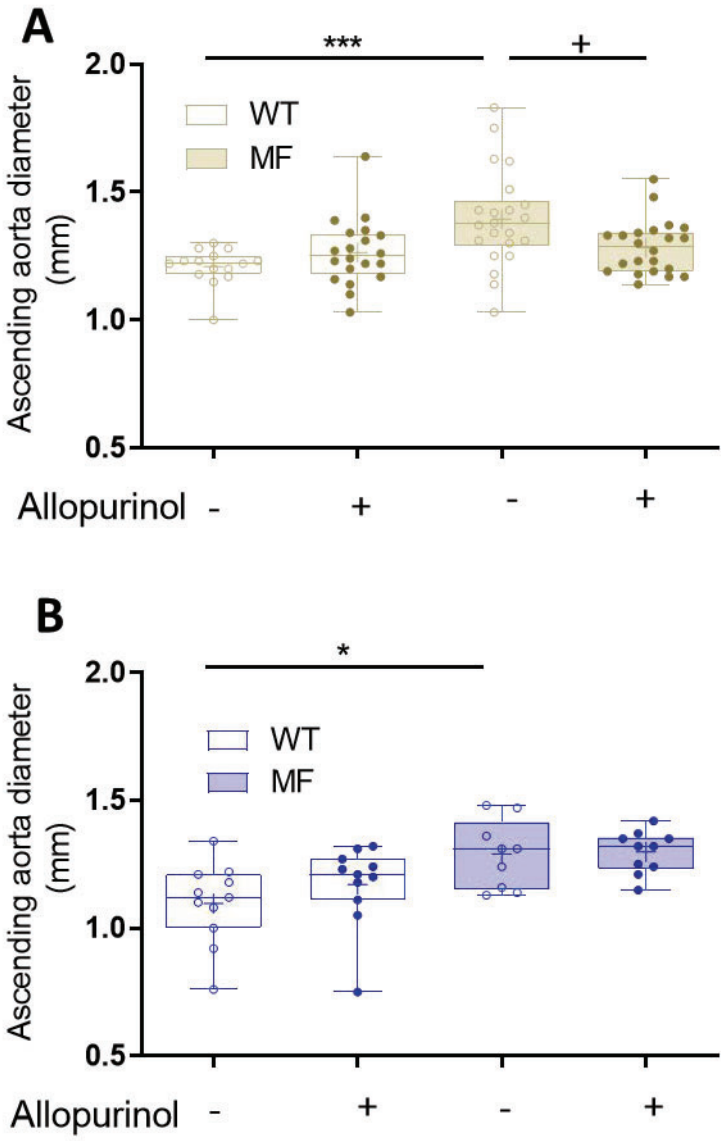

Figure S3. **Ascending aorta diameter in WT and MFS mice treated with allopurinol. (A)** Ultrasonography in WT and MFS mice of 6 months of age palliatively treated with allopurinol (PA1). See also Table S4. (**B)** Ultrasonography in 3 months of age WT and MFS mice preventively treated with allopurinol (PE). See also Table S5. Data represented as boxplots. Statistical analysis: Two-way ANOVA and Tukey post-test (A and B). ***$P \leq 0.001$ and $^{*}P \leq 0.05$; *effect of genotype; $^{+}$effect of treatment.

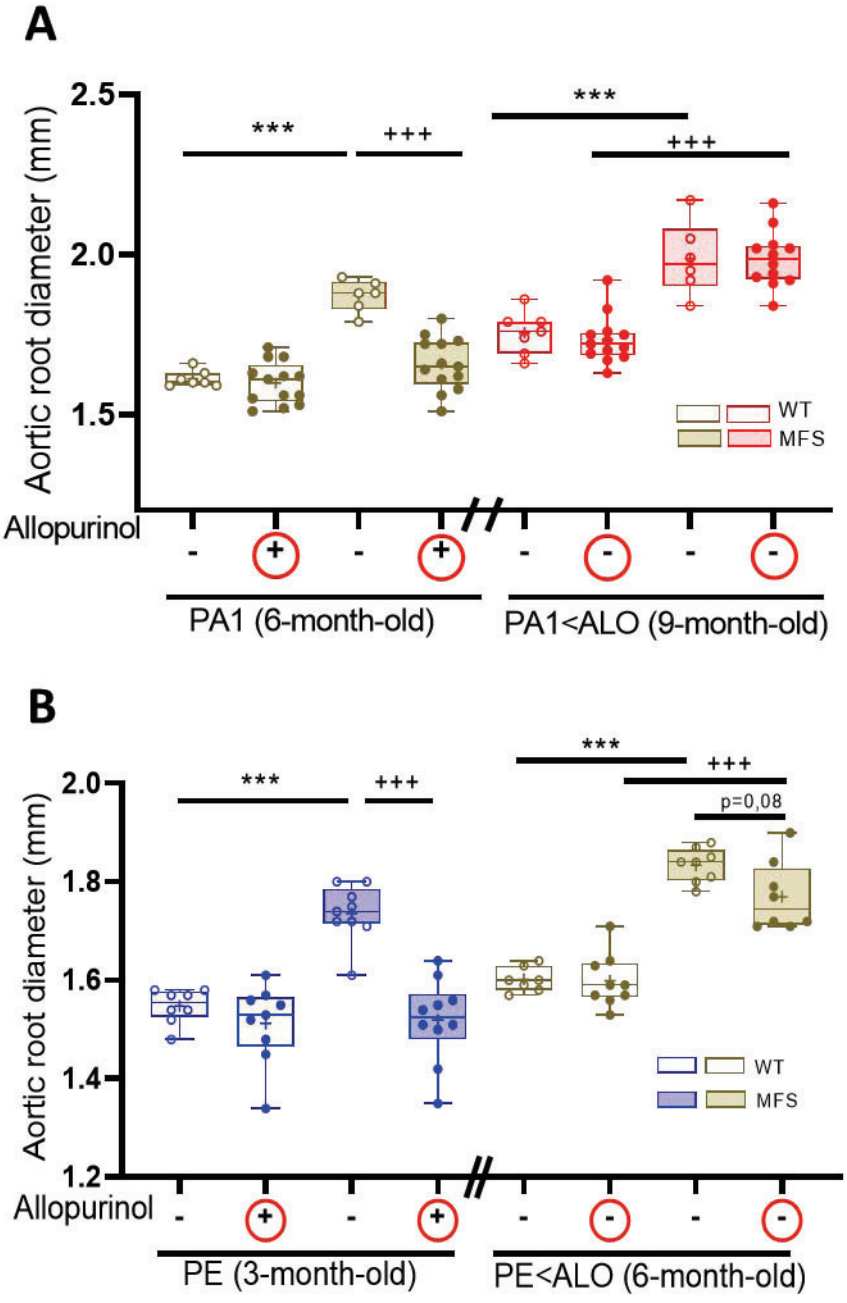

Figure S4. Reversion of aortic root dilation following the withdrawal of allopurinol. (**A**) WT and MFS mice were treated with allopurinol (ALO) following the palliative treatment from 2 to 6 months of age (PA1; 6-month-old). Thereafter, ALO was withdrawn from WT and MFS mice (+ inside red circles) until 9 months of age (PA1<ALO) (- inside red circles). The aortic root diameter

was measured by ultrasonography at 6- and 9-month-old (brown and red boxes, respectively). N= 6-13. See also Table S6. (**B**) WT and MFS mice were treated with allopurinol following the preventive treatment (PE, 3-months-old). Thereafter, allopurinol was withdrawn from WT and MFS mice (+ inside red circles) until 6 months of age (PE<ALO) (- inside red circles). The aortic root diameter was measured by ultrasonography at 3- and 6-month-old (blue and brown boxes, respectively). N= 6-10. See also Table S7. Statistical analysis in A and B: Two-way ANOVA and Tukey post-test. ***, $^{+++}$*P*≤0.001; *effect of genotype; $^{+}$effect of treatment.

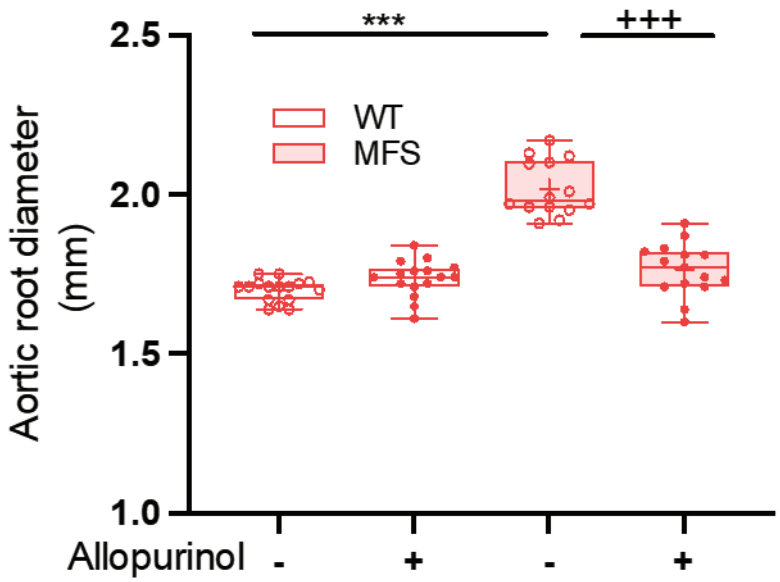

Figure S5. Aortic root diameter in WT and MFS mice palliatively treated with allopurinol (PA2). Data represented as boxplots. Statistical analyses: See also Table S6. Two-way ANOVA and Tukey's post-test. ***/+++$P \leq 0.001$; *effect of genotype; $^{+}$effect of treatment. n=14-16.

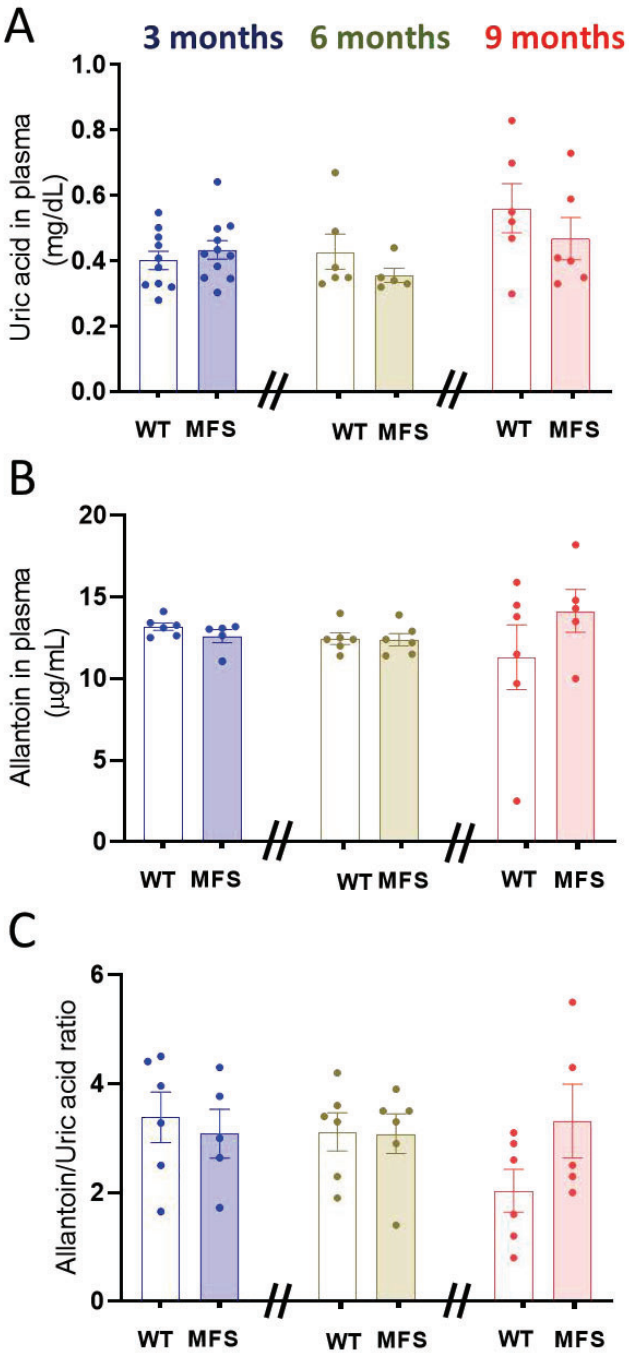

Figure S6. Uric acid and allantoin blood plasma levels are not altered in MFS mice. Blood plasma levels of uric acid (A), its catabolite allantoin (B) and their ratio (Allantoin/uric acid) (C) measured in WT and MFS mice of different ages (3-, 6-, and 9-month-old). Data as the mean ± SEM. Statistical analysis: Kruskal-Wallis with Dunn's multiple comparison test. n= 5-12.

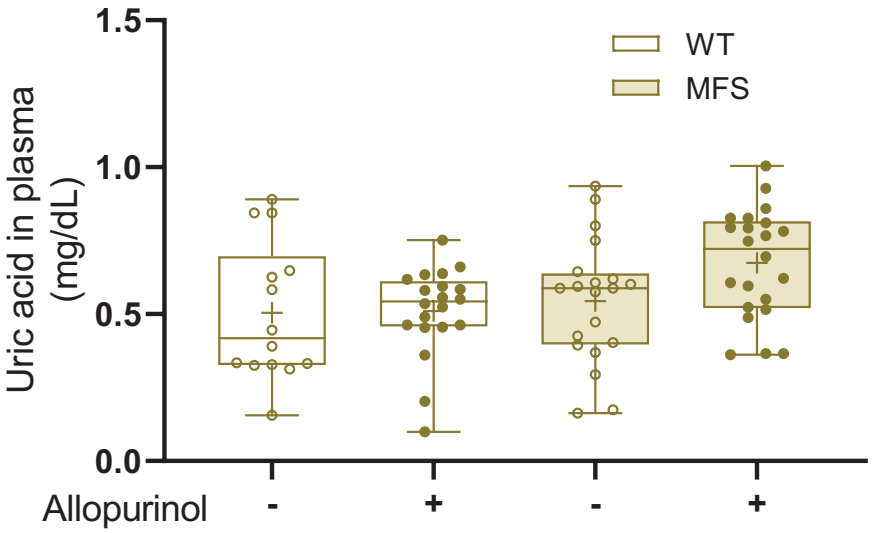

Figure S7. Plasma levels of uric acid do not change following allopurinol administration in WT and MFS mice. Uric acid blood plasma levels in WT and MFS mice palliatively treated with allopurinol (PA1) (n=14-22). Data represented as boxplots. Statistical test analysis: Two-way ANOVA with Tukey's post-test.

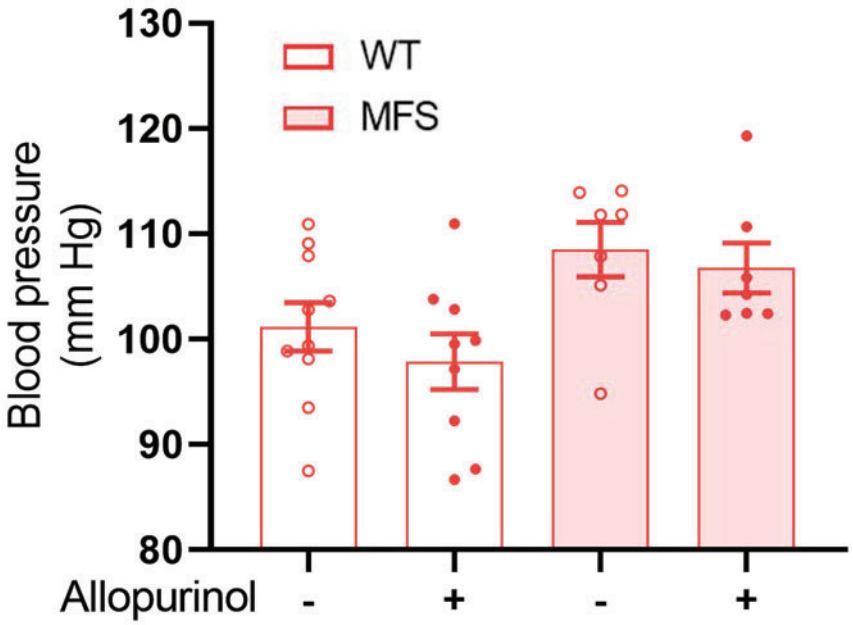

Figure S8. Allopurinol does not alter systolic blood pressure. Systolic blood pressure measurements in 9-month-old WT and MFS mice palliatively treated with allopurinol for 28 weeks (PA2) (n=6-10). Data as the mean ± SEM. Statistical test analysis: Kruskal-Wallis with Dunn's multiple comparison test.

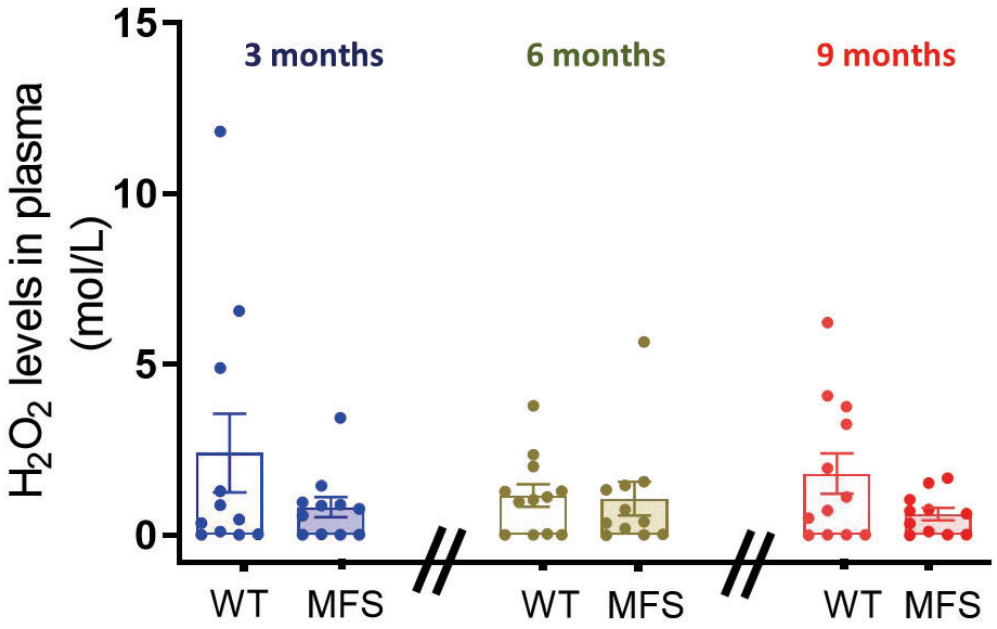

Figure S9. H_2O_2 plasma levels do not change with age in MFS mice. H_2O_2 levels in the blood plasma of WT and MFS of different ages (3-, 6-, and 9-monthold) (n=12-14). Data as the mean ± SEM. Statistical test analysis: Kruskal-Wallis with Dunn's multiple comparison test.

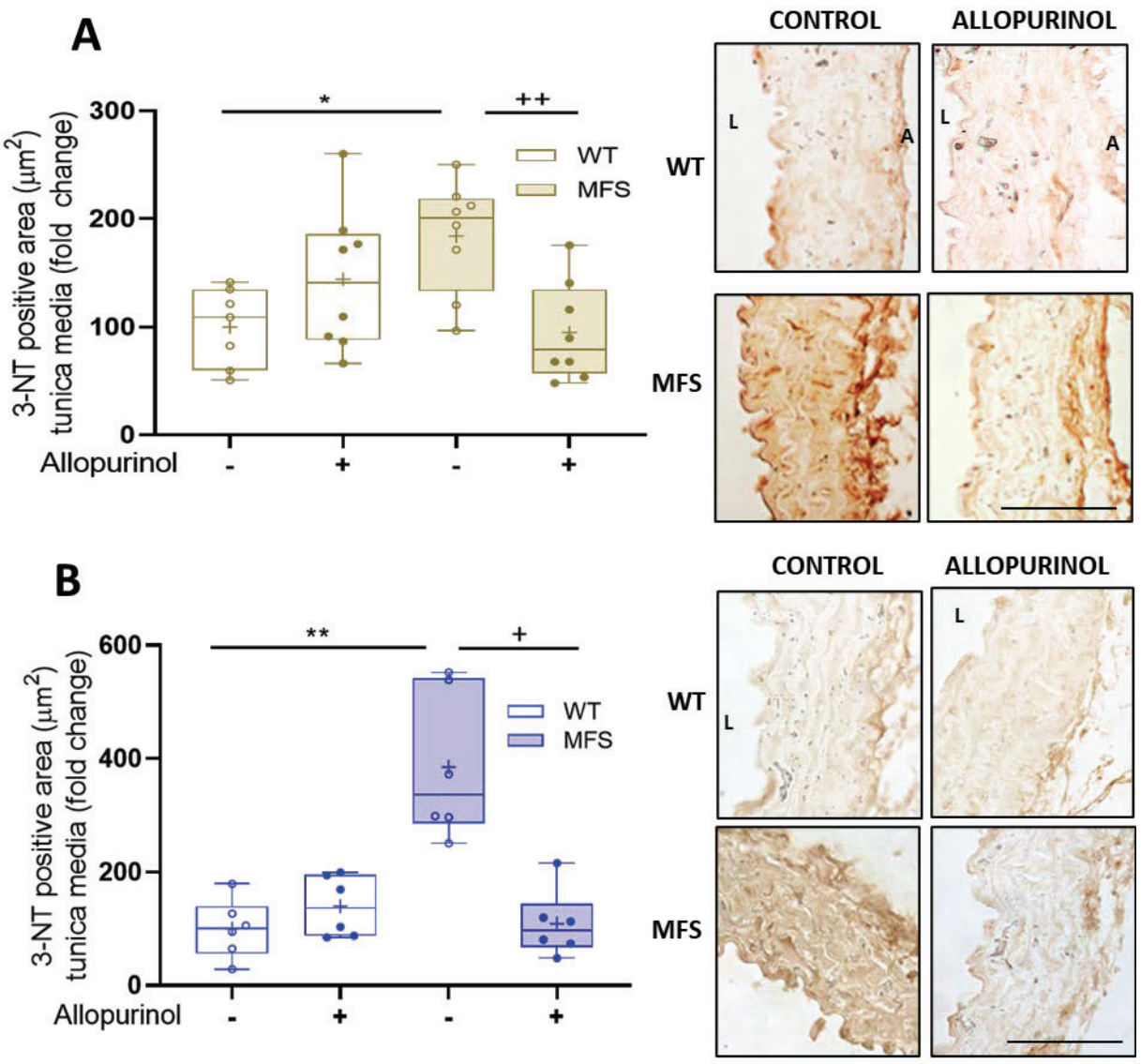

Figure S10. Allopurinol reduces redox stress-associated 3´-nitrotyrosine levels in the tunica media of MFS aorta. Quantitative analysis and representative images of the 3-NT levels in the aortic tunica media evidenced by immunohistochemistry with anti-3-NT antibodies after palliative (PA1) **(A)** and preventive (PE) **(B)** treatments with allopurinol in WT and MFS mice. Bar, 100 µm. Data represented as boxplots. Statistical test analysis: Two-way ANOVA and Tukey's post-test (A); Kruskal-Wallis and Dunn's multiple comparison tests (B). $^{**/++}P \leq 0.01$ and $^{*/+}P \leq 0.05$; *effect of genotype; $^{+}$effect of treatment.

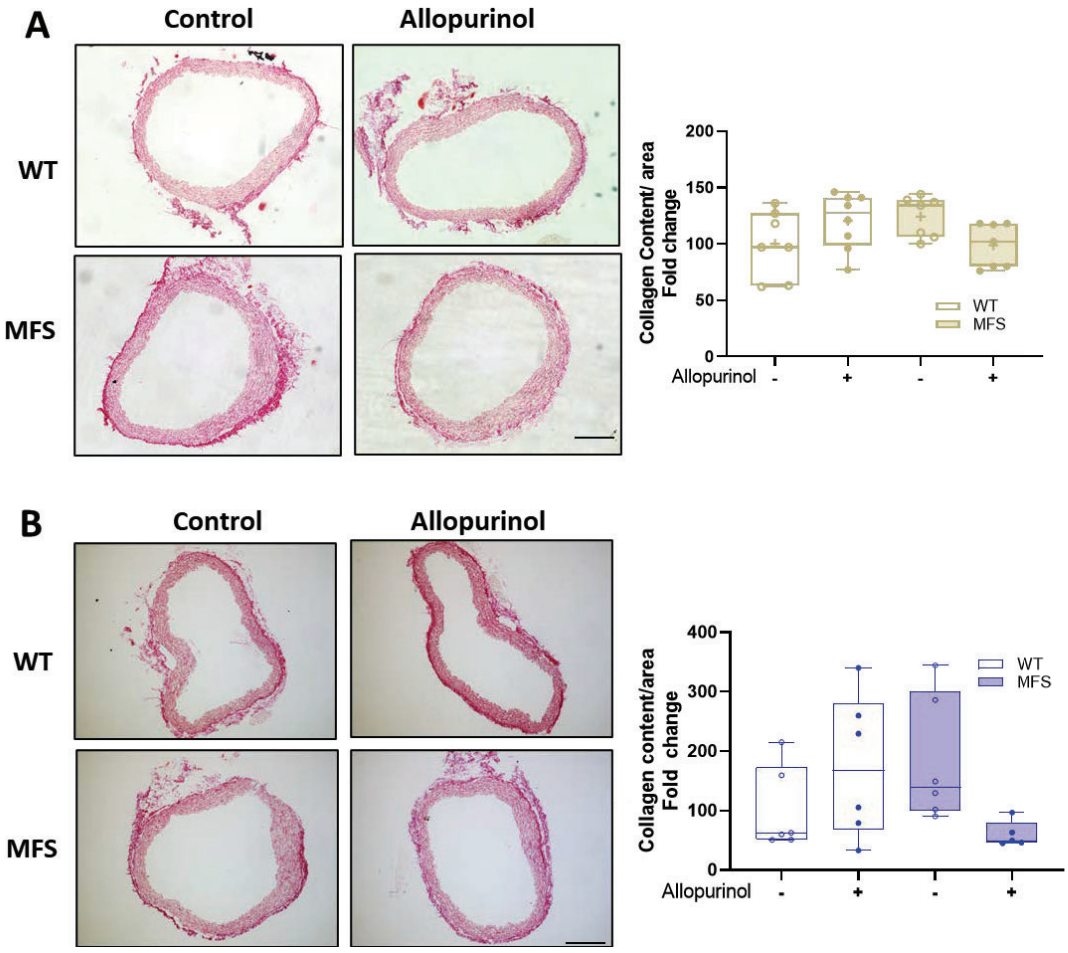

Figure S11. Collagen total content in the aortic tunica media of MFS mice following the administration of allopurinol. Picrosirius red staining of WT and MFS aortae from non-treated (control) or treated with allopurinol following its palliative (PA1) or preventive (PE) administration (A and B, respectively). At their respective side, the quantitative analysis of the staining at the media. Bar, 100 μm.

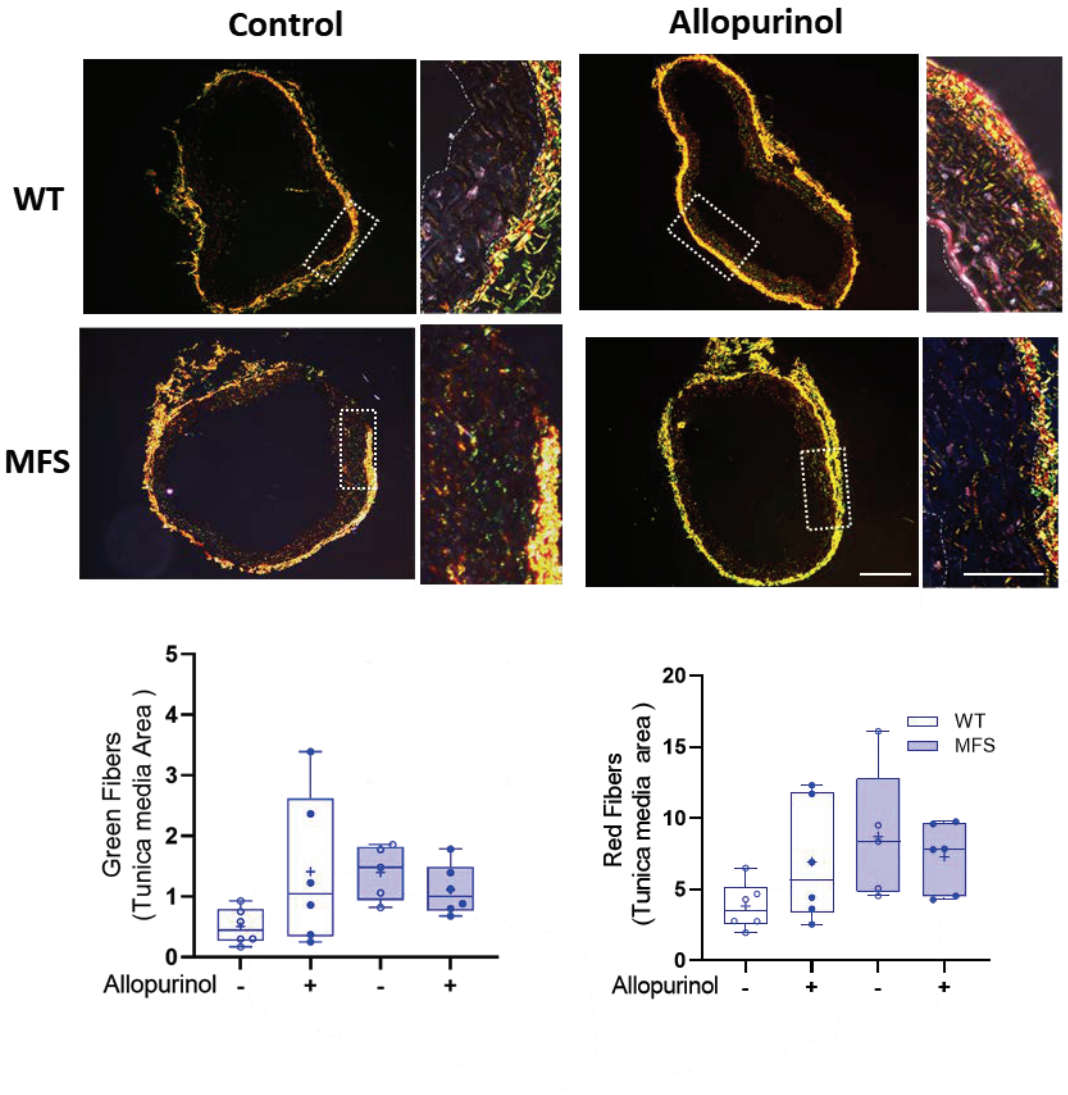

Figure S12. Collagen maturation state in the aortic tunica media of MFS mice following the preventive treatment with allopurinol. Immature (green) and mature (red) collagen fibers of the tunicae media and adventitia of WT and MFS aortae stained with Picrosirius red visualized under the polarized microscope see Fig. S11). WT and MFS mice were treated allopurinol in a preventive manner (PE) (n=5-6).). Representative fluorescence images of the whole aorta and enhanced indicated regions (white dashed lines). In enhanced images on the right of each panel, the media is at the center and the adventitia is on its right. The respective quantitative analysis of both types of collagen fibers is shown below images. Bar, 100 µm. Data represented as boxplots. Statistical test analysis: Kruskal-Wallis and Dunn's multiple comparison tests.

3. SUPPLEMENTAL TABLES

Table S1. Primers used in RT-PCR analysis in MFS mice.

Gene	Primer sequences
Xdh	Fw: 5´- GGAGATATTGGTGTCCATTGTG -3´ Rv: 5´- CCTGCTTGAAGGCTGAGAAA -3´
Nox4	Fw: 5'- ACGTCCTCGGTGGAAACTT-3' Rv: 5'-AGTGAATTGGGTCCACAACAG-3'
Gapdh	Fw: 5´- TTGATGGCAACAATCTCCAC -3´ Rv: 5´- CGTCCCGTAGACAAAATGGT-3´

Table S2. Echocardiographic values of the aortic root diameter (in mm) of WT and MFS mice subjected to palliative treatment (PA1) in the presence (+) or absence (-) of allopurinol after treatment for 4 months (from 2-to-6 month-old mice). Graphic shown in Fig. 3A. Data pooled by sex is included.

Aortic root diameter at 6-month-old mice (PA1)				
Allopurinol	**WT**		**MFS**	
-	**1.59±0.02**	**12**	**1.83±0.03*** **	**21**
	♂ 1.58±0.03	8	♂1.85±0.05***	11
	♀1.59±0.05	4	♀1.74±0.06***	10
+	**1.51±0.04**	**20**	**1.64±0.05^{++}**	**23**
	♂1.56±0.07	10	♂1,75±0.09	9
	♀1.45±0.03	10	♀1.57±0.04^{+}	14

Statistical analysis: Three-Way ANOVA. *Effect of genotype; $^{+}$effect of treatment. ***$p\leq0.001$; $^{++}p\leq0.01$; $^{+}p\leq0.05$. The number of animals is indicated on the right of each column. Sex: ♂ males, ♀ females.

Table S3. Echocardiographic values of the aortic root diameter (in mm) of WT and MFS mice subjected to preventive treatment (PE) in the presence (+) and absence (-) of allopurinol. Graphics shown in Fig. 3C.

Aortic root diameter at 3-month-old mice (PE)				
Allopurinol	**WT**		**MFS**	
-	1.45±0.04	11	1.71±0.04***	9
+	1.27±0.04	11	1.35±0.04^{+++}	10

Statistical analyses: Two-Way ANOVA followed by Tukey post-test. *effect of genotype; $^{+}$effect of treatment. ***, $^{+++}p\leq0.001$; $^{++}p\leq0.01$; *$p\leq0.05$. The number of animals is indicated on the right of each column.

Table S4 Echocardiographic values of the ascending aorta diameter (in mm) of WT and MFS mice subjected to palliative treatment (PA1) in the presence (+) or absence (-) of allopurinol after treatment for 4 months (2-to-6-month-old mice). Graphic shown in Fig. S3A.

Ascending Aorta diameter at 6-month-old mice (PA1)				
Allopurinol	**WT**		**MFS**	
-	**1.21±0.02**	**15**	**1.39±0.04*** **	**22**
	♂1.21±0.04	7	♂1.50±0.06	11
	♀1.21±0.01	8	♀1.28±0.04	11
+	**1.26±0. 03**	**20**	**1.32±0.05^{+}**	**22**
	♂1.34±0.04	10	♂1.47±0.11	9
	♀1.19±0.02	10	♀1.24±0.02	13

Statistical analyses: Two-way ANOVA followed by Tukey post-test. *Effect of genotype; $^{+}$effect of treatment. ***$p \leq 0.001$; $^{+}p \leq 0.05$. The number of animals is indicated on the right of each column.

Table S5. Echocardiographic values of the ascending aorta diameter (in mm) of WT and MFS mice subjected to preventive treatment (PE) in the presence (+) and absence (-) of allopurinol. Graphics shown in Fig. S3B.

Ascending aorta diameter at 3-month-old mice (PE)				
Allopurinol	**WT**		**MFS**	
-	1.10±0.16	11	1.29±0.13*	9
+	1.17±0.16	11	1.30±0.08	10

Statistical analyses: Two-way ANOVA followed by Tukey post-test. *Effect of genotype; $^{+}$effect of treatment. *$p \leq 0.05$. The number of animals is indicated on the right of each column.

Table S6. Echocardiographic values of the aortic root diameter (in mm) of WT and MFS mice subjected to preventive treatment with allopurinol from gestation until endpoint at 3-month-old /PE). Thereafter, allopurinol was withdrawn for 3 months, and mice subjected to ultrasonography (endpoint at 6-month-old/PE<ALO). Graphics shown in Fig. S4A.

	Aortic root diameter at 3-month-old mice (PE)				**Aortic root diameter at 6-month-old mice (PE<ALO)**			
Allopurinol	**WT**		**MFS**		**WT**		**MFS**	
-	1.54±0.01	8	1.73±0.02***	9	1.61±0.01	7	1.84±0.01***	8
+ (in PE only)	1.51±0.03	9	1.52±0.03^{+++}	10	1.60±0.01	9	1.77±0.02	8

Statistical analyses: Two-way ANOVA followed by Tukey post-test. *Effect of genotype; $^{+}$effect of treatment. ***,$^{+++}$$p$≤0.001. The number of animals is indicated on the right of each column.

Table S7. Echocardiographic values of the aortic root diameter (in mm) of WT and MFS mice subjected to palliative treatment with allopurinol (from 2-to-6-month-old/PA1). Thereafter, allopurinol was withdrawn for a period of 3 months (until 9-month-old), and mice were subjected to endpoint ultrasonography (9 month-old/PA1<ALO). Graphics shown in Fig. S4B.

	Aortic root diameter at 6-month-old mice (PA1)				**Aortic root diameter at 9-month-old mice (PA1<ALO)**			
Allopurinol	**WT**		**MFS**		**WT**		**MFS**	
-	1.61±0.01	7	1.87±0.02***	6	1.76±0.03	7	1.98±0.05***	6
+ (in PA1 only)	1.60±0.02	13	1.66±0.02^{+++}	13	1.73±0.02	13	1.97±0.02	12

Statistical analyses: Two-way ANOVA followed by Tukey post-test. *Effect of genotype; $^{+}$effect of treatment. ***,$^{+++}$$p$≤0.001. The number of animals is indicated on the right of each column.

Table S8. Echocardiographic values of the aortic root diameter (in mm) of WT and MFS mice subjected to palliative treatment (PA2) with allopurinol for 6 months (from 2- to 9-month-old mice). Data pooled for sex is also shown. Graphics shown in Fig. S5.

Aortic root diameter at 9-month-old mice (PA2)				
Allopurinol	**WT**		**MFS**	
-	**1.70±0.01**	**16**	**2.02±0.02*****	**14**
	♂ 1.69±0.02	7	♂2.07±0.03***	8
	♀1.72±0.02	9	♀1.94±0.01***	6
+	**1.74±0.01**	**16**	**1.76±0.02^{+++}**	**15**
	♂1.75±0.02	7	♂1.74±0.03^{++}	8
	♀1.73±0.02	9	♀1.79±0.03^{+++}	7

Statistical analysis: Three-Way ANOVA. *Effect of genotype; $^{+}$effect of treatment. ***, $^{+++}p\leq0.001$; $^{++}p\leq0.01$; $^{+}p\leq0.05$. The number of animals is indicated on the right of each column. Sex: ♂ males, ♀ females.

Table S9. Potency (pEC_{50}) and maximum response (E_{max}) of the concentration–response curves (CRCs) values for ACh- and NTP-induced relaxation response (%) in the ascending aorta from WT and MFS mice (9-months-old) in the presence (+) or absence (-) of allopurinol. Graphic shown in Fig. 4D.

Ascending aorta		**WT**				**MFS**			
Allopurinol		**-**		**+**		**-**		**+**	
CRC	***E_{max} (%FE)***	88.25±2.99	6	89.70±2.52	4	82.09±4.65	6	80.06±5.45	6
ACh	***pEC_{50}***	7.52±0.10		7.69±0.08		6.85±0.13***		7.49±0.19	
CRC	***E_{max} (%FE)***	90.21±4.75	5	102.8±2.94	4	102.1±3.45	4	106.7±7.27	5
NTP	***pEC_{50}***	7.69±0.11		7.96±0.07		7.96±0.08		7.66±0.18	

*Effect of genotype; ***$p\leq0.001$. The number of animals is indicated on the right of each column. Two-way ANOVA followed by Tukey post-test.

Table S10. KCl vascular tone was expressed as force units (mN). Potency (pEC_{50}) and maximum response (E_{max}) of the concentration-response curve (CRC) values for Phe-induced contraction response (%) in the ascending aorta of 9-month-old WT and MFS mice in the presence (+) or absence (-) of allopurinol. The number of animals is indicated on the right of each column. Graphic shown in Figs. 4B and 4E.

Ascending aorta		**WT**				**MFS**			
Allopurinol		**-**		**+**		**-**		**+**	
KCl	E_{max} ***(mN)***	4.70±0.52	6	4.56±0.80	5	4.43±0.60	6	4.32±0.49	6
CRC	E_{max} ***(%KCl)***	52.67±6.60	6	31.18±9.44	5	75.32±19.06	6	64.70±20.21	5
Phe	pEC_{50}	6.46±0.28		7.28±0.80		6.25±0.61		6.35±0.72	

OBJECTIVE 3: Determine the impact of uric acid in the progression of aortic aneurysm in Marfan syndrome

Rodriguez-Rovira I, Lopez-Sainz A, Palomo-Buitrago ME, Perez B, Jimenez-Altayó F, Campuzano V, Egea G.

HYPERURICAEMIA DOES NOT INTERFERE WITH AORTOPATHY IN A MURINE MODEL OF MARFAN SYNDROME.

BioRxiv 2023.05.21.541606; doi: https://doi.org/10.1101/2023.05.21.541606 under revision in International Journal of Medical Sciences)

Special Issue: New Advance in Rare Genetic Disorder

HYPERURICAEMIA DOES NOT INTERFERE WITH AORTOPATHY IN A MURINE MODEL OF MARFAN SYNDROME

Isaac Rodríguez-Rovira1, Angela López-Sainz2, Maria Encarnación Palomo-Buitrago1, Belén Pérez3, Francesc Jiménez-Altayó3, Victoria Campuzano1,4, and Gustavo Egea1,5,*
1Departament of Biomedical Sciences, University of Barcelona School of Medicine and Health Sciences, 08036 Barcelona (Spain).
2Department of Cardiology, Hospital Clínic de Barcelona, IDIBAPS, 08036 Barcelona (Spain).
3Department of Pharmacology, Autonomous University of Barcelona School of Medicine, 08192 Bellaterra (Barcelona, Spain).
4Centro de Investigación Biomédica en Red de Enfermedades Raras (CIBERER), ISCIII, 28029 Madrid (Spain).
5Center of Medical Genetics, University of Antwerp, Antwerp (Belgium).
*Correspondence: gegea@ub.edu.

ABSTRACT

Redox stress is involved in the aortic aneurysm pathogenesis in Marfan syndrome (MFS). We recently reported that allopurinol, an inhibitor of XOR, inhibited aortopathy in a MFS mouse model acting as an antioxidant without altering uric acid (UA) plasma levels. Hyperuricaemia is ambiguously associated with cardiovascular injuries as UA, having antioxidant or pro-oxidant properties depending on the concentration and accumulation site. We aimed to evaluate whether hyperuricaemia causes harm or relief in MFS aortopathy pathogenesis. Two-month-old male wild-type (WT) and MFS mice (Fbn1C1041G/+) were injected intraperitoneally for several weeks with potassium oxonate (PO), an inhibitor of uricase, an enzyme that catabolises UA to allantoin. Plasma UA and allantoin levels were measured via several techniques, aortic root diameter and cardiac parameters by ultrasonography, aortic wall structure by histopathology, and pNRF2 levels by immunofluorescence. PO induced a significant increase in UA in blood plasma both in WT and MFS mice, reaching a peak at three and four months of age but decaying at six months. Hyperuricaemic MFS mice showed no change in the characteristic aortic aneurysm progression or aortic wall disarray evidenced by large elastic laminae ruptures. There were no changes in cardiac parameters or the redox stress-induced nuclear translocation of pNRF2 in the aortic tunica media. Altogether, the results suggest that hyperuricaemia interferes neither with aortopathy nor cardiopathy in MFS mice.

Keywords: Uric acid, aortic aneurysm, Marfan syndrome, allopurinol, oxidative stress, oxonic acid, hyperuricaemia.

1. INTRODUCTION

Redox stress (RS) results from the chronic dysfunctional balance between the production and elimination of both reactive oxygen and nitrogen species (ROS and RNS; RONS). RS is largely involved in numerous pathological processes leading to the loss- or gain-of-function of lipids and proteins and changes in gene expression depending on the main subcellular location where it occurs [1,2]. With the accompanying cell signalling (growth factors, kinases), haemodynamics, and extracellular matrix alterations, RS is becoming increasingly clearly an aggravating driver of both thoracic and abdominal aortic aneurysms, including MFS syndrome (MFS) [3-8].

MFS is a genetic connective tissue disorder caused by mutations in the fibrillin-1 gene (FBN1) affecting cardiovascular, ocular, and musculoskeletal systems [9-14]. The aortic root aneurysm, with its usual subsequent dissection and rupture, is the principal cause of death in MFS patients and prophylactic surgical replacement is the main treatment option to increase life expectancy [15-17]. Nonetheless, current pharmacological treatments with beta-blockers (atenolol) and angiotensin II receptor type I (ART1) antagonists (losartan; LOS) have recently provided a minor, yet significant, improvement in aortopathy progression [18]. In any case, new complementary treatment strategies are necessary to achieve a substantial improvement in slowing or stopping aortopathy progression considering the variety of molecular mechanisms involved. It is at this point where anti- redox stress agents, such as resveratrol [19-21], allopurinol [22,23], and cobinamide [24] have recently appeared on the scene as potential new therapies.

We reported that upregulated NADPH (nicotinamide adenine dinucleotide phosphate) oxidase 4 (NOX4) aggravates aortic aneurysm progression in both in human and mouse MFS aortic samples, and other investigators have subsequently established specific signalling pathways mediating this injury [25-27]. Besides NOX4, nitric oxide synthase [28], mitochondria [29], endoplasmic reticulum [30-31], and xanthine oxidoreductase (XOR) are other important sources of ROS in the cardiovascular system [32]. XOR is a complex enzyme that, concomitantly with uric acid (UA) formation from purine metabolism, also forms ROS (superoxide and hydrogen peroxide) [33]. XOR also participates in MFS aortopathy [22, 34].

In humans and great apes, UA can abnormally accumulate in plasma and some tissues. However, in rodents, UA is quickly catabolised by uricase to allantoin, which is much more water-soluble than UA [35]. In humans, allantoin has been suggested as an oxidative stress biomarker because it is not produced metabolically [36]. Several epidemiological studies suggest a relationship between elevated serum UA and cardiovascular risk factors. However, this association remains controversial [37-41]. Thus, UA has a dual role in redox biopathology [36,38,42,43]. On the one hand, it accounts for as much as 50% of the total antioxidant capacity of biological fluids in humans [43,44,45], and it was postulated that higher UA levels protect against some peroxynitrite and inflammatory-induced CNS diseases [46]. On the other, when UA accumulates in the cytoplasm or the acidic/hydrophobic milieu, it becomes a pro-oxidant, promoting RS [47-49].

UA was found in the aortic walls of human aneurysms and atherosclerotic plaque arteries [50], and a positive correlation between serum UA levels and aortic dilatation and dissection has been reported [23,51-54]. Nonetheless, epidemiologic and biochemical studies on UA formation have demonstrated that it is not only UA itself that leads to a worse prognosis and increased cardiovascular events but also ROS

formed during XOR activity. Therefore, the resulting combined action of excessive UA and ROS formation along with enhanced XOR activity could significantly contribute to oxidative stress- linked endothelial dysfunction and heart failure, perhaps in aortopathies as well [55,56]. Interestingly, the LIFE (Losartan Intervention for Endpoint reduction) clinical trial demonstrated that LOS was superior to atenolol in reducing cardiovascular events and mortality in patients with hypertension [56]. This result was partially attributable to the intrinsic uricosuric effect of LOS via inhibition of the UA transporter URAT1 [57]. On the other hand, LOS normalised the aortic dilatation in MFS mice better than beta- blockers based on the rationale that LOS inhibited ATR1-mediated TGFβ hypersignaling [58]. Considering that Ang II activates endothelial XOR [59], it is possible that the reparatory effect of LOS on the aortic aneurysm in MFS mice might also be partially attributable to its uricosuric effect. Moreover, in the heart and circulatory system, UA also stimulates the production of ROS via the activation of TGFβ1 and NOX4 [60,61]. Therefore, considering all the above, it might be possible that UA participates, to some extent, in MFS aortopathy, aggravating it by acting as a pro-oxidant and/or promoting ROS production or, just the opposite, mitigating aneurysm progression by acting as an antioxidant. Nevertheless, knowing the broad pathological implication of increased plasma UA levels, we are inclined to think that UA's effect might be more aggravating than mitigating. Then, this study aimed to evaluate the impact of experimentally induced hyperuricaemia in aortic aneurysm progression in a murine model of MFS. Whereas in the observed allopurinol-induced blockade of aortopathy, plasma UA levels remained unaltered and its involvement was initially discarded, this cannot be definitive as, physiologically, UA in rodents is catabolised to allantoin by uricase. Therefore, to study our aim in MFS mice, it was necessary to generate and maintain increased plasma UA levels long enough to coincide with aneurysm formation to evaluate its progression. This transient hyperuricaemic model is feasible utilising uricase inhibitors like potassium oxonate (PO). Our results indicate that, despite the presence of high plasma UA levels, aortic aneurysm progression in MFS mice did not change in any way (aggravating or ameliorating), indicating that UA does not mediate in murine Marfan aortopathy.

2. RESULTS

2.1. Sex differences in uric acid and allantoin blood plasma levels in MFS mice.

We first measured plasma levels of UA and allantoin in two-month-old male and female WT and MFS mice (Figure 1), age of the basal start point of subsequent PO treatment (see supplementary Figure 1 for a scheme of experimental protocol followed in the study), and at which the aneurysm can already be clearly seen in both sexes (supplementary Figure 2). There were no differences in basal plasma UA levels between WT male and female. Unlike in male, there were significant differences between WT and MFS female as well as between MFS male and female being significantly higher in the former (Figure 1A). Plasma allantoin levels behaved almost in parallel with UA, showing significant sex differences between MFS mice but not between WT and MFS females, most likely due to the great variability of the measurements (Figure 1B). Considering sex differences in UA and allantoin plasma levels, we decided to continue working only with males because they are the most referentially studied sex for aortopathy progression as MFS patients have a significantly larger aortic root diameter than female patients. This phenotypic difference in aortic diameter between males and females is also recapitulated in MFS mice models. Moreover, male mice show minimal or no oestrogen modulation, which could additionally impact on results in females, and

there were no basal differences either in UA or allantoin plasma levels between WT and MFS animals at the starting point of the study.

2.2. Potassium oxonate transiently increased blood plasma levels of uric acid both in WT and MFS mice

Unlike humans and higher primates, rodents quickly catabolise UA to allantoin, which makes it difficult to study the impact of UA on the onset and/or progression of cardiovascular diseases using murine models. This problem can be transiently overcome with the administration of uricase inhibitors. Oxonic acid is the most efficient chemical inhibitor of uricase, administered as potassium oxonate (PO). Therefore, to study the impact of UA on MFS aortopathy and cardiopathy, we next generated a MFS murine model of hyperuricaemia with regular injections of PO. PO was administered to two-month-old WT and MFS mice for a period of 4, 8, and 16 weeks until three, four, and six months of age, respectively (Supplementary Figure 1). After four weeks of PO treatment, plasma UA levels increased significantly in both male WT and MFS mice (PO treatment; $p=0.0016$), their respective increases being highly similar and, therefore, not significant between them (interaction genotype/treatment $p=0.9737$) (Figure 2A). Strikingly, plasma allantoin levels exhibited highly similar behaviour to UA, being statistically significant for PO treatment ($p \leq 0.0001$) but not for the interaction genotype/treatment ($p=0.2966$) (Figure 2B). Some treated and untreated WT and MFS animals were euthanised for histopathological analysis of aortae (see below) and the rest continued PO treatment for 4 and 12 weeks more, receiving a total of 8 and 16 weeks of PO treatment, the mice reaching the age of four and six months, respectively (Supplementary Figure 1). Note that eight-week PO treatment maintained high plasma levels of both UA and allantoin compared with untreated male mice, which only reached statistical significance in WT mice most likely due to the large variability of values obtained in the other experimental groups (Supplementary Figures 3A and B). Following a further eight weeks of PO administration in these mice (16 weeks of treatment), UA and allantoin plasma levels showed no differences between treated and untreated animals, regardless of the genotype (Supplementary Figure 4). Therefore, the PO-induced hyperuricaemia in WT and MFS mice is transient but with an effective temporal window of eight weeks after PO injection (from two to four months of age mice), which, nonetheless, is long enough to evaluate the potential cardiovascular impact on both WT and MFS mice.

2.3. Aortopathy in MFS mice progressed regardless of the potassium oxonate-induced hyperuricaemia

Just before blood extraction to measure UA and allantoin levels in each PO-treated and untreated WT and MFS mouse, we analysed the aortic root diameter and cardiac parameters by 2D echocardiography. In three-month-old mice with four weeks of PO treatment, the aortic root diameter in MFS mice exhibited the characteristic aneurysm (WT/PO- vs. MFS/PO-) but showed no differences with PO treatment (WT/PO+ vs. MFS/PO+) (Figure 3). Similar results were observed when some WT and MFS animals continued receiving PO for an additional 4 or 12 weeks, reaching statistical differences between them. As expected, untreated MFS mice tended towards aortic dilatation compared with untreated WT mice, but not reaching significance due to the low number of analysed mice (Supplementary Figures 5 and 6).

The echocardiographic analysis of different cardiac parameters (IVSD, LVPWD, LVDD, and LVDS) did not show any significant difference between WT and MFS mice, regardless of the length of PO treatment (Table 1).

2.4. The characteristic structural disarray of MFS aorta persisted following potassium oxonate-induced hyperuricaemia.

We next analysed the structural organisation of the aortic wall in three- and six- month-old mice who received PO treatment for 4 and 16 weeks, respectively (Supplementary Figure 1 and Figure 4A and B). The tunica media of MFS aorta showed numerous characteristic ruptures of elastic laminae, whose extension and number were rather variable but always greater than in WT aorta. The large number of elastic breaks observed in PO-treated MFS mice aortae was indistinguishable from untreated MFS animals, regardless of the weeks of treatment (Figure 4A/4 weeks PO and 3 months of age mice and 4B/16 weeks PO and 6 months of age mice).

2.5. Potassium oxonate-induced hyperuricaemia does not modify the increased nuclear pNRF2 levels occurring in MFS mice

The nuclear factor erythroid 2-related factor 2 (NRF2) is a key transcription factor that regulates the expression of several antioxidant defence mechanisms. Oxidative stress triggers its phosphorylation (pNRF2), being subsequently translocated to the nucleus to activate the expression response of physiological antioxidant enzymes. Thus, we next evaluated the nuclear presence of pNRF2 in aortic paraffin sections from WT and MFS mice treated with PO for 4 and 16 weeks (Figures 5A and B, respectively). Aortic media showed a higher presence of nuclear pNRF2 in MFS than in WT smooth muscle cells, as previously observed [22], which is demonstrative of the MFS aorta suffering redox stress and cells consequently triggering the endogenous antioxidant response. However, after the administration of PO, this response did not change (Figure 5).

2.5. Blood pressure is not perturbed by potassium oxonate administration.

We also evaluated whether PO treatment might affect systolic blood pressure. This was measured after eight weeks of treatment (four-month-old mice) and presented no alteration (Supplementary Fig. 7).

3. DISCUSSION

In humans, the role of UA associated with oxidative stress and cardiovascular diseases is under debate. Most evidence comes from epidemiologic studies suggesting that increased serum levels of UA are a risk factor for cardiovascular diseases, knowing that oxidative stress is a relevant pathological mechanism in their pathogenesis and/or progression [62,63]. Allopurinol, a specific inhibitor of XOR that reduces serum levels of UA in humans [55], becomes protective in some cardiovascular diseases where oxidative stress is persistent (e.g., ischemia-reperfusion heart injury) [64]. Recently, we reported that allopurinol halts aortic aneurysm in a murine model of MFS, acting as an antioxidant both directly (ROS scavenger and XOR inhibitor) and indirectly by reducing the expression of metalloproteinase 2 and NADPH oxidase Nox4. We also realised that this antioxidant action was independent of UA as plasma levels did not change throughout several treatments [22].

In humans, UA is considered the main antioxidant of the organism and, thus, it has been proposed as a potential treatment for some pathologies that affect the central nervous system [46, 65]. However, this approach in humans cannot be easily conducted and,

therefore, it is necessary to first test this hypothesis in animal models. Nevertheless, in rodents, purine catabolism does not end with UA formation and, consequently, in its potential pathological accumulation (hyperuricaemia) either in serum or tissues. Hence, to study the relationship between UA and aortic aneurysm pathogenesis in a murine MFS model, we had to experimentally produce hyperuricaemia with oxonic acid, an inhibitor of uricase activity. Despite this intrinsic limitation, some hyperuricaemic mouse models have been generated that inhibit uricase, complemented or not with purine metabolism precursors where XOR is determinant for UA formation [66-69]. This pharmacological approach has been successfully used to study the impact of UA on cardio- and cerebrovascular diseases but not aortopathies [70,71].

We here have generated a hyperuricaemic male MFS mouse model following PO administration, and the main results obtained were the following: (i) despite aortic aneurysm occurring in MFS mice, their plasma UA levels are not significantly different from WT animals; (ii) oxonic acid, supplied as PO, produces a transient but significant elevation in plasma UA levels lasting long enough to evaluate its impact on aortopathy and cardiopathy progression in the MFS mouse model; (iii) PO-induced UA accumulation in blood plasma did not impact on either aortic aneurysm progression or the cardiac parameters examined in the MFS mouse model; and (iv) PO-induced hyperuricaemia does not modify the characteristic cellular anti-redox stress response occurring in MFS aortic media revealed by the nuclear translocation of pNRF2 in aortic vascular smooth muscle cells (VSMCs).

One striking observation was that plasma allantoin levels did not decrease in parallel with the increase in UA given that PO inhibits uricase activity. We think that this can be explained by the known non-enzymatic transformation of UA into allantoin. Thus, UA can react with anion superoxide, become oxidised and converted into allantoin. Likewise, UA can also be transformed into allantoin under alkaline conditions [72]. The overaccumulation of UA might explain the high allantoin levels.

Despite evidence supporting a role for RS in human aortic aneurysms, a clear relationship between systemic RS, serum UA levels, total antioxidant capacity, and ascending aortic aneurysms has not been definitively established. Nonetheless, serum UA concentrations and total antioxidant capacity have been reported to be associated with aortic dilatation in humans, suggesting serum UA levels as an indicator of oxidative stress [23,50, 51,73- 75]. However, this conclusion has not been confirmed in our PO-induced hyperuricaemic MFS mouse model. Of interest, in very a recent study [23] published while we were preparing our manuscript, it was reported a highly similar protective effect of allopurinol in the same MFS mouse model used here and in our previous study [22]. Strikingly, they show higher plasma UA levels in MFS mice. Our result, which contradicts their reported observations, is not easy to explain given that in our studies [22 and this study], we obtained highly similar plasma UA levels measured using two different techniques (chromatographic techniques in [22] and Spinreact Uric Acid kit, this study). Of note, we noticed that plasma UA values differed significantly depending on the blood extraction method used (infraorbital or cardiac punctures) being abnormally much higher when extracted from the heart (our unpublished observations), which is the source of measured plasma UA in [23].

We are aware that our study has some limitations. Firstly, the use of rodents to study the impact of UA, whose results are not easily translatable to humans because rodents very rarely accumulate UA. Secondly, we cannot exclude that despite the absence of any effect on aortopathy progression in hyperuricaemic MFS mice, there could be other alterations associated with hyperuricaemia such as kidney damage [76,77] or

phenotypic switching of VSMCs [78,79]. Fourthly, we only studied male mice as they have a greater aortopathy penetrance than females. Therefore, we cannot discard that females could show a different behaviour. Fifth, the use of PO generates a transient hyperuricaemic mouse model which limits the study of any potential long-term effects of hyperuricaemia. In this case, the generation of uricase (Uox)-deficient MFS mice would be a more suitable model.
Based on our findings, we can conclude that, unlike ROS, UA accumulation seems not to be instrumental in the aortopathy and cardiopathy of a murine model of MFS, at least once the aneurysm is already established and in male mice.

4. MATERIAL AND METHODS

4.1. Chemicals and reagents

Sodium carboxy methyl cellulose (0.5%; CMC-Na) (C5678 Sigma-Aldrich) was prepared with sterile physiological saline as the solvent for potassium oxonate (PO; 156124 Sigma-Aldrich). Potassium oxonate was suspended in CMC-Na. The injected dose was 250 mg/kg and adjusted to the weight of each animal.

4.2. Mice, experimental design, and study approval

Male MFS mice with a fibrillin-1 mutation (Fbn1C1041G/+) (hereafter, MFS mice) were purchased from The Jackson Laboratory (B6.129-Fbn1tm1Hcd/J; Strain #012885/Common name: C1039G; Bar Harbor, ME 04609, USA). MFS and sex- and age-matched wild-type littermates (WT mice) were maintained in a C57BL/6J genetic background. All mice were housed according to the University of Barcelona's institutional guidelines (constant room temperature at 22ºC, controlled environment 12/12-hour light/dark cycle, 60% humidity and ad libitum access to food and water). WT and MFS mice were randomly divided into four experimental groups: WT and MFS mice treated with CMC-Na (vehicle), and WT and MFS mice treated with PO. All four groups received the treatment by intraperitoneal injection of the corresponding reagent (CMC- Na: 0.5%; PO: 250 mg/kg) every 48 h (Supplementary Figure 1). Animal care and colony maintenance were carried out according to European Union (Directive 2010/63/EU) and Spanish guidelines (RD 53/2013) for the use of experimental animals. Ethical approval was obtained from the local animal ethics committee (CEEA protocol approval number: 357/22).

4.3. Uric acid and allantoin analysis in blood plasma

Plasma uric acid levels were measured using Spinreact (model Spinlab 100) with the Spinreact Uric Acid kit (SP41001). We followed the manufacturer's instructions.
For the determination of allantoin in blood plasma, an adapted protocol was used, as previously described [80]. Briefly, plasma (60 µl) was deproteinised with acetonitrile (25 µl). Samples were centrifuged (5 min, 12,000 g). Ten µl of supernatant was injected into the HPLC system. Separation of allantoin was performed on a Synergy Hydro-RP C-18 reversed-phase column (250 × 4.6 mm I.D., 5 m particle size) from Phenomenex (Torrance, CA, USA). Allantoin elution (at 4 min) was performed with potassium dihydrogen phosphate (10 mM, pH 2.7): acetonitrile (85:15) and ultraviolet detection (at 235 nm).

4.4. Echocardiography

Two-dimensional transthoracic echocardiography was performed in all animals under 1.5% inhaled isoflurane. Each animal was scanned 12–24 hours before sacrifice. Images

were obtained with a 10–13 MHz phased array linear transducer (IL12i GE Healthcare, Madrid, Spain) in a Vivid Q system (GE Healthcare, Madrid, Spain). Images were recorded and later analysed offline using commercially available software (EchoPac v.08.1.6, GE Healthcare, Madrid, Spain). Proximal aortic segments were assessed in a parasternal long-axis view. The aortic root diameter was measured from inner edge to inner edge in end-diastole at the level of the sinus of Valsalva. Left ventricle (LV) dimensions were assessed in 2D mode in a parasternal long-axis view at both end-diastole (LVDD) and end-systole (LVSD). The interventricular septum and posterior wall thickness at end-cardiac diastole were also measured. All echocardiographic measurements were carried out in a blinded manner by two independent investigators with no knowledge of genotype or treatment.

4.5. Histopathology

Paraffin-embedded tissue arrays of mice aortae from different experimental sets were cut into 5 µm sections. Elastic fibre ruptures were quantified by counting the number of large fibres breaks in tissue sections stained with Verhoeff-Van Gieson. Breaks larger than 20 µm were defined as evident large discontinuities in the normal circumferential continuity (360º) of each elastic lamina in the aortic media [81]. They were counted along the length of each elastic lamina in four different representative images of three non- consecutive sections of the same ascending aorta. Three sections per condition were usually studied, spaced 10 µm apart (two sections). All measurements were carried out in a blinded manner by two different observers with no knowledge of genotype and treatment. Images were captured using a Leica DMRB microscope (40x oil immersion objective) equipped with a Leica DC500 camera and analysed with Fiji Image J Analysis software.

4.6. Immunofluorescence staining

For pNRF2 immunofluorescence, paraffin-embedded aortic tissue sections (5 µm thick) were deparaffinised and rehydrated prior to unmasking the epitope. Sections were treated first with heat-mediated retrieval solution (1 M Tris-EDTA, 0.05% Tween, pH 9) for 30 min in the steamer at 95ºC. Next, sections were incubated for 20 minutes with ammonium chloride (NH_4Cl, 50 mM, pH 7.4) to block free aldehyde groups, followed by a permeabilisation step using 0.3% Triton X-100 for 10 min and then treated with 1% BSA blocking buffer solution for 2 h prior to overnight incubation with monoclonal anti- pNRF2 (1:200; Abcam ab76026) in a humidified chamber at 4°C. On the next day, sections were rinsed with PBS followed by 60 min incubation with the secondary antibody goat anti-rabbit Alexa 647 (1:1.000, A-21246, Invitrogen). Sections were counterstained with DAPI (1:10.000) and images were acquired using an AF6000 widefield fluorescent microscope. For quantitative analysis, four areas of each ascending aorta section were quantified with Image J software. All measurements were carried out in a blinded manner by two independent investigators.

4.7. Blood pressure measurements

Systolic blood pressure measurements were acquired by the tail-cuff method and using the Niprem 645 non-invasive blood pressure system (Cibertec, Madrid, Spain).

Mice were positioned on a heating pad and all measurements were carried out in the dark to minimise stress. All animals were habituated to the tail cuff by daily training one week prior to the final measurements. Then, the systolic blood pressure was recorded over the course of three days. For quantitative analysis, the mean value of three measurements per day was used per animal. All measurements were carried out in a blinded manner with no knowledge of genotype or experimental group.

4.8. Statistical analysis

Data were presented as bars showing the mean ± standard error of the mean (SEM). Firstly, normal distribution and equality of error variance data were verified with Kolmogorov-Smirnov/Shapiro-Wilk tests and Levene's test, respectively, using the IBM SPSS Statistics Base 22.0 before parametric tests were used. Differences between three or four groups were evaluated using one-way or two-way ANOVA with Tukey's post- hoc test if data were normally distributed and variances were equal, or the Kruskal-Wallis test with Dunn's post-hoc test if data were not normally distributed. A value of $P \leq 0.05$ was considered statistically significant. Data analysis was carried out using GraphPad Prism software (version 9.1.2; GraphPad Software, La Jolla, CA). Outliers (ROUT 2%, GraphPad Prism software) were removed before analysis.

Supplementary Materials: The following supporting information can be downloaded at: www.mdpi.com/xxx/s1,
Figure S1: Schematic representation of the experimental protocol followed in this study.
Figure S2: Aortic root diameter in WT and MFS mice at the start time of the study (two months old).
Figure S3: Uric acid and allantoin plasma levels following eight weeks of treatment with potassium oxonate.
Figure S4: Uric acid and allantoin plasma levels following 16 weeks of treatment with potassium oxonate.
Figure S5: Aortic root diameter in WT and MFS mice treated with PO for eight weeks.
Figure S6: Aortic root diameter in WT and MFS mice treated with PO for 16 weeks.
Figure S7: Blood pressure in WT and MFS treated with potassium oxonate.

Author Contributions: Conceptualisation, G.E.; methodology, I.R-R. A.L-S., M.P-B., B.P.; formal analysis, I.R-R, A.L.-S., V.C., G.E.; investigation, I.R.-R. A.L.-S., M.P-B. B.P., F.J-A., V.C., G.E.; resources, I.R.-R.; data curation, F.R-R, V.C., G.E.; writing—original draft preparation, G.E.; writing—review and editing, I.R-R., F.J-A, V.C., G.E.; supervision, F.J-A., V.C., G.E.; funding acquisition, F.J.-A., V.C., G.E. All authors have read and agreed to the published version of the manuscript.
Funding: This research was funded by poorly endowed grants from the Ministerio de Ciencia e Innovación PID2020-113634RB-C2 to G.E and F.J.-A, and from the Generalitat de Catalunya 2021 SGR 00029.
Institutional Review Board Statement: The animal study protocol was approved by the local Committee of Ethical Animal Experimentation (CEEA-PRBB; Protocol Number: 357/22) in accordance with the guidelines of the European Communities Directive 86/609/EEC. The PRBB has Animal Welfare Assurance (#A5388-01, Institutional Animal Care and Use Committee approval date 05/08/2009), granted by the Office of Laboratory Animal Welfare (OLAW) of the US National Institutes of Health.
Informed Consent Statement: Not applicable.

Data Availability Statement: Original data can be requested from the corresponding author.

Acknowledgements: We thank Fernando J. Pérez Asensio (Animal Room of the PCB, Barcelona) for uric acid measurements and Helena Kruyer for English editorial assistance.

5. REFERENCES

1. Sies H, Belousov VV, Chandel NS, Davies MJ, Jones DP, Mann GE, Murphy MP, Yamamoto M, Winterbourn C. Defining roles of specific reactive oxygen species (ROS) in cell biology and physiology. Nat Rev Mol Cell Biol. 2022, 23(7):499-515. doi: 10.1038/s41580-022-00456-z.
2. Sies H. Oxidative eustress: On constant alert for redox homeostasis. Redox Biol. 2021, 41:101867. doi: 10.1016/j.redox.2021.101867.
3. Portelli SS, Hambly BD, Jeremy RW, Robertson EN. Oxidative stress in genetically triggered thoracic aortic aneurysm: role in pathogenesis and therapeutic opportunities. Redox Rep. 2021, 26(1):45-52. doi: 10.1080/13510002.2021.1899473.
4. Salmon M. NADPH Oxidases in Aortic Aneurysms. Antioxidants (Basel). 2022, 16;11(9):1830. doi: 10.3390/antiox11091830.
5. Rysz J, Gluba-Brzózka A, Rokicki R, Franczyk B. Oxidative Stress-Related Susceptibility to Aneurysm in Marfan's Syndrome. Biomedicines. 2021, 6;9(9):1171. doi: 10.3390/biomedicines9091171.
6. Malecki C, Hambly BD, Jeremy RW, Robertson EN. The Role of Inflammation and Myeloperoxidase-Related Oxidative Stress in the Pathogenesis of Genetically Triggered Thoracic Aortic Aneurysms. Int J Mol Sci. 2020, 16;21(20):7678. doi: 10.3390/ijms21207678.
7. Pincemail J, Defraigne JO, Courtois A, Albert A, Cheramy-Bien JP, Sakalihasan N. Abdominal Aortic Aneurysm (AAA): Is There a Role for the Prevention and Therapy Using Antioxidants? Curr Drug Targets 2018, 19(11):1256-1264. doi: 10.2174/1389450118666170918164601.
8. Sánchez-Infantes D, Nus M, Navas-Madroñal M, Fité J, Pérez B, Barros-Membrilla AJ, Soto B, Martínez-González J, Camacho M, Rodriguez C, Mallat Z, Galán M. Oxidative Stress and Inflammatory Markers in Abdominal Aortic Aneurysm. Antioxidants (Basel) 2021, 14;10(4):602. doi: 10.3390/antiox10040602.
9. Judge DP, Dietz HC. Marfan's syndrome. Lancet 2005, 3;366(9501):1965-76. doi: 10.1016/S0140-6736(05)67789-6.
10. Asano K, Cantalupo A, Sedes L, Ramirez F. Pathophysiology and Therapeutics of Thoracic Aortic Aneurysm in Marfan Syndrome. Biomolecules 2022, 14;12(1):128. doi: 10.3390/biom12010128.
11. Milewicz DM, Braverman AC, De Backer J, Morris SA, Boileau C, Maumenee IH, Jondeau G, Evangelista A, Pyeritz RE. Marfan syndrome. Nat Rev Dis Primers 2021, 2;7(1):64. doi: 10.1038/s41572-021-00298-7.
12. Demolder A, von Kodolitsch Y, Muiño-Mosquera L, De Backer J. Myocardial Function, Heart Failure and Arrhythmia in Marfan Syndrome: A Systematic Literature Review. Diagnostics (Basel) 2020, 25;10(10):751. doi: 10.3390/diagnostics10100751.
13. Loeys BL, Dietz HC, Braverman AC, Callewaert BL, De Backer J, Devereux RB, Hilhorst-Hofstee Y, Jondeau G, Faivre L, Milewicz DM, Pyeritz RE, Sponseller PD, Wordsworth P, De Paepe AM. The revised Ghent nosology for the Marfan syndrome. J Med Genet. 2010, 47:476-85. doi: 10.1136/jmg.2009.072785.

14. von Kodolitsch Y, Demolder A, Girdauskas E, Kaemmerer H, Kornhuber K, Muino Mosquera L, Morris S, Neptune E, Pyeritz R, Rand-Hendriksen S, Rahman A, Riise N, Robert L, Staufenbiel I, Szöcs K, Vanem TT, Linke SJ, Vogler M, Yetman A, De Backer J. Features of Marfan syndrome not listed in the Ghent nosology - the dark side of the disease. Expert Rev Cardiovasc Ther 2019, 17(12):883-915. doi: 10.1080/14779072.2019.1704625.
15. Soto ME, Ochoa-Hein E, Anaya-Ayala JE, Ayala-Picazo M, Koretzky SG. Systematic review and meta-analysis of aortic valve-sparing surgery versus replacement surgery in ascending aortic aneurysms and dissection in patients with Marfan syndrome and other genetic connective tissue disorders. J Thorac Dis 2021, 13(8):4830-4844. doi: 10.21037/jtd-21-789.
16. Steinmetz LM, Coselli JS. Endovascular Repair in Patients with Marfan Syndrome: Concerns Amid Controversy. Ann Vasc Surg 2022, 17:S0890-5096(22)00236-9. doi: 10.1016/j.avsg.2022.04.049..
17. Moshirfar M, Barke MR, Huynh R, Waite AJ, Ply B, Ronquillo YC, Hoopes PC. Controversy and Consideration of Refractive Surgery in Patients with Heritable Disorders of Connective Tissue. J Clin Med 2021, 24;10(17):3769. doi: 10.3390/jcm10173769.
18. Pitcher A, Spata E, Emberson J, Davies K, Halls H, Holland L, Wilson K, Reith C, Child AH, Clayton T, Dodd M, Flather M, Jin XY, Sandor G, Groenink M, Mulder B, De Backer J, Evangelista A, Forteza A, Teixido-Turà G, Boileau C, Jondeau G, Milleron O, Lacro RV, Sleeper LA, Chiu HH, Wu MH, Neubauer S, Watkins H, Dietz H, Baigent C; Marfan Treatment Trialists' Collaboration. Angiotensin receptor blockers and β blockers in Marfan syndrome: an individual patient data meta-analysis of randomised trials. Lancet 2022, 10;400(10355):822-831. doi: 10.1016/S0140-6736(22)01534-3.
19. Hibender S, Franken R, van Roomen C, Ter Braake A, van der Made I, Schermer EE, Gunst Q, van den Hoff MJ, Lutgens E, Pinto YM, Groenink M, Zwinderman AH, Mulder BJ, de Vries CJ, de Waard V. Resveratrol Inhibits Aortic Root Dilatation in the Fbn1C1039G/+ Marfan Mouse Model. Arterioscler Thromb Vasc Biol 2016, 36(8):1618-26. doi: 10.1161/ATVBAHA.116.307841.
20. van Andel MM, Groenink M, Zwinderman AH, Mulder BJM, de Waard V. The Potential Beneficial Effects of Resveratrol on Cardiovascular Complications in Marfan Syndrome Patients-Insights from Rodent-Based Animal Studies. Int J Mol Sci 2019, 5;20(5):1122. doi: 10.3390/ijms20051122.
21. Mieremet A, van der Stoel M, Li S, Coskun E, van Krimpen T, Huveneers S, de Waard V. Endothelial dysfunction in Marfan syndrome mice is restored by resveratrol. Sci Rep 2022, 28;12(1):22504. doi: 10.1038/s41598-022-26662-5.
22. Rodríguez-Rovira I, Arce C, De Rycke K, Pérez B, Carretero A, Arbonés M, Teixidò- Turà G, Gómez-Cabrera MC, Campuzano V, Jiménez-Altayó F, Egea G. Allopurinol blocks aortic aneurysm in a mouse model of Marfan syndrome via reducing aortic oxidative stress. Free Radic Biol Med 2022, 20;193(Pt 2):538-550. doi: 10.1016/j.freeradbiomed.2022.11.001.
23. Yang L, Wu H, Luo C, Zhao Y, Dai R, Li Z, Zhang X, Gong Z, Cai Z, Shen Y, Yu F, Li W, Zhao H, Zhang T, Zhu J, Fu Y, Wang J, Kong W. Urate-Lowering Therapy Inhibits Thoracic Aortic Aneurysm and Dissection Formation in Mice. Arterioscler Thromb Vasc Biol 2023, In press. doi: 10.1161/ATVBAHA.122.318788.
24. Schwaerzer GK, Kalyanaraman H, Casteel DE, Dalton ND, Gu Y, Lee S, Zhuang S, Wahwah N, Schilling JM, Patel HH, Zhang Q, Makino A, Milewicz DM,

Peterson KL, Boss GR, Pilz RB. Aortic pathology from protein kinase G activation is prevented by an antioxidant vitamin B12 analog. Nat Commun 2019, 6;10(1):3533. doi: 10.1038/s41467-019-11389-1.
25. Jiménez-Altayó F, Meirelles T, Crosas-Molist E, Sorolla MA, Del Blanco DG, López-Luque J, Mas-Stachurska A, Siegert AM, Bonorino F, Barberà L, García C, Condom E, Sitges M, Rodríguez-Pascual F, Laurindo F, Schröder K, Ros J, Fabregat I, Egea G. Redox stress in Marfan syndrome: Dissecting the role of the NADPH oxidase NOX4 in aortic aneurysm. Free Radic Biol Med 2018, 118:44-58. doi: 10.1016/j.freeradbiomed.2018.02.023.
26. Huang K, Wang Y, Siu KL, Zhang Y, Cai H. Targeting feed-forward signaling of TGFβ/NOX4/DHFR/eNOS uncoupling/TGFβ axis with anti-TGFβ and folic acid attenuates formation of aortic aneurysms: Novel mechanisms and therapeutics. Redox Biol 2021, 38:101757. doi: 10.1016/j.redox.2020.101757.
27. Yu W, Xiao L, Que Y, Li S, Chen L, Hu P, Xiong R, Seta F, Chen H, Tong X. Smooth muscle NADPH oxidase 4 promotes angiotensin II-induced aortic aneurysm and atherosclerosis by regulating osteopontin. Biochim Biophys Acta Mol Basis Dis 2020, 1;1866(12):165912. doi: 10.1016/j.bbadis.2020.165912.
28. Toral M, de la Fuente-Alonso A, Campanero MR, Redondo JM. The NO signalling pathway in aortic aneurysm and dissection. Br J Pharmacol 2022, 179(7):1287-1303. doi: 10.1111/bph.15694.
29. Oller J, Gabandé-Rodríguez E, Ruiz-Rodríguez MJ, Desdín-Micó G, Aranda JF, Rodrigues-Diez R, Ballesteros-Martínez C, Blanco EM, Roldan-Montero R, Acuña P, Forteza Gil A, Martín-López CE, Nistal JF, Lino Cardenas CL, Lindsay ME, Martín-Ventura JL, Briones AM, Redondo JM, Mittelbrunn M. Extracellular Tuning of Mitochondrial Respiration Leads to Aortic Aneurysm. Circulation 2021, 25;143(21):2091-2109. doi: 10.1161/CIRCULATIONAHA.120.051171.
30. Siegert AM, García Díaz-Barriga G, Esteve-Codina A, Navas-Madroñal M, Gorbenko Del Blanco D, Alberch J, Heath S, Galán M, Egea G. A FBN1 3'UTR mutation variant is associated with endoplasmic reticulum stress in aortic aneurysm in Marfan syndrome. Biochim Biophys Acta Mol Basis Dis 2019, 1865(1):107-114. doi: 10.1016/j.bbadis.2018.10.029.
31. Meirelles T, Araujo TLS, Nolasco P, Moretti AIS, Guido MC, Debbas V, Pereira LV, Laurindo FR. Fibrillin-1 mgΔ(lpn) Marfan syndrome mutation associates with preserved proteostasis and bypass of a protein disulfide isomerase-dependent quality checkpoint. Int J Biochem Cell Biol 2016, 71:81-91. doi: 10.1016/j.biocel.2015.12.009.
32. Polito L, Bortolotti M, Battelli MG, Bolognesi A. Xanthine oxidoreductase: A leading actor in cardiovascular disease drama. Redox Biol 2021, 24;48:102195. doi: 10.1016/j.redox.2021.102195.
33. Bortolotti M, Polito L, Battelli MG, Bolognesi A. Xanthine oxidoreductase: One enzyme for multiple physiological tasks. Redox Biol 2021, 41:101882. doi: 10.1016/j.redox.2021.101882.
34. Yang HH, van Breemen C, Chung AW. Vasomotor dysfunction in the thoracic aorta of Marfan syndrome is associated with accumulation of oxidative stress. Vascul Pharmacol 2010, 52(1-2):37-45. doi: 10.1016/j.vph.2009.10.005.
35. Maiuolo J, Oppedisano F, Gratteri S, Muscoli C, Mollace V. Regulation of uric acid metabolism and excretion. Int J Cardiol 2016, 15;213:8-14. doi: 10.1016/j.ijcard.2015.08.109.

36. Seet RC, Kasiman K, Gruber J, Tang SY, Wong MC, Chang HM, Chan YH, Halliwell B, Chen CP. Is uric acid protective or deleterious in acute ischemic stroke? A prospective cohort study. Atherosclerosis 2010, 209(1):215-9. doi: 10.1016/j.atherosclerosis.2009.08.012.
37. Kanbay M, Segal M, Afsar B, Kang DH, Rodriguez-Iturbe B, Johnson RJ. The role of uric acid in the pathogenesis of human cardiovascular disease. Heart 2013, 99(11):759-66. doi: 10.1136/heartjnl-2012-302535.
38. Vassalle C, Mazzone A, Sabatino L, Carpeggiani C. Uric Acid for Cardiovascular Risk: Dr. Jekyll or Mr. Hide? Diseases, 2016, 26;4(1):12. doi: 10.3390/diseases4010012.
39. Masi S, Pugliese NR, Taddei S. The difficult relationship between uric acid and cardiovascular disease. Eur Heart J 2019, 21;40(36):3055-3057. doi: 10.1093/eurheartj/ehz166.
40. Yu W, Cheng JD. Uric Acid and Cardiovascular Disease: An Update From Molecular Mechanism to Clinical Perspective. Front Pharmacol 2020, 11:582680. doi: 10.3389/fphar.2020.582680.
41. Lee SJ, Oh BK, Sung KC. Uric acid and cardiometabolic diseases. Clin Hypertens
2020, 15;26:13. doi: 10.1186/s40885-020-00146-y.
42. Cortese F, Giordano P, Scicchitano P, Faienza MF, De Pergola G, Calculli G, Meliota G, Ciccone MM. Uric acid: from a biological advantage to a potential danger. A focus on cardiovascular effects. Vascul Pharmacol 2019, 120:106565. doi: 10.1016/j.vph.2019.106565.
43. Kang DH, Ha SK. Uric Acid Puzzle: Dual Role as Anti-oxidant and Pro-oxidant. Electrolyte Blood Press 2014, 12(1):1-6. doi: 10.5049/EBP.2014.12.1.1.
44. Glantzounis GK, Tsimoyiannis EC, Kappas AM, Galaris DA. Uric acid and oxidative stress. Curr Pharm Des 2005, 11:4145-51. doi: 10.2174/138161205774913255.
45. Itahana Y, Han R, Barbier S, Lei Z, Rozen S, Itahana K. The uric acid transporter SLC2A9 is a direct target gene of the tumor suppressor p53 contributing to antioxidant defense. Oncogene 2015, 34:1799-810. doi: 10.1038/onc.2014.119.
46. Scott GS, Hooper DC. The role of uric acid in protection against peroxynitrite-mediated pathology. Med Hypotheses 2001, 56(1):95-100. doi: 10.1054/mehy.2000.1118.
47. Sautin YY, Nakagawa T, Zharikov S, Johnson RJ. Adverse effects of the classic antioxidant uric acid in adipocytes: NADPH oxidase-mediated oxidative/nitrosative stress. Am J Physiol Cell Physiol 2007, 293(2):C584-96. doi: 10.1152/ajpcell.00600.2006.
48. Corry DB, Eslami P, Yamamoto K, Nyby MD, Makino H, Tuck ML. Uric acid stimulates vascular smooth muscle cell proliferation and oxidative stress via the vascular renin-angiotensin system. J Hypertens 2008, 26(2):269-75. doi: 10.1097/HJH.0b013e3282f240bf.
49. Yu MA, Sánchez-Lozada LG, Johnson RJ, Kang DH. Oxidative stress with an activation of the renin-angiotensin system in human vascular endothelial cells as a novel mechanism of uric acid-induced endothelial dysfunction. J Hypertens 2010, 28(6):1234-42.
50. Patetsios P, Rodino W, Wisselink W, Bryan D, Kirwin JD, Panetta TF. Identification of uric acid in aortic aneurysms and atherosclerotic artery. Ann N Y Acad Sci 1996, 18;800:243-5. doi: 10.1111/j.1749-6632.1996.tb33318.x.

51. Esen AM, Akcakoyun M, Esen O, Acar G, Emiroglu Y, Pala S, Kargin R, Karapinar H, Ozcan O, Barutcu I. Uric acid as a marker of oxidative stress in dilatation of the ascending aorta. Am J Hypertens 2011, 24(2):149-54. doi: 10.1038/ajh.2010.219.
52. Cai J, Zhang Y, Zou J, Shen Y, Luo D, Bao H, Chen Y, Ye J, Guan JL. Serum uric acid could be served as an independent marker for increased risk and severity of ascending aortic dilatation in Behçet's disease patients. J Clin Lab Anal 2019, 33(1):e22637. doi: 10.1002/jcla.22637.
53. Otaki Y, Watanabe T, Konta T, Watanabe M, Asahi K, Yamagata K, Fujimoto S, Tsuruya K, Narita I, Kasahara M, Shibagaki Y, Iseki K, Moriyama T, Kondo M, Watanabe T. Impact of hyperuricemia on mortality related to aortic diseases: a 3.8- year nationwide community-based cohort study. Sci Rep 2020, 31;10(1):14281. doi: 10.1038/s41598-020-71301-6.
54. Yang G, Chai X, Ding N, Yang D, Ding Q. A retrospective observational study of serum uric acid and in-hospital mortality in acute type A aortic dissection. Sci Rep 2022, 19;12(1):12289. doi: 10.1038/s41598-022-16704-3.
55. Kelkar A, Kuo A, Frishman WH. Allopurinol as a cardiovascular drug. Cardiol Rev 2011, 19(6):265-71. doi: 10.1097/CRD.0b013e318229a908.
56. Høieggen A, Alderman MH, Kjeldsen SE, Julius S, Devereux RB, De Faire U, Fyhrquist F, Ibsen H, Kristianson K, Lederballe-Pedersen O, Lindholm LH, Nieminen MS, Omvik P, Oparil S, Wedel H, Chen C, Dahlöf B; LIFE Study Group. The impact of serum uric acid on cardiovascular outcomes in the LIFE study. Kidney Int 2004, 65(3):1041-9. doi: 10.1111/j.1523-1755.2004.00484.x.
57. Hamada T, Ichida K, Hosoyamada M, Mizuta E, Yanagihara K, Sonoyama K, Sugihara S, Igawa O, Hosoya T, Ohtahara A, Shigamasa C, Yamamoto Y, Ninomiya H, Hisatome I. Uricosuric action of losartan via the inhibition of urate transporter 1 (URAT 1) in hypertensive patients. Am J Hypertens 200, 21(10):1157-62. doi: 10.1038/ajh.2008.245.
58. Habashi JP, Judge DP, Holm TM, Cohn RD, Loeys BL, Cooper TK, Myers L, Klein EC, Liu G, Calvi C, Podowski M, Neptune ER, Halushka MK, Bedja D, Gabrielson K, Rifkin DB, Carta L, Ramirez F, Huso DL, Dietz HC. Losartan, an AT1 antagonist, prevents aortic aneurysm in a mouse model of Marfan syndrome. Science 2006, 7;312(5770):117-21. doi: 10.1126/science.1124287.
59. Landmesser U, Spiekermann S, Preuss C, Sorrentino S, Fischer D, Manes C, Mueller M, Drexler H. Angiotensin II induces endothelial xanthine oxidase activation: role for endothelial dysfunction in patients with coronary disease. Arterioscler Thromb Vasc Biol 2007, 27(4):943-8. doi: 10.1161/01.ATV.0000258415.32883.bf.
60. Delbosc S, Paizanis E, Magous R, Araiz C, Dimo T, Cristol JP, Cros G, Azay J. Involvement of oxidative stress and NADPH oxidase activation in the development of cardiovascular complications in a model of insulin resistance, the fructose-fed rat. Atherosclerosis 2005, 179(1):43-9. doi: 10.1016/j.atherosclerosis.2004.10.018.
61. Nyby MD, Abedi K, Smutko V, Eslami P, Tuck ML. Vascular Angiotensin type 1 receptor expression is associated with vascular dysfunction, oxidative stress and inflammation in fructose-fed rats. Hypertens Res 2007, 30(5):451-7. doi: 10.1291/hypres.30.451.
62. Borghi C. The role of uric acid in the development of cardiovascular disease. Curr Med Res Opin 2015;31 Suppl 2:1-2. doi: 10.1185/03007995.2015.1087985.
63. Wang R, Song Y, Yan Y, Ding Z. Elevated serum uric acid and risk of cardiovascular or all-cause mortality in people with suspected or definite coronary

artery disease: A meta-analysis. Atherosclerosis 2016, 254:193-199. doi: 10.1016/j.atherosclerosis.2016.10.006.
64. Kinugasa Y, Ogino K, Furuse Y, Shiomi T, Tsutsui H, Yamamoto T, Igawa O, Hisatome I, Shigemasa C. Allopurinol improves cardiac dysfunction after ischemia-reperfusion via reduction of oxidative stress in isolated perfused rat hearts. Circ J. 2003, 67(9):781-7. doi: 10.1253/circj.67.781.
65. Hooper DC, Kean RB, Scott GS, Spitsin SV, Mikheeva T, Morimoto K, Bette M, Röhrenbeck AM, Dietzschold B, Weihe E. The central nervous system inflammatory response to neurotropic virus infection is peroxynitrite dependent. J Immunol 2001, 15;167(6):3470-7. doi: 10.4049/jimmunol.167.6.3470.
66. Lu J, Dalbeth N, Yin H, Li C, Merriman TR, Wei WH. Mouse models for human hyperuricaemia: a critical review. Nat Rev Rheumatol 2019, 15(7):413-426. doi: 10.1038/s41584-019-0222-x.
67. Lin C, Zheng Q, Li Y, Wu T, Luo J, Jiang Y, Huang Q, Yan C, Zhang L, Zhang W, Liao H, Yang Y, Pang J. Assessment of the influence on left ventricle by potassium oxonate and hypoxanthine-induced chronic hyperuricemia. Exp Biol Med 2023, 248(2):165-174. doi: 10.1177/15353702221120113.
68. Qian X , Wang X , Luo J , Liu Y , Pang J , Zhang H , Xu Z , Xie J , Jiang X , Ling W. Hypouricemic and nephroprotective roles of anthocyanins in hyperuricemic mice. Food Funct 2019, 20;10(2):867-878. doi: 10.1039/c8fo02124d.
69. Yasutake Y, Tomita K, Higashiyama M, Furuhashi H, Shirakabe K, Takajo T, Maruta K, Sato H, Narimatsu K, Yoshikawa K, Okada Y, Kurihara C, Watanabe C, Komoto S, Nagao S, Matsuo H, Miura S, Hokari R. Uric acid ameliorates indomethacin- induced enteropathy in mice through its antioxidant activity. J Gastroenterol Hepatol 2017, 32(11):1839-1845. doi: 10.1111/jgh.13785.
70. Cutler RG, Camandola S, Feldman NH, Yoon JS, Haran JB, Arguelles S, Mattson MP. Uric acid enhances longevity and endurance and protects the brain against ischemia. Neurobiol Aging 2019, 75:159-168. doi: 10.1016/j.neurobiolaging.2018.10.031.
71. Cutler RG, Camandola S, Malott KF, Edelhauser MA, Mattson MP. The Role of Uric Acid and Methyl Derivatives in the Prevention of Age-Related Neurodegenerative Disorders. Curr Top Med Chem 2015, 15(21):2233-8. doi: 10.2174/1568026615666150610143234.
72. Benzie IF, Chung Wy, Tomlinson B. Simultaneous measurement of allantoin and urate in plasma: analytical evaluation and potential clinical application in oxidant:antioxidant balance studies. Clin Chem 1999, 45(6 Pt 1):901-4.
73. Wang JC, Tsai SH, Tsai HY, Lin SJ, Huang PH. Hyperuricemia exacerbates abdominal aortic aneurysm formation through the URAT1/ERK/MMP-9 signaling pathway. BMC Cardiovasc Disord 2023 30;23(1):55. doi: 10.1186/s12872-022- 03012-x.
74. Zhang Y, Xu X, Lu Y, Guo L, Ma L. Preoperative uric acid predicts in-hospital death in patients with acute type A aortic dissection. J Cardiothorac Surg 2020, 15;15(1):21. doi: 10.1186/s13019-020-1066-9.
75. Jiang WL, Qi X, Li X, Zhang YF, Xia QQ, Chen JC. Serum uric acid is associated with aortic dissection in Chinese men. Int J Cardiol 2016, 1;202:196-7. doi: 10.1016/j.ijcard.2015.08.174.
76. Li H, Zhang H, Yan F, He Y, Ji A, Liu Z, Li M, Ji X, Li C. Kidney and plasma metabolomics provide insights into the molecular mechanisms of urate nephropathy in a

mouse model of hyperuricemia. Biochim Biophys Acta Mol Basis Dis 2022, 1;1868(6):166374. doi: 10.1016/j.bbadis.2022.166374.
77. Gherghina ME, Peride I, Tiglis M, Neagu TP, Niculae A, Checherita IA. Uric Acid and Oxidative Stress-Relationship with Cardiovascular, Metabolic, and Renal Impairment. Int J Mol Sci. 2022, 16;23(6):3188. doi: 10.3390/ijms23063188.
78. Crosas-Molist E, Meirelles T, López-Luque J, Serra-Peinado C, Selva J, Caja L, Gorbenko Del Blanco D, Uriarte JJ, Bertran E, Mendizábal Y, Hernández V, García-Calero C, Busnadiego O, Condom E, Toral D, Castellà M, Forteza A, Navajas D, Sarri E, Rodríguez-Pascual F, Dietz HC, Fabregat I, Egea G. Vascular smooth muscle cell phenotypic changes in patients with Marfan syndrome. Arterioscler Thromb Vasc Biol 2015, 35(4):960-72. doi: 10.1161/ATVBAHA.114.304412.
79. Pedroza AJ, Tashima Y, Shad R, Cheng P, Wirka R, Churovich S, Nakamura K, Yokoyama N, Cui JZ, Iosef C, Hiesinger W, Quertermous T, Fischbein MP. Single-Cell Transcriptomic Profiling of Vascular Smooth Muscle Cell Phenotype Modulation in Marfan Syndrome Aortic Aneurysm. Arterioscler Thromb Vasc Biol 2020, 40(9):2195-2211. doi: 10.1161/ATVBAHA.120.314670.
80. Onetti Y, Jiménez-Altayó F, Heras M, Vila E, Dantas AP. Western-type diet induces senescence, modifies vascular function in non-senescence mice and triggers adaptive mechanisms in senescent ones. Exp Gerontol 2013, 48(12):1410-9. doi: 10.1016/j.exger.2013.09.004.
81. Arce C, Rodríguez-Rovira I, De Rycke K, Durán K, Campuzano V, Fabregat I, Jiménez-Altayó F, Berraondo P, Egea G. Anti-TGFβ (Transforming Growth Factor β) Therapy with Betaglycan-Derived P144 Peptide Gene Delivery Prevents the Formation of Aortic Aneurysm in a Mouse Model of Marfan Syndrome. Arterioscler Thromb Vasc Biol 2021, 41(9):e440-e452. doi: 10.1161/ATVBAHA.121.316496.

FIGURE LEGENDS

Figure 1. Basal uric acid and allantoin blood plasma levels in male and female WT and Marfan syndrome mice. (A) Uric acid and (B) allantoin plasma levels in two-month-old WT and MFS mice (males and females). Results are the mean ± SEM. Statistical tests: Kruskal-Wallis, Dunn's post-hoc. *p ≤0.05, **p ≤0.01; ****p ≤0.0001.

Figure 2. Uric acid and allantoin plasma levels following four weeks of potassium oxonate treatment. Two-month-old male WT and MFS mice were treated for four weeks with potassium oxonate (PO); subsequently, uric acid (A) and allantoin (B) plasma levels were determined. Results are the mean ± SEM. Statistical test: Two-way ANOVA. **p
≤0.01; ****p ≤0.0001

Figure 3. Aortic root diameter in WT and MFS mice following four weeks of potassium oxonate treatment. The aortic root diameter was measured via 2D echocardiography in two-month-old male WT and MFS mice treated for four weeks with potassium oxonate (PO). An identified outlier is indicated with a red circle but was not included in the statistical analysis. Results are the mean ± SEM; Statistical test: Two-way ANOVA; genotype, ****p ≤0.0001

Figure 4. Aortic wall organisation in WT and MFS mice treated with potassium oxonate. Representative light microscope images of elastin histological staining (Elastin Verhoeff-Van Gieson) of aortic paraffin sections of the tunica media of the ascending aorta from WT and MFS mice treated or not with potassium oxonate (PO). The quantitative analysis of aortic elastic breaks after 4 and 16 weeks of PO treatment is also shown beside their respective images. Results are the mean ± SEM. Statistical analysis: Kruskal Wallis, Dunn's post-hoc, *p ≤0.05.

Figure 5. pNRF2 levels in WT and MFS mice treated with potassium oxonate. Representative images and quantitative analysis of the nuclear translocation of the phosphorylated form of NRF2 in VSMCs of the tunica media of WT and MFS mice treated with potassium oxonate (PO) for four weeks (A) and 16 (B) weeks (mice aged 3 and six months, respectively) (B). Bar, 100 µm. Statistical tests: Kruskal-Wallis and Dunn's multiple comparison tests. *p ≤ 0.05.

Figure 1

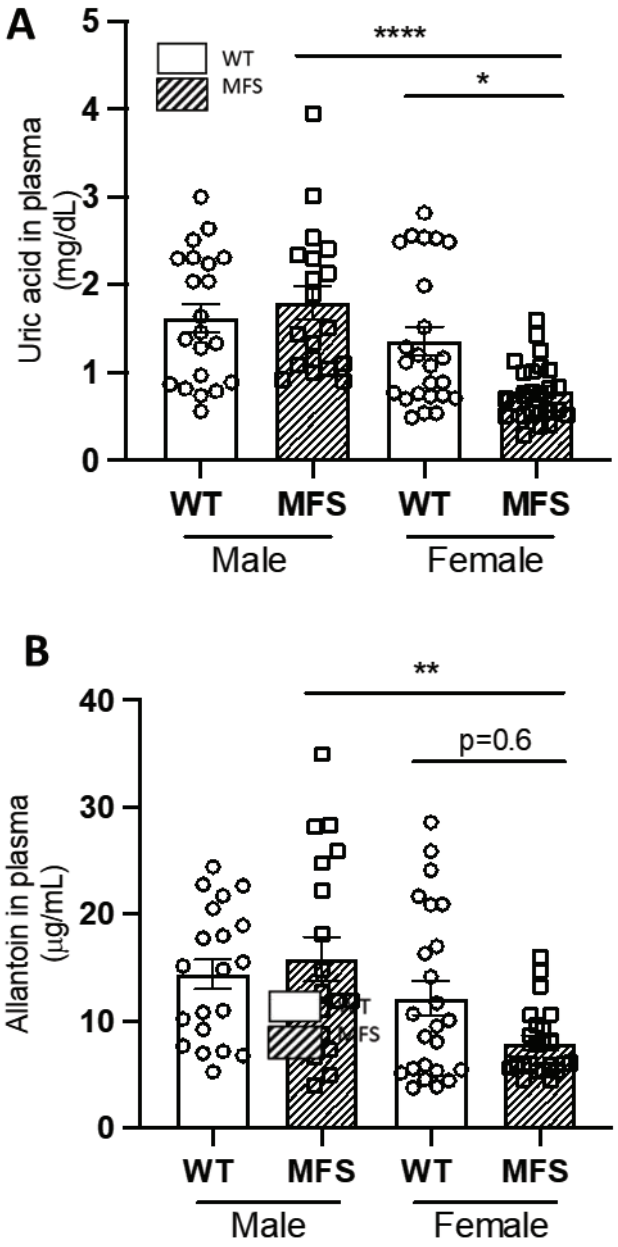
A
Uric acid in plasma (mg/dL)
WT
MFS
****
*
WT
MFS
WT
MFS
Male
Female
B
Allantoin in plasma (µg/mL)
**
p=0.6
WT
MFS
WT
MFS
Male
Female

Figure 2

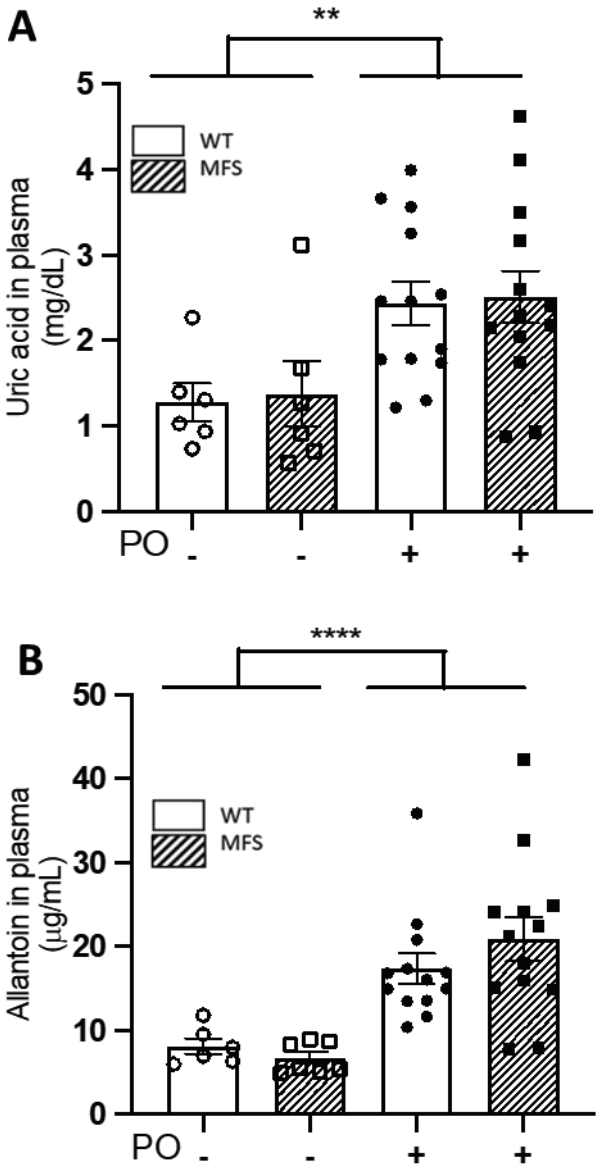
A
**
Uric acid in plasma (mg/dL)
WT
MFS
PO
B
****
Allantoin in plasma (μg/mL)
WT
MFS
PO

Figure 3

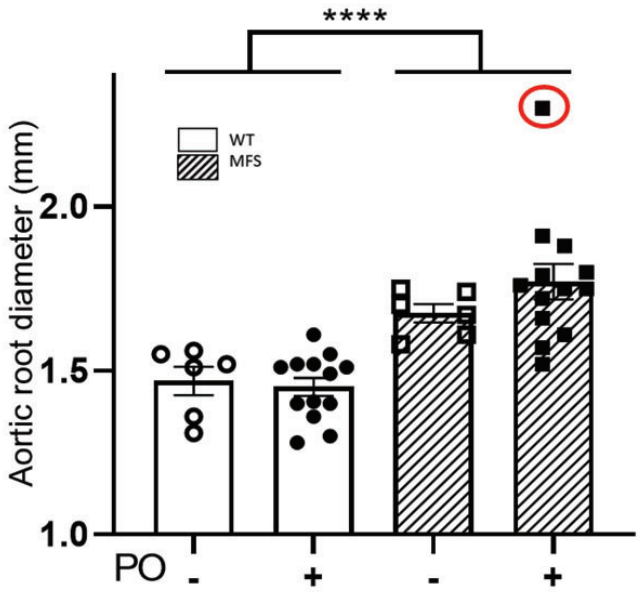

Figure 4

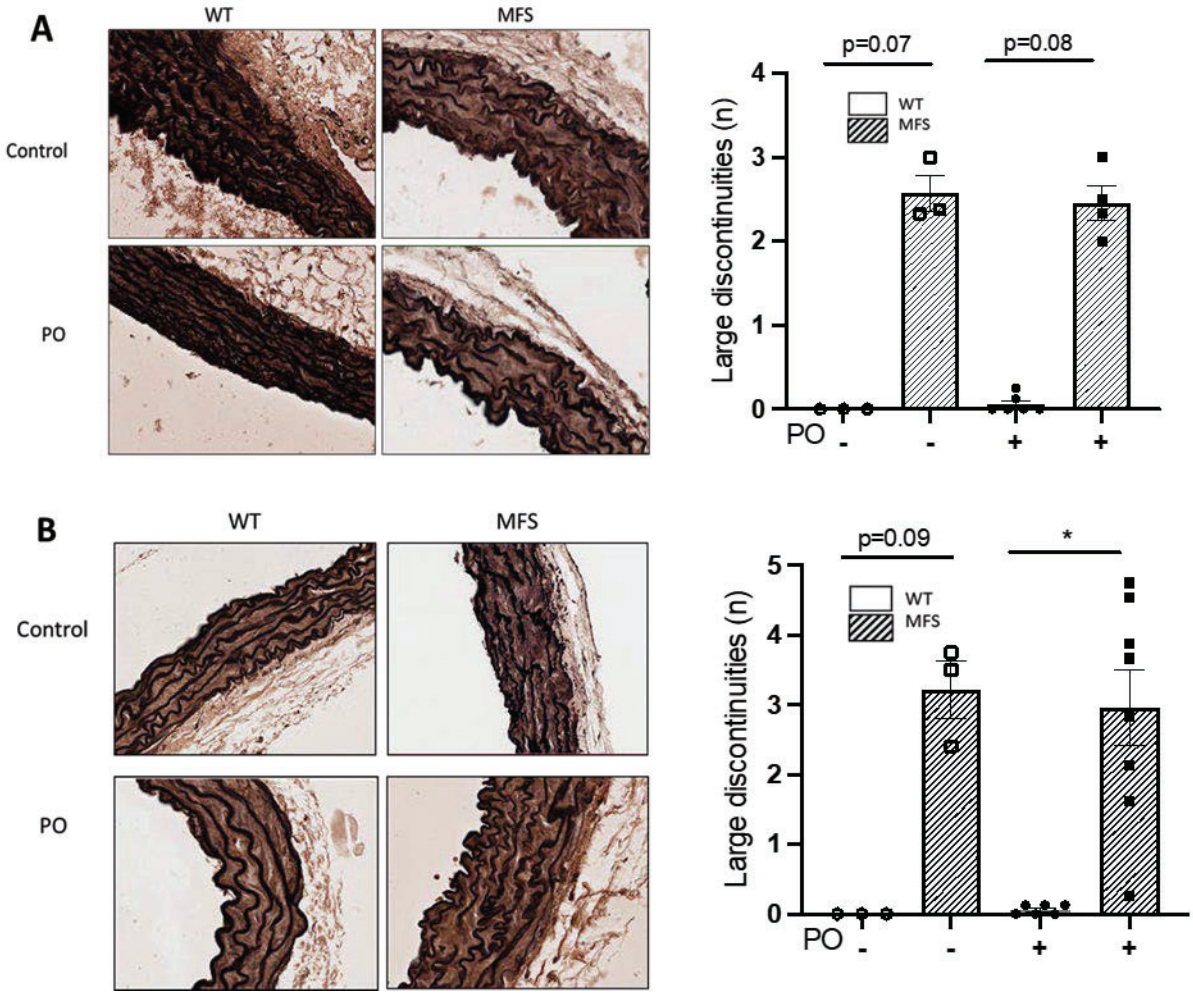
A
WT
MFS
Control
PO
p=0.07
p=0.08
WT
MFS
Large discontinuities (n)
0
1
2
3
4
PO
-
-
+
+
B
WT
MFS
Control
PO
p=0.09
*
WT
MFS
Large discontinuities (n)
0
1
2
3
4
5
PO
-
-
+
+

Figure 5

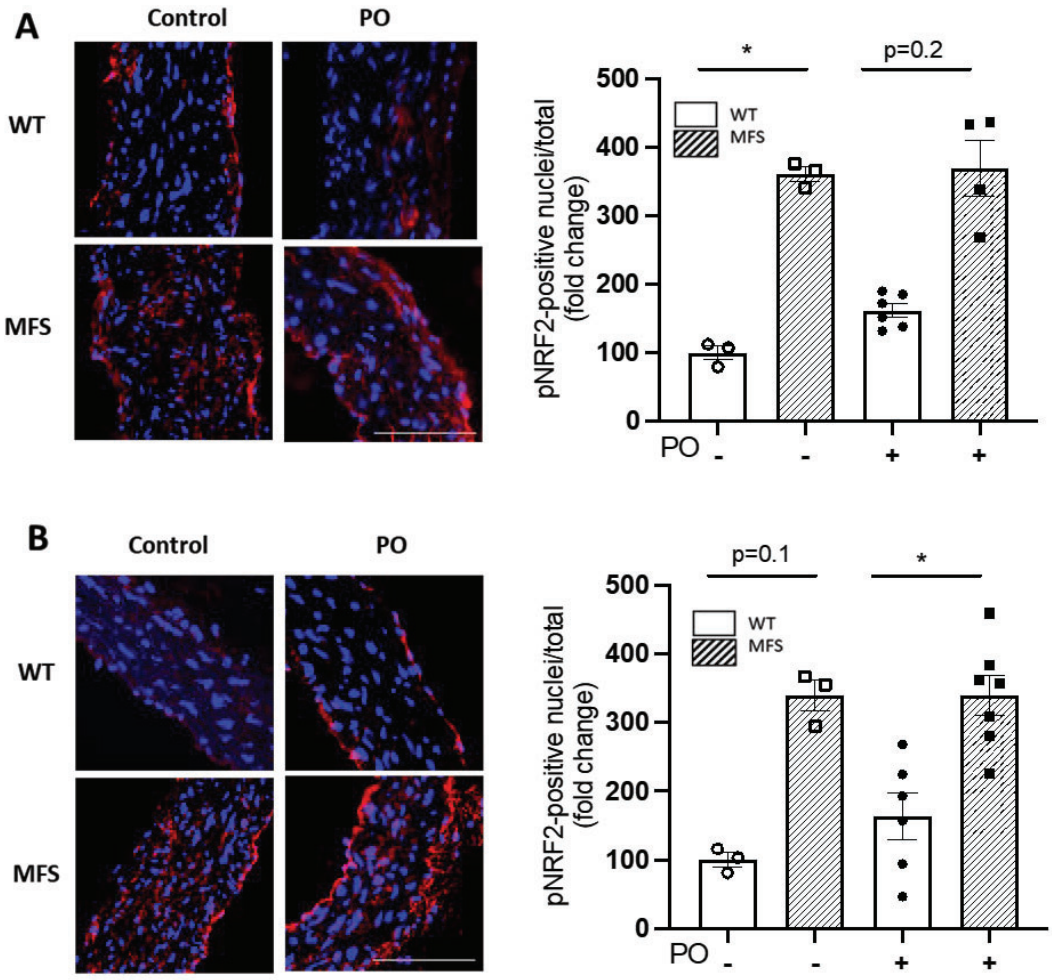
A
Control
PO
WT
MFS
*
p=0.2
WT
MFS
pNRF2-positive nuclei/total
(fold change)
500
400
300
200
100
0
PO
-
-
+
+
B
Control
PO
WT
MFS
p=0.1
*
WT
MFS
pNRF2-positive nuclei/total
(fold change)
500
400
300
200
100
0
PO
-
-
+
+

Table 1. Cardiac parameters measured by 2D ultrasound in WT and MFS treated (+) or not (-) with potassium oxonate (PO; in weeks).

		WT	WT	WT	WT	MFS	MFS	MFS	MFS
Potassium oxonate (PO)	Mice age (months)/ PO (weeks)	IVSD	LVPWD	LVDD	LVDS	IVSD	LVPWD	LVDD	LVDS
---------	2 m/0 w	0,82±0,01	0,79±0,01	1,98±0,02	1,27±0,03	0,81±0,01	0,77±0,01	1,98±0,03	1,25±0,03
-	3 m/4 w	0,80±0,02	0,76±0,03	2,07±0,11	1,27±0,04	0,80±0,02	0,78±0,02	2,06±0,04	1,36±0,04
-	4 m/8w	0,87±0,04	0,95±0,09	1,88±0,05	1,29±0,08	0,95±0,09	0,95±0,09	2,31±0,19	1,39±0,05
-	6 m/16w	0,87±0,03	0,85±0,03	2,05±0,07	1,40±0,04	0,87±0,01	0,83±0,02	2,01±0,03	1,32±0,01
+	3 m/4 w	0,83±0,01	0,80±0,002	2,03±0,05	1,38±0,02	0,82±0,01	0,81±0,01	2,07±0,06	1,41±0,04
+	4 m/8 w	0,84±0,04	0,93±0,02	2,21±0,19	1,43±0,07	1,01±0,05	1,06±0,02	2,52±0,07	1,71±0,08
+	6 m/16 w	0,79±0,01	0,80±0,02	2,11±0,06	1,35±0,04	0,79±0,02	0,75±0,03	2,00±0,06	1,34±0,02

IVSD: interventricular septum diameter; LVPWD: left ventricle posterior wall diameter; LVDD: left ventricle diameter in diastole; LVDS: left ventricle diameter in systole.

SUPPLEMENTARY MATERIAL

HYPERURICAEMIA DOES NOT INTERFERE WITH AORTOPATHY IN A MURINE MODEL OF MARFAN SYNDROME

Isaac Rodríguez-Rovira[1], Angela López-Sainz[2], Maria Encarnación Palomo-Buitrago[1], Belén Pérez[3], Francesc Jiménez-Altayó[3], Victoria Campuzano[1,4], and Gustavo Egea[1,5,*]

[1]Departament of Biomedical Sciences, University of Barcelona School of Medicine and Health Sciences, 08036 Barcelona (Spain).

[2]Department of Cardiology, Hospital Clínic de Barcelona, IDIBAPS, 08036 Barcelona (Spain).

[3]Department of Pharmacology, Autonomous University of Barcelona School of Medicine, 08192 Bellaterra (Barcelona, Spain).

[4]Centro de Investigación Biomédica en Red de Enfermedades Raras (CIBERER), ISCIII, 28029 Madrid (Spain).

[5]Center of Medical Genetics, University of Antwerp, Antwerp (Belgium).

*Correspondence: gegea@ub.edu.

ABSTRACT

Redox stress is involved in the aortic aneurysm pathogenesis in Marfan syndrome (MFS). We recently reported that allopurinol, an inhibitor of XOR, inhibited aortopathy in a MFS mouse model acting as an antioxidant without altering uric acid (UA) plasma levels. Hyperuricaemia is ambiguously associated with cardiovascular injuries as UA, having antioxidant or pro-oxidant properties depending on the concentration and accumulation site. We aimed to evaluate whether hyperuricaemia causes harm or relief in MFS aortopathy pathogenesis. Two-month-old male wild-type (WT) and MFS mice (*Fbn1*$^{C1041G/+}$) were injected intraperitoneally for several weeks with potassium oxonate (PO), an inhibitor of uricase, an enzyme that catabolises UA to allantoin. Plasma UA and allantoin levels were measured via several techniques, aortic root diameter and cardiac parameters by ultrasonography, aortic wall structure by histopathology, and pNRF2 levels by immunofluorescence. PO induced a significant increase in UA in blood plasma both in WT and MFS mice, reaching a peak at three and four months of age but decaying at six months. Hyperuricaemic MFS mice showed no change in the characteristic aortic aneurysm progression or aortic wall disarray evidenced by large elastic laminae ruptures. There were no changes in cardiac parameters or the redox

stress-induced nuclear translocation of pNRF2 in the aortic tunica media. Altogether, the results suggest that hyperuricaemia interferes neither with aortopathy nor cardiopathy in MFS mice.

SUPPLEMENTARY FIGURE LEGENDS

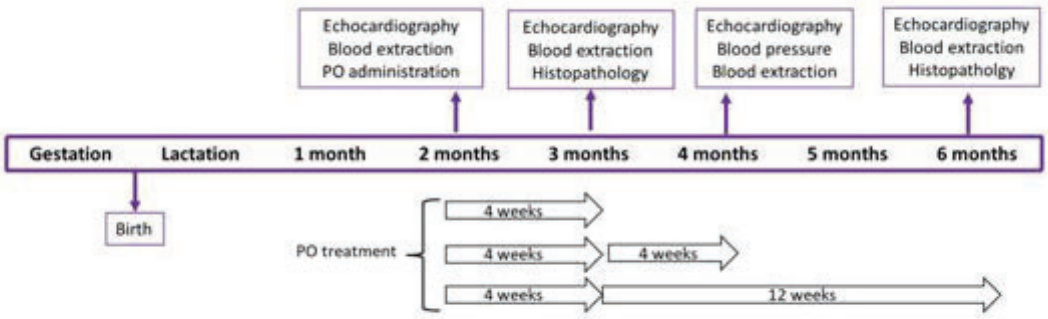

Supplementary Figure 1. Representative scheme of the experimental protocols for allopurinol treatments. PO: potassium oxonate. PO was administered to WT and MFS mice for four weeks, some animals were euthanized and other continued receiving PO for additional 4 weeks or 12 weeks for a total time of 8 and 16 weeks, respectively.

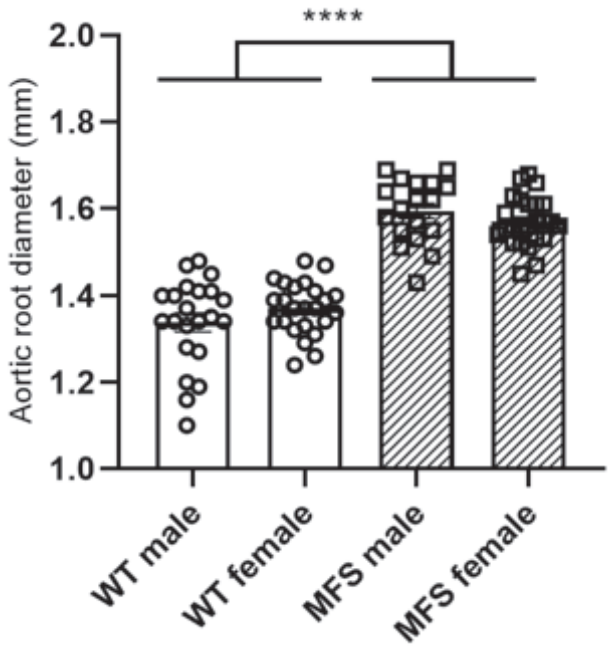

Supplementary Figure 2. Aortic root diameter in WT and MFS mice at the start point of the study (two months old). The aortic root diameter of male and female WT and MFS mice was measured with 2D echocardiography. Results are the mean ± SEM. Statistical test: Two-way ANOVA. ****$p \leq 0.0001$.

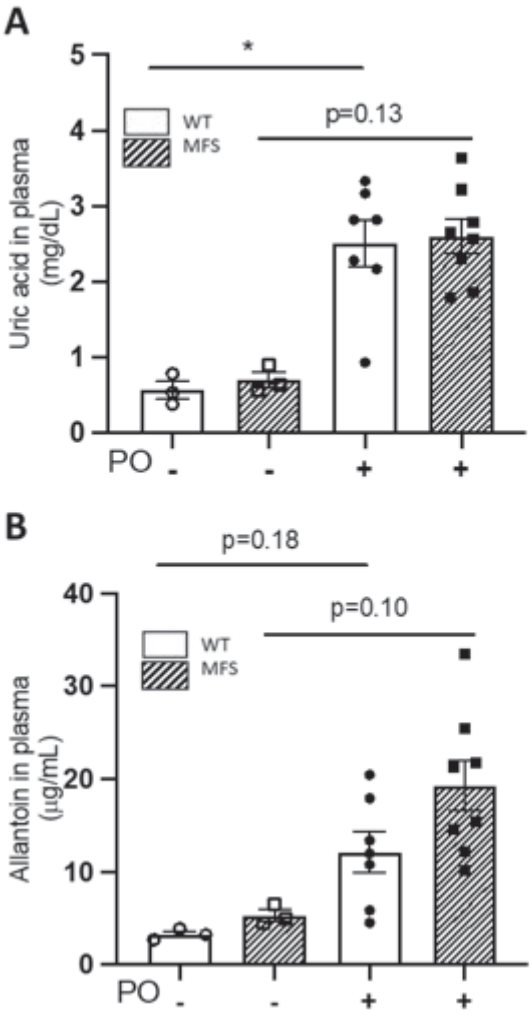

Supplementary Figure 3. Uric acid and allantoin plasma levels following eight weeks of potassium oxonate treatment. Three-month-old WT and MFS mice (treated with PO for four weeks) continued receiving PO treatment for four weeks more (total of eight weeks of PO treatment; four-month-old mice) and their uric acid (A) and allantoin (B) plasma levels were determined. Results are the mean ± SEM. Statistical tests: Kruskal Wallis, Dunn's *post-hoc*. *$p \leq 0.05$

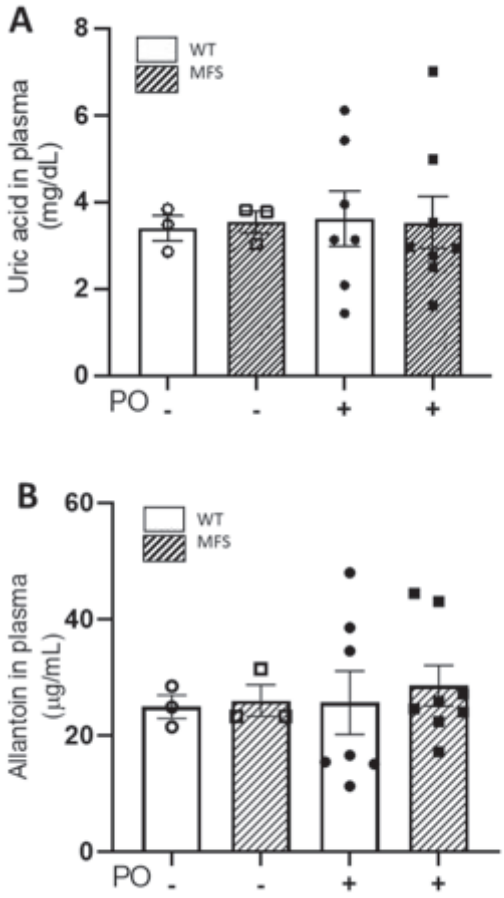

Supplementary Figure 4. Uric acid and allantoin plasma levels following 16 weeks of potassium oxonate treatment. Male WT and MFS mice treated for eight weeks with potassium oxonate (PO) were treated for an additional eight weeks (16 weeks of PO treatment; six-month-old mice) and uric acid (A) and allantoin (B) plasma levels were determined. Results are the mean ± SEM. Statistical test: Kruskal-Wallis.

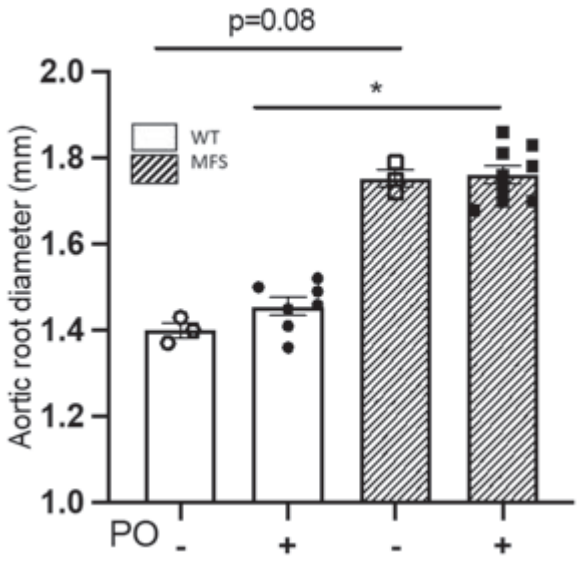

Supplementary Figure 5. Aortic root diameter in WT and MFS mice following eight weeks of potassium oxonate treatment. Male WT and MFS mice treated for four weeks with potassium oxonate (PO) were treated for an additional four weeks (eight weeks of PO treatment; four-month-old mice) and the aortic root diameter was measured again with 2D echocardiography. Results are the mean ± SEM. Statistical tests: Kruskal Wallis, Dunn's *post-hoc*. **p* ≤0.05.

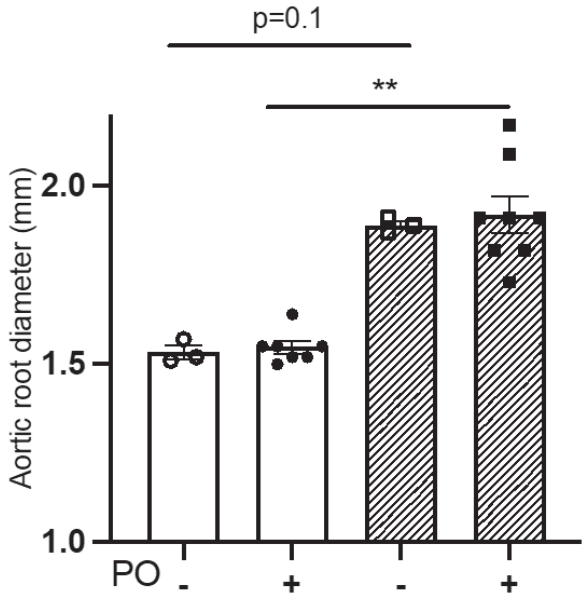

Supplementary Figure 6. Aortic root diameter in WT and MFS mice following 16 weeks of potassium oxonate treatment. Male WT and MFS mice treated for eight weeks with potassium oxonate (PO) were treated for an additional eight weeks (16 weeks of PO treatment; six-month-old mice) and the aortic root diameter was measured again with 2D echocardiography. Results are the mean ± SEM. Statistical tests: Kruskal Wallis, Dunn's *post-hoc*. ***p* ≤0.01.

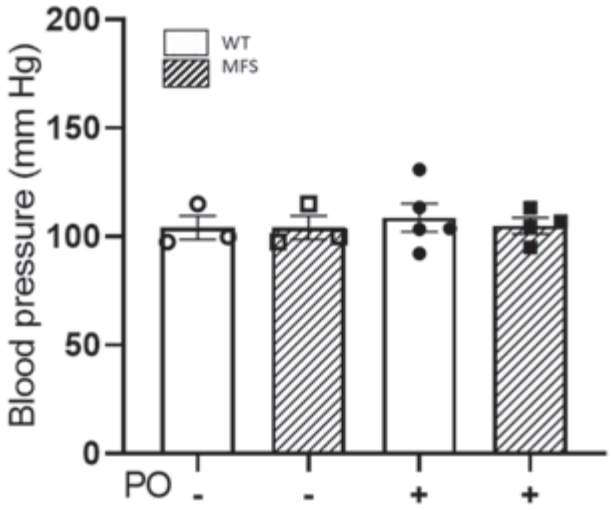

Supplementary Figure 7. Blood pressure in WT and MFS treated with potassium oxonate. Systolic blood pressure measurements in four-month-old WT and MFS mice treated with potassium oxonate (PO; eight weeks). Results are the mean ± SEM. Statistical test: Kruskal-Wallis with Dunn's multiple comparison test.

4. SUMMARY OF RESULTS

Contribution of the PhD candidate: report from the thesis supervisors As the supervisors of the doctoral thesis presented by Isaac Rodríguez Rovira, entitled "Insights in the pathogenesis of the aortic aneurysm in Marfan Syndrome and new therapeutic approaches", we certify his active participation in the experimental tasks, analysis of the results obtained and their discussion, formulation of conclusions and preparation of the manuscripts of the projects included in this thesis. The specific contributions of the PhD candidate for each project are listed below, along with the impact factors (IF) of the journals where results were published. None of the published articles have been presented as part of other doctoral theses.

Article 1: Arce C, Rodríguez-Rovira I, De Rycke K, Durán K, Campuzano V, Fabregat I, Jiménez-Altayó F, Berraondo P, Egea G. Anti-TGFβ (Transforming Growth Factor β) Therapy With Betaglycan-Derived P144 Peptide Gene Delivery Prevents the Formation of Aortic Aneurysm in a Mouse Model of Marfan Syndrome. Arterioscler Thromb Vasc Biol. 2021 doi: 10.1161/ATVBAHA.121.316496

IF 2021 = 8,313; Q1

Contribution of the PhD candidate: The candidate has significantly contributed to a large portion of the results presented in the article and supplementary figures. They have also participated in the discussion of the results, partially contributed to the writing of the manuscript, and participated in the discussion of the results.

Article 2: Rodríguez-Rovira I, Arce C, De Rycke K, Pérez B, Carretero A, Arbonés M, Teixidò-Turà G, Gómez-Cabrera MC, Campuzano V, Jiménez-Altayó F, Egea G. Allopurinol blocks aortic aneurysm in a mouse model of Marfan syndrome via reducing aortic oxidative stress. Free Radic Biol Med. 2022 20;193:538-550. doi:10.1016/j.freeradbiomed.2022.11.001.

IF 2022 = 8,313; Q1;

Contribution of the PhD candidate: The candidate has participated in the majority of the results presented in the article and supplementary figures, in experimental designs, and in the development of experimental techniques. They have contributed to the initial drafts of the article and have been actively involved in the discussion of both the results and the article itself.

Article 3: Rodriguez-Rovira I, Lopez-Sainz A, Palomo-Buitrago ME, Perez B, Jimenez-Altayó F, Campuzano V, Egea G. HYPERURICAEMIA DOES NOT INTERFERE WITH AORTOPATHY IN A MURINE MODEL OF MARFAN SYNDROME. BioRxiv 2023.05.21.541606; doi: https://doi.org/10.1101/2023.05.21.541606 under revision in International Journal of Medical Sciences)

IF 2022 = 6,208; Q1

Contribution of the PhD candidate: The candidate has participated in every presented result, in the development of the initial drafts of the article, and in the overall discussion of both the results and the article.

In summary, the candidate is a highly significant contributor to the articles presented for his thesis. Lastly, regarding the shared use of results for different theses, I guarantee that none of the co-authors of the articles provided by the candidate Isaac Rodríguez-Rovira for this thesis have used any results, either in whole or in part, for any other doctoral thesis.

Director, supervisor and tutor

Gustavo Egea Guri

EGEA GURI GUSTAVO - 46218960T
Firmado digitalmente por EGEA GURI GUSTAVO - 46218960T
Fecha: 2023.06.20 09:44:09 +02'00'

Signature

Summary of the results

Article 1: Anti-TGFβ (Transforming Growth Factor β) Therapy With Betaglycan-Derived P144 Peptide Gene Delivery Prevents the Formation of Aortic Aneurysm in a Mouse Model of Marfan Syndrome

In the two treatments that we performed in the article with P144, in the preventive approach, Marfan syndrome mice did not exhibit aortic dilation, whereas untreated Marfan syndrome mice of the same age already developed aneurysms. However, the palliative treatment with P144 did not effectively stop the progression of the aneurysm. In all instances, P144 enhanced the morphology of elastic fibers and restored the TGFβ signaling pathway mediated by pERK1/2 to normal levels. In contrast to the palliative treatment, the preventive approach resulted in reduced mRNA levels of Tgfβ1 and Tgfβ2.

Article 2: Allopurinol blocks aortic aneurysm in a mouse model of Marfan syndrome via reducing aortic oxidative stress.

In the aortic samples obtained from individuals with MFS, immunohistochemistry revealed an increase in XOR protein expression in both the tunica intima and media of the dilated area. In MFS mice (Fbn1C1041G/+), the mRNA transcripts of XOR and the enzymatic activity of the XO were found to be elevated in the aorta of 3-month-old mice but not in older animals. Treatment with the XOR inhibitor ALO effectively halted the progression of aortic root aneurysms in MFS mice. When ALO was administered prior to the onset of the aneurysm, it prevented its subsequent development. ALO also inhibited MFS-associated endothelial dysfunction, as well as elastic fiber fragmentation, nuclear translocation of pNRF2, increased levels of 3'-nitrotyrosine, and collagen remodeling in the tunica media. Furthermore, ALO reduced the excessive production of H_2O_2 in the large aorta of MFS mice, as well as the overexpression of NOX4 and MMP2 at the transcriptional level.

Article 3: HYPERURICAEMIA DOES NOT INTERFERE WITH AORTOPATHY IN A MURINE MODEL OF MARFAN SYNDROME

The administration of PO resulted in a significant increase in blood plasma levels of uric acid (UA) in both WT and MFS mice, with the highest levels observed at three to four months of age, followed by a decline at six months. Interestingly, hyperuricemic MFS mice did not exhibit any alterations in the typical progression of aortic aneurysms or the structural disarray of the aortic wall, characterized by ruptures in large elastic laminae. Additionally, there were no changes observed in cardiac parameters or the nuclear translocation of pNRF2 induced by redox stress in the aortic tunica media.

5. DISCUSSION

MFS is a rare disorder associated with multisystem manifestations in which cardiovascular one is the most serious. The development of animal models of the disease has allowed the study of the pathomechanisms underlying the different features of the syndrome unfortunately without establishing a clear phenotype associated to numerous mutations in *Fbn1*.

Until now, studies have been focusing in understanding the formation and development of the aneurysm by unraveling new molecular mechanisms that are involved in the aortopathy (Deleeuw et al. 2021). Furthemore, different studies have been suggesting new therapies and treatments that target different mechanisms and molecules in order to block or mitigate the progression of the aortic root dilation (Nettersheim et al 2022; Mieremet et al. 2022). So far, MFS main molecular studies have been focused on targeting TGF-ß but more recently other targets including oxidative stress are acquiring more relevance.

In this thesis we have carried out three different studies in which we evaluated the two known molecular pathways that significantly contribute to the formation and progression of the aortic aneurysm in MFS: The first study is focus on the TGF-ß signaling pathway, in which the excess of TGF-ß is abducted by a peptide (P144 peptide), and the other two studies focused on theredox stress, in which on one hand we study the contribution of XOR as an important source of ROS evaluating allopurinol as a potential new drug therapy; and on the other hand, we evaluate the impact of uric acid, as the final product of XOR activity (at least in humans)(Figure 11).

In the first study (P144), we focused in targeting the TGF-ß pathway, we investigated the potential of using the peptide P144 derived from betaglycan/TGFβ receptor III as a novel therapeutic approach to interfere in the development of aortic aneurysms in MFS. To assess its effectiveness, we administered P144 using an AAV-based expression vector in MFS mice (C1041G/+) before and after the formation of the aneurysm.

The key findings of the study are:

1. P144 is consistently expressed in the liver and also but to a lesser extent in the aorta, indicating its potential effectiveness in the latter.

2. P144 prevents the formation of the aneurysm, but once the aneurysm is already present, the peptide is unable to halt its progression.
3. The prevention of the aneurysm formation by P144 also avoids aortic wall disarrays and the TGFβ hypersignaling mediated by ERK1/2, both characteristic of MFS aorta
4. The early administration of P144 normalizes the elevated levels of Tgfβ1 and Tgfβ2 transcripts that are typically observed in MFS mice.

Many studies before last the decade indicated that TGFβ hypersignaling was fully determinant of aneurysm progression in MFS (Milewicz et al. 2017; Hoffman et al. 2019). Having this on mind, we hypothesized that the betaglycan-derived peptide P144 could be a promising therapeutic tool to regulate the excessive availability of active TGFβ in aortic mural cells. Using P144 as an anti-TGFβ agent had the advantage of partial inhibition of TGFβ signaling, which provided a better safety profile compared to complete inhibition, thus reducing the risk of tumor formation. In our study, we found that preventive administration of P144 effectively suppressed the overexpression of Tgfβ1 and Tgfβ2 in MFS mice without significantly affecting their normal levels in WT animals. These results indicate that P144 not only acts as a sequestering agent for excess TGFβ but also influences the transcription of these ligands within the aortic wall, suggesting a potential feedback or direct regulatory effect. While changes in mRNA expression levels may not necessarily reflect a reduced capability of P144 to sequester excess soluble TGFβ ligands at the protein level, it is worth noting that similar reductions in TGFβ expression have been observed when using TGFβ inhibitors in liver cancer patients. This reduction in expression is considered a diagnostic biomarker indicating the efficacy of the treatment. Importantly, the findings from our study demonstrate that while P144 can prevent the formation of aneurysms in both the short and long term, it does not halt the progression of existing aneurysms. This confirms the divergent role of TGFβ in the development and growth of aortic aneurysms in MFS, as previously reported. Ramirez's laboratory has shown that the impact of TGFβ on aneurysm formation and progression varies, with both protective and detrimental effects depending on the timing of cytokine activity interception and the therapeutic agent used (neutralizing anti-TGFβ antibodies or losartan) (Ramirez et al. 2015).

However, recent publications have evidenced that in fact TGFβ hypersignaling is a secondary driver of aneurysm progression in MFS (Tellides et al. 2017; Jones et al. 2009). Blocking TGFβ in young MFS animals at an early stage of the disease exacerbated the aneurysm, while treatment at later stages was beneficial. Similar findings were reported in another MFS mouse model,

where the loss of physiological (SMC)-associated TGFβ signaling enhanced aortopathy after postnatal SMC-specific deletion of TβRII. It was also observed that an anti-TGFβ neutralizing antibody exacerbated thoracic and abdominal aortic disease induced by Ang II infusion in mice. These findings indicate that maintaining a physiological basal level of TGFβ signaling is crucial for normal aortic development, and its imbalance can lead to aortopathy (Cook et al. 2015). Our results align with this notion, as the expression of the P144 peptide in MFS mice (C1041G/+) maintains TGFβ ligands and canonical (SMAD2) and noncanonical (ERK1/2) downstream signaling pathways at normal levels. However, when P144 was administered after aortic aneurysm progression had already begun, it did not effectively reduce the overexpression and availability of bioactive soluble TGFβ ligands, potentially becoming detrimental. It is possible that at this stage, the levels of aortic P144 expression are insufficient to counteract the excess TGFβ activity. Additionally, other mechanisms may come into play, particularly at advanced stages of aneurysm progression, interfering with TGFβ expression and function, and compensating for the local inhibitory effect of P144. One such mechanism could involve Ang II-AT1R, which dysregulates TGFβ-independent mechanisms that contribute to aortic aneurysm progression through vascular mechanical stress, hemodynamic force, and kinetic energy. These mechanisms may indirectly interfere with TGFβ-associated signaling pathways, including the SMAD pathway and the expression levels of TGFβ ligands and their receptors, ultimately influencing aneurysm growth and rupture. However, it is evident from our study and previous research that while TGFβ is necessary, it is not sufficient for aortic formation and growth. The context and timing of its signaling levels are critical in determining whether its potential therapeutic effect becomes detrimental or beneficial.

In the second study (XOR), we demonstrated a new source of oxidative stress in MFS and a new potential therapeutic treatment to block the formation and progression of the aortic aneurysm initially based on XOR overexpression both in MFS patients and mice.

In the last decade, there has been a huge progress in understanding the molecular mechanisms involved in the development and progression of aortic aneurysms in MFS. However, current pharmacological treatments such as angiotensin receptor blockers (ARBs) and β blockers have shown uncertain results in halting or slowing down the progression of aortic aneurysms. A recent meta-analysis of randomized trials indicated that the combination of ARBs and β blockers may be more effective than either treatment alone in reducing the enlargement of the aortic root in MFS patients. In this second study we aimed to deepen into the role of oxidative distress in the molecular pathogenesis of aortic aneurysms being focus on XOR.

The key findings of our study are the following:

(i) XOR, a potent ROS-generating system, is upregulated in the aorta of both MFS patients and young mice;

(ii) this upregulation is accompanied by increased enzymatic activity of the oxidase form (XO);

(iii) treatment with the XOR inhibitor allopurinol prevents the formation and progression of aortic root dilation;

(iv) the inhibitory effect of allopurinol on the aortic aneurysm is not permanent, as the aneurysm reappears upon withdrawal of the drug

(v) allopurinol prevents endothelial-dependent vasodilator dysfunction that occurs in MFS;

(vi) allopurinol inhibits the MFS-associated increase in aortic H_2O_2 levels and some representative redox stress-associated reactions as well as the collagen remodeling in the aortic media;

(vii) allopurinol inhibits the characteristic upregulation of NOX4 and MMP2 that happens in the aortic tunica media in MFS.

It is important to highlight that XOR overexpression also occurs in aortic samples from MFS patients. This finding was consistent with our observations in MFS mice at the protein and mRNA level. Notably, the increase in XOR expression was observed only in young mice (3 months old) and not in older mice (6 and 9 months old), suggesting that XOR upregulation may occur during the rapid growth phase of aortic dilation, which slows down in older animals. However, previous studies have reported conflicting results regarding XOR activity in MFS aortae, possibly due to different MFS mouse models or variations in XOR activity assays and experimental conditions.

ALO is mainly associated with treating UA-related conditions, but the inhibitory effect of ALO over the aortopathy both when administered preventively and palliatively was not accompanied by changes in UA plasma levels, suggesting that UA could not interfere in aortopathy in MFS mice. Interestingly, ALO did not lead to the expected reduction in allantoin plasma levels. Therefore, our results suggest that the blockade of MFS aortopathy by ALO is not directly linked to changes in UA levels, but it should involve other accompanying mechanisms.

In this sense, it has been reported that ALO possesses a ROS-lowering effect independent of its XOR inhibition activity, acting as a direct ROS scavenger (George et al. 2006). We demonstrated this by adding ALO to MFS aortic rings in vitro, and we observed that ALO rapidly attenuated their elevated H_2O_2 production levels regardless of the age of the mice. Importantly, this reduction was also observed in aortic rings from MFS mice treated with ALO in vivo. In addition to its direct scavenging role, ALO can effectively act as a indirect antioxidant by reducing the upregulation of NOX4, an NADPH oxidase responsible for H_2O_2 generation.

ALO treatment also resulted in the reduction or inhibition of various pathological responses associated with redox stress, such as the accumulation of 3-NT, the nuclear translocation of pNRF2, and the fibrotic remodeling in the aortic media. These findings have several implications in the pathophysiology of MFS aortic media: (i) the increase in 3-NT indicates abnormal RNS formation due to the pathological uncoupling of NO, leading to protein nitration via the highly reactive intermediate peroxynitrite and its subsequent product, 3-NT. The elevation of 3-NT in MFS aortic media aligns with recent evidence of NO uncoupling in aneurysm formation in MFS mice and patients . Actin, identified as a nitrated protein target in MFS aorta from MFS patients, contributes to the reported impaired contractile properties of VSMCs in MFS ; (ii) redox stress in MFS aorta is elevated to a degree that the intrinsic physiological antioxidant response mediated by pNRF2 nuclear translocation is insufficient to compensate. In contrast, ALO treatment allows for this compensation, normalizing endogenous redox levels in MFS aorta and associated modifications; and (iii) ALO normalized the content of immature collagen fibers, thereby mitigating the collagen remodeling response that typically accompanies aneurysm formation to compensate for elastic fiber disarray. It would be interesting to explore whether ALO can also prevent the characteristic phenotypic switch of VSMCs to a mixed contractile-secretory phenotype.

Finally, ALO normalized ACh-stimulated vasodilator function, improving endothelial function. This is not surprising given the reported effects of ALO in increasing NO bioavailability, partially or entirely attributable to reduced ROS production. Restoring endothelial function is crucial since it has been observed that flow-mediated dilatation, a noninvasive measure of endothelial function, correlates with aortic dilatation in MFS patients.

In sum, mechanistically talking, we show that allopurinol blocks the progression of MFS aortopathy by acting as a potent antioxidant. It directly inhibits XOR activity and acts as a scavenger of ROS, but also indirectly normalizing aortic NOX4 and MMP2 expression levels.

In the third study (uric acid), we studied the contribution of UA in the MFS aortopathy, whether acting as an antioxidant or a prooxidant. In humans, the role of UA in oxidative stress and CVD is still debated. Some epidemiological studies suggest that elevated levels of UA in the blood are a risk factor for CVD, which are characterized by oxidative stress.

In humans, UA is considered an important antioxidant in the body and has been proposed as a potential treatment for certain central nervous system disorders (Chamorro et al. 2014). However, studying the role of UA in these conditions is challenging, and animal models are often used to investigate these hypotheses. In rodents, the breakdown of purines does not stop at UA, resulting in the potential accumulation of UA (hyperuricemia) in the blood or tissues. To definitively study the potential relationship between UA and the development of aortic aneurysms in MFS, we had to induce hyperuricemia experimentally using oxonic acid, which inhibits uricase, which is the the enzyme that catabolizes UA to allantoin in mice.

In our study, we generated a transient mouse model of MFS with hyperuricemia by administering potassium oxonate (PO) in drinking water. The main findings we obtained were the following:

(i) Despite MFS mice developing aortic aneurysms, their UA plasma levels are not significantly different from those of WT animals.

(ii) PO administration causes a temporary but significant increase in plasma UA levels, allowing us to assess its impact on the progression of aortopathy and cardiopathy in the MFS mouse model.

(iii) The accumulation of UA in blood plasma induced by PO does not affect the progression of aortic aneurysms or the examined cardiac parameters in the MFS mouse model.

(iv) Hyperuricemia induced by PO does not alter the characteristic cellular anti-redox stress responses observed in MFS aortic media, as evidenced by the nuclear translocation of pNRF2 in aortic VSMCs.

Although there is evidence supporting the involvement of oxidative stress in human aortic aneurysms, the relationship between systemic oxidative stress, UA levels, and aortic dilatation has not been definitively established. Nonetheless, some recent studies have shown that higher serum UA levels and total antioxidant capacity are associated with aortic dilatation in humans,

indicating a link between UA levels and oxidative stress (Zhang et al. 2020; Jiang et al. 2016; Wang et al., 2023). However, our study using the hyperuricemic MFS mouse model induced by oxonic acid did not confirm this relationship (Scott et al. 2001; Hooper et al. 2001). Additionally, it had no effect on the cellular anti-oxidative stress response in the aortic smooth muscle cells of the MFS mice, as indicated by the absence of nuclear translocation of pNRF2, a marker of this response.

Strikingly, plasma levels of allantoin, a product of non-enzymatic transformation of UA, did not decrease in parallel with the increase in UA levels induced by oxonic acid. This discrepancy can be explained by the known non-enzymatic conversion of UA to allantoin, which can occur through oxidative reactions. The accumulation of UA might explain the elevated levels of allantoin.

Strikingly, in Yang et al. 2023 they showed higher uric acid levels in the MFS mice suggesting the UA is detrimental and is the main player in the formation of the aneurysms in different pathologies. We did not observe higher UA levels in none of our ages in our MFS mice model, and neither in the febuxostat study. A possible explanation could be the type of food administrated, the conditions they kept the mice, or even the extraction method they used for processing the blood regardless of the genotype.

Even though we did not obtain any relevant result in our UA study, we keep in mind that maybe the method we used to increase UA levels in plasma might not be the best. As stated before, UA if found in the plasma they suggest it has an antioxidant effect, whether if it is found in the cytoplasm of the cells could act as a prooxidant. This localization might play a crucial role, and in our hands, we did not control the exact location of UA with the oxonic acid treatment.

In addition, we consider that UA effect could be studied in a different manner. In order to persistently accumulate UA plasma levels and not transitionally as we have done with PO, we suggest the generation of a MFS mouse model knocked down for urate oxidase (*Uox*$^{-/-}$), the enzyme that transforms uric acid into allantoin, but only at the aorta Nonetheless, the expected higher accumulation of UA at blood plasma could be toxic to mice, as therefore quickly eliminated. In fact different studies that have used UOX-/- mice model have shown at short-term problems in mice survival.Actually, in Lu et al 2017, they developed a UOX KO mice model, and the survival rate decreased drastically after week 5 of age.

Another interesting manner to evaluate whether UA plays a key role in the MFS aortopathy, it would be by using probenecid (Colín-González et al. 2013), a drug used to properly eliminate UA, by blocking URAT1. This enzyme allows the UA to go back to the bloodstream, and probenecid increases the UA excretion through the urine. This method would provide new information by reducing UA levels in the MFS, and we plan to study it in the lab soon

Overall discussion: potential translationality of our results to MFS patients

These three studies presented in the present thesis have provided new knowledge in the MFS aortopathy development, but we consider that not all of them have potential translationality to the clinical practise.

In the P144 study, when we injected the peptide before the aneurysm was formed, the aneurysm did not appear, but once the aneurysm was established, P144 could not revert the aortic root dilation. This was not the case in the allopurinol (ALO) study, as ALO blocked the formation and development of the aneurysm regardless of the time was administrated.

Furthermore, P144 treatment is really difficult to be applied to patients because: (1) P144 is integrated into hepatocytes and we have not tested at long-term the effects of this incorporation in the liver cells and the secondary effects that it may have, whether affecting the expression of other genes or the cell proliferation, and (2) MFS patients that carry “de novo” mutations (and diagnosed of the disease) do not usually show the aortopathy until years of life (and highly variable) and , and the administration of AVV-P144 would require to have detected the disease but without having shown any dilatation of the aorta, with is not the usual situation in clinical practice. Only in those cases in which the disease has been transmitted from parents to children could it be theoretically possible, knowing that they are already carriers of the mutation.

However, ALO does not present the above problems with P144. As it is a safe drug that it is administered orally and from our study in MFS mice, ALO could be administered to MFS patients regardless whether have already developed or not the aneurysm since ALO blocked both the formation and the progression of the aortic aneurysm. Therefore, ALO is with much the most suitable drug for a translational approach to the aortopathy in patients.

It is curious that ALO already presents several capacities regardless of the main known one. It can inhibit the XOR activity (Lee et al. 2009), it is also used to treat the leishmaniosis in dogs (Manna et al. 2009), as it interdicts the "de novo" synthesis of pyrimidines, and it acts as a ROS scavenger (George et al. 2006). Little is known about the mechanisms underlying all these effects, but there might be a common one that could help to understand all of these. One interesting point that could provide more information about the ALO mechanism of action is evaluating the mRNA expression of TGF-ß levels in treated aortic samples. As known, P144 reduced the mRNA expression levels of TGF-ß1 and TGF-ß2 in the preventive treatment, and TGF-ß triggers the expression of NOX4 which is involved in oxidative distress in MFS. Furthermore, ALO reduced the mRNA expression levels of NOX4, and ALO could be acting as a negative feedback loop inhibiting directly, or indirectly, the H_2O_2 formation from NOX4 upregulated by TGF-ß.

Regardless of the specific mechanism of action, it is known that ALO and similar drugs that present the same effect have an effect in the MFS aortopathy. Our ALO study was the first one being published, and subsequently 2 more papers have been published demonstrating the same effects as us. In Yagi et al. 2022, they test the effect of febuxostat, a drug that also blocks XOR activity, and it has a similar effect as ALO, it blocks the aortic aneurysm in MFS. Moreover, in Yang et al 2023 they test ALO in our same MFS mouse model and the same dose we used, and they obtained the same results as we did, ALO indeed blocked the aortopathy in MFS.

In the recent years, researchers have tried to develop new strategies and treatments in order to block or mitigate the aortic aneurysm in MFS. As the final objective is to be able to translate this results in patients, all the strategies that are based on a knockingout or a knockdown genes are not suitable to be applyed in humans (e.g. XOR KO) (Yagi et al. 2022). Therefore, the only realistic strategy that left is combined drug treatments to avoid or delay as musc as possible aortic surgery. Nitro-oleic acid (Nettersheim et al. 2022), resveratrol (Mieremet et al 2022), rapamycin (Zaradzki et al 2022), Vitamin B (Huang et al. 2021) or apocynin (Yang et al 2010), among others (Deleeuw et al. 2021) are some of the published studies that have provided new information to the MFS aortopathy, nevertheless none of them have been applied into humans, whether some of them have strong secondary effects or are not completely safe, or because they are expensive.

We suggest that ALO is a great candidate to test in MFS patients. It is a safe and well-tolerated drug, economic and easy to administrate. Important to highlight is that the dose of ALO used in mice (20 mg/kg/day) if it was translated to humans, it would be a doses equivalent of ~120 mg/day (for a 70 kg individual). It is known that at these doses ALO does not reduce the normal UA plasma levels (6-7 mg/dL).

For a hypothetical clinical trial with ALO, we would suggest to administered together beta-blockers and/or losartan since in this way significant mechanisms involved in the aortopathy are pharmacologically targeted at the same time (heart rate/atenolol, TGF-ß/losartan and redox stress/ALO)

Even though our results with UA do not demonstrate an impact in MFS aortopathy, it has been reported that UA has an effect at cerebrovascular level particularly in stroke. In Chamorro et al. 2014, they examined the potential benefits of uric acid therapy in patients with acute ischemic stroke by studying its effects on functional outcomes after 90 days. Uric acid, known for its antioxidant properties and neuroprotective effects in experimental stroke models, was the focus of their assessment.

To sum up, in Figure 11 I show a summary of the main findings of this thesis. We have definitively provided new significant insights in the pathomechanism of the aortopathy in MFS involving altered TGF-ß signaling and oxidative stress. From our studies, we strongly bet for allopurinol as a realistic pharmacological drug that in combination with current ones (beta-blockers and angiotensin II receptor antagonists) could result together much effective than their single administration. Nonetheless more research is needed to understand completely the mechanisms and their role in the formation and development of the aortic aneurysm in MFS and surely on next years we will witness of it.

A

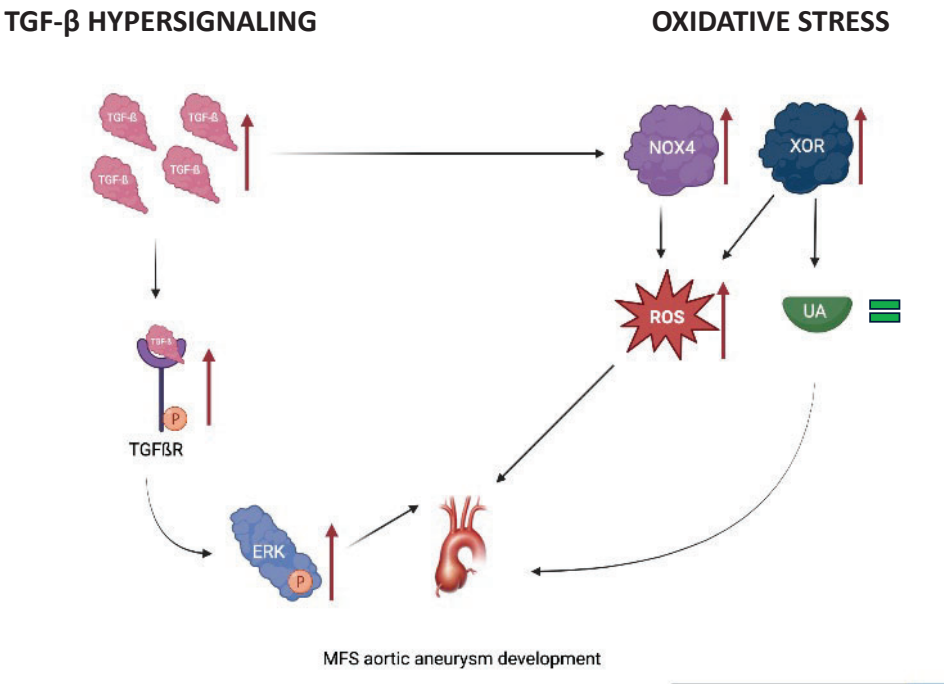

B

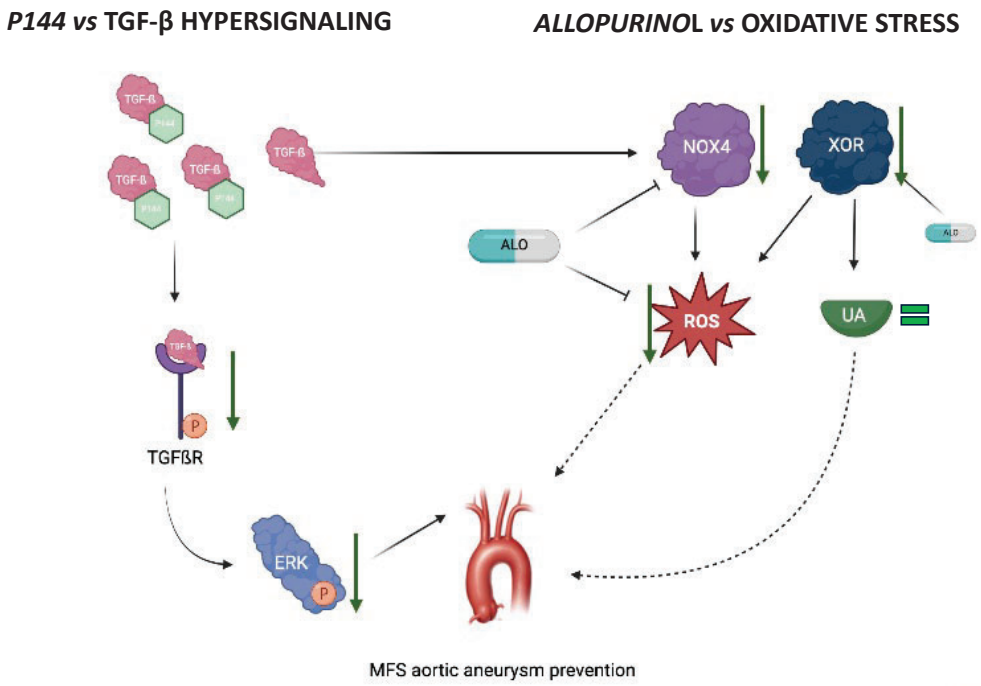

Figure 11. Summary of main findings in this thesis. (A) Pathological conditions in MFS and (B) after the different treatments.

5. CONCLUSIONS

(1) The soluble anti-TGF-β peptide P144 derived from the extracellular domain of betaglycan/TGFRβ III prevents the formation of aortic aneurysm, but not its progression in a murine model of Marfan syndrome (*Fbn1*$^{C1041G/+}$).

(2) Xanthine oxidoreductase as generator of oxidative stress is involved only in the early stages of aortopathy in a murine model of Marfan syndrome.

(3) Allopurinol blocks both the formation and the progression of the aortic aneurysm in a murine model of Marfan syndrome by acting directly as antioxidant and inhibitor of xanthine oxidoreductase, as well as indirectly inhibiting the overexpression of MMP2 and NADPH oxidase Nox4. We propose the use of allopurinol in a combinatory pharmacological therapy with other currently used drugs for patients with Marfan syndrome.

(4) Uric acid does not participate in the progression of aortic aneurysm in a murine model of Marfan syndrome.

6. REFERENCES

Akhtar K., Broekelmann T.J., Miao M., Keeley F.W., Starcher B.C., Pierce R.A., Mecham R.P., Adair-Kirk T.L. Oxidative and nitrosative modifications of tropoelastin prevent elastic fiber assembly in vitro. J. Biol. Chem. 2010;285:37396–37404. doi: 10.1074/jbc.M110.126789.

Annes JP, Munger JS, Rifkin DB. Making sense of latent TGFβ activation. J Cell Sci. 2003 Jan;116(Pt 2):217–24.

Araki K., Inaba K. Structure, mechanism, and evolution of Ero1 family enzymes. Antioxid. Redox Signal. 2012;16:790–799. doi: 10.1089/ars.2011.4418.

Arfin S, Jha NK, Jha SK, Kesari KK, Ruokolainen J, Roychoudhury S, Rathi B, Kumar D. Oxidative Stress in Cancer Cell Metabolism. Antioxidants (Basel). 2021 Apr 22;10(5):642. doi: 10.3390/antiox10050642.

Back M, Gasser TC, Michel J-B, Caligiuri G. Biomechanical factors in the biology of aortic wall and aortic valve diseases. Cardiovasc Res. 2013;99(2):232-241. doi:10.1093/cvr/cvt040.

Barcellos-Hoff MH, Dix TA. Redox-mediated activation of latent transforming growth factor-β1. Mol Endocrinol. 1996 Sep;10(9):1077–83.

Battelli M.G., Bolognesi A., Polito L. Pathophysiology of circulating xanthine oxidoreductase: new emerging roles for a multi-tasking enzyme. Biochim. Biophys. Acta. 2014;1842:1502–1517. doi: 10.1016/j.bbadis.2014.05.022

Battelli M.G., Polito L., Bortolotti M., Bolognesi A. Xanthine oxidoreductase in cancer: more than a differentiation marker. Cancer Med. 2016;5:546–557. doi: 10.1002/cam4.601

Battelli M.G., Bortolotti M., Polito L., Bolognesi A. The role of xanthine oxidoreductase and uric acid in metabolic syndrome. Biochim. Biophys. Acta (BBA) - Mol. Basis Dis. 2018;1864:2557–2565. doi: 10.1016/j.bbadis.2018.05.003

Berry CE, Hare JM. Xanthine oxidoreductase and cardiovascular disease: molecular mechanisms and pathophysiological implications. J Physiol. 2004 Mar 16;555(Pt 3):589-606. doi: 10.1113/jphysiol.2003.055913.

Boron WF, Boulpaep EL. Medical Physiology. Philadelphia: Elsevier; 2005.

Bortolotti M, Polito L, Battelli MG, Bolognesi A. Xanthine oxidoreductase: One enzyme for multiple physiological tasks. Redox Biol. 2021 May;41:101882. doi: 10.1016/j.redox.2021.101882.

Brand M.D. The sites and topology of mitochondrial superoxide production. Exp. Gerontol. 2010;45:466–472. doi: 10.1016/j.exger.2010.01.003

Calero A, Illig KA. Overview of aortic aneurysm management in the endovascular era. Semin Vasc Surg. 2016 Mar;29(1-2):3-17. doi: 10.1053/j.semvascsurg.2016.07.003.

Cañadas V, Vilacosta I, Bruna I, Fuster V. Marfan syndrome. Part 1: pathophysiology and diagnosis. Nat Rev Cardiol. 2010;7(5):256-265. doi:10.1038/nrcardio.2010.30.

Chamorro A, Amaro S, Castellanos M, Segura T, Arenillas J, Martí-Fábregas J, Gállego J, Krupinski J, Gomis M, Cánovas D, Carné X, Deulofeu R, Román LS, Oleaga L, Torres F, Planas AM; URICO-ICTUS Investigators. Safety and efficacy of uric acid in patients with acute stroke (URICO-ICTUS): a randomised, double-blind phase 2b/3 trial. Lancet Neurol. 2014 May;13(5):453-60. doi: 10.1016/S1474-4422(14)70054-7.

Chau KH, Elefteriades JA. Natural history of thoracic aortic aneurysms: size matters, plus moving beyond size. Prog Cardiovasc Dis. 2013;56(1):74-80. doi:10.1016/j.pcad.2013.05.007.

Chaudhry SS, Cain S a., Morgan A, Dallas SL, Shuttleworth CA, Kielty CM. Fibrillin-1 regulates the bioavailability of TGF β1. J Cell Biol. 2007;176(3):355–67.

Chung A.W.Y., Au Yeung K., Cortes S.F., Sandor G.G.S., Judge D.P., Dietz H.C., van Breemen C. Endothelial dysfunction and compromised eNOS/Akt signaling in the thoracic aorta during the

progression of Marfan syndrome. Br. J. Pharmacol. 2007;150:1075–1083. doi: 10.1038/sj.bjp.0707181

Cohn RD, van Erp C, Habashi JP, Soleimani A a, Klein EC, Lisi MT, et al. Angiotensin II type 1 receptor blockade attenuates TGF-β-induced failure of muscle regeneration in multiple myopathic states. Nat Med. 2007;13(2):204–10.

Colín-González AL, Santamaría A. Probenecid: an emerging tool for neuroprotection. CNS Neurol Disord Drug Targets. 2013 Nov;12(7):1050-65. doi: 10.2174/18715273113129990090.

Cook JR, Clayton NP, Carta L, Galatioto J, Chiu E, Smaldone S, Nelson CA, Cheng SH, Wentworth BM, Ramirez F. Dimorphic effects of transforming growth factor-β signaling during aortic aneurysm progression in mice suggest a combinatorial therapy for Marfan syndrome.Arterioscler Thromb Vasc Biol. 2015; 35:911–917. doi: 10.1161/ATVBAHA.114.305150

Cortese F, Giordano P, Scicchitano P, Faienza MF, De Pergola G, Calculli G, Meliota G, Ciccone MM. Uric acid: from a biological advantage to a potential danger. A focus on cardiovascular effects. Vascul Pharmacol 2019, 120:106565. doi: 10.1016/j.vph.2019.106565.

Cozijnsen L, Braam RL, Waalewijn RA, et al. What is new in dilatation of the ascending aorta? Review of current literature and practical advice for the cardiologist. Circulation. 2011;123(8):924-928. doi:10.1161/CIRCULATIONAHA.110.949131.

De Backer J, Renard M, Campens L, et al. Marfan Syndrome and Related Heritable Thoracic Aortic Aneurysms and Dissections. Curr Pharm Des. 2015;21(28):4061-4075. doi:10.1161/01.CIR.0000078634.33124.95.

Deleeuw V, De Clercq A, De Backer J, Sips P. An Overview of Investigational and Experimental Drug Treatment Strategies for Marfan Syndrome. J Exp Pharmacol. 2021 Aug 11;13:755-779. doi: 10.2147/JEP.S265271.

Di Guglielmo GM, Le Roy C, Goodfellow AF, Wrana JL. Distinct endocytic pathways regulate TGF-β receptor signalling and turnover. Nat Cell Biol. 2003;5(5):410–21.

Dietz HC, Cutting GR, Pyeritz RE, Maslen CL, Sakai LY, Corson GM, et al. Marfan syndrome caused by a recurrent de novo missense mutation in the fibrillin gene. Nature. 1991 Jul;352(6333):337–9.

Dijke P, Arthur HM. Extracellular control of TGFβ signalling in vascular development and disease. 2007;8(november).

Dotor J, López-Vázquez AB, Lasarte JJ, Sarobe P, García-Granero M, Riezu-Boj JI, Martínez A, Feijoó E, López-Sagaseta J, Hermida J, Prieto J, Borrás-Cuesta F. Identification of peptide inhibitors of transforming growth factor beta 1 using a phage-displayed peptide library. Cytokine. 2007 Aug;39(2):106-15. doi: 10.1016/j.cyto.2007.06.004.

Egea G, Jiménez-Altayó F, Campuzano V. Reactive Oxygen Species and Oxidative Stress in the Pathogenesis and Progression of Genetic Diseases of the Connective Tissue. Antioxidants (Basel). 2020 Oct 19;9(10):1013. doi: 10.3390/antiox9101013.

El-Hamamsy I, Yacoub MH. Cellular and molecular mechanisms of thoracic aortic aneurysms. Nat Rev Cardiol. 2009;6(12):771-786. doi:10.1038/nrcardio.2009.191.

Erbel R, Aboyans V, Boileau C, et al. 2014 ESC Guidelines on the diagnosis and treatment of aortic diseases. Eur Heart J. 2014;35(41):2873-2926. doi:10.1093/eurheartj/ehu281.

Ezquerro I.J., Lasarte J.J., Dotor J. A synthetic peptide from transforming growth factor β type III receptor inhibits liver fibrogenesis in rats with carbon tetrachloride liver injury. Cytokine. 2003;22:12–20. doi: 10.1016/S1043-4666(03)00101-7.

Faivre L, Collod-Beroud G, Loeys BL, Child A, Binquet C, Gautier E, et al. Effect of mutation type and location on clinical outcome in 1,013 probands with Marfan syndrome or related phenotypes and FBN1 mutations: an international study. Am J Hum Genet. 2007;81(3):454–66.

Fernandez ML, Stupar D, Croll T, Leavesley D, Upton Z. Xanthine Oxidoreductase: A Novel Therapeutic Target for the Treatment of Chronic Wounds? Adv Wound Care (New Rochelle). 2018 Mar 1;7(3):95-104. doi: 10.1089/wound.2016.0724.

Förstermann U., Münzel T. Endothelial nitric oxide synthase in vascular disease: From marvel to menace. Circulation. 2006;113:1708–1714. doi: 10.1161/CIRCULATIONAHA.105.602532.

Gallo-Oller G., Vollmann-Zwerenz A., Melendez B., Rey J., Hau P., Dotor J., Castresana J. P144, a Transforming Growth Factor beta inhibitor peptide, generates antitumoral effects and modifies SMAD7 and SKI levels in human glioblastoma cell lines. Cancer Lett. 2016;381:67–75. doi: 10.1016/j.canlet.2016.07.029

Gartner LP, Hiatt JL. Texto Atlas de Histología. 3rd ed. McGraw-Hill Interamericana; 2008.

Ge G, Greenspan DS. BMP1 controls TGFβ1 activation via cleavage of latent TGFβ-binding protein. J Cell Biol. 2006 Oct;175(1):111–20.

George J, Carr E, Davies J, Belch JJ, Struthers A. High-dose allopurinol improves endothelial function by profoundly reducing vascular oxidative stress and not by lowering uric acid. Circulation. 2006 Dec 5;114(23):2508-16. doi: 10.1161/CIRCULATIONAHA.106.651117.

Gordon KJ, Blobe GC. Role of transforming growth factor-β superfamily signaling pathways in human disease. Biochim Biophys Acta. 2008;1782(4):197–228.

Habashi JP, Doyle JJ, Holm TM, et al. Angiotensin II Type 2 Receptor Signaling Attenuates Aortic Aneurysm in Mice Through ERK Antagonism. Science (80-). 2011;332(April):361-366. doi:10.1126/science.1192152.

Hart PJ, Deep S, Taylor AB, Shu Z, Hinck CS, Hinck AP. Crystal structure of the human TβR2 ectodomain–TGF-β3 complex. Nat Struct Biol. 2002;(26587):203–8.

Hoffman Bowman M, Eage KA, Milewicz DM. Update on clinical trials of Losartan with and without ß-blockers to block aneurysm growth in patients with Marfan syndrome: a review. JAMA Cardiol. 2019; 4:702–707. doi: 10.1001/jamacardio.2019.1176

Holm TM, Habashi JP, Doyle JJ, et al. Noncanonical TGFbeta signaling contributes to aortic aneurysm progression in Marfan syndrome mice - supplementary. Science (80-). 2011;332(6027):358-361. doi:332/6027/358 [pii]\r10.1126/science.1192149.

Hooper DC, Kean RB, Scott GS, Spitsin SV, Mikheeva T, Morimoto K, Bette M, Röhrenbeck AM, Dietzschold B, Weihe E. The central nervous system inflammatory response to neurotropic virus infection is peroxynitrite dependent. J Immunol 2001,
15;167(6):3470-7. doi: 10.4049/jimmunol.167.6.3470.

Huang TH, Chang HH, Guo YR, Chang WC, Chen YF. Vitamin B Mitigates Thoracic Aortic Dilation in Marfan Syndrome Mice by Restoring the Canonical TGF-β Pathway. Int J Mol Sci. 2021 Oct 29;22(21):11737. doi: 10.3390/ijms222111737.

Huse M, Chen YG, Massague J, Kuriyan J. Crystal structure of the cytoplasmic domain of the type I TGF β receptor in complex with FKBP12. Cell. 1999 Feb;96(3):425–36.

Hutchison SJ. Enfermedades Aórticas: Atlas de Diagnóstico Clínico Por Imagen. Barcelona: Elsevier; 2010.

Isogai Z. Latent Transforming Growth Factor β-binding Protein 1 Interacts with Fibrillin and Is a Microfibril-associated Protein. J Biol Chem. 2003;278(4):2750–7.

Isselbacher, E. M., Preventza, O., Hamilton Black, J., 3rd, Augoustides, J. G., Beck, A. W., Bolen, M. A., Braverman, A. C., Bray, B. E., Brown-Zimmerman, M. M., Chen, E. P., Collins, T. J., DeAnda, A., Jr, Fanola, C. L., Girardi, L. N., Hicks, C. W., Hui, D. S., Schuyler Jones, W., Kalahasti, V., Kim, K. M., Milewicz, D. M., … Woo, Y. J. 2022 ACC/AHA Guideline for the Diagnosis and Management of Aortic Disease: A Report of the American Heart Association/American College of Cardiology Joint Committee on Clinical Practice Guidelines. Circulation. 2022;146(24):e334-e482. doi:10.1161/CIR.0000000000001106

Jiang WL, Qi X, Li X, Zhang YF, Xia QQ, Chen JC. Serum uric acid is associated with aortic dissection in Chinese men. Int J Cardiol 2016, 1;202:196-7. doi:10.1016/j.ijcard.2015.08.174.

Jiménez-Altayó F., Meirelles T., Crosas-Molist E., Sorolla M.A., Del Blanco D.G., López-Luque J., Mas-Stachurska A., Siegert A.-M., Bonorino F., Barberà L., et al. Redox stress in Marfan syndrome: Dissecting the role of the NADPH oxidase NOX4 in aortic aneurysm. Free Radic. Biol. Med. 2018;118:44–58. doi: 10.1016/j.freeradbiomed.2018.02.023.

Jondeau G, Michel JB, Boileau C. The translational science of Marfan syndrome. Heart. 2011;97:1206-1214. doi:10.1136/hrt.2010.212100.

Jones JA, Spinale FG, Ikonomidis JS. Transforming growth factor-beta signaling in thoracic aortic aneurysm development: a paradox in pathogenesis.J Vasc Res. 2009; 46:119–137. doi: 10.1159/000151766

Junqueira LC, Carneiro J. Histología Básica. 6th ed. Barcelona: Masson; 2005.

Kanbay M, Segal M, Afsar B, Kang DH, Rodriguez-Iturbe B, Johnson RJ. The role of uric acid in the pathogenesis of human cardiovascular disease. Heart 2013,
99(11):759-66. doi: 10.1136/heartjnl-2012-302535.

Kang DH, Ha SK. Uric Acid Puzzle: Dual Role as Anti-oxidant and Pro-oxidant.
Electrolyte Blood Press 2014, 12(1):1-6. doi: 10.5049/EBP.2014.12.1.1.

Karimi A, Milewicz DM. Structure of the Elastin-Contractile Units in the Thoracic Aorta and How Genes That Cause Thoracic Aortic Aneurysms and Dissections Disrupt This Structure. Can J Cardiol. 2016;32(1):26-34. doi:10.1016/j.cjca.2015.11.004.

Karnebeek CDM Van, Naeff MSJ, Mulder BJM, Hennekam RCM, Offringa M. Natural history of cardiovascular manifestations in Marfan syndrome Natural history of cardiovascular manifestations in Marfan syndrome. 2001;(June 2008):129–37.

Karnebeek CDM Van, Naeff MSJ, Mulder BJM, Hennekam RCM, Offringa M. Natural history of cardiovascular manifestations in Marfan syndrome Natural history of cardiovascular manifestations in Marfan syndrome. 2001;(June 2008):129–37.

Karpman C, Aughenbaugh GL, Ryu JH. Pneumothorax and bullae in Marfan syndrome. Respiration. 2011;82(3):219–24.

Kielty CM, Stephan S, Sherratt MJ, Williamson M, Shuttleworth CA. Applying elastic fibre biology in vascular tissue engineering. Philos Trans R Soc Lond B Biol Sci. 2007;362(1484):1293-1312. doi:10.1098/rstb.2007.2134.

Kierszenbaum AL, Tres LL. Histology and Cell Biology: An Introduction to Pathology. 4th ed. Philadelphia: Elsevier; 2016.

Kisker C, Schindelin H, Rees DC. Molybdenum cofactor-containing enzymes: structure and mechanism. Annu Rev Biochem. 1997;66:233–267

Koeppen BM, Stanton BA. Berne & Levy Physiology. 6th ed. Philadelphia: Mosby; 2008.

Kohler M, Pitcher A, Blair E, Risby P, Senn O, Forfar C, et al. The impact of obstructive sleep apnea on aortic disease in Marfan's syndrome. Respiration. 2013;86(1):39–44.

Krstic J, Santibanez JF. Transforming growth factor-β and matrix metalloproteinases: functional interactions in tumor stroma-infiltrating myeloid cells. ScientificWorldJournal. 2014;2014:521754.

Krstić J., Trivanović D., Mojsilović S., Santibanez J.F. Transforming Growth Factor-Beta and Oxidative Stress Interplay: Implications in Tumorigenesis and Cancer Progression. Oxid. Med. Cell. Longev. 2015;2015:654594. doi: 10.1155/2015/654594.

Kukreja R.C., Kontos H.A., Hess M.L., Ellis E.F. PGH synthase and lipoxygenase generate superoxide in the presence of NADH or NADPH. Circ. Res. 1986;59:612–619. doi: 10.1161/01.RES.59.6.612

Lacy F., Gough D.A., Schmid-Schönbein G.W. Role of xanthine oxidase in hydrogen peroxide production. Free Radic. Biol. Med. 1998;25:720–727. doi: 10.1016/S0891-5849(98)00154-3

Lassègue B., San Martín A., Griendling K.K. Biochemistry, physiology, and pathophysiology of NADPH oxidases in the cardiovascular system. Circ. Res. 2012;110:1364–1390. doi: 10.1161/CIRCRESAHA.111.243972

Lavall D, Schäfers H-J, Böhm M, Laufs U. Aneurysms of the ascending aorta. Dtsch Arztebl Int. 2012;109(13):227.

Lavoie P, Robitaille G, Agharazii M, Ledbetter S, Lebel M, Larivière R. Neutralization of transforming growth factor-β attenuates hypertension and prevents renal injury in uremic rats. J Hypertens. 2005;23(10). doi:16148614.

Lee SJ, Oh BK, Sung KC. Uric acid and cardiometabolic diseases. Clin Hypertens 2020, 15;26:13. doi: 10.1186/s40885-020-00146-y.

Lee BE, Toledo AH, Anaya-Prado R, Roach RR, Toledo-Pereyra LH. Allopurinol, xanthine oxidase, and cardiac ischemia. J Investig Med. 2009 Dec;57(8):902-9. doi: 10.2310/JIM.0b013e3181bca50c.

Liu R-M, Desai LP. Reciprocal regulation of TGF-β and reactive oxygen species: A perverse cycle for fibrosis. Redox Biol. 2015 Dec;6:565–77.

Llopiz D, Dotor J, Casares N, Bezunartea J, Díaz-Valdés N, Ruiz M, Aranda F, Berraondo P, Prieto J, Lasarte JJ, Borrás-Cuesta F, Sarobe P. Peptide inhibitors of transforming growth factor-beta enhance the efficacy of antitumor immunotherapy. Int J Cancer. 2009 Dec 1;125(11):2614-23. doi: 10.1002/ijc.24656.

Llopiz D., Dotor J., Zabaleta A., Lasarte J.J., Prieto J., Borras-Cuesta F., Sarobe P. Combined immunization with adjuvant molecules poly(I:C) and anti-CD40 plus a tumour antigen has potent prophylactic and therapeutic antitumor effects. Cancer Immunol. Immunother. 2008;57:19–29. doi: 10.1007/s00262-007-0346-8.

Loeys BL, Dietz HC, Braverman AC, Callewaert BL, De Backer J, Devereux RB, et al. The revised Ghent nosology for the Marfan syndrome. J Med Genet. 2010 Jul;47(7):476–85.

Lou Z., Wang A.-P., Duan X.-M., Hu G.-H., Song G.-L., Zuo M.-L., Yang Z.-B. Upregulation of NOX2 and NOX4 Mediated by TGF-β Signaling Pathway Exacerbates Cerebral Ischemia/Reperfusion Oxidative Stress Injury. Cell. Physiol. Biochem. 2018;46:2103–2113. doi: 10.1159/000489450

Lu P, Takai K, Weaver VM, Werb Z. Extracellular matrix degradation and remodeling in development and disease. Cold Spring Harb Perspect Biol. 2011;1–25.

Lyons RM, Keski-Oja J, Moses HL. Proteolytic activation of latent transforming growth factor-β from fibroblast-conditioned medium. J Cell Biol. 1988 May;106(5):1659–65.
Maiuolo J, Oppedisano F, Gratteri S, Muscoli C, Mollace V. Regulation of uric acid metabolism and excretion. Int J Cardiol 2016, 15;213:8-14. doi: 10.1016/j.ijcard.2015.08.109.

Manna L, Vitale F, Reale S, Picillo E, Neglia G, Vescio F, Gravino AE. Study of efficacy of miltefosine and allopurinol in dogs with leishmaniosis. Vet J. 2009 Dec;182(3):441-5. doi: 10.1016/j.tvjl.2008.08.009.

Mann DL, Zipes DP, Libby P, Bonow RO. Braunwald's Heart Disease: A Textbook of Cardiovascular Medicine. 10th ed. Philadelphia: Elsevier; 2015.

Manning G, Whyte DB, Martinez R, Hunter T, Sudarsanam S. The protein kinase complement of the human genome. Science. 2002 Dec;298(5600):1912–34.

Martínez-Revelles S., García-Redondo A.B., Avendaño M.S., Varona S., Palao T., Orriols M., Roque F.R., Fortuño A., Touyz R.M., Martínez-González J., et al. Lysyl Oxidase Induces Vascular Oxidative Stress and Contributes to Arterial Stiffness and Abnormal Elastin Structure in Hypertension: Role of p38MAPK. Antioxid. Redox Signal. 2017;27:379–397. doi: 10.1089/ars.2016.6642.

Masi S, Pugliese NR, Taddei S. The difficult relationship between uric acid and cardiovascular disease. Eur Heart J 2019, 21;40(36):3055-3057. doi: 10.1093/eurheartj/ehz166.

Maumenee IH. The eye in the Marfan Syndrome. Trans Am Ophthalmol Soc. 1981;79:684–7337.

Miah R, Fariha KA, Sony SA, Ahmed S, Hasan M, Mou AD, Barman Z, Hasan A, Mohanto NC, Ali N. Association of serum xanthine oxidase levels with hypertension: a study on Bangladeshi adults. Sci Rep. 2022 Dec 16;12(1):21727. doi: 10.1038/s41598-022-26341-5.

Milewicz DM. Treatment of Aortic Disease in Patients With Marfan Syndrome. Circulation. 2005;111(11):e150–7.

Milewicz DM, Braverman AC, De Backer J, Morris SA, Boileau C, Maumenee IH, Jondeau G, Evangelista A, Pyeritz RE. Marfan syndrome. Nat Rev Dis Primers. 2021 Sep 2;7(1):64. doi: 10.1038/s41572-021-00298-7.

Milewicz DM, Prakash SK, Ramirez F. Therapeutics targeting drivers of thoracic aortic aneurysms and acute aortic dissections: insights from predisposing genes and mouse models. Annu Rev Med. 2017; 68:51–67. doi: 10.1146/annurev-med-100415-022956

Mieremet A, van der Stoel M, Li S, Coskun E, van Krimpen T, Huveneers S, de Waard V. Endothelial dysfunction in Marfan syndrome mice is restored by resveratrol. Sci Rep. 2022 Dec 28;12(1):22504. doi: 10.1038/s41598-022-26662-5.

Mo L, He Q, Wang Y, Dong B, He J. High prevalence of obstructive sleep apnea in Marfan's syndrome. Chin Med J (Engl). 2014;127(17):3150–5.

Murillo-Cuesta S., Rodríguez-de la Rosa L., Contreras J., Celaya A.M., Camarero G., Rivera T., Varela-Nieto I. Transforming growth factor β1 inhibition protects from noise-induced hearing loss. Front. Aging Neurosci. 2015;7:32.

Neogi T., George J., Rekhraj S., Struthers A.D., Choi H., Terkeltaub R.A. Are either or both hyperuricemia and xanthine oxidase directly toxic to the vasculature? A critical appraisal. Arthritis Rheum. 2012;64:327–338. doi: 10.1002/art.33369

Neptune ER, Frischmeyer P a, Arking DE, Myers L, Bunton TE, Gayraud B, et al. Dysregulation of TGF-β activation contributes to pathogenesis in Marfan syndrome. Nat Genet. 2003;33(3):407–11.

Nettersheim FS, Lemties J, Braumann S, Geißen S, Bokredenghel S, Nies R, Hof A, Winkels H, Freeman BA, Klinke A, Rudolph V, Baldus S, Mehrkens D, Mollenhauer M, Adam M. Nitro-oleic acid reduces thoracic aortic aneurysm progression in a mouse model of Marfan syndrome. Cardiovasc Res. 2022 Jul 20;118(9):2211-2225. doi: 10.1093/cvr/cvab256.

Oller J, Gabandé-Rodríguez E, Ruiz-Rodríguez MJ, Desdín-Micó G, Aranda JF, Rodrigues-Diez R, Ballesteros-Martínez C, Blanco EM, Roldan-Montero R, Acuña P, Forteza Gil A, Martín-López CE, Nistal JF, Lino Cardenas CL, Lindsay ME, Martín-Ventura JL, Briones AM, Redondo JM, Mittelbrunn M. Extracellular Tuning of Mitochondrial Respiration Leads to Aortic Aneurysm. Circulation. 2021 May 25;143(21):2091-2109. doi: 10.1161/CIRCULATIONAHA.120.051171.

O'Connell MK, Murthy S, Phan S, et al. The three-dimensional micro- and nanostructure of the aortic medial lamellar unit measured using 3D confocal and electron microscopy imaging. Matrix Biol. 2008;27(3):171-181. doi:10.1016/j.matbio.2007.10.008.

Polito L, Bortolotti M, Battelli MG, Bolognesi A. Xanthine oxidoreductase: A leading actor in cardiovascular disease drama. Redox Biol. 2021 Nov 24;48:102195. doi: 10.1016/j.redox.2021.102195.

Ramirez F, Sakai LY, Rifkin DB, Dietz HC. Extracellular microfibrils in development and disease. Cell Mol Life Sci. 2007;64(18):2437–46.

Reinhardt DP, Ono RN, Notbohm H, Müller PK, Bächinger HP, Sakai LY. Mutations in Calcium-binding Epidermal Growth Factor Modules Render Fibrillin-1 Susceptible to Proteolysis A POTENTIAL DISEASE-CAUSING MECHANISM IN MARFAN SYNDROME. J Biol Chem. 2000;275(16):12339–45.

Rybczynski M, Koschyk D, Karmeier A, Gessler N, Sheikhzadeh S, Bernhardt AM, Habermann CR, Treede H, Berger J, Robinson PN, Meinertz T, von Kodolitsch Y. Frequency of sleep apnea in adults with the Marfan syndrome. Am J Cardiol. 2010 Jun 15;105(12):1836-41. doi: 10.1016/j.amjcard.2010.01.369.

Robinson PN, Booms P, Katzke S, Ladewig M, Neumann L, Palz M, et al. Mutations of FBN1 and genotype-phenotype correlations in Marfan syndrome and related fibrillinopathies. Hum Mutat. 2002;20(3):153–61.

Ross MH, Kaye GI, Pawlina W. Histología: Texto Y Atlas Color Con Biología Celular Y Molecular. 4th ed. Buenos Aires: Editorial Médica Panamericana; 2004.

Sakai LY, Keene DR, Renard M, De Backer J. FBN1: The disease-causing gene for Marfan syndrome and other genetic disorders. Gene. 2016;591(1):279–91.

Sankar S, Mahooti-Brooks N, Centrella M, McCarthy TL, Madri JA. Expression of transforming growth factor type III receptor in vascular endothelial cells increases their responsiveness to transforming growth factorβ2. J Biol Chem. 1995 Jun;270(22):13567–72.

Santiago B., Gutierrez-Canas I., Dotor J., Palao G., Lasarte J.J., Ruiz J., Prieto J., Borras-Cuesta F., Pablos J.L. Topical application of a peptide inhibitor of transforming growth factor-beta1 ameliorates bleomycin-induced skin fibrosis. J. Investig. Dermatol. 2005;125:450–455. doi: 10.1111/j.0022-202X.2005.23859.x.

Schardinger F. Über das Verhalten der Kuhmilch gegen Methylenblau und seine Verwendung zur Unterscheidung von ungekochter und gekochter Milch. Untersuch Nahrungs Genussmittel. 1902;5:1113–1121

Scherer LR, Arn PH, Dressel DA, Pyeritz RM, Haller JAJ. Surgical management of children and young adults with Marfan syndrome and pectus excavatum. J Pediatr Surg. 1988 Dec;23(12):1169–72.

Scott GS, Hooper DC. The role of uric acid in protection against peroxynitrite- mediated pathology. Med Hypotheses 2001, 56(1):95-100. doi: 10.1054/mehy.2000.1118.

Seet RC, Kasiman K, Gruber J, Tang SY, Wong MC, Chang HM, Chan YH, Halliwell B, Chen CP. Is uric acid protective or deleterious in acute ischemic stroke? A 10.1016/j.atherosclerosis.2009.08.012.

Shi Y, Massagué J. Mechanisms of TGF-β signaling from cell membrane to the nucleus. Cell. 2003;113(6):685–700.

Siegert AM, García Díaz-Barriga G, Esteve-Codina A, Navas-Madroñal M, Gorbenko Del Blanco D, Alberch J, Heath S, Galán M, Egea G. A FBN1 3'UTR mutation variant is associated with endoplasmic reticulum stress in aortic aneurysm in Marfan syndrome. Biochim Biophys Acta Mol Basis Dis. 2019 Jan;1865(1):107-114. doi: 10.1016/j.bbadis.2018.10.029.

Sies H, Berndt C, Jones DP. Oxidative Stress. Annu Rev Biochem. 2017 Jun 20;86:715-748. doi: 10.1146/annurev-biochem-061516-045037.

Sies H. Chapter 1 - Oxidative eustress and oxidative distress: Introductory remarks. 2020. In H. Sies (Ed.), Oxidative Stress (pp. 3-12). Academic Press. ISBN 9780128186060.

Sies H, Jones DP. Reactive oxygen species (ROS) as pleiotropic physiological signalling agents. Nat Rev Mol Cell Biol. 2020 Jul;21(7):363-383. doi: 10.1038/s41580-020-0230-3.

Sies H. Oxidative eustress: the physiological role of oxidants. Sci China Life Sci. 2023 Apr 6. doi: 10.1007/s11427-023-2336-1.

Sponseller PD, Hobbs W, Riley LH 3rd, Pyeritz RE. The thoracolumbar spine in Marfan syndrome. J Bone Joint Surg Am. 1995 Jun;77(6):867–76.

Tellides G. Further Evidence Supporting a Protective Role of Transforming Growth Factor-β (TGFβ) in Aortic Aneurysm and dissection. Arterioscler Thromb Vasc Biol. 2017;37:1983-1986. doi:10.1161/ATVBAHA.117.310031.

Testut L, Latarjet A. Compendio de Anatomía Descriptiva. Barcelona: Salvat; 1983.

Tremblay D, Leask RL. Remodelling and pathology development associated with aneurysmal ascending aortic tissues. Can J Chem Eng. 2011;89(1):13-22. doi:10.1002/cjce.20455.

Tsamis A, Krawiec JT, Vorp DA. Elastin and collagen fibre microstructure of the human aorta in ageing and disease: a review. J R Soc Interface. 2013;10:1-22. doi:10.1098/rsif.2012.1004.

Vassalle C, Mazzone A, Sabatino L, Carpeggiani C. Uric Acid for Cardiovascular Risk: Dr. Jekyll or Mr. Hide? Diseases, 2016, 26;4(1):12. doi: 10.3390/diseases4010012.

Viveiro C, Rocha P, Carvalho C, Zarcos MM. Spontaneous pneumothorax as manifestation of Marfan syndrome. BMJ Case Rep. 2013;1–3.

Wagenseil JE, Mecham RP. Vascular extracellular matrix and arterial mechanics. Physiol Rev. 2009;89(3):957-989. doi:10.1152/physrev.00041.2008.

Wang JC, Tsai SH, Tsai HY, Lin SJ, Huang PH. Hyperuricemia exacerbates abdominal aortic aneurysm formation through the URAT1/ERK/MMP-9 signaling pathway. BMC Cardiovasc Disord 2023 30;23(1):55. doi: 10.1186/s12872-022- 03012-x.

Waud WR, Rajagopalan KV. Purification and properties of the NAD+-dependent (Type D) and O2-dependent (Type O) forms of rat liver xanthine dehydrogenase. Arch Biochem Biophys. 1976a;172:354–364

Wilson NK, Gould RA, Gallo E, Consortium ML. Pathophysiology of aortic aneurysm: insights from human genetics and mouse models. Pharmacogenomics. 2016;17(18):2071-2080

Wolinsky H, Glagov S. Structural Basis for the Static Mechanical Properties of the Aortic Media. Circ Res. 1964;14(5):400-413. doi:10.1161/01.RES.14.5.400.

Wolinsky H, Glagov S. A Lamellar Unit of Aortic Medial Structure and Function in Mammals. Circ Res. 1967;20(1):99-111. doi:10.1161/01.RES.20.1.99

Yagi H, Akazawa H, Liu Q, Yamamoto K, Nawata K, Saga-Kamo A, Umei M, Kadowaki H, Matsuoka R, Shindo A et al. Aberrant mechanosensitive signaling underlies activation of vascular endothelial xanthine oxidoreductase that promotes aortic aneurysm formation in Marfan syndrome. bioRxiv 2022; doi: 10.1101/2022.01.30.478356.

Yang H.H.C., van Breemen C., Chung A.W.Y. Vasomotor dysfunction in the thoracic aorta of Marfan syndrome is associated with accumulation of oxidative stress. Vascul. Pharmacol. 2010;52:37–45. doi: 10.1016/j.vph.2009.10.005

Yang L, Wu H, Luo C, Zhao Y, Dai R, Li Z, Zhang X, Gong Z, Cai Z, Shen Y, Yu F, Li W, Zhao H, Zhang T, Zhu J, Fu Y, Wang J, Kong W. Urate-Lowering Therapy Inhibits Thoracic Aortic Aneurysm and Dissection Formation in Mice. Arterioscler Thromb Vasc Biol 2023, In press. doi: 10.1161/ATVBAHA.122.318788.

Yasui H., Hayashi S., Sakurai H. Possible involvement of singlet oxygen species as multiple oxidants in p450 catalytic reactions. Drug Metab. Pharmacokinet. 2005;20:1–13. doi: 10.2133/dmpk.20.1

Yu Q, Stamenkovic I. Cell surface-localized matrix metalloproteinase-9 proteolytically activates TGF-β and promotes tumor invasion and angiogenesis. Genes Dev. 2000 Jan;14(2):163–76.

Yu W, Cheng JD. Uric Acid and Cardiovascular Disease: An Update From Molecular Mechanism to Clinical Perspective. Front Pharmacol 2020, 11:582680. doi: 10.3389/fphar.2020.582680.

Zaradzki M, Mohr F, Lont S, Soethoff J, Remes A, Arif R, Müller OJ, Karck M, Hecker M, Wagner AH. Short-term rapamycin treatment increases life span and attenuates aortic aneurysm in a murine model of Marfan-Syndrome. Biochem Pharmacol. 2022 Nov;205:115280. doi: 10.1016/j.bcp.2022.115280.

Zhang Y, Xu X, Lu Y, Guo L, Ma L. Preoperative uric acid predicts in-hospital death in patients with acute type A aortic dissection. J Cardiothorac Surg 2020,
15;15(1):21. doi: 10.1186/s13019-020-1066-9.